Efficient stabilization with hydraulic binders of local earth for building construction applications

Noha Al Haffar

N° d'ordre NNT : 2021LYSET006

THESE DE DOCTORAT DE L'UNIVERSITE DE LYON

opérée au sein de
ECOLE NATIONALE DES TRAVAUX PUBLICS DE L'ETAT
LGCB-LTDS UMR 5513

Ecole doctorale N°162
MEGA (Mécanique, Energétique, Génie Civil, Acoustique)

Spécialité : Génie Civil

Soutenue publiquement le 28/06/2021, par :

Noha AL HAFFAR

Efficient stabilization with hydraulic binders of local earth for building construction applications

---

Stabilisation performante au liants hydrauliques des terres locales pour la construction

Devant le jury composé de :

Venkatarama REDDY B. V.	Professeur (Indian Institute of Science)	Rapporteur
Céline PERLOT-BASCOULÈS	Maître de conférences (BTP ISA, Anglet)	Rapportrice
Mathilde MORVAN	Maître de conférences (UCA, Clermont-Ferrand)	Examinatrice
Guillaume HABERT	Professeur (ETH Zürich)	Examinateur
Jean-Claude MOREL	Directeur de recherche (ENTPE, Lyon)	Examinateur
Antonin FABBRI	Directeur de recherche (ENTPE, Lyon)	Directeur
Fionn MCGREGOR	Chargé de recherche (ENTPE, Lyon)	Encadrant
Laurent IZORET	Directeur délégué Produits : Applications & Recherche (ATILH, Paris)	Co-Encadrant

If we knew what it was we were doing, it would not be called research, would it?

Albert Einstein [1879-1955]

Acknowledgement

First, I would also like to thank the jury members for their interest and participation in this thesis. Special thanks go to Prof. Jean Claude MOREL for agreeing to chair the thesis jury. I would also like to thank Dr. Celine PERLOT-BASCOULÈS and Prof. Venkatarama REDDY B. V., who kindly and graciously accepted to review the manuscript. I am also very grateful to Prof. Guillaume HABERT and Dr. Mathilde MORVAN for examining my thesis. I appreciate the opportunity I have been given to share my work with them, and to discuss the application of the ecological criteria to the challenge of building with earth today.

The present Doctoral thesis is the outcome of 39 months of research activity carried out in the LTDS (Laboratory of Tribology and System Dynamics) of the ENTPE (National School of Public Works of the State) and sponsored by the ATILH (French Technical Association of Industries of Hydraulic Binders) and the ANRT (French National Association of Research and Technology) under the CIFRE convention n˚2017/1512. The achievement of this Doctoral thesis would not have been made possible without the support and advice of a number of people, who deserve my sincere acknowledgments.

I am truly indebted to my main supervisor Prof. Antonin FABBRI for his valuable comments, suggestions and criticisms with regards to my research and the manuscripts, which compose the core of this thesis. I have learnt a lot during the time I had the privilege to work close to him. He was always there for me when I needed him and gave me some key advice, without losing his status as the cool boss! Thank you, Antonin, for believing in my potentials since our very first meeting during my Master project and for introducing me to the world of earthen materials which broadened my experience in the field of eco-friendly building materials. I would like also to express my sincere thanks to my co-supervisor Dr. Fionn MCGREGOR, who was always provided valuable insights leading to the successful completion of my project. He is kindly acknowledged for introducing me to the topic of Moisture Buffering Capacity of building materials. A big thanks goes to Dr. Horacio COLINA for the efforts he had made to support this project and for the continuous follow-up of the project progress as a co-supervisor in the ATILH for two years. A big thanks goes also to Dr. Laurent IZORET who came in later as a co-supervisor in the ATILH but also provided valuable guidance and feedback. I would like also to thank the representatives of the cement companies' members of the ATILH who intervened in the steering committee of this thesis for their continuous advice and for the discussions we made on cementitious materials and soil stabilization. I mention in particular: Eng. Claire CAPRA, Eng. Laetitia BESSETTE, Dr. Fabien BARBERON Dr. Nathalie GINEYS and Dr. Jaouad NADAH.

I must not forget to thank all members of the technical, IT and administrative units of the ENTPE and the ATILH for their help and guidance. Mr. Stephane COINTET is acknowledged for his technical assistance during manufacturing samples, performing mechanical tests, and preparing the experimental setup of the durability tests. Eng. Joachim BLANC-GONNET is acknowledged for his technical assistance during the performance of the thermographic measurements. Mr. Laurent BIDAULT is acknowledged for his technical assistance during the

microstructural analysis of cement-earth mixtures with thermogravimetry. I would also like to thank Mrs. Francette PIGNARD, Mrs. Sonia CENILLE, Mrs. Emmanuelle BUBOIS-TREPAT, Mrs. Fanny BLANCON, Mrs. Muriel MUDRY, Mrs. Martine KRIEF and Mrs. Nathalie HOUËL.

I would also like to express my thanks to all my colleagues at the ENTPE, especially to Mohamed Saïd ABBAS, Lassana Bakary TRAORÉ, Thibaud MAUFRE, Rudy BUI, Youssra LAAROUSSI, Youneng LIU and Xin LI for the fruitful and stimulating discussions we had together. I would like also to thank Nancy HAMIEH, my first student-intern, for her important contribution to chapter 5 and I wish her every success in pursuing a PhD thesis.

Living abroad away from your family and beloved ones is not easy. So I could not forget my friends in France who turned into my family: Hafsa EL AMINE, Dalia KHALIL, Soha BAYDOUN, Orsola BAYDOUN and Mahdis ABADEHZADEH. I am grateful for having you by my side during this journey, and hope we will always be there for each other. As the distance is not a barrier for the friendship, I like to remember my friends in Lebanon, Elham EL-ETER and Zahraa OSMAN, with whom I've shared good laughs and great moments.

Finally, but by no means least, boundless thanks to my family members, especially to my mother Iman AL-DHAYBI, my father Abdulhakim and my two brothers, Mouhammad and Abdallah, for almost unbelievable support throughout this thesis and all these years. They are the most important people in my world, and I dedicate this thesis to them.

Grenoble, France, the 26th of September 2021

Noha Al Haffar

Abstract

The lack of optimization in the formulation of stabilized compacted earth is a major brake on its development as a modern building material. This PhD thesis aims at producing tools for quantification of impacts of cement composition and raw earth nature, as well as their dosages, on the performance of compressed stabilized earth block (CSEB). Firstly, a performance analysis of the cement-earth mixtures was carried out with respect to their mechanical resistance, hygroscopic properties, and durability toward water, to optimize the formulation and the curing conditions. These tests were interpreted from a microstructural point of view to understand the chemical impact of the different selected cements on the studied earths, before concluding on the factors affecting stabilization. Secondly, a method for evaluating the durability of CSEB under realistic conditions was developed. For this purpose, an experimental device that simulates the erosion induced by the cyclical and coupled effects of wind and precipitation has been developed. Finally, the formulation of mortar joints, and moisture transfers at the block-mortar interfaces, were studied. The latest study builds on previous results obtained at the material-scale to interpret the behavior at the scale of the block-mortar element in a real structure.

Keywords: CSEB, low-carbon cements, mechanical and hygroscopic properties, durability toward water, cyclic erosion test, masonry.

Résumé

Le manque d'optimisation dans la formulation de la terre compactée stabilisée au ciment est un frein majeur à son développement en tant que matériau de construction moderne. Cette thèse vise à produire des outils de quantification des impacts de la composition du ciment et de la nature de la terre crue, ainsi que de leurs dosages, sur les performances du bloc de terre compactée stabilisée au ciment (BTCS). Dans un premier temps, une analyse de performances des mélanges ciment-terre a été réalisée en fonction de leur résistance mécanique, échanges hygroscopiques et durabilité vis-à-vis de l'eau liquide, afin d'optimiser la formulation et les conditions de cure. Ces essais ont été interprétés d'un point de vue microstructural pour comprendre l'impact chimique des différents ciments sélectionnés sur les terres locales étudiées, avant de conclure sur les facteurs affectant la stabilisation. Deuxièmement, une méthode d'évaluation de la durabilité des BTCS dans des conditions réalistes d'utilisation a été développée. Dans ce but, un dispositif expérimental qui simule l'érosion induite par les effets cycliques et couplés du vent et des précipitations a été mis au point. Enfin, la formulation des joints de mortiers, et les transferts d'humidité à l'interface bloc-mortier, ont été étudiés. Cette dernière étude s'appuie sur les résultats précédents acquis à l'échelle des matériaux pour interpréter le comportement à l'échelle de l'élément bloc-mortier dans une structure réelle.

Mots clés : BTCS, ciments bas carbone, propriétés mécaniques et hygroscopiques, durabilité à l'eau, essai d'érosion cyclique, maçonnerie.

Dissemination

Publications in scientific journals

2021	*Materials and Structures* Al Haffar, N., Fabbri, F., McGregor, F. Curing conditions impact on compressive strength development in cement stabilized compacted earth. DOI: 10.1617/s11527-021-01702-0
2019	*Comptes Rendus Mécanique* Fabbri, F., Al Haffar, N., McGregor, F. Measurement of the air relative permeability of compacted earth in the hygroscopic regime of saturation. DOI: 10.1016/j.crme.2019.11.017
Under preparation	Al Haffar, N., Fabbri, F., McGregor, F. What factors matter most in the effectiveness of cement-soil stabilization?
Under preparation	*Construction and Building Materials* Al Haffar, N., Fabbri, F., McGregor, F. Innovative method to assess the durability of cement stabilized earth blocks.
Under preparation	*Construction and Building Materials* Al Haffar, N., Hamieh, N., Fabbri, F., McGregor, F. Assessment of bond development in earth block masonry.

Proceeding of international conferences with acts and peer review

2021	*13th fib International PhD Symposium in Civil Engineering, Marne-la-Vallée, Paris, France.* Al Haffar, N., Fabbri, F., McGregor, F. Toward a new assessment method of the durability of stabilized compacted earth blocks.
2019	*Symposium on the infrastructure development - shaping the future using bio-based solutions for structures & buildings, Liverpool, UK.* Al Haffar, N., Fabbri, F., McGregor, F. Assessment of the durability of cement stabilized compacted earth.
2019	*5th International Conference on Sustainable Construction Materials and Technologies (SCMT5), London, UK.* Al Haffar, N., Fabbri, F., McGregor, F., Colina, H. Cement stabilization effect on mechanic and hygric properties of compacted earth. DOI: 10.18552/2019/IDSCMT5159

Proceeding of national conferences with acts and peer review

2019 *5èmes Rencontres Interdisciplinaires Doctorales de l'Architecture et de l'Aménagement Durables RIDAAD 2019, ENTPE, Vaulx-en-Velin, France.*
Al Haffar, N., Fabbri, F.
Stabilisation performante aux liants hydrauliques des terres locales pour la construction.

Contents

Table of figures

List of tables

List of abbreviations and symbols

Abbreviations	
cc	Cement content
CSEB	Compressed Stabilized Earth Block
DSC	Differential Scanning Calorimetry
DTA	Differential Thermal Analysis
DVS	Dynamic Vapor Sorption
ISO	International Organization for Standardization
ISS	Interface Shear Strength
MBV	Moisture Buffer Value
MDD	Maximum Dry Density
OMC	Optimum Moisture Content
OPC	Ordinary Portland Cement
SEM	Scanning Electron Microscopy
TGA	Thermal Gravimetric Analysis
UCS	Uniaxial Compression Strength
XRD	X-Ray Diffraction

Symbols		
Symbol	Description	Units
d_a	Thickness of the air layer in the cup	[m]
δ_a	Water vapour permeability of air	[$kg.m^{-1}.Pa^{-1}.s^{-1}$]
δ_p	Water vapour permeability	[$kg.m^{-1}.Pa^{-1}.s^{-1}$]
ρ_d	Dry density	[$g.cm^{-3}$]
ρ_L	Liquid density	[$g.cm^{-3}$]
ρ_s	Density of solid grains	[$g.cm^{-3}$]

C_p^0	is the volumetric heat capacity of the dry material,	[J.m^{-3}.K^{-1}]
D_L	Hydraulic conductivity	[kg.m^{-1}.Pa^{-1}.s^{-1}]
P_L	Liquid pressure	[Pa]
c_L	Specific heat capacity of water	[J.kg^{-1}.K^{-1}]
A	Area of the specimen	[m²]
G	Total moisture flux	[kg.s^{-1}]
L	Thickness of the sample	[m]
$P_{v,sat}$	Saturation water vapour pressure	[Pa]
RH	Relative Humidity	[%]
u	Water content	[-]
w	Water content	[%]
β	Water vapour surface transfer coefficient	[kg.m^{-2}.s^{-1}.Pa^{-1})]
μ	Water vapour resistance factor	[-]
ξ	Moisture capacity	[kg.m^{-3}]
φ	Relative Humidity	[-]
T	Temperature of the material	[K]
λ	Thermal conductivity	[W.m^{-1}.K^{-1}]

General introduction

General context

Excavation work is an important aspect in civil engineering projects used during the construction process of almost every structure. It generates waste soils that the holder discards or intends to discard or is required to discard. In Europe, soils extracted from construction sites are five times higher than the amount of household waste, which make them the biggest source of waste produced every year [1]. In France, tons of inert materials are extracted each year from various earthworks prior to the foundations of infrastructure, roads, and other transport networks (example Figure 0.1). In the Greater Paris area, the total volume of spoil generated by all the constructions is estimated to reach 400 million tons by 2030 [2]. Theses volumes are out of all proportion to those that were processed in the past and they no longer allow a balance to be struck between muck and backfill [3]. Several management scenarios have emerged, depending on the nature of the geological terrains and their different physical, chemical, and mechanical properties.

Figure 0.1. Inert waste storage quarry at Thivernal-Grignon – Yvelines (credit to Simon Schnepp and Morgane Renou [4])

An innovative solution is to transform waste earth produced locally to a construction product. Indeed, earth had been used for more than 10,000 years by man in various forms for constructions [5] and are still used for todays. It is estimated that about one third of the word population lies in earthen houses [6]. Numerous impressive historical architectures are still standing in every continent and about 20% of cultural sites of the UNESCO World Heritage List are fully or partially made of earth (Figure 0.2) [7]. To cite few examples: The Great Mosque of Djenne in Mali, the walled city of Shibam in Yemen, the massive ramparts of Alcazaba, the Bam citadel in Iran, the old town of Ghadames in Libya, the Ksar of Aït-Ben-Haddou, the Jiayuguan Great Wall in China and the village of Taos Pueblo in New Mexico (Figure 0.3).

The earth-built heritage reflects the diversity of the manufacturing techniques, born from different lifestyles, varied climates and the type of the available soils [8]. The most common traditional techniques are wattle and daub, cob, rammed earth, adobe and compacted earth blocks [9], but about 12 techniques are used todays to turn earth into a construction product as illustrated in Figure 0.4. Thus, the construction technique and process could be adapted to the existing excavated material. These construction processes distinct by the hydric state of the

mixture (plastic, solid and liquid), the type of implementation and the hydric state of the material during the implementation, and the structural role of the earth element (load-bearing or a non-load-bearing) [10]–[13].

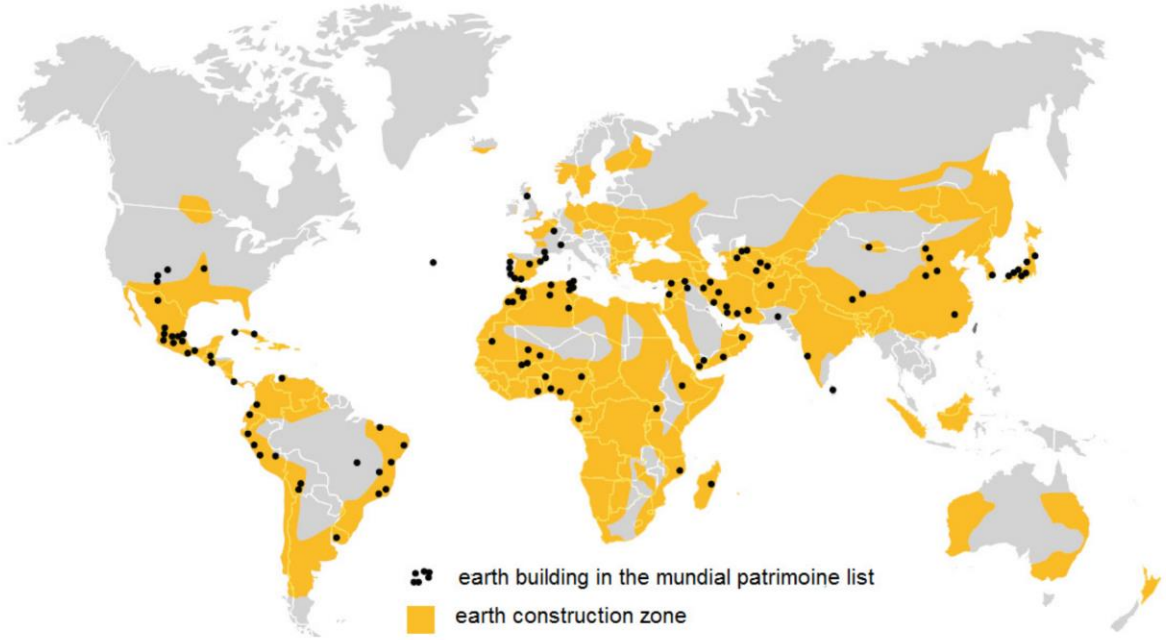

Figure 0.2. Earth construction in the world with patrimonies UNESCO (after [14])

Generally speaking, the use of earth for construction provide a valuable stimulus for new-build applications in response to the growing awareness of the need for sustainable development in building sector [15]. Actually, earthen construction materials are known by their low embodied energy [10], [16]. Firstly, earth is a local material that can be produced and used immediately on the construction site or nearby and does not require industrial processing [17]. Secondly, the well-established ability of earth walls to store and manage heat and moisture improve indoor comfort [18]–[21], thanks to their high thermal mass and hygroscopicity [20], [22]–[25]. This property allows reducing the energy consumption required for heating, ventilation and cooling during the lifespan of the building [26]. Thirdly, earth grant low-energy reuse of the material for construction by virtue of the reversible binding action of clay [27], [28].

The common point between earthen structures is that their mechanical strength depends essentially on the cohesive-frictional property of the soil used. However, cohesion significantly drops if the material is exposed to important hydric changes in humid environments, which may be prejudicial to the construction. For example, the investigations made in [29] showed that an increase from 2% to 12% in the water content of compacted earth lead to reducing the compressive strength and the stiffness by a factor of 4. In the same vein, similar findings were pointed out by different researchers [30]–[32]. It is also worth noting that the collapse induced by an increase in the water content is a well-known phenomenon in soil mechanics and it's taken into account in most of the elastoplastic constitutive laws [33], [34]. On the other side, even though some earths can be directly used as a building material in their immediate environment, others may be inadequate.

(a) Great Mosque of Djenné, Timbuktu, Mali [35]

(b) Old Walled City of Shibam, Yemen [36]

(c) Massive ramparts of Alcazaba, fortress the Alhambra complex, Granada, Spain

(d) Bam citadel (Arg-e Bam), Iran [37]

(e) Old town of Ghadames, Libya (@ George Steinmetz)

(f) Ksar of Aït-Ben-Haddou, Morocco

(g) Jiayuguan Great Wall, Gansu, China [38]

(h) Village of Taos Pueblo, New Mexico, USA (@Gimas/Shutterstock)

Figure 0.3. Examples of earthen architecture's heritage

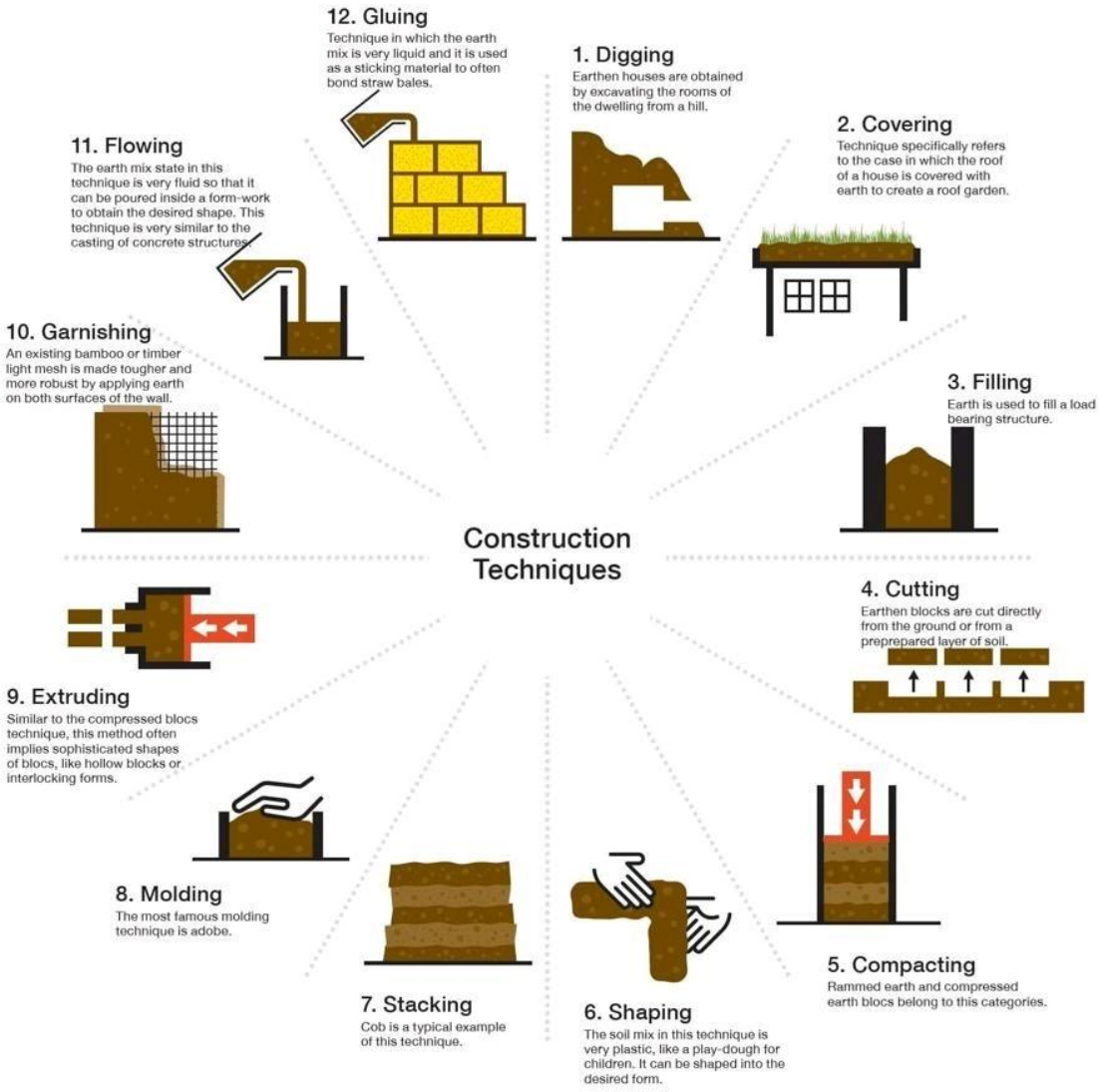

Figure 0.4. Variety of the earthen construction techniques (after [39])

To face these problems, the characteristics of earth are usually modified to enhance its physical and/or mechanical properties for a specific application. The modification of earth characteristics is known as stabilization [40], [41]. Different stabilization methods exists, depending on the mineralogical composition of the earth material and the construction technique [42], [43]. Organic stabilizers like plant aggregates, plant fibers, animal waste and natural polymers could be added to improve the characteristics of wattle and daub, cob and adobe [44]–[47]. While hydraulic binders like lime and cement are particularly appropriate for stabilizing compacted earth block and rammed earth [48]–[51]. These stabilizers are also used to enhance the mechanical characteristics of infrastructure embankments or soil subgrades during road construction. Between them, cement produces the highest improvement of strength and durability and it is the more spread stabilization method especially in Anglo-Saxon countries such as Australia, USA and India, where proportions of added cement range from 6% to 15% [52].

However, the lack of optimization in the formulation of cement stabilized earth is a major brake on its wider acceptance as a modern building material, especially in France. Despite years of research in this field since 1920s [53], a deep understanding of cement stabilization of earth in

building sector remains complex. The complexity of this up-growing science may find its origin in the variability of the available earths/soils which is complex in nature. This complexity led researchers to "case-by-case" investigations by focusing on stabilization with Ordinary Portland cement (OPC), which is the most popular chemical stabilizing agent used in different countries across the world [54]–[57]. While studies on the impact of cements other than OPC are limited. In any case, the attention is often given to the mechanical aspect of the final product. Whereas the limitation of stabilization benefits to the sole increase of mechanical resistance would undeniably lead to the conclusion that it not an environmentally advisable technology [58].

CIFRE project N°2017/1512

In this context, a collaboration has been initiated in this thesis between French industrial manufacturers of hydraulic binders, represented by their technical association (ATILH) and the Laboratory of Tribology and System Dynamics (LTDS - ENTPE) with his team specialized in Geo-based and Bio-based materials, to answer stakes related on the efficient stabilization of local earth with hydraulic binders having lower environmental impact than OPC. The study is concerned by the compressed stabilized earth block (CSEB) because it is the most stabilized earthen building material produced at the industrial scale.

It is worth noting that in the beginning of the thesis, it had been planned to conduct the study on some types of earths excavated in works of the *Grand Paris Express* construction worksite in Ile de France, in the perspective of studying the performance of excavated materials after stabilization. However, we encountered many problems in delivering the material, so it was decided finally to conduct the study on materials suitable for construction from the Auvergne Rhône-Alpes region.

Challenges

Although numerous studies were carried out to assess the influence of cement stabilization on mechanical and hygrothermal properties of compacted earth block, the effectiveness of cement stabilization is still not totally understood. Studies have shown for instance that mechanical resistance depends on many factors like cement dosage, clay fraction of earth, density of the sample and its water content. But the question is, what are the minimum required tools to judge the effectiveness of cement stabilization for building construction applications? And what is the pre-characterization of earth required before proceeding to stabilize compacted earth blocks with cement?

Secondly, the mechanical performance of masonry does not depend only on the quality of the block. The past literature reveals that bond in masonry is function of mortar composition, water quantity in the fresh mortar, and the water content of the block at the time of masoning. However, studies on the moisture transport phenomenon and their influence on the bond strength development in the stabilized earth block masonry are limited.

Lastly, even if stabilization increases the durability of the materials, the use of chemical stabilizer may generate new durability issues, while no uniformly accepted expression for the durability of stabilized earth exists. Furthermore, laboratory methods to assess the durability of stabilized block are still needed.

Objectives and methodology

The objectives of this PhD thesis can be summarized into three tasks:

- Analysis of the performance of cement stabilized earth block with respect to cement and earth characteristics.
- Development of laboratory assessment test to evaluate the durability of cement stabilized earth block toward water erosion.
- Assessment of moisture transport and bond strength development in the stabilized earth block masonry.

For the first task, a performance-based approach was used. Two natural earths were chosen based on the available types already studied in our laboratory. Five types of cement were proposed by cement manufacturers intervened in the steering committee of this thesis. They differ mainly in their composition and physical and chemical properties. The performance of cement-earth formulations was analyzed on the light of the physical and mineralogical composition of the earth and the cement type used in each case. The term performance includes mechanical resistance, hygroscopic capacities, and durability toward water.

Regarding the second task, a cyclic wetting and drying test inspired from the drip erosion test was developed to mimic the effect of wind driven rainfall on stabilized earth block surface.

Finally, moisture transport in the block-mortar assembly and their influences on the mechanical behavior of the assembly were assessed experimentally.

Organization of the thesis manuscript

This thesis manuscript is organized as follows:

- In Chapter 1, a state-of-the-art presentation will be given. This chapter is divided into five main sections. The first section introduces the CSEB technique. The second and third sections addresses the characteristics of soil and cement that can affect the performance of CSEB. The fourth section deals with the state of knowledge on the evaluation methods of the performance aspects of CSEB, including mechanical, hygroscopic and durability. The last section in Chapter I presents a review on the block mortar interface in CSEB's masonry. This chapter conclude on the research problem and the scientific approach adopted.

- Chapter 2 is dedicated for the characterization of the materials of the study, and it details the manufacturing procedure of all the type of samples used. The utilization of representative small samples for experimental test instead of blocks is justified and the representativity criteria is determined for all formulations. Finally, the problematic of sample conditioning was addressed. A focus is made on optimizing and discussing curing of cement stabilized earth samples.

- Chapter 3 represent a core part of the thesis that deals with the effectiveness of cement stabilization based on a performance approach. Firstly, the performance of different cement-earth mixtures is evaluated based on three aspects: the mechanical resistance the hygroscopic capacities and the durability toward water. Secondly, a microstructural analysis of mixtures is presented to identify the processes behind the evaluated performance of the materials. Thirdly, the performance of cement-earth mixtures is

discussed based on cement and earth characteristics. Finally, recommendations on the evaluation of the effectiveness of cement stabilization are proposed.

- In Chapter 4, a new laboratory testing method is developed to assess the durability of stabilized earth bocks toward water driven rainfall. It consists of a cyclic wetting-drying test. Methods for quantification of the test results are proposed and evaluated based on their advantages and limitations.

- Chapter 5 deals with the compressive and shear behavior of masonry with respect to block and mortar composition. In a second step, a method was proposed based on the hydrothermal behavior of mortar-block assembly in the aim of indirectly estimating water transported from mortar to block.

- Finally, conclusions and perspectives on this PhD thesis will be given.

Chapter 1. State of the art

In this chapter, we will draw up a state of the art of the various knowledge already acquired around compacted earth blocks. Different characteristics of earth and cement used will be identified and presented. The different performance aspects of compressed stabilized earth blocks will be described. The methods used for the assessment of different parameters related to these aspects will be presented and discussed. Finally, we conclude on the research problem and the scientific approach adopted in this thesis.

1.1 CSEB: the origin and the technique

1.1.1 The origin of CSEB

The first attempts at compacted earth block were tried in France, in the first years of the 19th century when the architect Francois Cointeraux tried to pre-cast small blocks of rammed earth. He used hand rammers to compress humid soil into small wooden molds which were held with the feet. The turning point came with effect from 1956, following the invention of the famous little CINVA-RAM press (Figure 1.1), designed by engineer Raul Ramirez at the CINVA centre in Bogota, Columbia [59]. Since its inception, compacted earth block technique has been gaining popularity in many countries (African countries, India, South Asia, Sri Lanka, New Zealand and Australia, Colorado, Texas, New Mexico, Germany, France, and Switzerland, etc.).

Today, compacted earth blocks are almost systematically stabilized with lime or cement. Different designation of compacted earth blocks exists in the literature like compressed earth block [60], pressed brick [61], pressed block [62], compressed stabilized earth block – CSEB [63], [64], soil cement solid bricks [65], [66], soil–cement block [67], ground blocks cements [68], compressed earth brick [62] or stabilized soil blocks [69]. In this manuscript, it will be designed by CSEB.

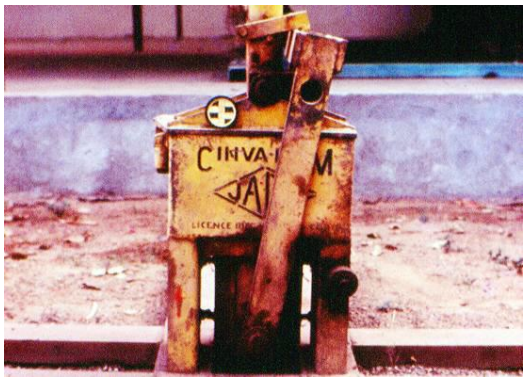

Figure 1.1. Cinva Ram, the first press for compressed earth blocks

1.1.2 Production technique

The production of CSEB consists of moistening earth/soil with stabilizer then pouring into a steel press and compressing either with a manual or motorized press. The compaction can be done with a single ram press of double compaction plate press or a press with double plate compaction ram. There is no fixed value for the compaction energy used to produce CSEB but

they are commonly compacted at compaction pressure between 3MPa and 8MPa [6]. The stages involved in the static compaction of CSEB are illustrated in Figure 1.2 as found in [70].

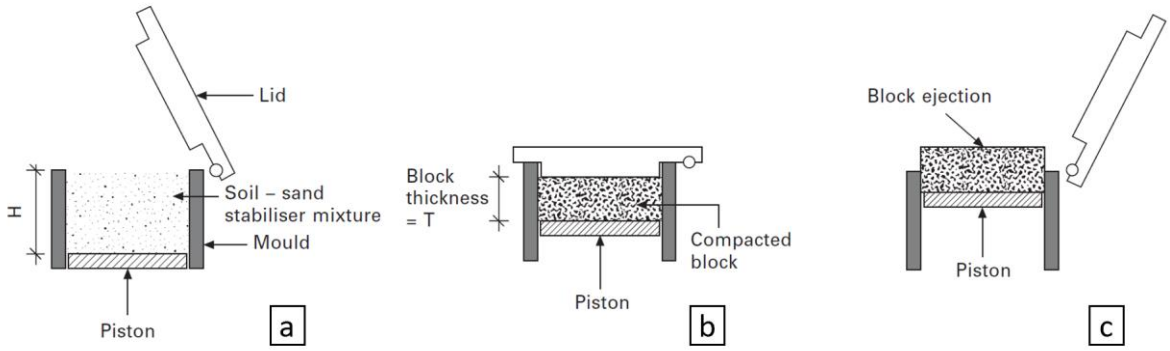

Figure 1.2. Stages of the static compaction process: (a) mold filling with processed mix, (b) compaction through lid closure and piston movement, (c) ejection of compacted block (after [70]).

Blocks can be compressed in many different shapes and sizes. The most common format is a rectangular parallelepiped (prismatic) and its dimensions vary depending on the press used. Figure 1.3 summarize the sizes of the block accepted in the official normative of the countries that have a standard of earth block. The most common block dimensions in use today are 29.5×14×9 cm (L×W×H) consistent with a unit weight in the order of 6 to 8 kg, a dry density in the range of 1.8 – 2.0g/cm^3 and with the possibility of building walls of 15, 30 or 45cm in thickness [71].

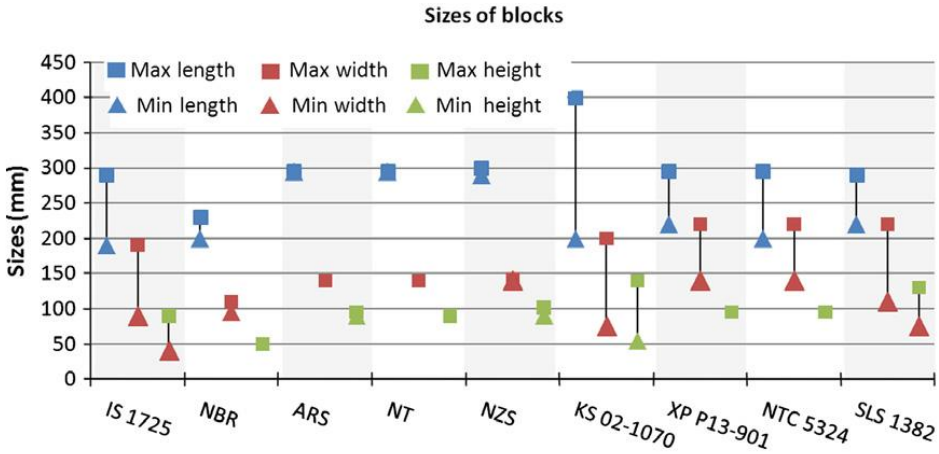

Figure 1.3 - Size of compressed earth blocks in international normatives (after Cid-Falceto J. et al., 2012 [72])

After compaction, CSEB could be stacked immediately but it is important to prevent rapid drying for delivering better gain in strength. Thus, they require curing for the development of cement hydration products. However, no unified curing method exists, and blocks studied in the literature are not always cured before testing. CSEB could be cured under polythene sheet in the open air in a humid atmosphere where air relative humidity is higher than 70% for about 28 days [73], [74]. Another curing method consists of staking CSEB one above the other and sprinkling water on them three to four times daily for four weeks then they are dried in the open air [70]. Reducing the curing period to 10-12 hours could be made by conditioning blocks

at high temperatures (80°C) at atmospheric pressure [75], but this method is rather proposed for lime and fly ash stabilized blocks.

1.1.3 Advantages and disadvantages of CSEB

CSEB has many advantages in comparison to similar building materials. A striking contrast between CSEB and conventional bricks is the greenhouse gas emissions during the production process and carbon emission. To have an idea on the trends, CSEB emit 22 kg CO_2/tons while concrete blocks emit 143 kg CO_2/tons, common fired clay bricks emit 200kg CO_2/tons and aerated concrete blocks emit between 280 and 375 kg CO_2/tons [76]. Thus, CSEB consumed, in average, less than 10% of the input energy as used to manufacture similar fired clay and concrete masonry unit [77]. According to [78], the use of cement stabilized earth blocks resulted in a reduction by 62% in the embodied energy in comparison with reinforced concrete framed structure and by 45% in comparison with burnt clay brick masonry and reinforced concrete solid slab construction. Referring to [79], [80], the embodied energy of masonry made with CSEB is in the range of 550–700 MJ/m^3, while it is about 2200 MJ/m^3 in case of burnt clay bricks.

In addition, CSEB can be used for load bearing structures and do not necessarily need to be plastered. Another advantage of CSEB is that equipment for its production is available from manual to motorized machinery ranging from village to industry scale.

However, CSEB is still “banned” nowadays in construction in height like the various earth construction techniques. Further, the social acceptance of CSEB is low due to counter examples done by unskilled people or wrong selection of the soil or the equipment or because it gives the impression of a poor building material to most people.

1.2 Earth properties influencing the performance of CSEB and their characterization methods

Earth/soil is the basic material in CSEB and it is very complex in nature. It is formed from the long-term transformation of the underlying parent rock by the simultaneous and evolutionary interaction of climatic factors and other physico-chemical and biological processes [81]–[83]. This reveals a wide variation in its physical, geotechnical, chemical, and mineralogical properties. Thus, the evaluation of earth properties through laboratory testing is essential for interpreting how it will behave when stabilized. In this section, the review of literature will focus on the properties of earth, common procedures followed to characterize them, their known effect on the performance of CSEB and current suitability criteria of earth for CSEB production.

1.2.1 Particle size distribution

The particle size distribution, also known as grain size, determine the amount of particles present in a soil sample [84] and it gives information on its ability to pack into a dense structure [6]. In almost every paper dealing with CSEB, the particle size distribution of the earth used is presented because it is considered one of the most important physical characteristics of soils.

1.2.1.1 Characterization method

The procedures for soil classification vary with existing standards but they are very similar, and they could be separated in two main types. The wet sieving particle size for the coarser particles larger than 80 µm and the sedimentation for the fine fraction (1 to 80 µm). These two procedures are included in the European standard EN ISO 17892-4 (2018) [85], the British standard BS 1377 Part 2.9 (1990) [86], Quebec standard BNQ-2501-025 (2013) [87] and North American standards (ASTM C136 (2014) [88] and ASTM D422 (2011) [89]). In general, a combination of a sieve test and a sedimentation should be performed to determine the full-particle size distribution.

The sieving procedure consists of separating the agglomerated grains from a known mass of soil by fractionating it under water with a series of sieves and weighing the cumulative 105°C-dried rejection mass on each sieve. The obtained value for each sieve is related to the total dry mass of the soil sample submitted for analysis. The sieves sizes recommended in the standard EN ISO 17892-4 (2018) are 63mm, 20mm, 6.30mm, 2.0mm, 0.63mm, 0.20mm, 0.0063 mm. These sizes also represent the size limits for coarse materials in the standard (cf. Table 1-1).

The sedimentation procedure completes the sieving analysis for particles with a diameter lower than 80µm. It is based on the measurement of the sedimentation time of solid particles in suspension in a solution of water mixed with a deflocculating agent. The principle of this method follows Stokes' law that links the diameter of the grains to their sedimentation rate. Thus, this law is applied to the elements of a soil to determine the equivalent diameters of the particles.

The terms used in the EN ISO 14688-1 (2018) [90] to identify each size fraction in a soil are presented in Table 1-1. The limits between the particle size and their names can vary with standards, especially the silt – sand's limit. This limit is fixed to 0.063mm, 0.05mm and 0.075mm in EN ISO 14688-1 (2018), USDA (1987) [91] and ASTM-D2487 (2017) [92], respectively.

Soil group	Particle size fractions	Range of particle sizes D [mm]
Very coarse soil	Large boulder	$D > 630$
	Boulder	$200 < D \leq 630$
	Cobble	$63 < D \leq 200$
Coarse soil	Gravel	$2.0 < D \leq 63$
	Coarse gravel	$20 < D \leq 63$
	Medium gravel	$6.3 < D \leq 20$
	Fine gravel	$2.0 < D \leq 6.3$
	Sand	$0.063 < D \leq 2.0$
	Coarse sand	$0.63 < D \leq 2.0$
	Medium sand	$0.20 < D \leq 0.63$
	Fine sand	$0.063 < D \leq 0.20$
Fine soil	Silt	$0.002 < D \leq 0.063$
	Coarse silt	$0.02 < D \leq 0.063$
	Medium silt	$0.0063 < D \leq 0.02$
	Fine silt	$0.002 < D \leq 0.0063$
	Clay	$D \leq 0.002$

Table 1-1. Soil classification with respect to particle size fractions according to the EN ISO 14688-1 (2018)

1.2.1.2 Examples from the literature

Most of the recommendations on criteria for selecting suitable soils for construction are based on its particle size distribution. Some of these recommendations are summarized in Table 1-2. It appears clearly that there is no single recommendation for particle size accepted worldwide. According to Olivier and Mesbah [93], the best soil to be used to manufacture compacted earth blocks contain 50 to 70% sand and 15 to 30% clay.

Author	Clay	Silt	Sand & Gravel
Fitzmaurice, 1958	20-30%	-	33-40%
United Nations, 1964	10%	15%	75%
Spence and cook, 1983	0-30%	10-40%	60-90%
Stulz and Mukerji, 1988	20%	20%	60%
Peter Walker et al., 2005	5-20%	10-30%	45-80%
Alley, 1948 [1]	25-30%	50-80%	10-20%
Schrader, 1981[1]	20-30%	-	70-80%
McHenry, 1984[1]	30-35%	-	65-70%
Norton, 1997	10-30%	15-30%	45-70%
Houben & Guillaud, 1994[1]	0-20%	10-30%	45-75%
Radanovic, 1996[1]	30-35%	-	65-75%
SAZS 724:2001, n.d.[1]	5-15%	15-30%	50-70%
Bolton, 2001	5-15%	15-30%	40-70%
HB-195, Peter Walker & Standards Australia, 2002[2]	5-20%	10-30%	45-75%
MOPT (1992)[3], spain	5-26%	Not available	Not available
IETcc (1971)[3]	10-40%	20-40%	10-20%
McHenry, 1984[3]	15%	32%	30% (Sand) + 23% (Gravel)
Smith and Austin (1996)[3], New Mexico	4-15%	40%	60-80%
Gomes & Folque (1953)[4]	15-31%	7-17%	28-51% (Sand) + 0-33% (Gravel)
Doat, et al. (1979)[4], CRATerre	15-25%	20-35%	40-50% (Sand) + 0-15% (Gravel)
Keable (1996)[4]	5-15%	15-30%	50-70%
Keefe (2005)[4]	7-15%	10-18%	45% (Sand) + 30% (Gravel)

Table 1-2. Recommendations on particle size distribution limits for compacted earth block

Gravels are the cohesionless part of earth [94] and they are important to produce CSEB. This refers to their loose packing and stability, which limit shrinkage and capillarity in earth. However, an excess of 10% is not recommended for use in CSEB production [53]. Some authors recommend a maximum size fraction between 15 and 20mm for gravels to be used in CSEB [6], while others recommend 6mm [95], but this is not standardized. Sand particles are very stable, lack cohesion, non-sticky with a gritty texture, they have a very high degree of internal friction and do not shrink. Silts are identical in nature to sand particles, but their internal friction is less than that of sand. Gravels, sands, and silts should not be used alone to produce CSEB because they lack cohesion. The finest fraction of soil is clay that have an average size less than 2μm [96] and its characteristics are not similar to those of the other three fractions.

[1] As cited in [384]
[2] As cited in [385]
[3] As cited in [386]
[4] As cited in [158]

Clays are cohesive and form a coherent mass at suitable moisture contents [97] and they have important engineering properties in a CSEB.

In general, earth is sieved at 5mm to eliminate the gravel portion [70]. An experimental study on optimum soil grading for the soil-cement blocks was done by Venkatarama Reddy and Richardson (2007) [98]. This study concluded that maximum strength is obtained for a clay content between 14 and 16% and that initial rate of absorption decreases with the increase in clay content of the block. In another study, Venkatarama Reddy and Latha [99] examined strength, durability, and absorption characteristics of CSEB of 14 different types of soil grading curves with three cement dosages. They found that optimum clay content leading to the maximum compressive strength is 10% for fine grained soil and 14% for coarse grained soils. CSEB made with the latter soil showed a lower strength and durability than those made with fine grained soils. Investigations made in [100] show that CSEB stabilized at 8% cement show satisfactory strength when there is 13% clay content in the soil and that strength reduces with increasing clay content. Outcomes of the study made in [101] on engineered soil indicates that strength and dry density increase with the fineness of soil particles. While the optimum of strength, dry density and water absorption were obtained for mixture of 35% soil and 65% sand.

1.2.2 Geotechnical characteristics

1.2.2.1 Characterization methods

a. Atterberg limits

Atterberg limits provide an estimation of clay minerals present in the soil [102]. The European standard that deals with critical water contents of a fine-grained soil is defined by EN ISO 17892-12 (2018) [103], BS 1377-2 (1990) [86], and ASTM D4318 (2017) [104]. The tests defined in these standards originate from the work of Atterberg, which was then standardized. Limits commonly required for geotechnical engineering tests are the liquid limit (LL) and the plastic limit (PL). They are the most frequent geotechnical test characteristics of earth for construction provided in scientific articles.

LL represents the empirical moisture content at which a soil passes from a liquid state to a plastic state. It could be measured with Casagrande method. Thus, a portion of the earth specimen is spread in a brass cup, divided in two by a grooving tool, and subsequently allowed to flow together from the shocks caused by dropping the cup in a standard mechanical device. According to the number of drops, the test follows a one-point method or a multipoint method. The number of drops to decide on the method may vary according to standards. The multipoint method is generally more precise. The water content is determined on the soil in the cup at the end of the test.

PL is defined as the empirical moisture content at which a soil is too dry to be plastic, which is the transition from a ductile to a brittle behavior (BS 1377-2 (1990)). It is measured internationally by pressing and manually rolling a thread of plastic soil on a glass plate until the water content is reduced to the point the thread crumbles and can no longer be pressed again and rerolled. The soil is rolled to a thread diameter of 3.0mm (UK and Quebec standard) or 3.2mm (ASTM standard). The soil water content is determined at the breaking point.

Lastly, the plasticity index (PI) is calculated as the numerical difference between LL and PL. Cohesive soils are classified in the BS 1377-2, 1990 based on a graphical representation of the PI that determine boundaries between consistency states of plastic soil.

b. Activity of clay minerals (Methylene blue value)

The activity of clay minerals could be deduced from the methylene blue test that aims to detect clay minerals in fines aggregates. The amount of absorbed methylene solution varies according to the amount of clay minerals and clay type, cation exchange capacity and specific surface area. In general, the test is undertaken at the 400µm fraction of the soil.

The testing method described in the NF P 94-068 (1998) [105] is called spot-test. It consists of dissolving a mas of 30 to 60g for high clayey soil and 60 to 120g for less clayey soil in 500ml of distilled water. Then methylene blue solution (10 g/l) is added to the soil solution by a step of 5ml and after 1 min, one drop of the mixture is placed onto a paper filter. The test ends when the dye forms a second lighter colored blue halo around the aggregate dye spot and stays stable over five consecutive spots without addition of methylene blue to the soil solution. As a result, the methylene blue value (V_{BS}) is reported in mg/g. Six categories of soil are described in the standard NF P11-300, 1992 [106] based on this value Table 1-3.

V_{BS}	Soil categories
$0.1 \leq V_{BS} < 0.2$	Water insensitive
$0.2 \leq V_{BS} < 1.5$	Sandy and Silty
$1.5 \leq V_{BS} < 2.5$	Sandy-Clay
$2.5 \leq V_{BS} < 6$	Silty moderately plastic
$6 \leq V_{BS} < 8$	Clayey
$8 \leq V_{BS}$	Heavy clayey

Table 1-3. Definition of soil categories according to Methylene Blue Value (NF P11-300, 1992)

The clay activity index A_{CB} is defined to purely reveal the activity of clay fraction in soil and it is calculated from the ratio between V_{BS} and the clay content in the 0-80µm fraction of the earth (C_B). This index enables to identify the soil's mineralogical composition following an Abaqus (blue activity diagram) given by Lautrin (1989) [107] and reused by Chiappone et al., 2004 [108]. The classes shown on the blue activity diagram classify soils as follows:

- 1 – non-clayey soil
- 2 – soil with interactive clay fraction
- 3 – soil with not much active clay fraction
- 4 – soil with normal clay fraction
- 5 – soil with active clay fraction
- 6 - soil with very active clay fraction
- 7 – soil with noxious clay fraction.

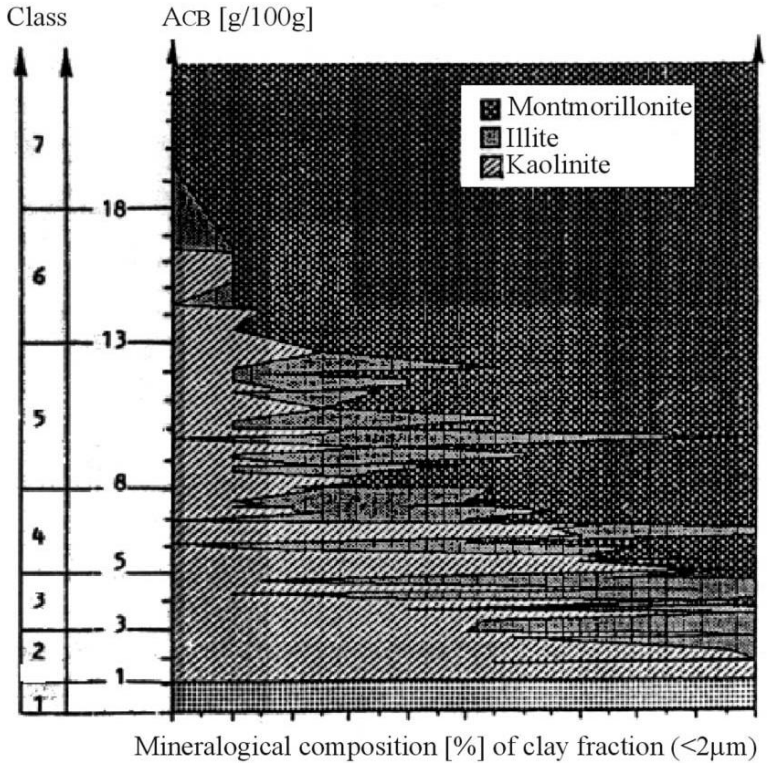

Figure 1.4. Blue activity diagram

c. Compaction characteristics

The compacity of a soil is defined as its ability to be compacted by static or dynamic compaction so that its volume is reduced. The compaction characteristics of a soil are determined from the maximum compaction state which allows particles to be moved into the denser possible configuration with a corresponding water content (that is the mass of water within the soil divided by the mass of dry material) called "optimum water content". Proctor test is the method followed for determining the compaction characteristics of soil. It is defined in different standards: ASTM D698, 2012 [109], BNQ 2501-250, 2013 [110], BS 1377, 1990 [86] and NF P94-093, 2014 [111]. This test consists of determining the relationship between molding water content and dry unit weight of soils compacted in mold with a 24.5N rammer dropped in a free fall from a height of 305 mm producing a compacting volumetric energy of 600 kN.m/m^3.

1.2.2.2 Examples from the literature

The most frequently presented geotechnical properties of soils in the literature of CSEB are Atterberg limits. In general, most of studied earths have a liquid limit value between 25 and 45% and a plastic limit value between 15 and 29%. Atterberg limits recommended by the French standard XP P13-901, 2001 [112] for CEB production are presented in Figure 1.5.

In the literature, recommendations on the suitability of soil for stabilization with cement based on their Atterberg limits exist. For example, a chart of Atterberg limits that determine the suitability of soil that needs stabilization (lime, cement, bitumen) to function satisfactorily as a building material was developed by Doat et al. [113] (Figure 1.6). This chart was later used by Stulz and Mukerji [102] and Norton [114]. It indicates that for cement stabilization, the limits are between a plasticity index of 7% to 29% and a liquid limit of 25% to 50%.

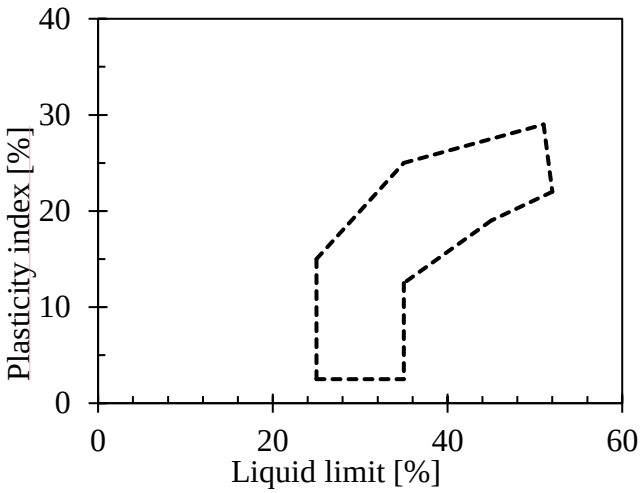

Figure 1.5. Plasticity nomograms of suitable soils for construction with CEB (AFNOR, 2001 [112])

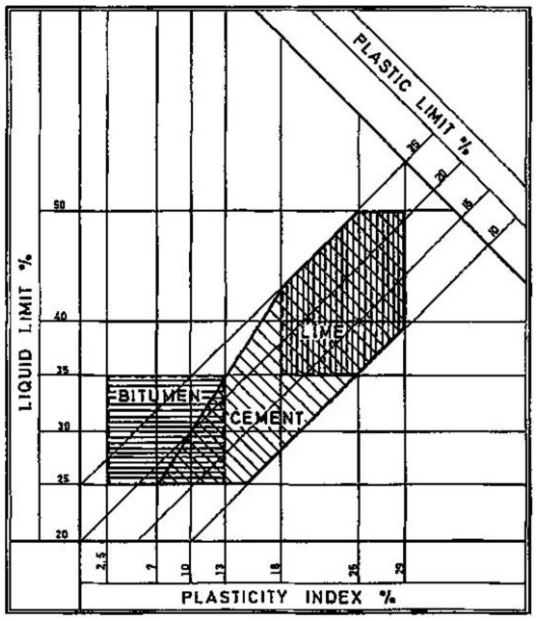

Figure 1.6. Atterberg limits chart for soils that need stabilization (from Doat et al. [105])

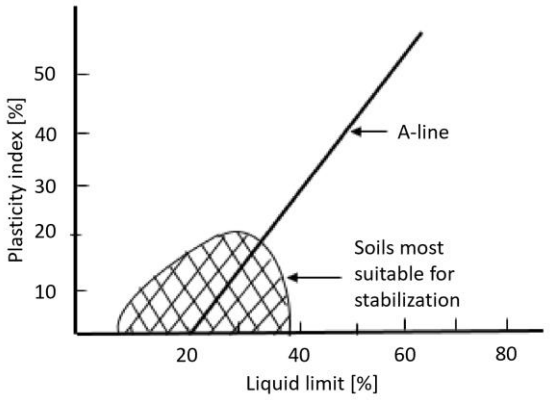

Figure 1.7. Plasticity chart for soils that need stabilization (from Spence and Cook [115])

Another proposition of Atterberg limits zone corresponding to soil suitability for stabilization is given by Spence and Cook [115] (Figure 1.7). The limits are between a plasticity index of 0% to 22% and a liquid limit of 7% to 39%. However, the latter recommendations are for stabilization in general without specifying the stabilizer (i.e., cement, lime, or bitumen), which could explain the difference between the two presented recommendations.

In this context, investigations made in [101] show that the strength of CSEB is significantly reduced with increasing plasticity index or liquid limit of the earth. Results obtained in [77] indicate that CSEB compacted with manual press and made with soils having a plasticity index above 20-25% developed excessive drying shrinkage, low compressive strength and they don't have adequate durability.

Concerning the optimum compaction characteristics (maximum dry density MDD and optimum water content OWC), the past literature shows that they depend on the compaction effort, the composition of the soil and cement addition.

For example, Olivier and Mesbah [93] studied the effect of compaction pressure on the compaction characteristics of the "Isle d'Abeau" earth. They performed their tests on cylindrical samples at different pressure levels varying between 1.2 MPa and 10 MPa. Their results presented in Figure 1.8 shows that increasing the compaction effort leads to a higher value of MDD and lower OMC. The optimum water content's values of earth used for compacted earth block found in existing studies varies between 9% and 18% [116]–[119].

Venkatarama Reddy *et al.* has demonstrated in [50] that optimum water content and dry density of earth-cement mix are not very sensitive to the variation of cement content between 5 and 12%. Whereas the increase in clay content implies a steep increase in the optimum water content of the mix.

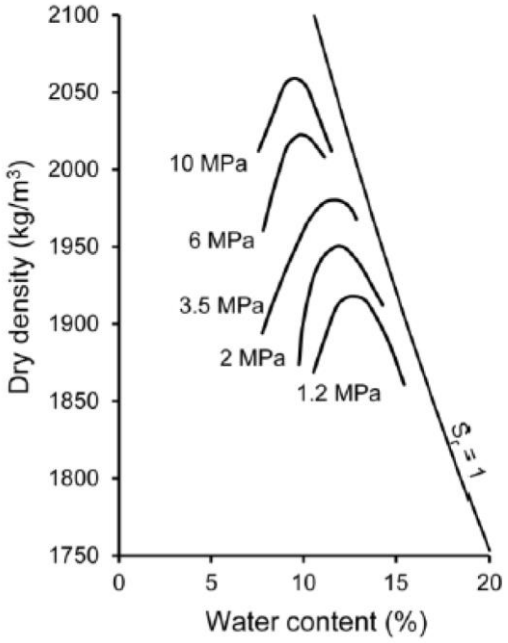

Figure 1.8. Variation of compaction curves with compaction pressure [120]

1.2.3 Chemical characteristics

1.2.3.1 Characterization methods

a. Major chemical elements

The major chemical elements present in a soil could be determined by X-ray fluorescence spectroscopy that consists of analyzing the X-ray emitted by the matter excited by an incident X-ray source. This test is carried out on pressed tablets of the material in powder (≤ 80μm), or on beads prepared from soil sample melted in combination with lithium metaborate and/or lithium tetraborate. Other techniques like the Electron Dispersive Spectrometer (EDS) analysis coupled with Scanning Electron Microscope (SEM) or microprobe analysis. These techniques give an image of the small zone analyzed of the sample, but the result may not be representative of the entire material.

b. Organic matter content

The amount of organic matter is often negligible in earths used for constructions. Anyhow, organic soil should be prevented for construction as recommended by different classification systems [121]–[125]. However, it is necessary to measure the organic matter content of the earth when it is extracted from regions rich in organic matter such as Canada [126].

Organic matter content can be determined either by the calcination method (XP P94-047, 1998 [127]) or the chemical method (XP P94-055, 1993 [128]). In the first method, the organic matter is equal to the mass loss of soil sample heated at 450°C to 550°C for 3 hours. In the second method, a soil sample is mixed with an oxidizing solution (potassium dichromate with sulfuric acid), the organic matter is then determined from the quantity of products which have reacted with the carbon of the soil after oxidation.

c. Calcite content

Physical and chemical properties of soil could be affected by the presence of free carbonates like calcite. Thus, the determination of calcite content or equivalent CO_2 is important. It can be realized by various techniques like titration (BS 1377-3, 1990 [129]), gravimetric (BS 1881-124, 2015 [130]) and volumetric measurement (EN ISO 10693, 2014 [131] and NF P94-048, 1996 [132]). The principle of these methods is based on the determination of the volume of CO_2 released by the soil sample under the action of excess hydrochloric acid. It consists of measuring the CO_2 formed by the dissociation of carbonates from a quantity of soil mixed with a solution of hydrochloric acid. Thus, the amount of acid consumed by the reaction is measured according to the BS 1377-3 (1990). In the standards EN ISO 10693 (2014), ASTM D4373 (2014) [133] and NF P94-048 (1996), the CO_2 is recovered by the intermediary of a calcimeter from the volume of gas produced.

d. Loss on ignition

The loss on ignition (LOI) is defined as the mass fraction lost by a dried sample by ignition at a specified temperature. It is related to the organic content of certain soils and the procedure to determine it is specified in standards BS 1377-3 (1990) and XP P94-047 (1998) [127]. LOI is determined from the ratio between the mass loss of soil samples passing the 2 mm heated to a constant mass at 550°C for at least 3 hours and the initial dried mass of the sample. While the total mass loss of the sample including organic matter hydroxyl for clay minerals and carbonate is determined by heating soil sample at 1000°C for two hours.

e. pH

The pH of soil is useful to know its minerals solubility and its ion mobility. Its measurement is performed on air dried samples of the soil fraction ≤ 2 mm. The soil sample is mixed with either a pure water, a 0.01 mol/l solution of chloride calcium ($CaCl_2$) or 1 mol/L solution of potassium chloride then the suspension is stirred for a few minutes, covered with a cover glass, and allowed to stand for a couple of hours that varies with standards. The suspension needs to be stirred right before the pH value measurement. The European standard (EN 15933, 2012 [134]) and International standard (EN ISO 10390, 2020 [135]) recommend a volumetric ratio of 1:5 and a rest at most 3 hours, while the British standard (BS 1377-3, 1990 [129]) recommend a volumetric ratio of 1:2.5 and a rest of at least 8 hours, and the American one (ASTM D4972, 2001 [136]) states a mass concentration (10g of air-dried soil for 10 ml of solution) and a rest of 1 hour.

f. Cation exchange capacity

Clay minerals contained in soil have a negative surface charge balanced by bound cations at the mineral surface. These bound cations can be exchanged by other cations in the pore water. Cation-exchange capacity (CEC) is defined as the amount of positive charge, generally calcium (Ca), sodium (Na), magnesium (Mg) and potassium (K), that can be exchanged per mass of soil. It could be used as a tool to estimate the cationic exchanges between cement and clays which reflect the behavior of soil during stabilization. The CEC is usually measured in centimoles of positive electric charge. Habitually, CEC is measured by displacing all the bound cation with a concentrated solution of another cation, and then measuring either the displaced cations or the amount of added cations that is retrained. Standards focused mostly on three procedures using ammonium acetate (NF X31-130, 1999 [137] and ASTM 7503-18, 2018 [138]), cobalt hexamine trichloride (NF X31-130, 1999; ISO 23470, 2018 [139]) and barium chloride (ISO 11260, 2018 [140]).

The first method was proposed by Metson (1956) [141] and it is widely used throughout the world. The saturation of the exchange sites by ammonium is carried out by percolating a 1mol/l ammonium acetate solution (75ml) through a test portion of 2.5g of soil. The excess reagent is eliminated with several rinses with ethanol (75ml). After drying in air, the solid phase is agitated in 50ml of a 1mol/l solution of sodium chloride. The CEC is determined from the exchanged ammonium measured by spectrocolorimetry. This procedure is recommended for soil with a pH value of 7.

In the second method, the exchange is carried out by simply shaking the test portion in the reagent. For a given volume of reagent (100ml), the quantity of sample weighed (2.5, 5 or 10g) is such that a sufficient concentration of cobalt hexamine ions remains in solution. This concentration is determined by spectrocolorimetry without chemical pretreatment of the solution. Then the CEC of the sample is determined from the loss of cobalt hexamine from solution. This procedure is recommended for soil with a natural pH value lower than 6.5.

In the third method, a soil test portion of 2.5 g (< 2 mm) is shaken for 1h with 30ml of 0.1mol/l $BaCl_2$ solution. The solid and liquid phases are separated by centrifugation. This operation is repeated twice, and the three supernatants are collected for the determination of exchanged cations. After equilibrating under shaken overnight the soil with 30ml of 0.0025mol/l $BaCl_2$, the solid phase is shaken once again, but this time with 30ml of 0.02mol/l magnesium sulphate ($MgSO_4$) solution overnight. The adsorbed barium exchanges with magnesium and precipitates

in the form of $BaSO_4$. The CEC value is determined for the difference between the residual content of magnesium in leaching solution and subtracted from the initial content.

g. Soluble salt content

Soluble salt content of soil is considered as an important element that determines the quality of earth used in construction. For example, in SAZS 724, 2001 [123] soil used for construction should be free from salts such as sulphates. While Walker et al., (2005) and New México Code, (2006) indicate that the salt content of a soil should be lower than 2% [121], [142].

Standard ISO 11265 (1994) [143] present a method to quantify the soluble salt content. Thus, the soil sample is extracted with water with an extraction ratio of 1:5 (m/V). The specific electrical conductivity (ECe in µS/cm) of the extract is then measured.

In the BS 1377-3 (1990) [129] and ISO 11048 (1995) [144], the sulfate amount is quantified by extraction from the dried soil samples using dilute hydrochloric acid or water in a soil/added water ratio of 1:2 or 1:5 (m/V). The sulphate content of these extracts is determined by a gravimetric method according to which barium chloride is added to the aqueous or acid extract. The precipitate of barium sulphate is dried and weighed and the sulphate content is then calculated from the mass of the soil used in the analysis and the mass of precipitated barium sulphate.

Chloride is quantified based on Charpentier-Volhard's method [129]. The chloride is extracted from the dried soil samples water. Silver nitrate ($AgNO_3$) is added to the aqueous soil extract. The solution is then diluted and then titrated using a solution of potassium thiocyanate (KSCN) in the presence of ammonium ferric sulphate as a colored indicator. The soluble chloride is calculated based on the volume of silver nitrate added and on the mass of the soil used in the analysis.

Method for quantification of nitrate and ammonium is described in ISO 14256-2 (2005) [145] using automatic measurement by spectrophotometry. The homogenized soil samples are extracted using a potassium chloride solution (1mol/l). The concentrations of mineral nitrogen compounds are then determined in the extracts by automated spectrophotometric methods.

1.2.3.2 Examples from the literature

The chemical composition of earth used in CEB/CSEB is not always presented in studies. Examples of major elements are presented in Table 1-4 as found in some references.

Major elements [% expressed as oxydes]												Reference
SiO_2	Al_2O_3	CaO	Fe_2O_3	K_2O	MgO	Na_2O	TiO_2	P_2O_5	MnO	SO_3	LOI	
79.4	11.9	0.03	1.8	0.3	-	0.0	1.3	ND	0.0	0.0	6.3	[146]
22.3	6.0	31.8	1.7	0.5	2.1	0.3	0.2	0.8	0.1	1.29	32.9	[146]
54.7	19.7	0.9	8.6	3.9	3.6	1.8	1.0	0.2	0.1	-	5.0	[147]
18.73	7.47	35.3	3.39	0.9	1.27	0.09	0.39	0.09	0.03	-	31.92	[117]

Table 1-4. Examples of chemical composition of the soils used in the fabrication of CEB in studies from the literature

Interesting element is the calcium because some soils may not contain it at all (~0.03% in [146]) while others contain it in high concentrations (31.8 in [146] and 35.3% in [117]). In the

latter case, the loss on ignition (LOI) is always high and it could be said that the corresponding earths contain calcite ($CaCO_3$). Besides calcium, silicone and aluminum are the two major elements in the studied earths since phyllosilicates (clay) are rich in these elements.

Besides chemical composition, pH and organic matter content of earth used in the CEB are also given as chemical characteristics by some researchers in the literature. Examples of the values that could take in CEB are presented in Table 1-5. It shows that pH values vary between 4.80 and 8.95. Concerning organic matter, the values reported in the presented studies are lower than 2 or slightly higher than 2. Walker et al. [142], the authorized content of organic matter in organic soil for construction should be lower than 2% and according to Houben and Guillaud [148] it could be between 2 and 4%.

pH	Organic content [%]	Reference
-	0.78	Hakimi *et al.*, (1996) [119]
8.95	0.67	Venkatarama Reddy, (2002) [75]
8.05	2.32	
7.22	1.40	
6.58	1.26	
8.00	0	Galán-Marín *et al.* (2010) [147]
-	2.10	Turanli and Saritas (2011) [149]
7.40	1.70	Uguryol and Kulakoglu (2013) [150]
4.80	-	Dove *et al.* (2016) [151]
6.80	-	
6.90	-	

Table 1-5. Examples of pH values and organic matter contents of the earths used in studies from the literature

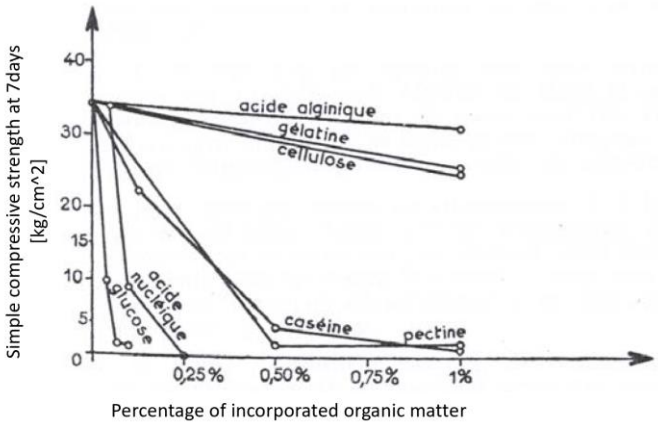

Figure 1.9. Effects of incorporating various organic matter into the soil at various percentages (after [152])

Certain active organic materials contained in a soil can delay the setting and hardening of cements [153] and the influence of certain types is well known. Peltier [152] quantified the effect of adding selected types of organic matter to a sandy soil stabilized at 10% of OPC by means of the compressive strength at 7 days (Figure 1.9). He shows that a low sugar or glucose content is sufficient to prevent the cement from setting. While cellulose and gelatin do not seems to have significant effect on the treatment at the concentrations studied. On the other hand, organic acid like acetic acid, humic acids and tannic acids prevent cement setting [154].

Finally, it is rare to find information in the literature on soluble salt contents of the earth used in CEB/CSEB. In some studies, the soluble chlorides and sulphates contents are determined. For example, in a study conducted by Hakimi *et al.* (1996) [119], the measured content of soluble chlorides and sulphates are equal to 0.07% and 0.64% respectively. In another study, the measured soluble chloride content in earth used by Galán-Marín *et al.* (2010) [147] is equal to 0.03%.

1.2.4 Mineralogical characterization

The mineralogical characterization permits to complete the chemical analysis by determining the nature and, under certain conditions, the quantity of the minerals contained in a sample. In what follow, the most used techniques for the characterization of clay materials are described than a Examples from the literature is presented.

1.2.4.1 Characterization methods

a. X-ray diffraction

XRD is an analytical technique used for phase identification of a crystalline material and can provide information on unit cell dimensions. The principle consists of placing the crystallized material in an intense beam of X-rays, usually of a single wavelength (monochromatic X-rays). This beam of X-rays is diffracted by the materials: the angles and intensities of diffracted X-rays are measured, with each compound having a unique diffraction pattern. The nature of the crystallized phases contained in the sample could be obtained by comparison with existing standards.

This technique is sufficient for materials without clay minerals or soil containing illite and kaolinite. It is necessary to complete the test by another one on oriented aggregates using three preparations: air-dried or natural, after glycolation and after heat treatment at 500°C if the soil contains clay minerals with a basal reflection (001) at 14 Å (i.e., chlorite, vermiculite or smectite) [155], [156].

b. Thermal Analysis

The XRD analysis could be completed with three types of thermal analyses: Differential Thermal Analysis (DTA), Differential Scanning Calorimetry (DSC) and Thermal Gravimetric Analysis (TGA). The principle of TGA consists in weighing the sample over time as the temperature increases. DTA and DSC are relatively similar techniques. In DTA, the material under study and an inert reference are submitted to identical thermal cycles while recording any temperature difference between the two samples. The exothermic or endothermic changes in the sample are detected by comparison to the inert reference. In DSC, the difference in the amount of heat required to increase the temperature of a sample and a reference is measured as a function of temperature.

The DTA usually confirms the qualitative characterization of soil performed by XRD. The results of DSC are less used for the characterization of soil but could be used for the determination of the thermal properties of earth construction materials such as the heat capacity. TGA is very useful because it permits to calculate the content of some minerals contained in soil such as goethite, clay minerals and calcite.

c. Scanning Electron Microscopy

The mineralogical characterization of soil is sometimes completed with SEM (Scanning Electron Microscopy) that permits to show some pictures of the microstructure of the soil. These observations could be completed by a very useful isolated chemical analysis using Energy Dispersive X-ray Spectroscopy (EDS).

1.2.4.2 Examples from the literature

Most of mineralogical characterization made in the literature using X-ray diffraction are qualitative and it is hard to find a study on CEB that provide quantitative characterization of the soil used.

In a study that aim at assessing the effect of cement stabilization on two different soils made by Ouedraogo *et al.* (2020) [157], the mineralogical characterization was performed through XRD analysis on crushed powder. The main identified constituents of the studied soils are quartz (SiO_2), calcite ($CaCO_3$), feldspar (albite ($NaSi_3AlO_8$) and orthoclase (KSi_3AlO_8)) and goethite (FeO(OH)). In order to determine the nature of clays, the XRD analysis was made on oriented aggregate. The identified clays minerals in the first soil are illite/muscovite and kaolinite and in the second one are illite, chlorite and montmorillonite.

In a study published by Gomes *et al.* (2014) [158], semi-quantitative analysis of soil used was provided with respect to the intensity of the diffraction peaks of X-ray powder diagrams. Three proportion levels were proposed: high, intermediate, or low.

In some publications, robust qualitative characterization by XRD are coupled with a calculation using the chemical composition of the studied soils are made. For example, Millogo *et al.* (2016) [44] presented in his study XRD spectrum of the soil used that compromise kaolinite ($Al_2(Si_2O_5)(OH)_4$), quartz (SiO_2) and goethite (FeO(OH)) only. Given the chemical composition, it becames simple to determine the amount of each mineral because the studied soil contain mainly kaolinite having a simple chemical formula. Thus, the amount of kaolinite could be calcylated by using the the content of Al_2O_3, quartz by the content of SiO_2 (corrected to the amount of SiO_2 contained in kaolinite) and the amount of goethite from Fe_2O_3.

However, the chemical composition of soils containing clay minerals like illite, montmorillonite or chlorite is complex and in their presence the calculation of the mineralogical composition becomes more complicated [159]. In this case, thermal gravimetric analysis (TGA) could be used as a complementary tool to improve the accuracy of the calculation. It could be used also to check the results obtained by the calculation.

1.3 Cement properties influencing the performance of CSEB

The composition of different types of cements are summarized in Table 1-6 and Table 1-7 according to the standard NF EN 197-1 [160]. According to this standard, cements are identified by a series of letters and numbers. The letters CEM, followed by numbers (from I to V), indicate the family of the binder, while other letters (A, B, C or D) provide an indication of the proportion of the other constituents (apart from clinker). These constituents are specified by a symbol according to their nature (D, L, P, S, etc.). The strength class is indicated by a number: 32.5 - 42.5 - 52.5. Within each strength class the performances define from an early

stage the distinction between the ‘Normal’ (N) and ‘Rapid’ (R) version (see Appendix Appendix A).

In this section, the main properties of cement that could affect the performance of CSEB are presented as found in concrete literature.

Cement type		Number of cements	Clinker [%]	Other constituents [%]	Secondary constituents [%]
Portland cement	CEM I	1	95 to 100	0	0 to 5
Hybrids of Portland cement	CEM II	19	65 to 94	6 to 35 of S/D/P/Q/V/W/T/L/LL	0 to 5
Blast furnace cement	CEM III	3	5 to 64	S: 36 to 95	0 to 5
Pouzzolanic cement	CEM IV	2	45 to 89	D/P/Q/V/W: 11 to 55	0 to 5
Composite cement	CEM V	2	20 to 64	S/P/Q/V: 28 to 80	0 to 5
K: Clinker, **S**: Blast furnace slag, **D**: Silica fume, **P**: Natural pozzolans, **Q**: Natural calcined pozzolans, **V**: Siliceous fly ash, **W**: Calcium fly ash, **T**: Charred schist, **L** and **LL**: Limestone					

Table 1-6. Cement’s composition according to EN 197-1

The letters A, B, C and D specify the clinker content:

	CEM II	CEM III	CEM IV	CEM V
A	80 to 94 %	35 to 64 %	65 to 89 %	40 to 64 %
B	65 to 79 %	20 to 34 %	45 to 64 %	20 to 38 %
C	-	5 to 19 %	-	-
D	CEM II with silica fume 90 to 94%	-	-	-

Table 1-7. Clinker content of cements according to EN 197-1

1.3.1 Cement properties

1.3.1.1 Physical properties

The main physical properties of cement are the fineness, soundness, setting time, heat of hydration, loss on ignition.

The fineness of cement represents the particle size of cement. If the cement contains coarser particles, it reduces the workability, rate of hydration, which directly affects the gain in strength. This property of cement helps the concrete to attain the strength earlier. At the same time, more fineness of cement may lead to form cracks in the concrete surface and affect the durability of concrete. The air permeability test is used to determine the fineness of the cement. It has been measured by specific surface area [161].

Soundness refers to the ability of cement to not shrink upon hardening. Good quality cement retains its volume after setting without delayed expansion, which is caused by excessive free lime and magnesia. Unsoundness of cement may appear after several years, so tests for

ensuring soundness must be able to determine that potential like Le Chatelier test Autoclave test. The first method done by using Le Chatelier apparatus, tests the expansion of cement due to lime. Cement paste (normal consistency) is taken between glass slides and submerged in water for 24 hours at 20+1°C. It is taken out to measure the distance between the indicators and then returned under water, brought to boil in 25-30 mins and boiled for an hour. After cooling the device, the distance between indicator points is measured again. In a good quality cement, the distance should not exceed 10mm. In the second method, cement paste (of normal consistency) is placed in an autoclave (high-pressure steam vessel) and slowly brought to 2.03 MPa, and then kept there for 3hours. The change in length of the specimen (after gradually bringing the autoclave to room temperature and pressure) is measured and expressed in percentage. The requirement for good quality cement is a maximum of 0.80% autoclave expansion [162].

Cement sets and hardens when water is added. This setting time can vary depending on multiple factors, such as fineness of cement, cement-water ratio, chemical content, and admixtures. Setting time can be an indicator of hydration rate. Cement used in construction should have an initial setting time that is not too low and a final setting time not too high. Hence, two setting times are measured. The initial set corresponds to the moment when the paste begins to stiffen noticeably (typically occurs within 30-45 minutes). While the final set corresponds to the moment when the cement hardens, being able to sustain some load (occurs below 10 hours) [163].

When water is added to cement, the reaction that takes place is called hydration. Hydration generates heat, which can affect the quality of the cement and be beneficial in maintaining curing temperature during cold weather. On the other hand, when heat generation is high, especially in large structures, it may cause undesired stress. The heat of hydration is affected most by C_3S and C_3A present in cement, and by water-cement ratio, fineness and curing temperature. The heat of hydration of Portland cement is calculated by determining the difference between the dry and the partially hydrated cement (obtained by comparing these at 7th and 28th days) [164].

The cement loses its weight when it is heated at 900 – 1000°C and the weight loss of cement due to heating is called loss of ignition. The cement may be subjected to pre-hydrate or carbonation because of extended storage. The cement weight loss on ignition test is used to find the pre-hydration or carbonation of cement. The setting time and strength of the cement will be affected by the pre-hydration [165].

1.3.1.2 Chemical composition of cement

The raw materials for cement production are limestone (calcium), sand or clay (silicon), bauxite (aluminum) and iron ore, and may include shells, chalk, marl, shale, clay, blast furnace slag, slate. Anhydrous cement is mainly composed by the following phases:

- Tricalcium aluminate (C_3A): Low content of C_3A makes the cement sulfate resistant. Gypsum balance the hydration of C_3A, which liberates a lot of heat in the early stages of hydration.
- Tricalcium silicate (C_3S) causes rapid hydration as well as hardening and is responsible for the cement's early strength gain an initial setting.
- Dicalcium silicate (C_2S) helps the strength gain after one week.

- Tetra-calcium aluminoferrite (C_4AF) is a fluxing agent. It reduces the melting temperature of the raw materials in the kiln from 1648°C to 1426 °C. It does not contribute much to the strength of the cement.
- Magnesia (MgO) present in excess amount in cement may make the cement unsound and expansive, but a little amount of it can add strength to the cement. Production of MgO-based cement also causes less CO_2 emission.
- Sulphur trioxide impacts the soundness of cement and expands it if used in high percentages. So, the percentage of Sulphur trioxide should not be more than 2%.
- Iron oxide Ferric oxide Aside is mainly responsible for the color of the cement and it adds strength and hardness.
- Alkali content of the cement are determined by the amounts of potassium oxide (K_2O) and sodium oxide (Na_2O). Cement containing large amounts of alkali can cause some difficulty in regulating the setting time of cement. Low alkali cement, when used with calcium chloride in concrete, can cause discoloration.
- Free lime, which is sometimes present in cement, may cause expansion. The proportion of lime is the major constituent of cement, which influences the strength and setting time of cement. The percentage of lime should be added carefully else it impacts the soundness of cement (expands) and makes it disintegrated.
- Silica fume is added to cement concrete to improve a variety of properties, especially compressive strength, abrasion resistance and bond strength. Though setting time is prolonged by the addition of silica fume, it can grant exceptionally high strength.
- Alumina is chemical-resistant. It quickens the setting but weakens the cement.

1.3.2 Stabilization mechanism in CSEB

Clinker is comprised of four major oxide phases: tricalcium silicate (C_3S), dicalcium silicate (C_2S), tricalcium aluminate (C_3A), and tetracalcium aluminoferrite (C_4AF). According to the standard notation used in cement chemistry, C = CaO, S = SiO_2, A = Al_2O_3, and F = Fe_2O_3.

The most important phases in soil stabilization through the cation exchange and flocculation-agglomeration are the two calcium silicate phases, C_3S and C_2S. Their hydration reactions at ambient temperature are:

$$2C_3S + 6H \rightarrow C_3S_2H_3 + 3CH \quad (1\text{-}1)$$

$$2C_2S + 4H \rightarrow C_3S_2H_3 + CH \quad (1\text{-}2)$$

Where C = CaO, S = S_iO_2 and H = H_2O

According to Gartner and Gaidis (1985) [166], the resulting solution is saturated with $Ca(OH)_2$ within 12 minutes of the time and Portland cement first come in contact with water. Gypsum in cement has a solubility equal to 2 g/l of water at 25°C similar to that of $Ca(OH)_2$ and the solution is saturated with respect to gypsum within approximately 6 minutes. When gypsum is dissolved, ions Ca^{2+} and SO_4^{2-} are generated. The drop of Ca^{2+} concentration at 12 hours is related to the setting of cement when a substantial amount of calcium is consumed from the solution to produce $C-S-H$ and $Ca(OH)_2$. During this process, a substantial amount of water is also consumed.

In typical cement types CEM I and CEM II, the combined amount of C_3S and C_2S is approximately equal to 75% of the total weight. The hydration of cement grains may continue for years depending on its fineness. Thus, $Ca(OH)_2$ is produced over the same period. Consequently, mortar and concrete containing Portland cement maintain a pH equal approximately to the pH of a saturated lime solution (~12.5).

The calcium hydroxide is formed through-solution process as a by-product of the hydration reaction of the calcium silicate phases in Portland cement. The released Ca^{2+} ions in the pore fluid stabilize the surrounding clay soil. Then the absorption rate slows down as it becomes increasingly diffusion dependent after the initial adsorption of ions by clay. In these conditions, Ca^{2+} ion concentration may rise locally to a level high enough to cause precipitation of $Ca(OH)_2$. This process depends on the rate of supply of Ca^{2+} by the hydrating cement particles. However, the opportunity of $Ca(OH)_2$ crystals to grow is very low due to the high dispersion of cement particles in stabilized soils. Therefore, they stay in the form of very fine particles of $Ca(OH)_2$, which is chemically known as hydrated lime.

Rather than the formation of $Ca(OH)_2$, the strength development in stabilized earth blocks in mainly due to the formation of $C-S-H$ [167]. This latter can form either from the hydration of calcium silicate phases (cf. reactions (1-3) and (1-4)) or from a pozzolanic reaction between $Ca(OH)_2$ and the silica (which can be supplied by the soil or the cement). Calcium may also react with alumina and produce $C-A-H$, which is the phase leading to strength development in calcium aluminate cements. The reactions are as follows:

$$Ca(OH)_2 + SiO_2 \rightarrow C-S-H \quad (1\text{-}3)$$

$$Ca(OH)_2 + Al_2O_3 \rightarrow C-A-H \quad (1\text{-}4)$$

The solubilization of silica and alumina from the soil components may be required for the formation of these additional cementing materials ($C-S-H$ and $C-A-H$) [168]. Solubility and surface reactivity of silica and alumina are increased in the high pH conditions that prevail in Portland cement-soil systems [169][168].

The possible sources of silica and alumina in typical soil are clay minerals, quartz, feldspars, and micas. Other silicates and alumino-silicates, either crystalline or amorphous, may also be present [170]. For example, Eades and Grim (1960) [171] speculated the dissolution of silica from the clay lattice in high pH, then combines with Ca^{2+} ions to form $C-S-H$. Diamond (1963) [172] speculated that the calcium adsorbed on the clay surfaces reacts with adjacent clay surfaces and the reaction products are formed as precipitates (agglomeration process).

The latter studies hypothesized the occurrence of a clay-calcium reaction exclusively through a solution process. But another possibility is a direct reaction of $Ca(OH)_2$ at the clay surface. For example, Stocker (1975) [173] proposed a diffused cementation theory based upon evidence that montmorillonite is the exclusive reactant with calcium and the concept that the bulk of the reaction takes place at the montmorillonite crystal edges. The formation of new phases upon the reactions at clay surfaces has also been reported in studies on lime-kaolinite and lime-montmorillonite [174], and lime-clay-water systems [175], [176].

1.4 Performance properties of CSEB and their assessment methods

1.4.1 Mechanical parameters

The main mechanical parameters are compressive strength, stiffness, shear resistance and tensile strength. In this section, the most common methods followed to measure them are presented and discussed based on the literature data.

1.4.1.1 Compressive strength

The most studied mechanical parameter of CSEB is the compressive strength. Several studies investigated the effect of different factors on this parameter. For example, the increases of compressive strength of the block with increasing the dry density has been consistently proven over the past 20 years. In some regions like India the compressive strength is controlled through density [177].

Many publications report that the strength increases with cement content and reduces by increasing clay contents [178]–[180]. In a study conducted by Venkatarama Reddy and Gupta (2005) [181], the effect of cement dosage on various characteristics of CSEB were investigated. They show that increasing cement dosage from 6 to 10% increase the strength of the block by 2.5 time and increasing cement dosage for 6 to 8% increases the elastic modulus by 2.5 time. However, the increase in the elastic modulus was not significant when cement dosage increased from 8 to 12%. The improvement of compressive strength with cement dosage was also investigated in [182], where increasing this latter from 5 to 10% improved the strength measured on air-dried samples by 33% only.

Another important factor that affects the strength of the block is its moisture content. Increasing moisture content of the block implies a reduction of the compressive strength of the block due to the softening of binders by water and development of pore water pressures. Results obtained by Walker (1995) [77] show that the compressive strength of saturated CSEB is typically around half the dried at ambient temperature.

However, the compressive strength does not depend only on soil and cement properties, but on sample geometry and testing method. Habitually, testing methods of CEB/CSEB's strength have followed procedures developed for fired clay and concrete block units [183], but a general consensus on a unified procedure is not reached yet. There are several pending questions on the strength's determination of CEB/CSEB, regarding the sample size and the testing procedure itself [184]–[186]. The most common testing methods are presented in what follow:

a. Direct compression test

This method consists of carrying test directly on the block in the direction in which is manufactured. It is the most used testing procedure for fired brick and solid or hollow concrete blocks. The test could be also made on cubes or cylinders extracted from the block or prepared from the same material in a convenient mold. However, there is no clear correlation between the cube or cylinder compressive strength and the block compressive strength [187]. Addedly, the impact of sample's extraction from blocks on compressive strength needs further investigation [188].

The sample's opposite surfaces should be plan and a capping (wood or Teflon sheet) should be placed between the specimen surface and the platen to ensure a close fit with the platen. Some

standards propose a correction of the measured strength in function of the aspect ratio and sample shape. However, proposed correction factors are admitted from studies developed for fired clay blocks and there is a lack of information regarding their reliability on compacted earth block [187]. To eliminate the platen restraint effect in compressive strength, sample dimensions should satisfy an aspect ratio greater than or equal to 2.

Figure 1.10. Example of direct compression test on cylindrical sample (from [189])

b. Half-bonded block test (RILEM test)

French standard XP P13-901 [190] recommends compression test that double the aspect ratio of the block to counter problems faced in testing the block directly. The setup of the test was developed firstly by Olivier *et al*. [191] then adopted by the RILEM Technical Committee 164 (Figure 1.11). The procedure consists of cutting the block in two perfect halves and superposing them to increase the aspect ratio and thus reduce the effects of confinement. The two halve blocks are stacked one above the other by providing a mortar joint. The mortar used shall be of the same material used to manufacture the blocks. In addition, the specimen is capped with a layer of neoprene to enable the even distribution of load between the platen and the block.

According to the comparative study carried out in [187], the results of compressive strength obtained from the RILEM test were lower than those obtained from the direct compression test after correction. This reduction in strength can refer to the inaccuracy of correction factor used in the direct compression test and/or to the effect of mortar in the RILEM procedure. A good correlation between the two tests could be established only if the effect of these two factors is eliminated, which requires further developments.

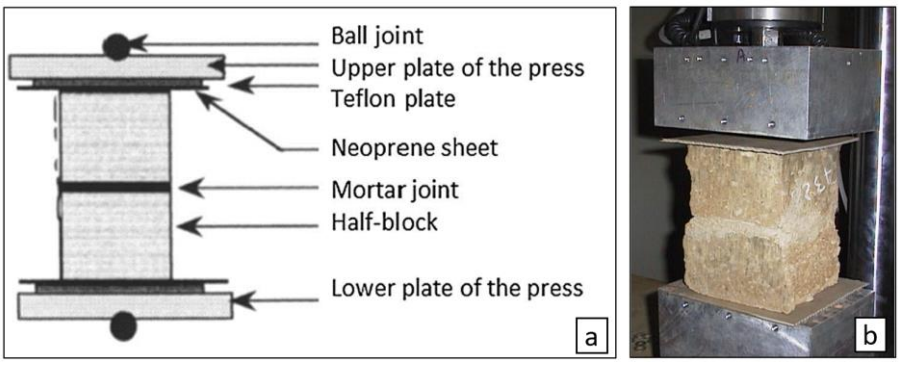

Figure 1.11. Experimental device developed by Olivier et al. [8] for compressive strength testing of CEB (a), RILEM test set-up

c. Three-point bending test

This test (Figure 1.12) proposes an indirect method to estimate the compressive strength of the block, but it is less accurate, and it underestimates the compressive strength of the block. Despite this, it is widely accepted to be sufficient to predict the strength [187]. It consists of calculating the compressive strength from the flexural stress obtained in pure bending, based on the traction/bending stress theory. A 'compression strength model for the 3 point bending test' is proposed in [192], which assumes that arch behavior of two beam and calculates the compressive strength of the block with the help of failure load from 3 point bending test. However, only limited samples were used to validate this model. Thus, further investigations are needed to evaluate its accuracy in calculating compressive strength needs to be carried out.

This test is advantageous because it can be done with minimal requirements and it does not require sample preparation or capping. On the opposite side, it does not account for susceptibility of defects in blocks such as shrinkage cracks.

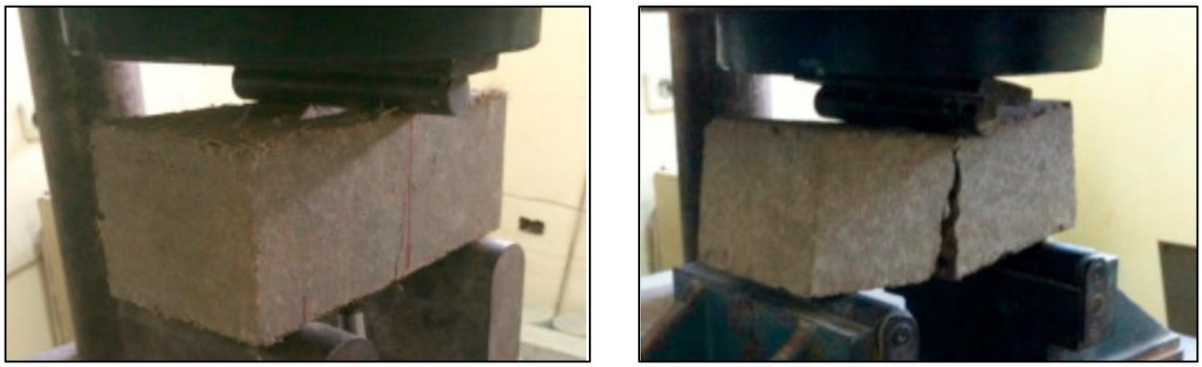

Figure 1.12. Setup of three-point bending test (from [193])

1.4.1.1 Stiffness

Stiffness could be accurately determined by local measurement methods during compression test by clipping extensometers on the sample or through photogrammetry [188]. It is important to mention that the displacements measured with the sensors of the press do not lead to accurate data because of the deformability of interface between the specimen and the press platens [184].

In a limited domain of small stress corresponding to less than 5% of the compressive strength, earth-based materials follow the Hooke's law. Thus, to measure the elasticity modulus, cycles must be applied during the compression test.

1.4.1.1 Flexural and tensile strength

In general, the tensile strength of CSEB could be determined through flexural tests or splitting tensile tests on cylindrical specimens [194]. Both test's equipment can be found in all conventional civil engineering laboratories. The flexural strength and modulus of rupture could be obtained following the procedure mentioned in [195] by testing the block under four-point bending test. The tensile strength of earth material is commonly estimated through direct traction test [196] or using the Brazilian test [197]. The ratio between tensile and compressive strength is approximately 1/10 based on these tests. Thus, CSEB can be considered as a non-tensile resistant material, and if the design cannot avoid tensile stresses, it is necessary to reinforce the structure.

1.4.2 Hygroscopic properties

One generally qualifies as hygroscopic any porous material which allow a regulation of the indoor variation of humidity within a dwelling. The characteristics of the inside air are very important for a building's inhabitants because it can significantly influence their comfort, health, and productivity. Extremely low levels of relative humidity (below 20%) may cause eye or skin irritations and dry the nasal mucous membranes, resulting in a higher risk of respiratory infections. On the other hand, high levels of relative humidity may lead to the development of fungi, which can cause allergies as manifested by asthma and rhinitis [198], [199] and the emission of volatile organic compounds is favored [200].

For that purpose, the material should have the ability of a material to adsorb (and release) water vapor molecules from (to) the surrounding atmosphere. But it is not sufficient since the velocity at which the water molecules are adsorbed is at least as important as the total amount of water molecules that can be adsorbed. Therefore, a proper estimation of hygroscopicity requires good knowledge of both sorption properties and vapor/liquid water transfer.

1.4.2.1 Adsorption-desorption properties

To properly describe sorption properties of earthen material, it is first important to understand its inner structure, which can be defined as an arrangement of solid particles with voids between them. Porosity, denoted by ϕ is the ratio of these voids. When the whole porous network is filled with air or liquid, the material is said to be dried or saturated. When the material is partially saturated, the total pore space is divided into two parts: one that is filled by the liquid phase and the other by the gaseous phase (which is composed by dry air and vapour). In the earth construction's scientific community, the relative proportion of liquid and gas is commonly depicted by the gravimetric water content, denoted by u, and which is defined by the ratio between the mass of water within the material and its dry mass:

$$u = \frac{m_w}{m_s} \tag{1-5}$$

We can however wonder what are the physical processes which lead to this coexistence between water and gas within the porous network of the material. Actually, earth is a hygroscopic material capable of fixing a quantity of moisture from the surrounding air on its surface and in its pores according to two processes depending on the relative humidity (Figure 1.13). At a low to 50% relative humidity, water is adsorbed on the surface of solid particles in the form of thin or superimposed layers; this is called surface absorption. When the RH is high enough, the captured water molecules are able to form capillary bridges between solid particles; this is called capillary condensation [201].

The evolution of the water content of the material, at a given temperature, in function of the relative humidity of the surrounding air is called the sorption isotherm. Several methods exist to estimate it, but the two most widely used are the desiccator and dynamic gravimetric vapor sorption methods.

The experimental protocol of the desiccator method is precisely defined in the international standard ISO 12751 [202]. The adsorption stage consists in successively putting a previously dried sample in several environments of increasing relative humidity and constant temperature. The sample is periodically weighed, and it stays within a given environment until mass constant. The desorption stage consists in successively putting a sample previously equilibrated at 95% RH (at least) in several environments of decreasing relative humidity until mass

constant and at constant temperature. The relative humidity of the environments is fixed by equilibrium with saturated saline solutions.

The dynamic gravimetric sorption method, commonly called the DVS (dynamic vapor sorption) method, consists in measuring uptake and loss of moisture by flowing a carrier gas at a specified relative humidity (or partial pressure) over a small sample (from several milligrams to several grams depending on the device used) suspended from the weighing mechanism of an ultrasensitive recording microbalance. Variations in the gas's relative humidity are automatically calculated by the device when the target condition in mass stability is reached. A sorption-desorption loop can thus be made in approximatively 1-2 weeks for earthen materials and hemp concretes, while a period of 2-4 months is necessary if the desiccator method is used. On the other hand, the desiccator method can test several specimens at the same time, and it is the only way to test specimens with high levels of heterogeneity.

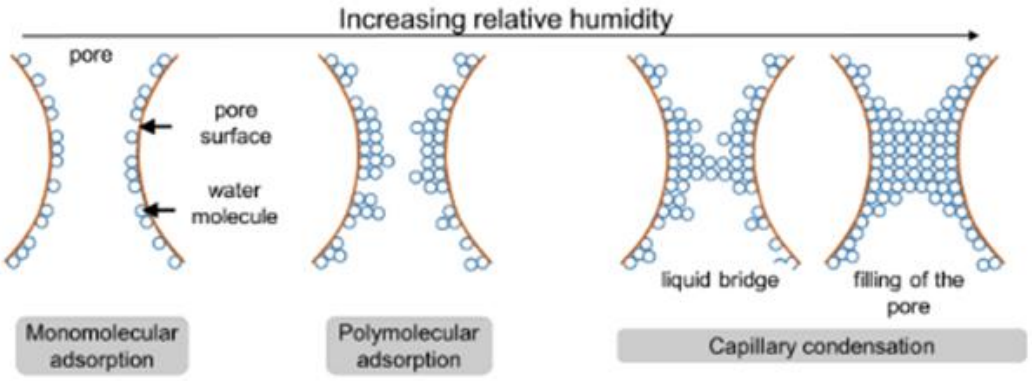

Figure 1.13 - Adsorption phenomenon from one layer to the total filling of the pore (after [201]).

For practical reasons, the use of single parameter can be preferred than the use of the sorption curves in order to give an idea of the sorption capability of a material. For that purpose, even if there is not yet a consensus, two parameters appear to be commonly used: the hydric capacity, denoted by ξ, and equal to the slope of the linear part of the desorption curve (typically between 30%RH and 80%RH) multiplied by the dry density of the material and $w_{\rho,80}$ which is the water content for a relative humidity of 80%.

$$\xi = \rho_d \frac{\partial u}{\partial \varphi} \; ; w_{\rho,80} = \rho_d \, u(\varphi = 80\%) \tag{1-6}$$

where ρ_d is the dry density, φ is the relative humidity and u is the water content.

For compacted earth blocks, either stabilized or not, ξ is generally in the range of 30kg/m^3 to 100kg/m^3 and $w_{\rho,80}$ is in the range of 60kg/m^3 to 120kg/m^3 [203]–[205].

1.4.2.2 Transport properties

a. Vapor permeability

The water vapor permeability is a property that characterizes the material ability to transport water vapor under a vapor pressure gradient. It is defined as the mass of vapor transferred

through the specimen per second and per unit area. It is commonly measured according to the "wet cup" or "dry cup" methods, which are described in the EN ISO 12572 standard [206]. The experimental protocol used for these two tests consists in placing the sample on top of a cup whose relative humidity is controlled by saline solution or salt powder.

To seal the samples to the cup, a vapor-tight tape should be used. Aluminum tape is recommended by Svennberg [207] since it does not adsorb a significant quantity of moisture itself. The samples with the cup were then stored in a climatic chamber or a ventilated box that was maintained at constant levels of RH (50% for example) and temperature (23°C for example). The ventilation kinetic within the box or the climatic chamber must be homogeneous and at least equal to 2m/s.

For the wet cup, the humidity within the cup is higher than that in the box/climatic chamber. For the dry cup it is the opposite.

After a transitional state where water vapor flow within the material is impacted by adsorption/desorption processes, a linear relation between mass variations of the cup and time is reached. During this permanent state, the vapor pressure gradient through the sample becomes homogeneous its mass conservation equation allows to write the apparent water vapor permeability as:

$$\delta_p = \frac{G.L}{A.\Delta P_v - G.\left(\frac{d_a}{\delta_a} + \frac{1}{\beta}\right)} \tag{1-7}$$

Where:

- G [kg/s] is the decrease of mass with time,
- L [m] is the thickness of the sample,
- A [m^2] is the average exposed area,
- ΔP_v [Pa] is the water vapor pressure difference between the cup and the box/climatic chamber.
- d_a [m] is the thickness of the air layer,
- δ_a is the water vapor permeability of air at 21°C, $\frac{d_a}{\delta_a}$ is a corrective term proposed in the EN ISO 12572 standard to take into consideration the effect of the air layer between the lower surface of the sample and the saline solution inside the cup,
- $\frac{1}{\beta}$ [m^2.s.Pa/kg] is a corrective term that consider the effect of the external surface film resistance. It could be estimated from the analysis of vapor diffusion tests on samples of different thicknesses.

Finally, in function of cup geometry, a mask edge correction may be also applied.

For convenient purposes, the vapor resistance factor (μ) is often used to present experimental results. It is linked to apparent water vapor permeability through the relation:

$$\mu = \frac{\delta_a}{\delta_p} \tag{1-8}$$

μ -values commonly obtained for earthen materials, and for some other classical construction materials, are reported in Table 1-8 and Table 1-9.

Material	μ [−]
Cellular Concrete	7.7 – 7.1
Lime silica brick	27 – 18
Solid brick	9.5 – 8
Gypsum board	8.3 – 7.3
Concrete	260 – 210
Lime Plaster	7.3 – 6.4

Table 1-8. μ-values of some classical construction materials (data from (Künzel, 1995) [208])

Material	μ [-]	Reference
Light earth	2 – 7	(Labat *et al.*, 2016) [209], (Volhard, 2016) [210]
Earth Plasters	7 – 10	(McGregor *et al.*, 2017) [211]
Rammed earth Compressed earth block	6 – 14	(D Allinson and Hall, 2010), (Liuzzi *et al.*, 2013), (Chabriac, 2014), (Fabbri, Al Haffar and McGregor, 2019) [212]–[215]
Adobe/Cob/Wattle and Daub	3 – 9	(Cagnon *et al.*, 2014) [216]

Table 1-9. Some typical values of μ of earthen materials

b. Liquid water and air permeability

The permeability characterizes the ability of a fluid mass to move through the porosity of a material. It is expressed as the product between the intrinsic permeability and the relative permeability coefficient. The intrinsic permeability depends only on the geometry of the porous network. However, in practical cases, a difference up to one order of magnitude can be observed between gas and liquid water intrinsic permeability that is commonly attributed to the differences between water/solid and gas/solid interactions and slip effects during gas permeability measurement [217]. For earthen materials, studies have focused on the liquid water permeability. The relative permeability depends on the volumetric proportion of the pore space occupied by adsorbed and/or condensed water molecules and it varies between 0 and 1. No clear methods for the estimation of this latter were made for earthen materials due to the complexity of the task especially for low saturation ratio.

To measure the liquid permeability of earth-based materials, the water absorption experiment is used. In the British standard BS 3921, the method consists in measuring the Initial Rate of Suction (IRS) by immerging a sample in water to a depth of 3mm during 1min. In the European standard EN 1015-18, the method consists of measuring the A-value, which is the total amount of water absorbed (in kg) per the surface in contact with water (in square meters) and per the square root of the immersion time (in seconds). Past publications underline significant differences on the sample geometry, its conditioning and the weighting frequency [218]–[220]. Although the variability of existing experimental protocol, the A-value method is commonly preferred due to the lack of accuracy of the IRS measurements.

The literature report a dependency of the A-value on the density of the samples [219]. Figure 1.14 report the A-value of 12 compacted earth samples having different densities as found in [221]. It shows that a linear correlation between the density and the A-value could be drawn and that A-value decreases as the density increases.

It is worth mentioning that the absorption tests do not directly give the permeability of the material. Even if some relations linking the A-Value to water diffusion and/or permeability coefficients exist [208], their accuracy for earth-based materials is not proven.

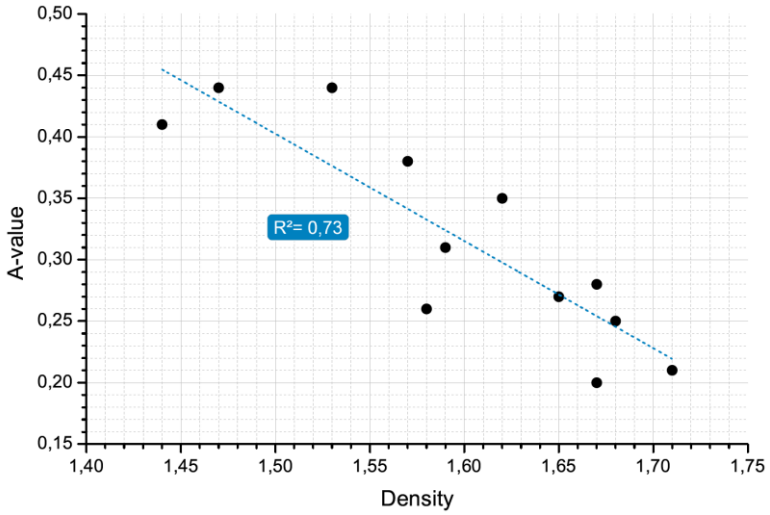

Figure 1.14. Variation of A-value [kg/m^2.s] with the dry density [g/cm^3] (from [221])

Finally, almost no study can be found concerning the evaluation of the gas relative permeability for earthen materials. To fill this gap, a first study was made during the very first part of my thesis. This study is not developed in the core of the manuscript, but the paper which was published on this topic is reported in Appendix B.

1.4.3 Durability toward water

The use of stabilizer significantly increases the durability to water of earthen material, but at the same time it may generate new durability issues. Nowadays, no uniformly accepted expression for the durability of CSEB exists. In this work, we assume that the durability can be regarded as "the ability of a block to resist deterioration". The benefit of this definition is its consideration of the durability-time relation, since due to deterioration, the durability of a block can fall with time. In this section, the main modes of block deterioration by water are identified and the laboratory measurement methods of the durability toward water are presented. Then, some publications that assessed the durability of compacted earth block and earth-based materials are reviewed.

1.4.3.1 Modes of CSEB deteriorations by water action

The main sources of water deterioration mechanisms are rain, rising damp, and condensation. Due to the action of water on the block, deterioration can occur following several ways:

Solvent action : It is the main mechanism occurring in many building materials. The block is vulnerable to the solvent action of water because of its surface ability to easily get wet and its capacity to absorb and retain water for sufficient long periods of time. As mentioned earlier, the process of cement-stabilization is known not to affect all the constituents in the block. Thus, the microstructure of a block consists of a material juxtaposed with pores, which means that it can attract water and retain it. Consequently, any unstabilized soil fraction present with the freed calcium hydroxide from the hydration of cement can be dissolved. The effect of this repeatable action can lead to overall softening of the block.

Surface erosion : When a block is stroked by rainwater, it is directly impacted with part turning into a spray. The impact is linked to the removal of loose particles, while the effect of spray is more likely to wet the block surface. Therefore, any unstabilized fraction of the block surface can be easily removed by the resulting wall surface flow. The effects of surface erosion include lowering the compressive strength, loss of rigidity and increase in permeability.

1.4.3.2 Laboratory measurement of the durability of CSEB toward water action

Existing testing laboratory methods designed to estimate the durability of compacted earth block toward water could be classified in three main categories:

a. Water erosion

The first one aims at assessing the resistance to water erosion like the so-called spray erosion test and drip erosion test.

The spray test (Figure 1.15) mimics the effects of wind driven rain erosion by spraying water on one surface of the block with a constant pressure for a certain amount of time. The durability of the block is evaluated from the rate of erosion calculated from the maximum depth of erosion measured with a 10mm flat ended rod. Different international standards propose this method of assessment like the Australian earth building handbook (HB-195) [222], and the New Zealand Standards (NZS 4297) [223]. The main differences between these Standards concern the exposed area of the sample, the spraying time, the spray application distance, and the water pressure (see Table 1-10).

As for the drip erosion test, it consists of evaluating the damage caused by submitting earth block inclined at 27° from the horizontal to a continuous stream of water suspended at a fixed level above the sample's upper surface. The erosion resistance is evaluated based on the average pitting depth measured with a 3mm probe. In the Australian earth building handbook (HB-195) there is two examples of this test, namely the Geelong drip test and the Swinburne accelerated erosion test. They differ mainly in the level from which the waterfall, the way in which water droplets are generated and the dropping duration.

The first method consists of releasing 100ml of water within 20 to 60 minutes via a wet cloth wick, which then falls 400mm in height onto the surface of a block sample inclined of an angle of 27^{o} from the horizontal (Figure 1.16 – a). At the end of the test, the pitting depth is measured with a 3mm probe and the depth of moisture penetration is determined by breaking the specimen across the point of greatest erosion. The maximum measured pitting depth is related to an erodibility index which is used, with the penetration depth, to evaluate the durability of the tested block (Table 1-11). The results of this test are considered acceptable in areas where annual precipitation is around 500mm while its application to areas of higher rainfall are not confirmed [224]. From a practical point of view, controlling the water falling onto the block using the wet wick is not accurate, which verify the reason behind the unproven reliability of this test.

In the second method, a continuous stream of water is generated by a glass tube of 5mm in internal diameter at 1.5m above the block, which falls onto its inclined surface at 27° from the horizontal (Figure 1.16 – b). The erosion performance is assessed from the average pitting depth measured with a 3mm probe (Table 1-12).

Figure 1.15. Setup of the spray erosion test (from the Australian earth building handbook (HB 195))

	HB 195	NZS	SLS 1382	ASTM E2395M-10	EBAA 2001	Bulletin 5
Sample	Whole block	Whole block	Whole block	Whole block	Whole block	Whole block
Tested face	Table of block	Table of block	Orientation as intended in wall construction	Table of block	Table of block	Table of block
Number of samples	5	-	3	-	5	1
Exposed area Ø [mm]	70-150	150	150	150	70-150	150
Spray time [min]	60	60	60	60	60	60
Application distance [mm]	470	470	500	470	470	470
Pressure (kPa)	50	50	50	50	50	50
Outlet nozzle Ø [mm]	-	153	-	153	-	-

Table 1-10. Main Specifications of spray erosion test according to international standards

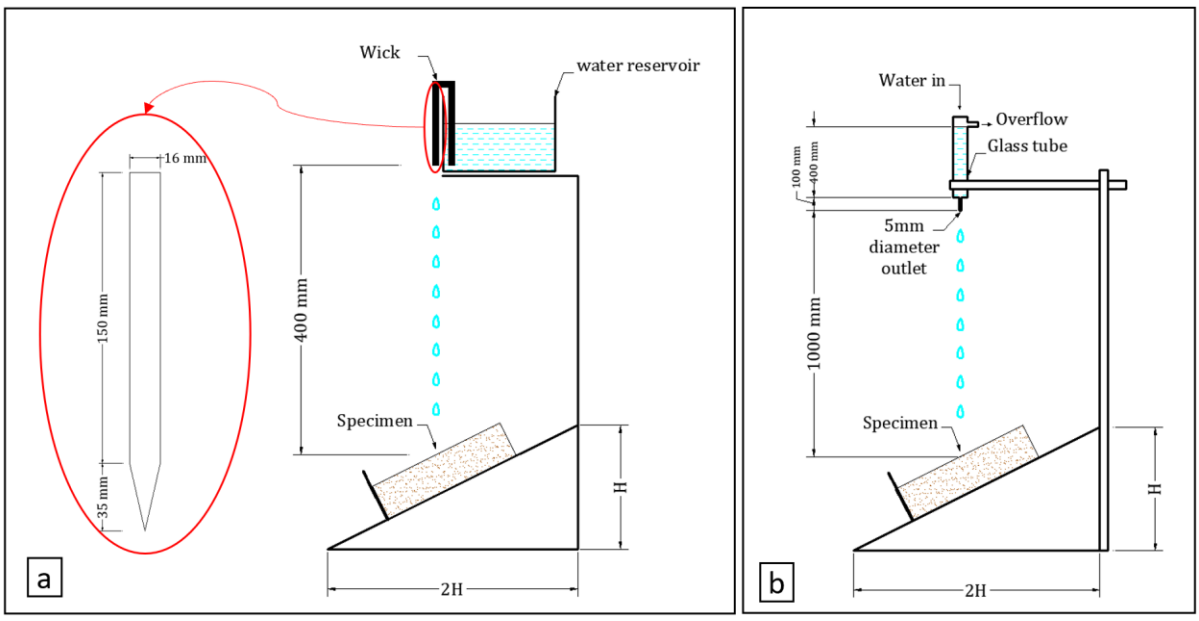

Figure 1.16. Schematic representations of the Geelong drip test (a) and Swinburne accelerated erosion test (b)

Characteristic	Criteria	Erodability Index	Note
Maximum pitting depth d [mm]	$0 < d < 5$	2	Slightly erosive
	$5 \leq d < 10$	3	Erosive
	$10 \leq d < 15$	4	Very erosive
	≥ 15	5	Fail
Depth of moisture penetration	< 120 mm		Pass
	> 120 mm		Fail

Table 1-11. Scale of assessment for Geelong drip test

Average pitting depth D [mm]	Classifications
$0 < D \leq 10$	Excellent
$10 < D \leq 20$	Good
$20 < D \leq 30$	Fair
$D > 30$	Poor

Table 1-12. Erosion classifications according to Swinburne accelerated erosion test

Due to the severe conditions of the spray erosion test, no unstabilized material reported in the literature data passed it. However, all stabilized materials resist to high water pressure beyond a certain dosage of stabilizer depending on the earth properties [225]. Thus, this test is more used as a tool to evaluate the efficacy of stabilizer rather than the durability of the material toward erosion. In this context, Ogunye and Boussabaine [226] indicate that natural exposure does not compromise extreme events, but degradation generally arises from alternative mechanisms like prolonged wetting and drying cycles. This issue was also noted by Van Damme and Houben in [58].

Concerning the drip test, most of literature data indicates that compacted earth block passed it, like the unstabilized earth samples with applied surface coating in [227], [228] and the stabilized samples with fibers in [229] or fly ash with activators in [230]. Some examples of materials that failed the drip test could found in [228] for unstabilized poured earth samples and in [227] for unstabilized adobes coated with natural polymer. In a study conducted by Seco et al. [231], compacted earth samples stabilized with 11% OPC passed the drip test but showed unacceptable degradation in natural exposure conditions.

b. Durability against an abnormal and/or cyclic excess supply of water

The second category of tests looks at the durability against an abnormal, and potentially cyclic, excess supply of water. In the Australian earth building handbook (HB 195), this problem is assessed though the wet-dry appraisal test. It consists in placing the specimen in 10mm of water for 30s and then dry it at ambient temperature until no color changes, then repeating this cycle six times. After the final cycle, the durability is evaluated based on the surface cracking patterns, the local swelling, the pitting, the loss of soil layers, the penetration of water by more than 70% of specimen, the loss of fragments greater than 50mm and the surface salt deposits. In the German Standard (DIN 18945) [232] this durability issue is assessed through other methods like the contact test and the suction test. The first one aims to reproduce the contact between an earth block and a 15mm thick mortar layer. It consists of putting a wet cellulose cloth, containing an amount of water of $0.5 g/cm^2$, onto the surface of earth block. The specimen is then stored for 1 day in an ambiance at 100% of relative humidity before being exposed to natural atmospheric conditions for 2 days. The durability assessment is made from the analysis

of cracks and/or irreversible swelling deformations. The second one was designed to represent the impact of capillary rises, and/or exterior timber frame walls during driving rains [233]. It consists of placing the sample on a conventional fired brick with an absorbent cloth on its top. This assemblage is placed inside a pan filled with water up to 1-5 mm below the upper edge of the fired brick. The durability assessment is made through visual detection of cracks and permanent deformations after 30min, 3h and 24h. On the other hand, the Bureau of Indian Standards (IS 3495 [234]) propose a simpler method which is the immersion test. In this latter, sample is fully immersed in room temperature water over a definite period or until reaching a constant value. The performance of the sample is evaluated based on the absorbed water content and the mass loss of the sample.

The simplicity of the latter test makes it one of the most methods performed in literature data. The tested specimens fail the immersion test generally if more than 15% water is absorbed, but higher limits could be found in the past studies, like 20% in [235] and [236]. According to Medero et al. [237], the immersion test could provide a good indication of the efficacy of cement stabilization and the short term performance of material subjected to prolonged contact with pooling water. While Guettala et al. [74] compared results of immersion test and those observed due to natural exposure and deduce that this test is too severe for the stabilized earth concrete tested in his study.

The absorption tests (wet-dry appraisal test and suction test) are also simple and popular in the literature data, but they are less severe than the immersion test. Hall and Djerbib [219] noted that evaporation at the dry surfaces during the absorption test establishes a hygrothermal gradient across the specimen. This issue promotes salt dissolution or deposition and efflorescence which cannot be examined when specimens are submerged in the immersion test. In [74], CEB stabilized with combinations of cement and lime higher than 5% survived the test for 7 days. In a comparison made in [74] and [231] between the results of absorption test and degradation of samples exposed to natural conditions, it had been observed that materials that performed the worst under natural exposure also show the higher final absorption rate.

c. Durability against wetting collapse

The last category concerns the assessment of risk of wetting collapse, which is commonly checked through saturated uniaxial compressive strength as recommended for example in the French Standard XP P13-901 [238]. The most common method that belong to this category is the saturated to dry strength testing. Given the demonstrated dependency between the strength of earthen materials and the amount of water trapped within the material and its distribution. The concept of this assessment method is that if the material has sufficient strength in saturated state, it will withstand the normal operating conditions of a building without problem.

In the IS 3495 [234] and HB-195 [222], the saturated unconfined compressive strength is determined after submerging the sample for 24 to 48 hours. While the dry strength is measured on air-dried or oven-dried (60 - 70°C) samples. To pass this test and to consider that the material is sufficiently durable, a minimum saturated and dry plus a minimum saturated to dry strength ratio are required, and they vary from author to another. In general, a wet to dry strength ratio of 0.5 is accepted (as reported in [239])

This test is relatively popular in literature data because compressive strength of compacted earth blocks is always evaluated. Heathcote [239] consider that the wet to dry strength ratio could be used as indicator for passing the spray erosion test rather than to provide long-term durability information about the material. He proposed more relaxed ratio of 0.33.

1.5 Block-mortar interface in CSEB's masonry

The behavior of masonry structure varies according to the performance of its components and the interaction between them. Indeed, it is essential to have adequate bond strength and durable bond throughout the life of the structure to achieve an efficient connection between the mortar and the blocks that resists to the action of exterior factors such as wind, earthquakes, and rain penetration. The deeper the mortar penetrates the crevices of the block the better the adhesion will be, improving the bond between the two elements.

1.5.1 Characteristics of mortar joint

Mortar, a bonding agent between CSEB to form a masonry, is mainly a mixture of water, fine aggregates, and cement or other binding material. Its role varies depending on the nature and purposes of the work required. Mortar is not strong as other building elements; it is used as a glue and controls weak points in a structure. Primarily, it serves to join the CSEB together in a strong bond yet keeps them at a specified distance from each other. It produces tight seals to provide a waterproof structure preventing the passage of moisture. In addition, it is used for architectural effects on masonry to give them aesthetic appearances [240].

Mortar is an integral part of the masonry and must be of good quality for good structure performance. Therefore, it is crucial to consider the properties of the mortar, which can affect the bond and the durability of the masonry, such as workability, water retention potential and strength. These properties describe the mortar and specifies it under two categories: plastic properties of fresh mortar and the hardened properties.

A key property of unset mortar is the workability, so it can spread easily to be paved evenly over the blocks and support their weight. Consistency, plasticity and cohesiveness are the main factors constituting the property of workability of the mortar, so it resists deformation and retains its deformed state. Fine materials improve the cohesiveness of the mortar, so less water is required to impart workability.

A desirable workability of the mortar requires high water content and only about 20-25% of this water is needed to sustain cement hydration [241]. The compressive strength of a mortar is related to water-cement ratio but the addition of water, for the required consistency and workability, remains in control of the mason [242]. When excess water is added to the mortar, the water-cement ratio increases resulting in a reduction in strength and durability performance of the mortar. This excess of water may be reduced or removed depending on the block absorption and water retention capacities of the mortar.

A good water retention is needed to maintain the plasticity of the mortar long enough to prevent breaking the bond when laying the blocks [243]. A very comprehensive study of bond strength in function of block and mortar properties such as block suction, water retaining capacity and strength of mortar was done by [244] on 50 mortars and 6 different blocks. They found that masonry constructed with porous dry clay blocks were more watertight with cement mortars of high-water retention potential than with cement mortars of low one and have a better bond strength. Results also conducted that the bond strength increased with the Portland cement content of the block and with mortars having highest compressive strength.

When hardened, mortar must be durable to transfer the compressive, tensile and shear stresses between blocks over the life of the structure. However, the strength of a mortar improved by

adding more cement should not exceed that of the blocks which may result a vertical cracking passing through blocks and mortar joints. In the opinion of masons, if cracks occur in the masonry, it will be much easier to repair if it tends to follow the joint than the failure of the blocks.

1.5.2 Block-mortar bonding and moisture transfer

The bond existing between the block and the mortar is a very important factor to ensure the stability of the structure since it is often the weakest zone in the masonry. A durable bond guarantees a watertight structure strong enough to resist stresses from different exteriors factors. Boynton and Gutschick [245] have highlighted the complexity of the bond to masonry and discussed many factors affecting its strength and water penetration properties. There are very surveys that provided quantitative evidence on the factors that affect the bond strength and durability such as the surface texture, the connection of pores, the mortar water retention, the block suction rate and its moisture content. The adhesion surface is therefore affected by the properties of both mortar and block.

According to the literature, there are no research projects aimed at understanding the moisture ingress at the interface between the compacted earth block and the earth mortar joint. A much more detailed understanding of the parameters affecting the penetration of moisture into earthen masonry is required as well as appropriate suggestions for reducing the impact of water on masonry performance. This section contains the main results of some studies based on water penetration for other types of masonry. Many uncertainties remain when taking these results into account due to the lack of knowledge about water penetration into earthen masonry.

The effect of surface texture on bond and water penetration was studied by a series of experiments of capillarity done by [246] on sand finished blocks and smooth blocks. He showed that mortar does not stick on a rough surface of the block regardless of the size of the pores and so the mortar is needed with sufficiently high workability to fill the voids and sufficient water retention to nullify the surface capillarity that can draws the moisture before even having a good bond.

Very low rate of absorption tends to decrease the bond strength, same as a high rate of absorption that also led to high leakage rates. The increase of the mortar flow and the water retention have a beneficial effect on both bond strength and resistance to water. A way to make the bond better is that the mason set immediately the blocks after laying the mortar and tapping it with a trowel at the time of laying [247]. For earthen masonry, [248] found from mechanical tests, that moistening the blocks was effective when it is laid on a mortar with low water retainment improving the shear strength of the masonry.

Palmer et Hall [249] investigated the strength between blocks made from clay and shale and cement-lime mortar and reached two most important conclusions. They conclude that vertical joints in masonry are most likely to bond failure and comment about the importance of pre-wetting the porous block to obtain a proper bond. A block with high rate of absorption tends to dry the fresh mortar that loses its plasticity, and at the same time a little suction of the block is necessary to form the best bond. So an optimum value of moisture content, which is about the two third of the water absorption of blocks determined by the 2h immersion test, is needed to obtain a strong and durable bond and prevent loss of moisture due to block suction [250].

Hall and Hoff [251] studied the relevant and important concepts of water transport through porous materials such as blocks. Water in masonry can be described in terms of absorption,

transfer, or desorption. When a fresh mortar is spread to bond the blocks, water is desorbed from the mortar and absorbed by the block. This mechanism is a main problem relating to durability issues and deterioration of the masonry. [252] studied the effects of water on mortar-block bond with blocks with low and high rate of absorption (fine or coarse pores) and cement-lime mortar. He showed that the water transfer from fresh mortar to block causes changes in material composition and water distribution over the joint and explained that the hydration of cementitious products in the body of the mortar joint differs from that at the bonding interface.

Groot [253] used neutron radiography to detect the water in the masonry and measure its velocity during the first minutes of the contact between block and mortar. He reported that the influence of gravity on water transfer is negligible since water contents was high in both below and above block. He observed that the initial seconds of contact between block and mortar is critical since the velocities of water decrease sharply over time affecting the bond development. He concluded that the transport of fine elements with water towards the interface also have effects on the bond strength. Fine materials are steeply transported with high flow velocities than low flow velocities.

In a further study Groot and Larbi [254] analyzed models of capillary water pressure and water transport for cylindrical capillaries (blocks) and water containing particle systems (mortars) in an attempt to study the water loss from the fresh mortar by the block suction. Modelling the pore structure as capillary tubes was an idealization, knowing that it depends on its shape, various diameters, closed and open pores. They were able to show that the coarse pores exert a low capillary pressure, and the fine pores exert a high one. Capillary pressure of the water in the mortar increases by the decreasing of the water content causing compaction and densification of the mortar. They concluded that reversed water flow from block to mortar, that can be the cause of the differences between the interface and the blocks strengths showed by the microscopic analysis, may influence the bond strength development. This release of water can be influenced by the effects of gravity.

Long term movement in masonry is influenced by the moisture transfer due to the bloc water absorption that reduces shrinkage and creep of mortar but increases the deformations of the blocks [255].

Water transfer across the interface is influenced by the curing conditions of the mortar and by the imperfect contact between block and mortar. The ratio water-cement of the mortar decreases due to the extraction of water by the block resulting in the decrease of the permeability of the cement paste. Insufficient contact between a dry cured mortar and the block is the result of the formation of air voids, called compaction pores, at the mortar interface due to the reduction of the water-cement ratio, unlike the wet cued mortar which represents no voids. The presence of compaction pores explains the existence of an interface resistance for joint mortars causing a reduction in flow through the interface [256].

1.5.3 Shear testing at the interface

Tests designed to assess the shear behavior of the interfaces of compacted earth masonry are similar to the test designed for the baked brick masonry [257]–[259]. The main tests that could be found in the literature are the triplet test [260], [261] (Figure 1.17), diagonal compression test [262], [263], shear box test [264], [265] and the triaxial test [196], [266]. Presently, the cohesion and the friction angle given by Mohr-Coulomb criterion are the two parameters that define the limits of the shear stresses.

Figure 1.17. Triplet test specimens and setup (from [261])

1.5.4 Failure modes in a masonry

The behavior of a masonry structure is dominated by tension and shear when subjected to a lateral loading. Usually, the tensile and shear bond strengths are quite low and hence the masonry fails through block-mortar interface. Failure can be represented by diagonal cracking of mortar layers and debonding of the block-mortar interface. This interface weakness can be avoided through usage of high adhesive mortars with high tensile and shear bond strengths [267] [268] but also it can modify the mode of failure to a combination of debonding and block cracking.

Failure mode of a masonry construction is governed by the behavior of discontinuities due to its heterogeneity induced by the mortar joint and the bock. Frequently these failures occur in the joints leading to diagonal cracks in the vertical and horizontal joints or passing through bed joints only [250].

Shear failure is an important and often governing the mode of failure in masonry structure. A complex relationship exists among joint normal stiffness, normal displacement and shear displacement. When displacement is controlled, shear strength increases with the increase of the normal load produced by the dilatancy [269]. Under high compression , dilatancy have a small effect and can be neglected [270].

When a masonry is solicited to simple compression in its plane, we observe three modes of failure according to the direction of solicitation. If the load is perpendicular to the mortar joints the cracks are vertical and if parallel, cracks are horizontal. In the case of biaxial compression, the failure mode is based on the ratio of the intensity of the vertical and horizontal loads [271] The masonry shows very good resistance to axial compression stresses. Shaan [271] says at failure if the load is perpendicular to the mortar joints, cracks will be vertical. According to [272] the difference between the rigidity of the block and the mortar causes triaxial compression of the mortar joint while the blocks are subjected to biaxial compression. A failure can therefore occur by vertical cracking or by crushing of the blocks.

In case that the load is parallel to mortar joints, cracks are horizontal [271]. Page [273] suggest that failure is reached as long as horizontal joints are cracked even if the masonry can support more loading. He also studied the influence of the orientation of the mortar joint with respect to the applied stresses. Rupture occurs by cracking and sliding in mortar joints and can be combined with the rupture of the block (Figure 1.18). In case of biaxial compression, [274] showed that failure is influenced by the quality of mortar joints acting as planes of weakness.

He expressed the failure surface in terms of local constraints relating to the mortar joints because they represent most of the time the plane of the rupture in the masonry.

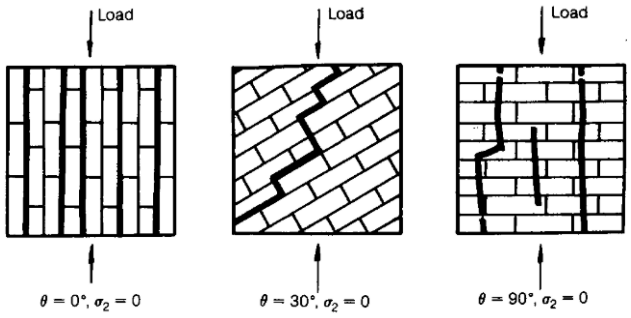

Figure 1.18. Failure modes in uniaxial compression (Page, 1981, [273]).

1.6 Conclusion on the research problem

Previous sections of this chapter presented the main factors that could affect the evaluated performance of CSEB, and therefore the efficacy of cement stabilization, from the materials characteristics (earth and cement) to the testing conditions of the final product. The reviewed literature indicated that an important number of studies were made to investigate the effect of these factors on the performance of compacted earth. While the effect of some properties on the performance of CSEB are relatively known (like clay content, dry density, water content, etc.), other may be questionable (particle size distribution, OMC, cement composition, cement dosage, etc.). In addition, the high variability in the characteristics of existing earths and cements lead in general to case-by-case studies. Further, the performance of a block having the same composition can vary when different methods are applied to assess the same property, like compressive strength or erosion resistance, etc. Finally, curing conditions affect the hydration process of cement in the CSEB, and therefore its performance. However, no unified curing method exists, neither on-site nor in laboratory.

It follows that to investigate the efficacy of cement stabilization, the first mission is to perform an exhaustive characterization of earth properties, to design the setup of robust manufacturing method and to define an optimized curing protocol.

The second mission is to quantify the impact of cement stabilization on the performance of the block. Even if some studies have already been made on that subject, as it is highlighted in this bibliographic review, the aim here is to perform a multi-criteria analysis which consider simultaneously compressive strength, hygroscopic properties, and durability toward water with respect to cement and earth characteristics. What is more, contrary to what it is commonly made in a large number of previous scientific studies, it was decided to not study OPC, but selected cements with lower clinker content and strength classes. Finally, even if some extensive studies have already been done concerning the block-mortar interface, it appears that it still lacks some data concerning the compatibility in composition between both, especially when block-mortar assemblage goes form dry to wet conditions.

Chapter 2. Materials sampling and curing

2.1 Experimental plan design

As presented in the literature review, many factors influence the performance of CSEB. For investigating stabilization effectiveness, it was decided to fix some factors while varying others to discuss the performance from the perspective of material's composition. The main fixed and variable factors are presented in Figure 2.1. Fixed factors include manufacturing dry density and water content, sample geometry and curing conditions. Here let recall that fixing manufacturing sample properties was done by formulation, which means that they vary from one to another, but they were fixed for the same cement-earth couple. Variable factors are therefore cement and earth characteristics. Main input variables of the experimental design are summarized in Table 2-1.

Cement characteristics examined are dosage, strength class, fineness, and composition. It was decided to select moderate dosages of 5 and 8% by dry mass of earth. The selected cements differ mainly in term of their strength class, clinker content, and composition. Earth characteristics that were inspected in the study are clay content, granulometry, mineralogy, toxicity, and alkalinity. It was decided to select two earths that differ in their geotechnical and chemical characteristics and that are suitable for construction at the same time. The first one (DAG) is finer than the second one (STA) and contain lower clay content. A third earth referenced as STAmix was prepared from STA earth while maintaining its mineralogical composition by milling it to approach from DAG earth by its fineness. A fourth earth named Lim was introduced for analyzing results and it is similar to DAG in term of fineness, but it contains the highest clay content in comparison with DAG and STA. It is worth noting that the mineralogical composition, the toxicity, and alkalinity of earths were not determined as pre-characterization input, but they were used to explain and justify hypothesis made on the effectiveness of cement stabilization in function of the performance of cement-earth couples.

The performance assessment procedure consists essentially of a comparative examination of the effect of stabilization based on performance indicators that enables covering three aspects: the mechanical performance, the hygrothermal performance and the durability toward water. The main engineering performance indicators of earth-based materials are summarized in Figure 2.2.

Concerning samples, the experimental campaign requires the production of three types of sample's geometry. The first one is evidently the compacted earth block which is the subject of the thesis. The available block press in the laboratory produces blocks of size 295mm×140mm×95mm. It was not possible to perform all tests on blocks due to the huge materials quantity that demands the manufacturing of all blocks required for the planned experiments. At the beginning of the thesis, it was estimated that the experimental campaign demands a minimum number of 1000 blocks, but the available earth quantities were not sufficient. Another reason is the difficulty encountered during tests if blocks will be used, both in terms of manipulating the block or in terms of time that each test will require. Therefore, it was decided to use cylindrical samples having 35mm in diameter and 70mm in height, whose are typically used in our laboratory for mechanical tests on earthen materials. While experiments that aim at quantifying the durability and the hygroscopicity were conducted on cylindrical samples having 100mm in diameter and a height that varies between 20 and 40mm depending on the test. It's worth noting that earth blocks were used in Chapter 4 for validating the durability test developed and in Chapter 5 for the analysis of block-mortar interlocking.

The initial step consists of fixing the manufacturing properties to ensure that samples of different geometry are similar in term of their compaction water content and dry density. These manufacturing properties were based on the optimum state of each mixture that are determined in §2.3, while the curing conditions of samples are addressed in §2.4. In the remaining chapters of the thesis, the experimental investigations are made on selected mixtures based on their relevancy for each subject treated in the study.

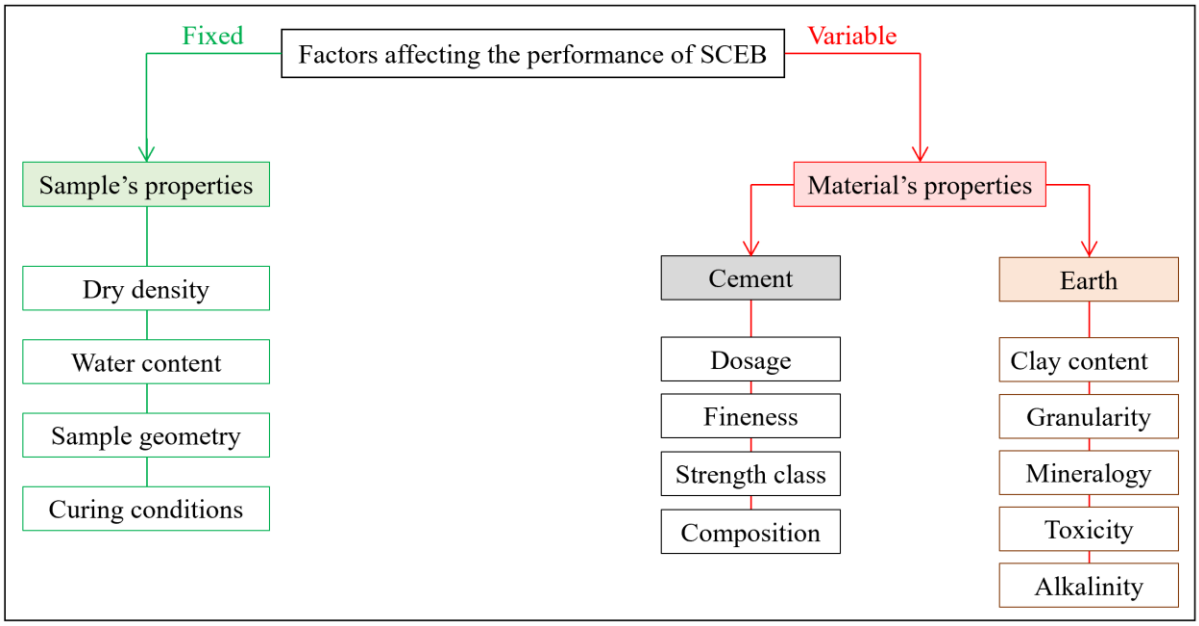

Figure 2.1. Visualization of main factors affecting the performance of CSEB as considered in the thesis.

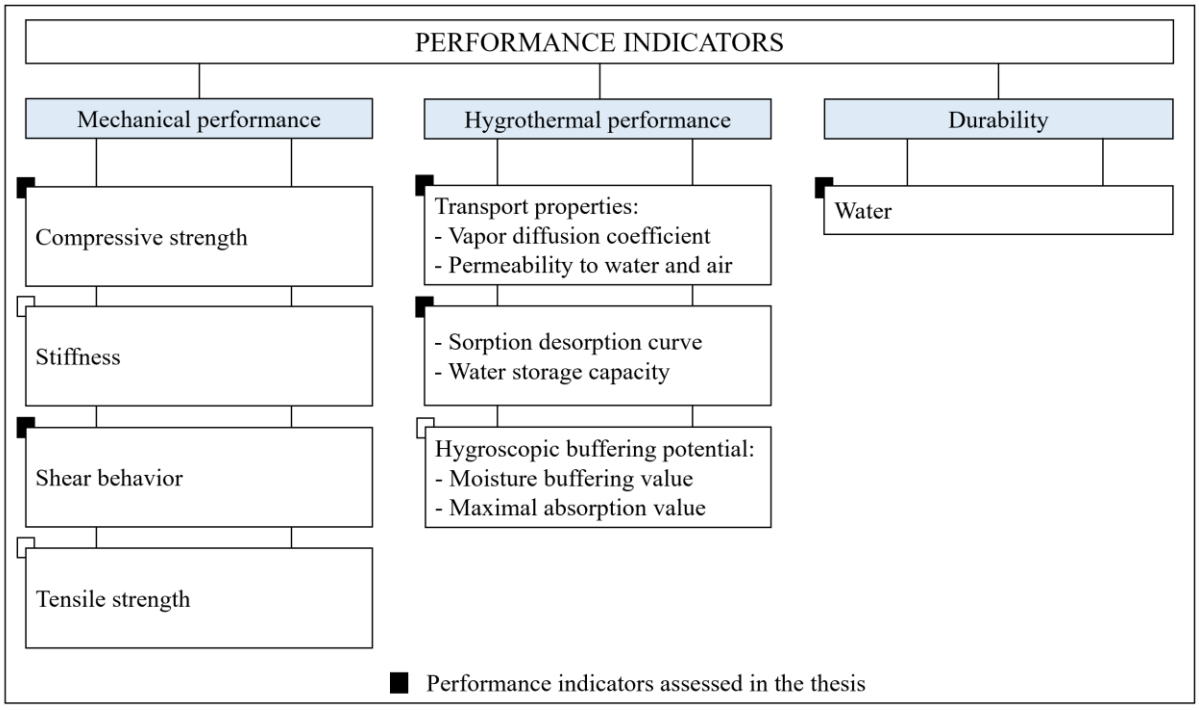

Figure 2.2. Main engineering performance indicators of earth-based materials

Materials		
Earths	Dagneux (DAG) St. Antoine L'Abbaye (STA)	▪ Main earths of the study.
	Limonest (Lim)	▪ Introduced for analysis purposes in section 3.4.2.
Cements	CEM II/A-LL – 42.5R CEM II/B-LL – 32.5R CEM V/A (S-V) – 42.5N MC 12.5 Prompt natural cement	▪ Cement dosage: 5 and 8% by dry mass of earth.
Manufacturing		
Mix-water	Optimum water content	▪ Corresponds to the maximum dry density of each formulation.
Compaction pressure	4 N/mm^2 ± 0.3 N/mm^2 250bars	▪ Cylindrical samples compacted with hydraulic press. ▪ Maximum pressure of the block press used.
Samples dimensions	Φ35mm×h70mm	▪ Uniaxial compression tests (direct method).
	Φ100mm×h40mm Φ100mm×h30mm Φ100mm×h20mm	▪ Moisture buffer tests. ▪ Water vapor permeability test. ▪ Accelerated erosion test. ▪ Immersion test.
	297mm×140mm×95mm	▪ Uniaxial compression tests (half-block method) ▪ Shear test (triplet test). ▪ Durability tests (contact test and drip test). ▪ Water adsorption test (on parts of block).
Conditioning		
Initial curing	21˚C ± 2˚C/~100%RH	▪ 7 days after compaction.
Drying conditions	21˚C ± 2˚C/50% ± 2%RH	▪ Drying conditions until reaching constant mass before each test.

Table 2-1. Summary list of the main constituent materials and input variables used in the production of samples

2.2 Materials

2.2.1 Earths

Three different natural earths coming from the "Auvergne Rhône-Alpes" region in southeastern France were selected for testing. Their location is shown in Figure 2.3. The first one is referenced as DAG and it was collected from centenarian rammed earth construction located at the city of "Dagneux". The second one is referenced as STA and it was extracted from subsoil at the village of "Saint Antoine l'Abbaye". The third one is referenced as Lim and it comes from ancient construction located at the village of "Limonest" (Figure 2.4). It is worth noting that the selected earths were used in different Ph.D. theses undertaken at our laboratory that investigated the mechanical [275], hygrothermal [221] and hydro-mechanical [276] behaviors of earth as a building materials, which oriented the initial selection of earths. The latter works treated the unstabilized materials while the present research is concerned by the stabilized ones.

Figure 2.3. Location of the selected earths on the map

The collected earths were crushed and sieved at 5mm because the material used must not contain grains with a diameter greater than fifth of the shortest dimension of the samples produced in the rest of this thesis. Sieved earths were homogenized then their particle size distribution was determined according to the French Norms NF P94-056 and NF P94-057. The obtained granular distribution is reported in Figure 2.5. It indicates that the three earths are quite fine. Concerning the granular stacking, DAG and Lim are similar in term of the absence of coarse gravel and sand since more than 90% of their particles is lower than 80µm. While STA shows a wider granular distribution. Only the latter earth lies in the recommended region of the particle size distribution for the manufacture of CEB given in the norm AFNOR XP-P13-901 [277]. Here let underline that the objective of the presented upper and lower limits is to provide a kind of recommendations and not to constitute a rigid regulation. Given that DAG

and Lim come already from existing constructions. In general, an earth is considered suitable for construction if it contains fine gravel and sand with cohesive fraction (i.e., silt and clay) that acts as a natural binder between grains [158], [278]. Anyhow, the aim of this study is not to judge the suitability of earth for building with CEB, but to investigate the influence that may have different properties of earth on the action of cement stabilization. And the granulometry is one of these properties.

Figure 2.4. Origin of the three earths

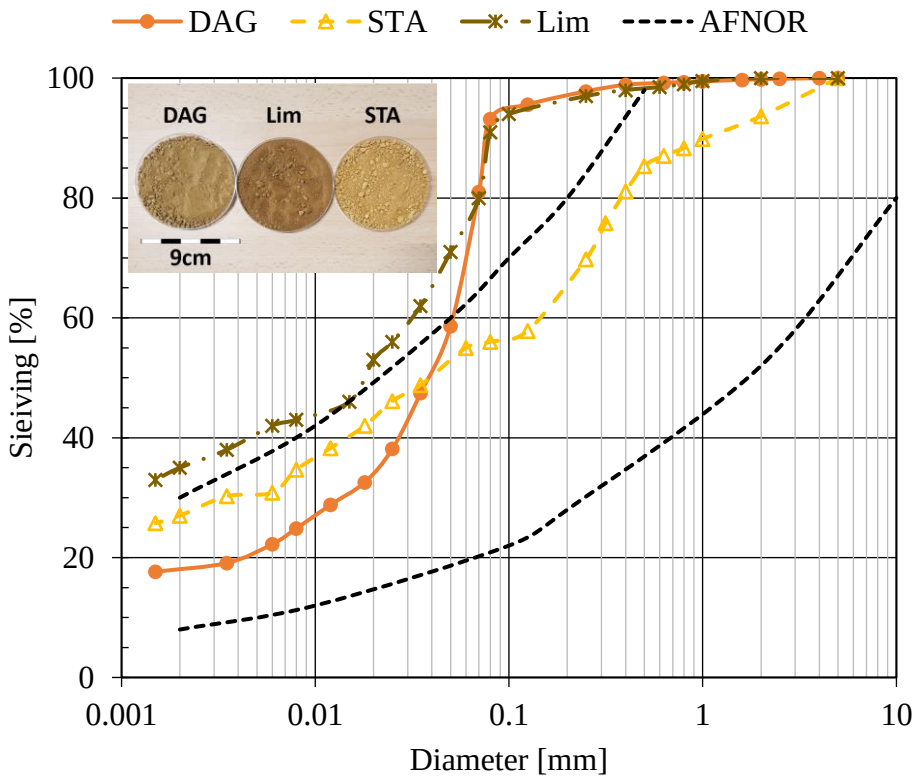

Figure 2.5. Particle size distribution of the three earths after sieving at 5mm.

Another factor that could influence the efficacy of cement treatment is the quantity and activity of the fine fraction of the earth (<2µm). In term of clay content, Lim contains the highest percentage (35%) when compared to STA (27%) and DAG (18%). Knowing that high clay content may negatively impact the action of cement stabilization because clay grains can compete for the mix-water required for cement hydration due to their high specific area (>10 m^2/g). To get information about the activity of this clayey fraction, the methylene blue value

(V_B) was used as indicators since methylene blue is preferentially absorbed by clays and organic materials. The methylene blue test was carried out on the 400µm fraction of the earths following the French Standard NF P 94-068. The ratio between V_B and the clay content in the 0-80µm fraction of the earth (C_B) enables the deduction of the clay activity index (A_{CB}). Results given in Table 2-2 indicates that the clay minerals contained in DAG possesses the highest activity, and clay in Lim has almost proximate activity. In contrary, clay minerals presenting in STA are not very active. Further, Atterberg limits were determined in agreement with the French Standard NF P 94-051. As expected, the plasticity index increases with the rise of clay content for the three studied earths.

		DAG	**STA**	**Lim**
Granulometry	Sand and fine gravel (5-0.06mm) [%]	27	45	25
	Silt (60-2µm) [%]	55	28	40
	Clay (<2µm) [%]	18	27	35
Activity	Methylene Blue value (V_B)	1.8	1.5	3.0
	Clay content in the 0-80µm (C_B) [%]	19.3	48.2	38.5
	Clay activity index (A_{CB})	9.33	3.11	7.79
Plasticity	Plastic limit (W_P) [%]	17.9	21.9	14.3
	Liquid limit (W_L) [%]	31.2	40.3	33.4
	Plasticity index (I_P) [%]	13.3	18.4	19.1

Table 2-2. Main properties of the three earths

2.2.2 Cements

A conscious decision was made to examine the effectiveness of stabilization with cements having lower clinker content than OPC, generally used for stabilization. To do so, five blended cements having different physical and chemical characteristics were selected based on the propositions of the cement manufacturers intervened in the steering committee of this thesis. Their main characteristics are summarized in Table 2-3 as provided by the manufacturers.

Firstly, CA was chosen as being relatively rich in clinker (86% by total mass). Thus, the results of treated earths with this cement could be compared to some extent with findings from the literature that dealt with OPC (i.e., cement type I).

The two cements CB and CM were selected to analyze the impact of reducing clinker content. In them, a percentage of the clinker content is substituted by limestone fillers. As another option, CM (i.e., masonry cement) may provide a win-win solution for both CEB and mortar joining it. On the other hand, the cement CV was suggested as it is rich in flash ash and furnace slag. This kind of cement is used sometimes by practitioners to improve the stability of soils for road applications. Finally, Prompt cement (CP) was proposed to verify its application in the stabilization of geo-based materials since its efficient employment in bio-based concrete is already proven. It is worth noting that no published works were found in the beginning of the thesis on stabilizing earthen materials with Prompt cement.

Selected cements were viewed as follow: CA is the cement with the highest clinker content (86%) and highest strength (54MPa at 28days) while CM is the cement with the lowest clinker content (20%) and lowest strength (20 MPa at 28 days). CB is a cement with average characteristics between the two extremes (77%; 40MPa). CV is of similar mechanical characteristics to CA but with low clinker content like CM. In the composition of CV, about

40% of clinker is substituted by siliceous fly ash and blast furnace slag. While limestone is used to replace a part of clinker in the first three cements. Finally, CP is a particular cement that differs totally from the remaining cements, despite that its mechanical strength is slightly close to that of CM. From an ecological point of view, the main assets of this cement are that it is burned at similar temperature to lime and that it contains nothing more than what is dug from the earth. It follows that characteristics of the selected cements here could lead to fruitful discussion.

Cement type			CEM II/A-LL – 42.5R	CEM II/B-LL – 32.5R	CEM V/A (S-V) – 42.5N	MC 12.5	CNP
Designation			**CA**	**CB**	**CV**	**CM**	**CP**
Composition by mass [%]	Clinker		86	77	58	57	100*
	Limestone		13	22	-	42	-
	Siliceous fly ash		-	-	21	-	-
	Blast furnace slag		-	-	20	-	-
	Minor additional constituents		1	1	1	1	-
Physical properties	Fineness [cm^2/g]		4176	4123	4425	5241	7950
	Average initial setting time [min]		155	150	168	145	2.5
	Average compressive strength of cement pastes [MPa]	At 7days	46	33	22	15	20.5
		At 28days	54	40	54	20	27.9
			* depends on the source of the natural raw material				

Table 2-3. Summary of the main characteristics of the chosen cements.

2.3 Sample's manufacturing

The first step consists of determining the optimum manufacturing properties of different cement-earth couples that could be produced in equipment of our laboratory. In this context, the well-known Proctor test is used for the determination of the "optimum water content" that corresponds to the maximum dry density of a soil in road geotechnics based on dynamic compaction.

However, the optimum Proctor could not be representative of the optimum state of CEB as discussed by P'KLA (2002) [279] in his PhD thesis conducted in the LTDS/ENTPE. He shows that no relation could be established between static compaction of CEB and Proctor compaction. The compaction energy in the latter method is inappropriate because it is not equivalent to that one of the block presses. For practical purposes, the optimum state should be determined using the block press as it is the case on site.

To that end, the optimum state is based in this thesis on the optimum CEB. The procedure followed to determine the latter state is presented in the following sub-sections.

2.3.1 Determination of the optimum state of the formulations

The determination of the optimum state of CEB consists of compacting blocks at different water contents with different materials quantities using the available CEB press following with the next steps:

1. Mixing earth with an initial fixed water content (w_1), then filling the mold of the press with a mass ($M_{1,1}$) and compacting to get a first block ($B_{1,1}$). In case of cement stabilized formulations, earth should be mixed with the required quantity of cement before adding water.
2. Increasing the mass of the earth to be introduced in the mold ($M_{1,2}$) while keeping the same water content (w_1) and repeating this until reaching the maximum mass ($M_{1,\,max}$) that could be compacted by the press in question.
3. Increasing water content (w_2, w_3, ..., w_n) and repeat steps 1 and 2 for each water content.
4. Calculating the maximum dry density for each water content form the ratio between the dry mass of the block obtained at 105°C and its corresponding apparent volume.
5. Plotting the calculated maximum dry densities in function of their corresponding water content.
6. The optimum water content (OWC) corresponds to the maximum dry density (MDD).

It follows that the quantity of earth required for the determination of the optimum state of stabilized and unstabilized formulations is huge, given that dry mass of one CEB varies between 6 and 7 kg, and that at least three blocks from each mixture (w_1, $M_{i,\,j}$) must be prepared to verify the repeatability of the results. For that reason, the optimum state was determined from CEB compaction for one unstabilized formulation only, made with DAG earth and designed by DUS. The resulting blocks could be crushed again and used in the fabrication of samples for the experiments, which is not the case of stabilized formulations. This part of the work was done in the framework of the Master project that preceded this Ph.D. thesis. The available block press was a manual Geo50.

For the remaining formulations, the optimum state was determined by compacting small samples inside homemade cylindrical mold using a hydraulic press that had been developed in a previous Ph.D. thesis [8]. This led to important saving of material and human effort. To do so, the compaction effort that enables the fabrication of cylindrical samples of 35mm in diameter and 70mm in height having the same MDD and OWC of blocks compacted with block's press should be determined firstly. Thus, series of cylindrical samples were compacted at the determined optimum state of DUS by controlling the press in displacement until reaching the target height. The average force recorded by the system of the hydraulic press at the end of compaction was registered and the average value was calculated and noted F_{comp}. It was equivalent to a compaction pressure of 4MPa±0.3MPa. Thereafter, the hydraulic press was turned on force-controlled program by fixing the maximum compaction force at F_{comp}. At the end, the same steps described earlier were followed again but on small cylindrical samples.

The obtained results are summarized in Table 2-4. It shows that OWC and MDD are not sensitive to the type of cement type used. Further, a small-scale variation in optimum water content with cement dosage between 5 and 8% was detected. This observation is in accordance with existing literature in this field. The remarkable difference in optimum moisture content of DAG, Lim, and STA could be attributed to the clay content in their 0-80µm fraction (DAG = 19.3%, STA = 38.5%, and Lim = 48.2%). The higher is the clay content the higher is the OWC. On the other side, the decrease in MDD after stabilization may be attributed to the difference in the specific gravities of earth and the stabilizer [280].

Formulation	Earth	Cement	Cement Dosage [%]	MDD [g/cm^3]	OWC [%]
DUS	DAG	-	-	1.85±0.03	14.0±0.15
DA5		CA	5	1.77±0.03	14.5±0.15
DB5		CB			
DV5		CV			
DM5		CM			
DP5		CP			
DA8		CA	8		14.8±0.15
DB8		CB			
DV8		CV			
DM8		CM			
DP8		CP			
SUS	STA	-	-	1.73±0.03	19.0±0.15
SA5		CA	5	1.66±0.03	20.0±0.15
SB5		CB			
SV5		CV			
SM5		CM			
SP5		CP			
SA8		CA	8		20.5±0.15
SB8		CB			
SV8		CV			
SM8		CM			
SP8		CP			
LUS	Lim	-	-	1.90±0.03	16.0±0.15
LB8		CB	8	1.79±0.03	16.8±0.15
LP8		CP			

Table 2-4. Summary of the formulation's manufacturing properties.

2.3.2 Fabrication of cylindrical samples

Manufacturing cylindrical samples was done in two stages, mixing and compaction. A "careful" manual mixing respecting the "three heaps rule" ("*règle des trois tas*" in french) was followed. This mixing procedure ensure a good distribution of cement and water and it was adopted and verified in the geomaterials ENTPE Lab since 1980 in studies undertaken on the factors affecting mixing, fabrication and rheology of compacted earth blocks [93], [281], [282]. Moreover, it is the mixing procedure preferred in our laboratory for the preparation of earth batches of small quantity (lower than 10kg). Addedly, investigations made in the master project that preceded the present thesis demonstrated that the performance of samples made after a manual mixing were repeatable in term of compressive strength. While a big dispersion was obtained in results of those obtained on samples prepared after mixing with electric blender, that we dispose in the laboratory. Which means that manual mixing enables producing a better homogeneous mixture. Let mention here that this issue was demonstrated on quantities of about 2kg only. And maybe other electric blender could ensure a better homogeneity of the mixture.

The manual mixing consists of moving a quantity of material 3 times by turning it over. The mixing consists in spreading the earth in a uniform layer thickness, then in spreading the cement in a uniform way on earth layer. Earth and cement are then mixed until obtaining a

uniform color of the mixture. Then this dry mixture is again spread in a uniform layer thickness. Water is then poured with a sprayer in two separate times with mixing each time and re-spreading in uniform layer thickness before adding water. The obtained wet mixture is reformed a last time then sealed in hermetic plastic bag to avoid contamination and variations in moisture content.

It is worth noting that proportioning out of earth, cement and water was done by mass, not by volume. And each batch was prepared to produce 6 samples only to not exceed a laps time of 1 hour between wet mixing and compaction. Knowing that laps time should be lower than initial setting time of cement to prevent considerable difference in the compressive strength of the produced samples [53].

Compaction consists of molding samples in two different cylindrical molds. The first one enables the production of samples having 35mm in diameter and 70mm in height (Figure 2.6 – a, c). It was developed by F. Champire in his thesis done at the ENTPE and the mold filling methodology is shown in Figure 2.7. The second one enables the production of samples having 100mm in diameter (Figure 2.6 – b, d) with different thicknesses (40mm, 30mm and 20mm). Filling the two molds was done in one layer for all samples. A hydraulic press was used for compaction and it was controlled in displacement until reaching the target height. The two types of cylindrical samples were compacted with similar compaction stress equal to 4MPa ± 0.2MPa.

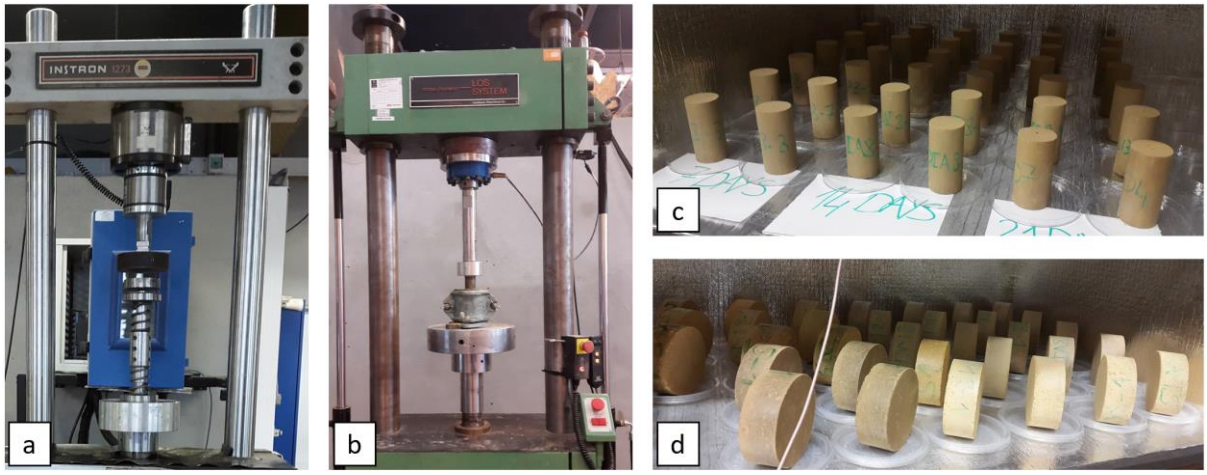

Figure 2.6. Mold of 35mm in internal diameter during compaction with hydraulic press (a), Mold of 100mm in internal diameter during compaction with hydraulic press (b), examples of the produced cylindrical samples having 35mm in diameter and 70mm in height (c), examples of the produced cylindrical samples having 100mm in diameter and 40mm in thickness (d).

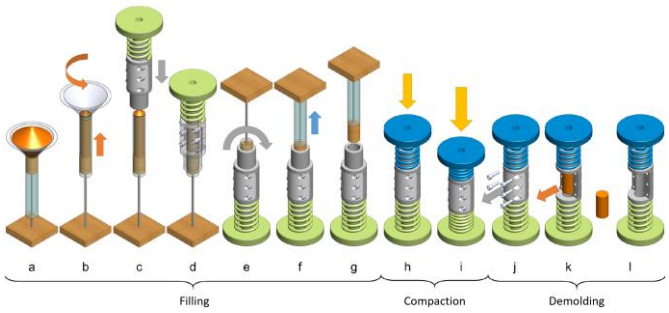

Figure 2.7. Mold filling methodology of cylindrical samples Φ35mm×h70mm (after [8])

2.3.3 Fabrication of earth blocks

Block's fabrication requires mixing about 50kg per batch of 6 blocks, thus, industrial mixing procedure was followed using electrical mixer of 120 litters and of vertical axis, used for mixing traditional mortars. The mixer used here enables mixing granular products with a grain size up to 8 mm (Figure 2.8 - a). To obtain a good mixing quality, the total material quantity should not exceed 60 kg in similar mixer used here. Like the manual mixing, earth and cement are firstly dry mixed for 2 minutes, then water is added gradually and mixed for 8 minutes. Counting the discharging of the mixer, one mixing cycle lasts about 15 minutes.

Due to the paddle's system of the mixer, big balls of wet earth with a diameter of 2 to 4 cm were formed at the end of the mixing stage. The discharge end of the mixer was large (Figure 2.8 - d) so it enables the recuperation of the formed balls, which was not convenient to produce homogeneous blocks. This problem was fixed by adding a metallic grid with round holes of 5mm in diameter at the discharge end of the mixer to facilitate sieving the mixture at the end of the mixing stage (Figure 2.8 - e). Thereafter, the prismatic mold of the press was filled with the required mass of the prepared mixture and compacted with a pressure of 250 bars (Figure 2.8 - b).

The hydraulic block press used was designed by press manufacturer for this study is such a way that it enables the production of blocks (Figure 2.8 - c) having the same dimensions of the blocks compacted with the manual press Geo50. However, the hydraulic press applies a simple compaction while the Geo50 is a double compaction press. A simple compaction means that the sample will be compact from one side more than the other. Thus, the manufacturing MDD of blocks produced by the simple compaction press were checked on earth blocks from the DUS formulation. To do so, each block dried at 105°C was sawn into 12 parts (Figure 2.9) to check the density gradient between the top and the bottom of the block on one side, and between the center and the outer on the other side. It was not possible to make precise calculations of the volume form the measured dimensions of the sawed block parts due to some irregularities. Thus, the apparent volume of each part was determined from the hydrostatic weighting method, which is commonly used in the construction industry for the determination of the volume of irregularly shaped object. Earth block parts were coated with paraffin wax before been immerged in water to avoid water adsorption during the test.

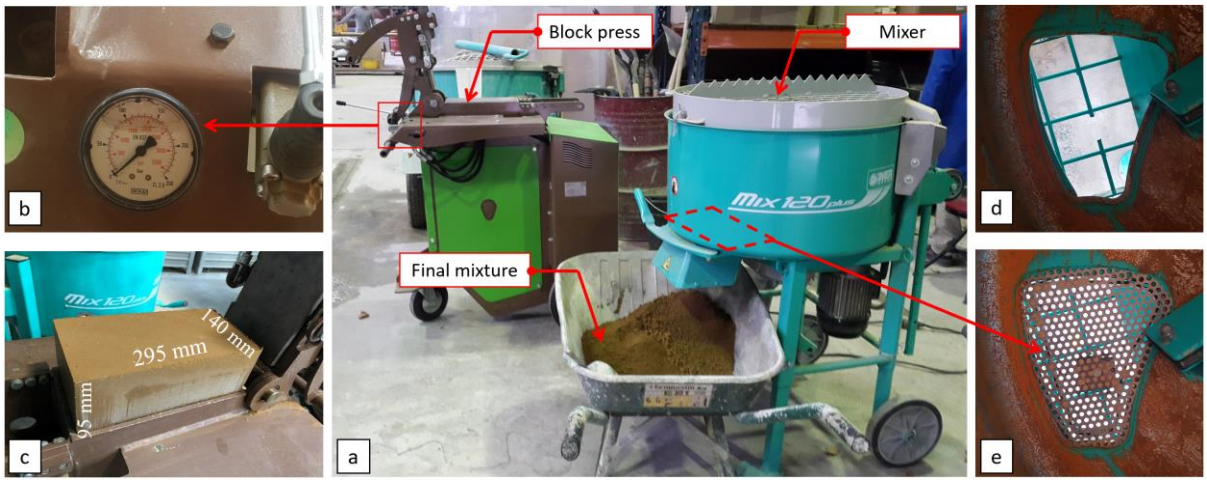

Figure 2.8. Manufacturing earth blocks (a), 250 bars pressure gauge of the block press (b), earth block directly after compaction (c), initial discharge end of the mixer mix 120 plus (d),

modified discharge end of the mixer with a metallic grid sieve with round holes of 5mm in diameter (e).

The calculated densities are presented in Figure 2.10. As expected, the central parts are slightly denser than the outer parts and the bottom parts are denser than those of the top since the direction of compaction is from the bottom to the top. Although this variation, the level of homogeneity of the fabricated blocks is quite high, given the maximum deviation between part of the same block is about 2.7%. It's worth noting that the maximum deviation in density of cylindrical samples prepared by double compaction is 1.5% along height as demonstrated in [8]. While for samples produced by Proctor compaction, the variation of dry density from top to bottom can reach 11% [275]. Therefore, the variation in the dry density along the block was not considered sufficiently important to impact the performance of the block measured in the present work.

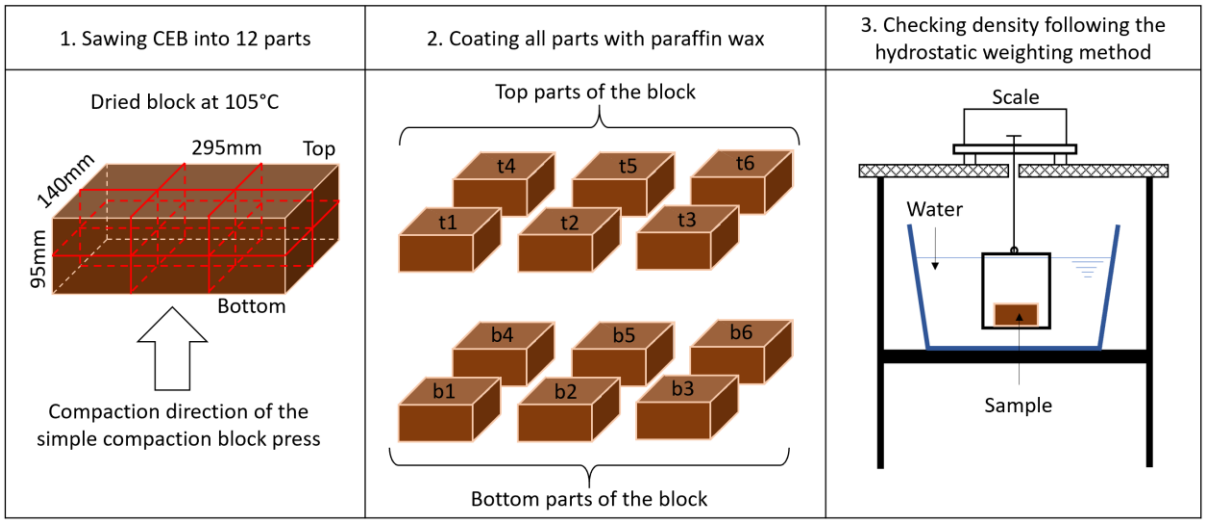

Figure 2.9. Schematic representation of the density-checking procedure of the blocks produced by the simple compaction press designed in this study.

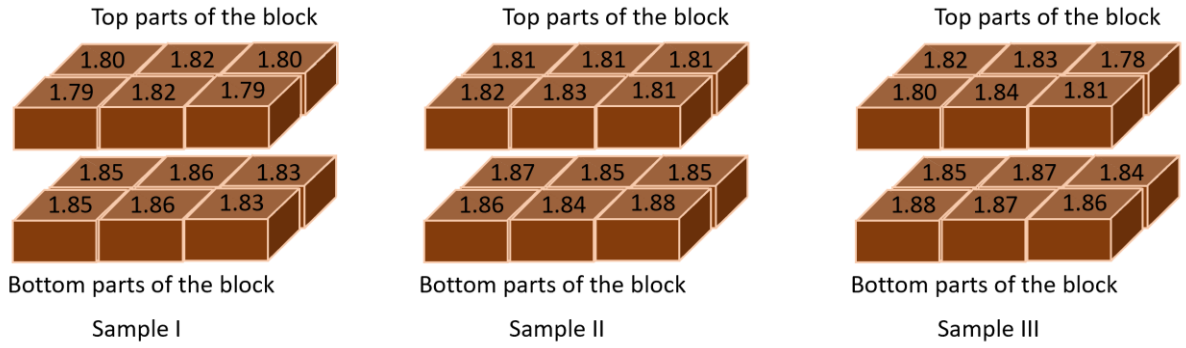

Figure 2.10. Results of the dry densities [g/cm^3] measured on earth DUS blocks compacted by the simple compaction block press.

2.4 Optimization of curing conditions

2.4.1 Motivation of this exploration

The employment of cement in compacted earth blocks requests and demands an effective curing method to obtain satisfactory performances (i.e., gain in strength and durability). In that regards, many practitioners propose covering stabilized compacted earth with waterproof plastic sheets for four weeks [283], a duration inspired from the familiar curing period of traditional cementitious materials. While other recommend keeping cement stabilized compacted earth in humid environment between one and four weeks before being dried in the open air and used for construction. In this context Rigassi V. has already compared in his manual of CEB's production [53] published in 1995 four conditionings of OPC's stabilized compacted earths: exposing to direct sun and wind, sheltering from direct sun and wind, covering with moist clothes and conditioning in relative humidity approaching 100%. He has demonstrated that the last method is the most effective when the dry compressive strength at 28 days is concerned.

So, it was necessary to define the same curing conditions for all samples after manufacturing. However, it was difficult to find at the beginning of the thesis a recent study that discuss curing method and that optimized duration of curing CSEB. Knowing that the performance of stabilized material will evidently depends on the curing conditions of samples. For these reasons, an attempt was made here to optimize initial curing conditions of CSEB.

To achieve this, the uniaxial compressive strength was used as a practical indicator to inspect dry compressive strength development at 28 days. Let recall here that cement stabilization is applied usually to increase the resistance of the material against water rather than to induce strength development as discussed in Chapter 1. But the choice of compressive strength as indicator of curing efficacy was made here for two main reasons. At first, unconfined compressive strength (UCS) is a common accepted property between practitioners and scientists. It is a basic measure of performance for compacted earth blocks, and it is practically the most important characteristic for design operations. It follows that there is an abundance of literature that examined factors affecting this parameter (like soil grading [93], [284]–[286], compaction energy [287], [288], moisture content and dry density [29], [30], [188]). The second reason is that UCS is measured through a test which will not impact the hardening process of cement (no variation of temperature and water content during the test), and the duration of the test (a few minutes) can reasonably be considered sufficiently low regarding curing period.

2.4.2 Method

2.4.2.1 Formulations

It was decided to conduct this part of the study on stabilized formulations made with both earths, DAG and STA, to verify if they behave in a similar manner with the curing duration. Unstabilized formulations (i.e., DUS and SUS) were used as reference formulations since strength of unstabilized material is not supposed to increase with initial moist curing conditions. Stabilized formulations concerned are those treated with 8% of CA, CB, CV and CM.

2.4.2.2 Curing

It consists of conditioning specimens obtained directly after casting in hermetic boxes where the relative humidity was maintained at 99.8% ± 0.2%RH. The boxes themselves were stored in air-conditioned room at 21˚C ± 2˚C. Moist curing duration was varied between 0 (no curing) and 21 days. After this stage, specimens were dried at 21˚C ± 2˚C and 50%RH ± 2%RH until the age of 28 days.

Specimen's masses were measured to ensure that drying did not occur during moist curing. All specimens had quasi-constant masses for the entire moist curing period (see Appendix C). The monitored masses indicate a rapid decrease in water content when samples were moved to drying conditions. Then, specimen moisture continued to decrease marginally until reaching an equilibrium state. The remaining water content in the unstabilized samples is linked to the water absorption ability of earth's mixtures in the drying conditions (21˚C and 50%RH).

In what follows, compressive strength measured after a drying period to constant mass at 21˚C/50%RH is termed as dry compressive strength, regardless of the initial curing conditions.

2.4.2.3 Testing

The uniaxial compressive strengths were determined at 28 days by applying a continuous loading at a steady rate of 0.02mm/s up to failure. Compressive strength of each sample was determined from its failure load and averaged cross-sectional area. Directly after the compression test, samples were sawn into three parts. The first part was crushed then dried by solution exchange method to arrest cement hydration at 28 days. This part of the sample was used for measurements of sorption isotherms and thermogravimetric analysis that will used in Chapter 3 as a tool for analyzing the impact of cement hardening on the material.

The second part was dedicated for porosity measurement. To do so, the sample was dried to a constant mass by the action of dry airflow at 21˚C inside a hermetic basket as schematized in Figure 2.11(d). It had been admitted that the water content of the entire sample is equal to the water content of each part of the sample. Thus, the "dry" mass of the entire sample (M_d) can be written in the following form:

$$M_d = \frac{M_i}{(1+w_1).(1+w_2)} \tag{2-1}$$

Where M_i [g] is the initial wet mass of the entire sample, w_1 [%] is the water content calculated with respect to the dry mass at 28 days and w_2 [%] is the remaining water content calculated with respect to the dry mass obtained after the second drying phase as shown in Figure 2.11 (b&d). The latter dried part of the sample was used to measure the skeletal volume (V_{sk}) with nitrogen pycnometer. Hence, the total porosity denoted $\emptyset$ was deduced from the relation between V_{sk} and the total volume (V_t) that have the form given in eq. (2-2):

$$\emptyset = 1 - \frac{V_{sk}}{V_t} \tag{2-2}$$

It should be noted that information provided by the pycnometer method was employed here for comparison purposes only and not for obtaining absolute values of sample's porosities.

The last part was conserved at 21°C/50%HR for analysis by scanning electron microscope (SEM) and X-ray diffraction (XRD). These analyses were performed in the laboratories of the

cement companies' members of the industrial partner of the thesis and were used for identifying the key chemical processes involved.

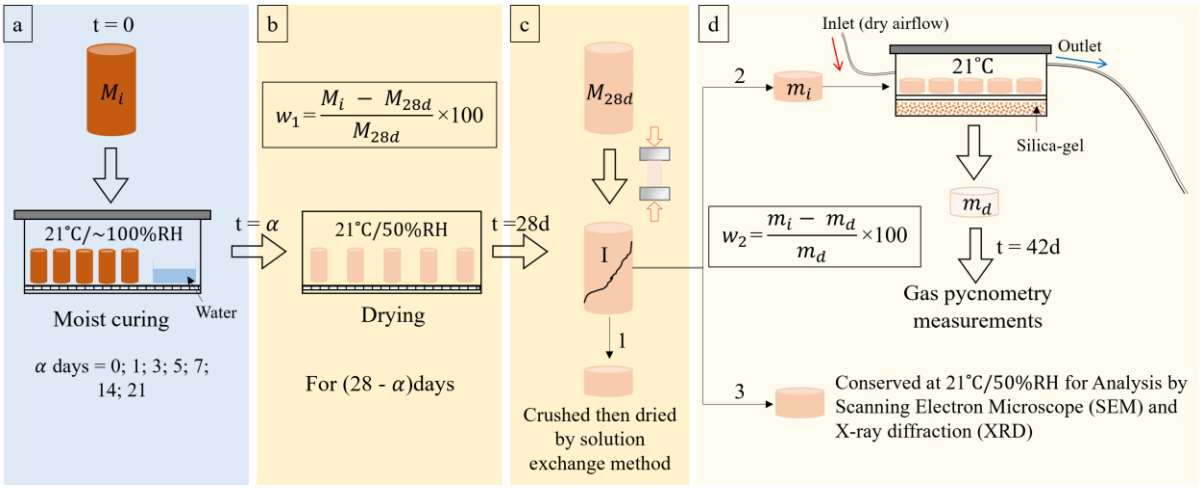

Figure 2.11. Illustration for the experimental campaign

2.4.3 Results

2.4.3.1 Influence of moist curing duration on the dry UCS

For comparison reasons, results will be presented in this section as normalized values as given in (2-3):

$$\text{Relative strength} = \frac{\text{UCS}_{\text{Stab}}}{\text{UCS}_{\text{Unstab}}} \quad (2\text{-}3)$$

Where UCS_{Stab} [MPa] and $\text{UCS}_{\text{Unstab}}$ [MPa] are the compressive strengths of stabilized and unstabilized earth, respectively.

Results shown in Figure 2.12 and Figure 2.13 indicate clearly that strength development was affected by the moist curing duration. Firstly, it appears that moist curing remains beneficial until 7 days, regardless of earth-cement combination. Thereafter, strength improvement becomes relatively negligible with respect to curing duration for all formulations. Another detail in these observations is that DA8 and SA8 are the formulations the most impacted by moist curing duration. A significant increase of strength by 50% and 32% were recorded between 0 and 7 days for DA8 and SA8, respectively. For all other formulations, the income of moist cure is less important with an average increase of 15% between 0 and 7 days. Consequently, it could be assumed that the more the cement contains clinker, the better will be the effect of curing duration on the compressive strength at 28 days Result of pycnometer measurements presented in Figure 2.14 revealed an apparent porosity in line with compressive strength obtained after different curing durations: the porosity tends to decrease with increasing curing duration.

Brief investigations on the effect of curing consisting of sealing samples can be found in [157]. In the latter study, authors have varied curing period between 0 (no curing), 7 and 21 days to choose an appropriate conditioning for their studied materials. Despite that CEM I 52.5 R was used as stabilizer, which is a cement rich in clinker (95%-100%), the increase in the dry compressive strength from 0 to 21 was about 10% only. Authors demonstrated that the effect

of this curing method was most notable on the wet compressive strength, which was not possible to be measured before 7 days of curing.

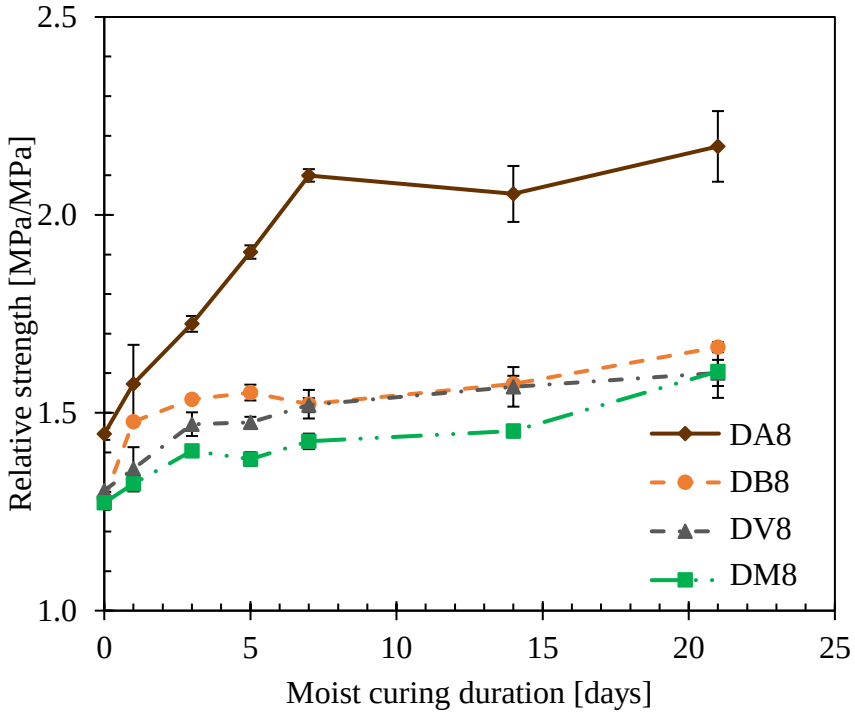

Figure 2.12. Impact of moist curing duration on the dry compressive strength of DAG earth with respect to cement type

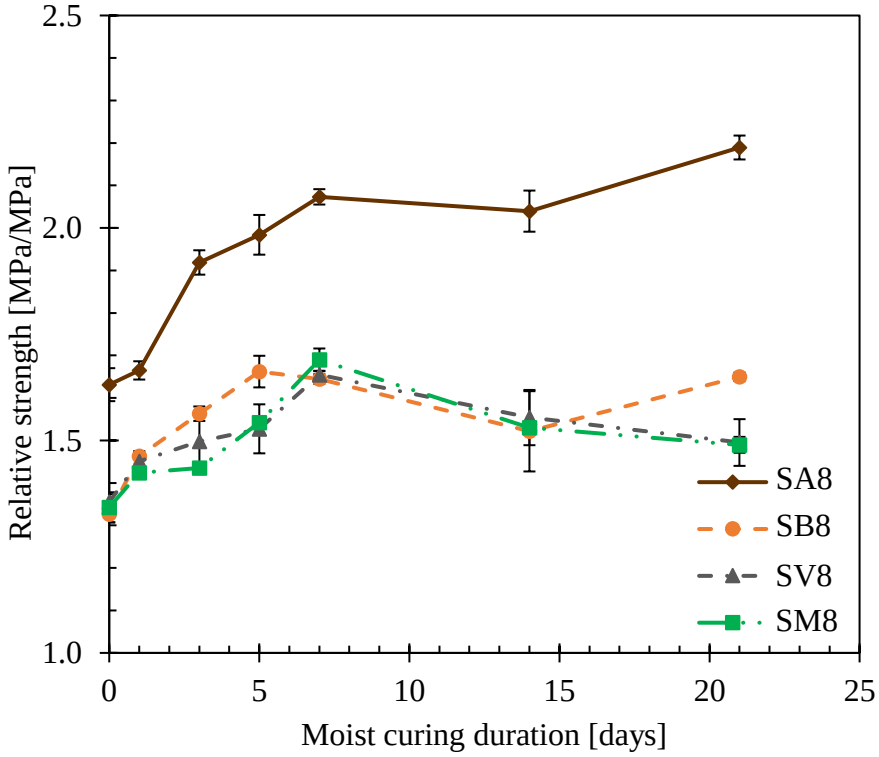

Figure 2.13. Impact of moist curing duration on the dry compressive strength of STA earth with respect to cement type

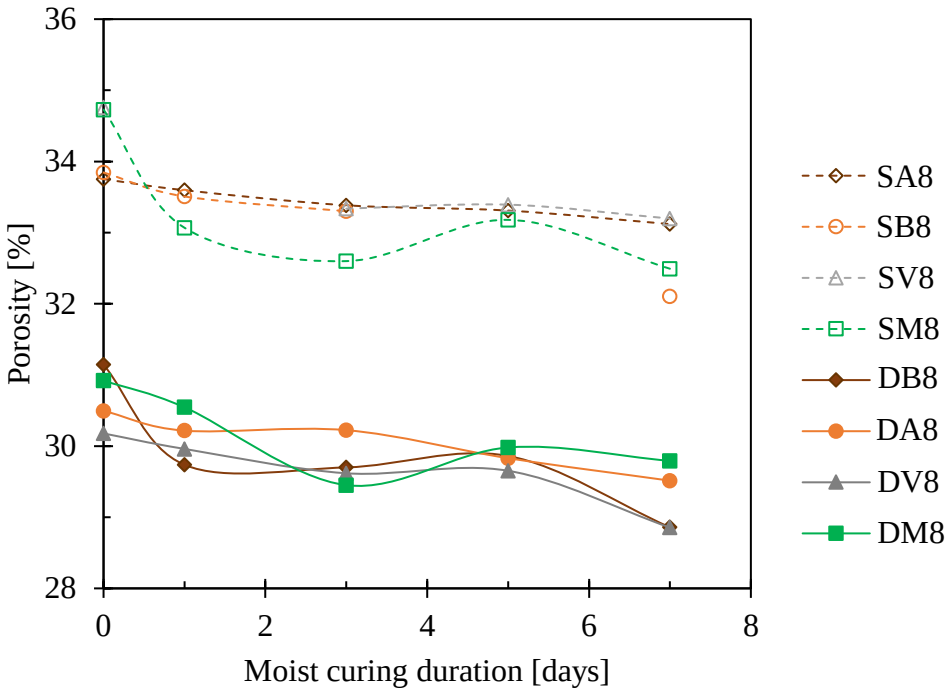

Figure 2.14. Evolution of the apparent porosity of stabilized earth samples in function of moist curing duration

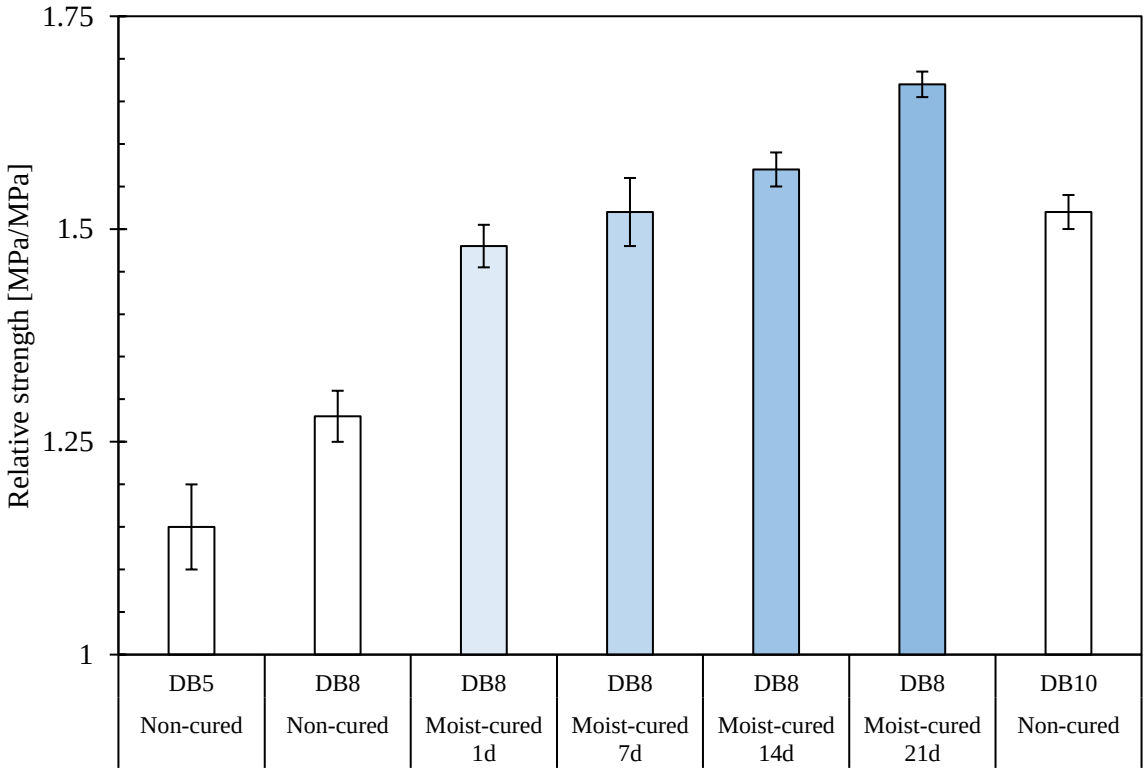

Figure 2.15. Dry strength on 28 days of DAG earth stabilized with 5, 8 and 10% of CB cement.

Nonetheless, the effect of sealing samples remains less significant than the moist curing applied in the present study. In this respect, Rigassi V. has already compared in his manual of CEB's

production [53] published in 1995 four conditionings of OPC's stabilized compacted earths: exposing to direct sun and wind, sheltering from direct sun and wind, covering with moist clothes and conditioning in relative humidity approaching 100%. He has demonstrated that the last method is the most effective when the dry compressive strength at 28 days is concerned.

Besides, and in the aim of insisting on the importance of initial moist curing, DAG samples stabilized with 5 and 10% of CB cement were tested dry at 28 days without being initially cured. Firstly, and as expected, results presented in Figure 2.15 show that dry compressive strength increase with increasing cement dosage. But the important indication of these results is that non-cured DB10 samples reached lower strength values when compared to those recorded by DB8 after curing. These results led us to look at curing from an "ecological" perspective. Since boosting strength through curing in humid environment is more attractive than increasing cement dosage. To that end, it is noteworthy that a correct curing should not be overlooked when employing cement as stabilizer.

2.4.3.2 Microstructural explanation of curing conditions

The manufacturing water content of cement stabilized earth blocks is usually not sufficient to meet the needs of cement, which compete with the clays present in the soil. The moist curing prevents loss of water and brings a continuous source of moisture for the sample, which enhance the chance of cement hydration. But anyhow, a fully hydrated cement is not possible, even in concrete mixtures. That is why cement is not usually used at its best level in stabilized compacted earth. This evidence had been manifested in the present study by a stagnation tendency of the compressive strength despite the availability of free water for three weeks. It seems that cement achieves an optimal hydration's degree during the first few days of moist curing. To verify these assumptions, scanning electron microscopy (SEM) was performed on the 7-days cured samples after 18 months of the compression test. Let recall that during this period, samples were conserved at ambient conditions of temperature and relative humidity.

Examples of the SEM images of stabilized DAG and STA earths are presented in Figure 2.16. Observations of 6 different blocks of compacted earth stabilized with different types of cements show heterogeneous microstructures. No major difference in microstructure can be observed for samples made of the same earth but stabilized with different cements. Going into detail, samples stabilized with CA (Figure 2.16 – a, b) seem to show smaller and more numerous cement grains than the samples stabilized with CB (Figure 2.16 – c, d). For samples stabilized with masonry cement (Figure 2.16 – e, f) a lower proportion of cement grains can be observed. These observations justify the highest compressive strength of samples stabilized with CA. On the opposite, noticeable differences can be observed between the two earths. In particular, all the blocks made with DAG earth (Figure 2.16 – a, c, e) seems to have a higher proportion of pores of sizes ranging between 20µm to 200µm than STA ones (Figure 2.16 – b, d, f).

Another remarkable feature in this analysis is that all the samples show numerous cement grains that are still anhydrous (in white color). The small-sized grains of cement are completely hydrated but the larger-sized grains of cement (equal to or greater than approximately 50µm) are partially hydrated. This issue could be observed clearly on Figure 2.17 that shows a partially hydrated cement grains where hydrated cement pastes engulf and encapsulate the core of the grain that remain anhydrous. These observations provide a useful information concerning the understanding of the stagnation tendency of compressive strength after 7 days of moist curing. It appears that the formed cement hydrates tend to block a part of cement particles inside its impermeable matrix, which prevent water accessibility. Therefore, the moisture availability

after the very first days seems to be useless comparing to its active contribution to strength development.

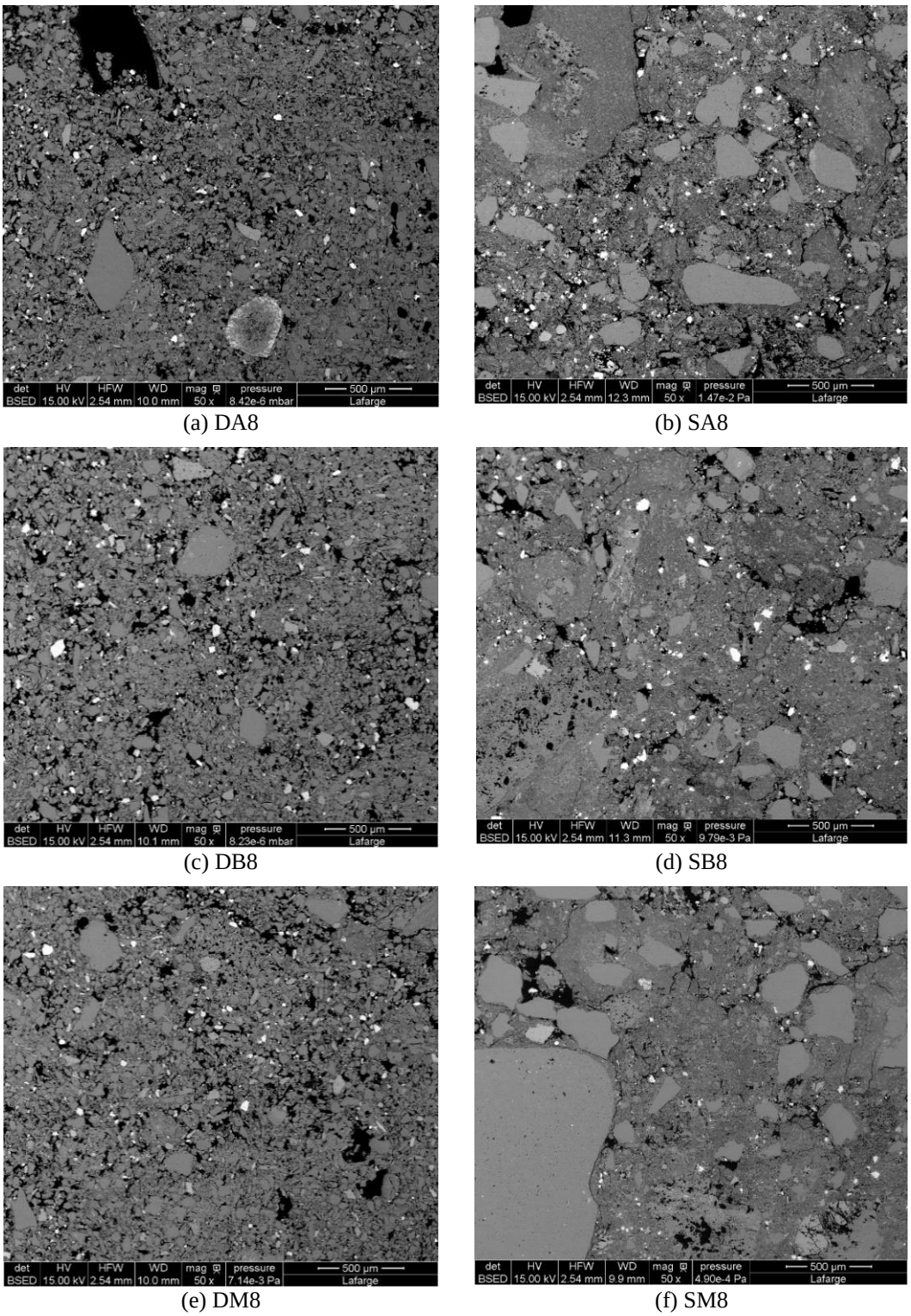

(a) DA8 (b) SA8

(c) DB8 (d) SB8

(e) DM8 (f) SM8

Figure 2.16. Microstructure of stabilized samples made with DAG (left) and STA (right) earths after 18 months of the compressive strength test.

However, we are not yet at the level to generalize this finding because longer moist curing conditions were not performed (i.e., several months or even several years). It was not planned

in this work because a curing duration of more than several weeks is obviously outside the range of optimization. The point here is simply that regular curing duration of 28 days could be reduced without really losing strength capacity of the product. Anyhow supplementary investigations are required to inquire further into the mechanism that dominant kinetics rate of hydration in stabilized compacted earth, which is the diffusion of free water through the layer of hydrates.

It is eventually important to mention that linking morphological properties of cement pastes microstructure to the evolution of concrete mechanical properties was the subject of many studies (cf. [289], [290] and references therein). However, this subject is not yet deeply analyzed in cement stabilized compacted earth. For this latter, the presence of clay (in term of type and quantity) could strongly affect hydration process, notably due to their strong specific surface area and their high affinity with water molecules. It follows that, even if the present study gives some ways forward, further investigations are needed to conclude on the link between microstructure and stabilization effectiveness.

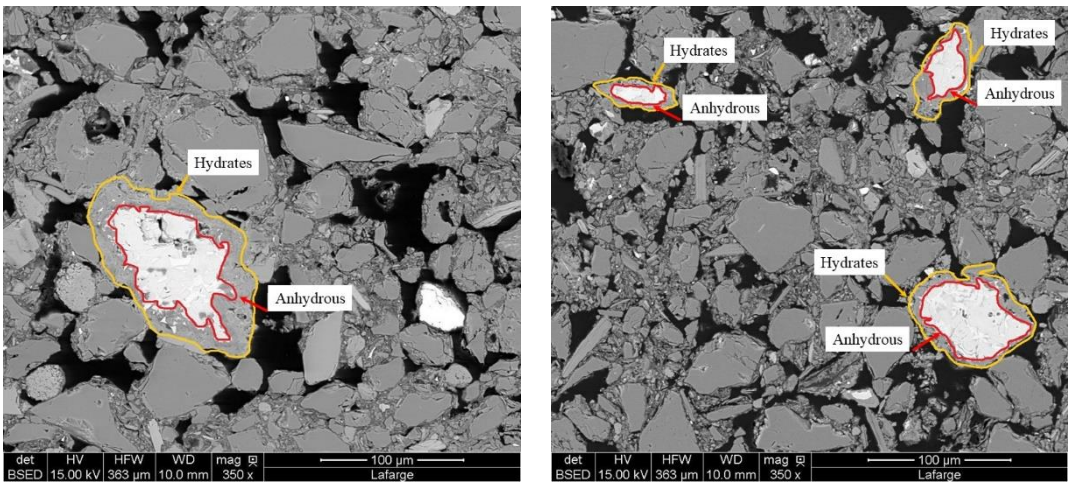

(a) DB8 (b) DM8

Figure 2.17. SEM figures (mag ×350) of DB8 and DM8 after 18 months of the compressive strength test.

2.4.4 Discussion on the effectiveness of curing

The hydration phenomenon in cement-based materials, such as pastes, mortars and concretes, is a thermo-activated process [291]–[293]. An elevated curing temperature between 40˚C and 100˚C can accelerate both pozzolanic and hydration reactions leading to achieving greater compressive strength at the early ages. Therefore, to go one-step further with the interpretation of the results, it would be useful to take a brief look at the role of elevated curing temperature in developing strength in cement stabilized compacted earth. To do so, DB5 samples were subjected to initial curing at 60˚C in moist and normal conditions of humidity as summarized in Table 2-5. Curing conditions. Initial curing in moist environment at ambient temperature (C-Ref.) was considered as a reference curing method based on the above findings and DUS was used as a reference formulation.

Strength variations with curing conditions presented in Figure 2.18 indicate that elevated temperature is not sufficient for proper strength development at 28 days, where stabilized samples show a 20% lower strength than the unstabilized ones. The major cause behind this reduction is the shortage of the inner water present in the samples, which prevent cement

hydration. Likewise, the dominant effect of moist curing was reinforced by the minor increase in strength between C-Ref. and C-T.H., which emphasize again that strength development in cement stabilized earth block is principally controlled by the moisture availability.

Against the best outcome of C-T.H., let recall that curing cement-based materials at elevated temperature can lead to a lowering of strength at the later ages (usually above 28 days) because of the unsuitable arrangement of hydrates during accelerate hydration, which is called crossover effect [294], [295]. This phenomenon was observed for example by Sajedi and Razak [296] in compressive strength of OPC mortars at the age of 56 and 90 days after 20 hours curing in bath water heater at 60˚C. In the same context, Teixeira *et al*. [297] observed more uniformly distributed hydration products on SEM images of cement pastes cured at room temperature than on those cured at 60˚C. Accordingly, it could be admitted that C-T.H. is serving the 28th day compressive strength at the cost of the long-term performance of the product. However, strength after 28 days was not measured in this work to validate this hypothesis. Nevertheless, this examination insists once more on the moist curing approach as an optimized method for cement stabilized compacted earth.

	C-T.	C-N.	C-Ref.	C-T.H.
Initial curing (2 weeks)	60˚C/50%RH	21˚C/50%RH	21˚C/99.8%RH	60˚C/99.8%RH
Conditioning until the 28th day	21˚C/50%RH		21˚C/50%RH	21˚C/50%RH

Table 2-5. Curing conditions

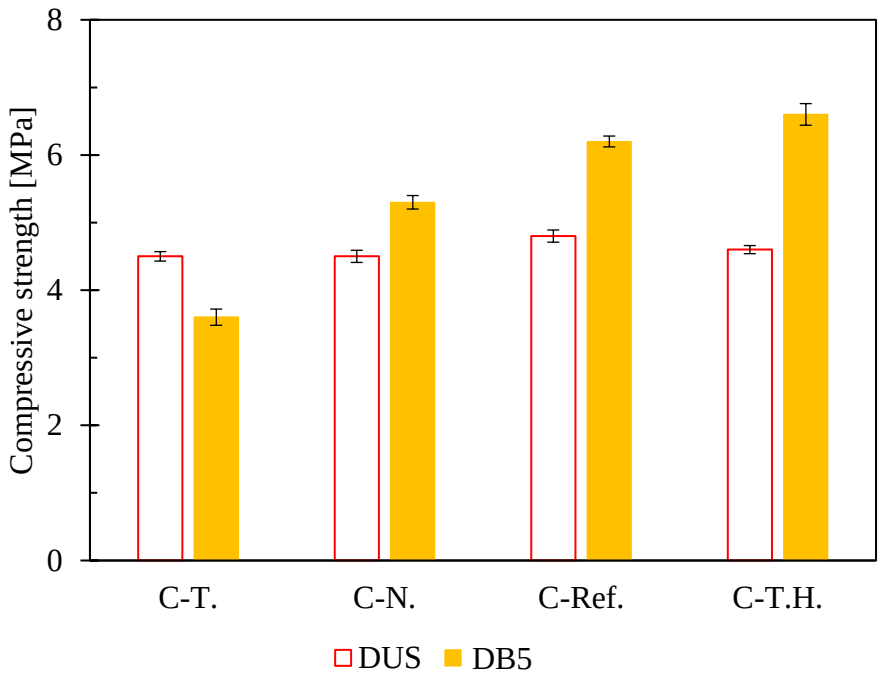

Figure 2.18. Variation of the dry compressive strength at the age of 28 days with respect to curing conditions.

2.4.5 Conclusion

In this chapter, the contribution of curing conditions to improving strength of cement stabilized compacted earth was addressed. The focus was made on evaluating the effectiveness of the duration of moist curing, consisting of conditioning samples in moist environment (∼100%RH) at ambient temperature (21˚C). The duration of moist curing was varied between 0 (no-curing) and 21 days. It had been demonstrated that moist curing at ambient temperature is beneficial for strength development until 7 days based on the 28^{th} day dry compressive strength. The stagnation tendency of compressive strength after 7 days of moist curing was justified by the detection of numerous partially hydrated cement grains on SEM images of stabilized DAG and STA. The water accessibility was prevented by the formed hydrated cement pastes that engulfed and encapsulated the core of the grain that remain anhydrous. Thus, hydration process was slowed down, which explained why no significant improvement in compressive strength was recorded after 7 days.

On the other side, the effectiveness of moist curing was discussed on the light of the effect of accelerated curing temperature of 60˚C in moist (100%RH) and normal conditions (50%RH) of relative humidity. The obtained results supported the moist curing method.

Finally, and based on the outcomes of this chapter, all samples that will be tested in the remaining parts of the work will be cured in humid environment at 21°C/∼100%HR for 7 days after demolding.

Chapter 3. Performance of cement-earth mixtures

3.1 Introduction

In the above chapter, it had been demonstrated that moist curing influences the dry compressive strength of DAG and STA in a similar way. No significant differences were observed in the gain in dry compressive strength after stabilization with 8% cement with CA, CB, CV, and CM.

However, dry compressive strength could not be used alone as a performance indicator to judge the efficacy of treating earthen materials with cement when the product is destined for building construction applications. In this chapter, the performance of different cement-earth mixtures is evaluated by considering three different aspects of the compacted product. Firstly, the compressive strength was reconsidered for the analysis. But here strength was evaluated in wet and dry conditions and by varying cement dosages between 5 and 8%. Secondly, the hygroscopic properties are assessed. Thirdly, the durability towards water is addressed.

Thereafter, microstructural analysis of cement-earth couples was made to investigate chemical impact of cement on the two earths. Lastly, a discussion was made on factors influencing cement stabilization efficacy based on cement and earth properties.

3.2 Evaluation of cement-earth mixture's performance

3.2.1 Compressive strength

3.2.1.1 Testing conditions

Compressive strengths of the samples were measured in wet and dry states. Based on the results of the previous chapter, sample conditioning for dry compressive test measurements has consisted in 7 days of moist curing followed by 21 days at 50% ± 2%RH and 21˚C ± 2˚C.

Sample conditioning for wet compressive strength has consisted in 28 days of moist curing (that is at 99.8% ± 0.2%RH and 21˚C ± 2˚C). It follows that wet samples are not saturated, but they are close to their endogenous saturation. For the record, sample water content was checked after each uniaxial compression test.

3.2.1.2 Results

Results obtained in dry and wet conditions at 28 days for all the tested formulation are presented in Table 3-1. To ease the data analysis, results are presented in terms of relative strengths as a function of cement dosage in Figure 3.1 for the dry condition and in Figure 3.2 for the wet condition. We recall that the relative strength, which is defined by the relation (2-3), as the ratio of stabilized over unstabilized unconfined compressive strengths from samples with identical curing conditions.

The first remarkable result is that a kind of hierarchical relation exits between relative strengths and cements. As expected, CA improved the resistance of samples with the highest action. No clear difference is observed between CB, CV, and CM. And finally, CP seems to provide the lower results.

Another clear point is that the effect of increasing cement dosage is more significant for DAG than STA earth. For this latter, there is hardly any improvement in strength between 5 and 8% cement.

	Cement type	Cement dosage	DAG		STA	
			Wet UCS [MPa]	Dry UCS [MPa]	Wet UCS [MPa]	Dry UCS [MPa]
Unstabilized	-	-	0.614	3.572	0.992	2.239
Stabilized	CA	5	3.462	4.696	2.668	4.362
		8	4.319	7.733	2.649	4.648
	CB	5	3.166	4.540	2.441	3.983
		8	3.435	5.459	2.117	3.684
	CV	5	1.881	4.248	2.006	3.587
		8	2.733	5.451	2.135	3.706
	CM	5	1.796	3.683	2.685	3.253
		8	2.397	5.122	2.030	3.783
	CP	5	1.308	3.026	1.611	3.108
		8	1.465	3.510	1.617	3.365

Table 3-1. Summary of the average dry and wet UCS of DAG and STA formulations

If we look on results in dry condition, the strength increase induced by stabilization appears to be more important for STA than for DAG. It can be even noticed that the dry strength of DAG earth samples stabilized with CP give a slightly lower resistance than unstabilized ones (relative strength between 0.8 and 1).

Note that stabilization with CP requires adding initial setting retarder, like citric acid, to fabricate samples in good conditions, which was not done here. Knowing that citric acid is effective in low concentrations and it has a retarding effect on the hydration in the system C_3A–gypsum–portlandite–water and C_3S [298]. It enables extending the initial setting time of CP to 30 minutes approximately at 20°C. The determination of an "optimum" dosage of citric acid is therefore desirable and/or required. In Figure 3.3, the evolution of wet UCS at 7 days of DP8 with citric acid dosage is presented. It indicates an increase by about 20% in UCS between 0 and 1% of citric acid. This increase was considered low with respect to citric acid dosage added. On the other hand, there is a possibility that samples stabilized with CP requires higher water content than other cements. However, here the samples were prepared at their optimum water content. After discussion with the industrial partner on these points, it was concluded that stabilization with CP requires further specific research that was found to be out of the scope of this study.

Now if we look on results in wet conditions the improvement in compressive strength due to stabilization appears to be significantly more important for DAG samples than for STA ones (Figure 3.2). One explanation of this behavior may be the higher clay content of STA. Indeed similar behavior had been expressed by OPC stabilized earth blocks tested in [299], where increasing the clay fraction of the soil was accompanied by a reduction in the saturated compressive strength.

To sum up, compressive strength results underlined a significant difference in behavior between dry and wet conditions. While the strength development due to stabilization appears to be higher for STA samples in dry conditions, the opposite is observed in wet conditions. To go further on this point, we will now analyze the ratio between wet and dry compressive strengths.

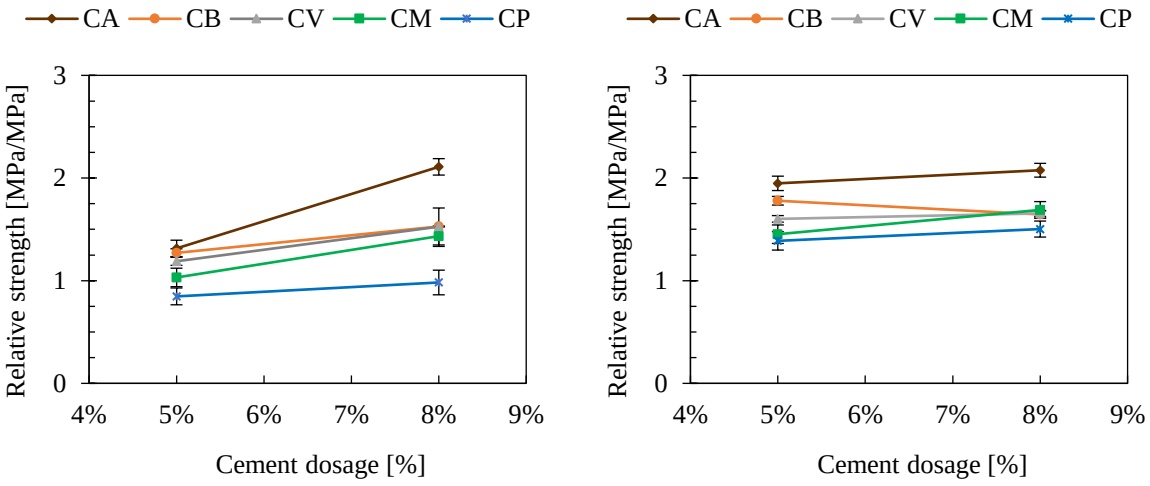

(a) DAG (b) STA

Figure 3.1. Relative 28-days dry strength of DAG and STA formulations stabilized with 5 and 8% cement by dry mass of earth.

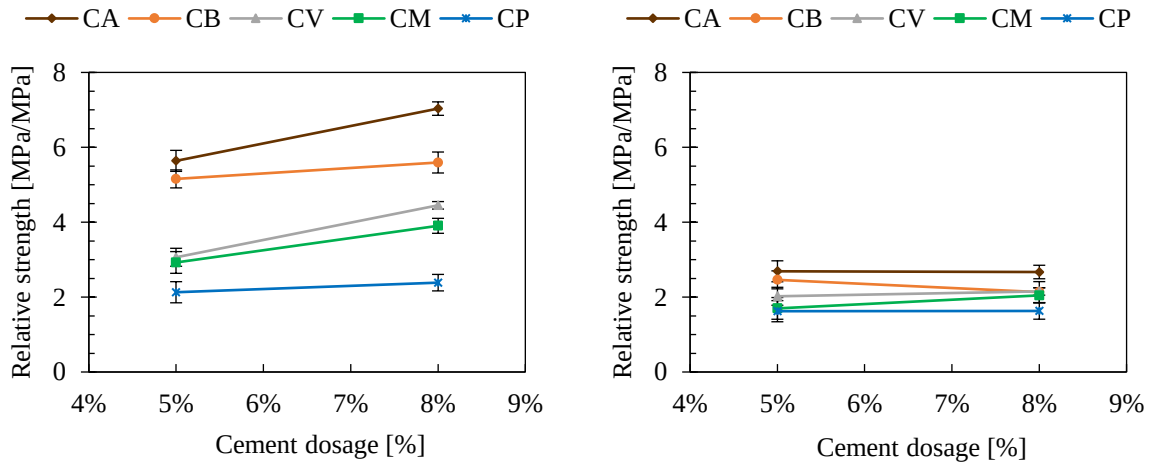

(a) DAG (b) STA

Figure 3.2. Relative 28-days wet strength of DAG and STA formulations stabilized with 5 and 8% cement by dry mass of earth.

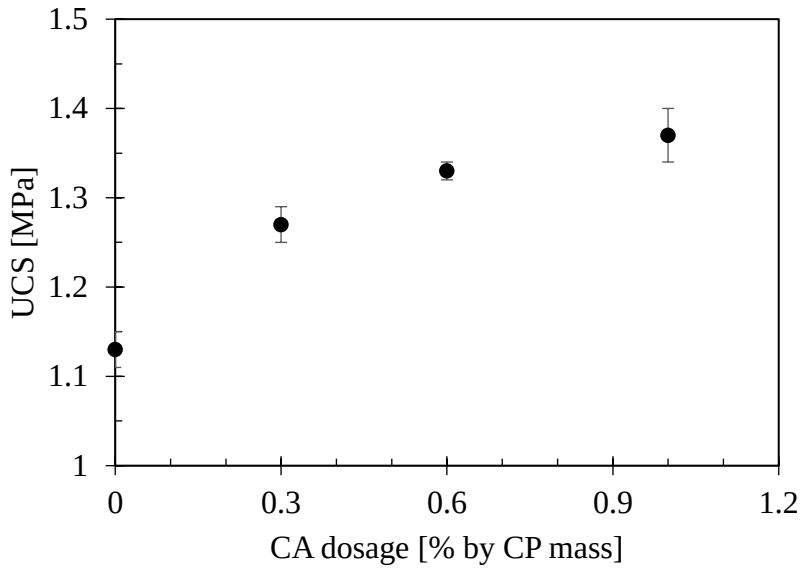

Figure 3.3. Influence of citric acid dosage on wet UCS of DP8 measured at 7 days

3.2.1.1 Analysis of the wet to dry strengths ratio

The wet to dry strengths ratio of stabilized earth blocks is commonly used to have a first insight of their durability against water. A minimum saturated and dry strengths of 1MPa and 2MPa, respectively, and a minimum saturated to dry strength ratio of 0.5, are sometimes used as reference values [224]. However, contrary to what is done here, wet strength should be measured on samples soaked for 24-48 hours in water and dry strength on 60°C-dried samples. Anyway, literature related to this field shows that there is no consensus on a unified testing method of strength. Depending on authors, sample geometry, definition of "saturated" and "dry" strengths may vary. Thus, rather than considering this strength ratio as an indicator of durability (this latter will be assessed in §3.2.3 and in Chapter 4), we will use it as a tool to sketch stabilizer efficiency, as it is supported by different authors [224], [225], [300].

Results of wet to dry strength ratio of DAG and STA formulations are presented in Figure 3.4. At first, stabilization leads to a noticeable increase of wet to dry ratio of DAG formulations, from 0.2 for unstabilized sample to 0.4-0.7 for stabilized ones. In case of STA, the values lie between 0.5 and 0.6 whatever the tested formulation. Another interesting point is that the increase of cement content does not seem to increase this ratio, and it may even reduce it (for example DA5 vs. DA8 and DB5 vs. DB8). In other terms, it means that in these cases the increase of cement content lead to a higher development of the dry strength than the wet one. One of the possible consequences of this result is that if the goal of the stabilization is to increase the wet strength, but not necessarily the dry one, a moderate to low cement content might be sufficient, even if it does not produce a significant increase in dry strength. In other words, the "optimum cement content" might be lower for wet strength development than for dry strength one.

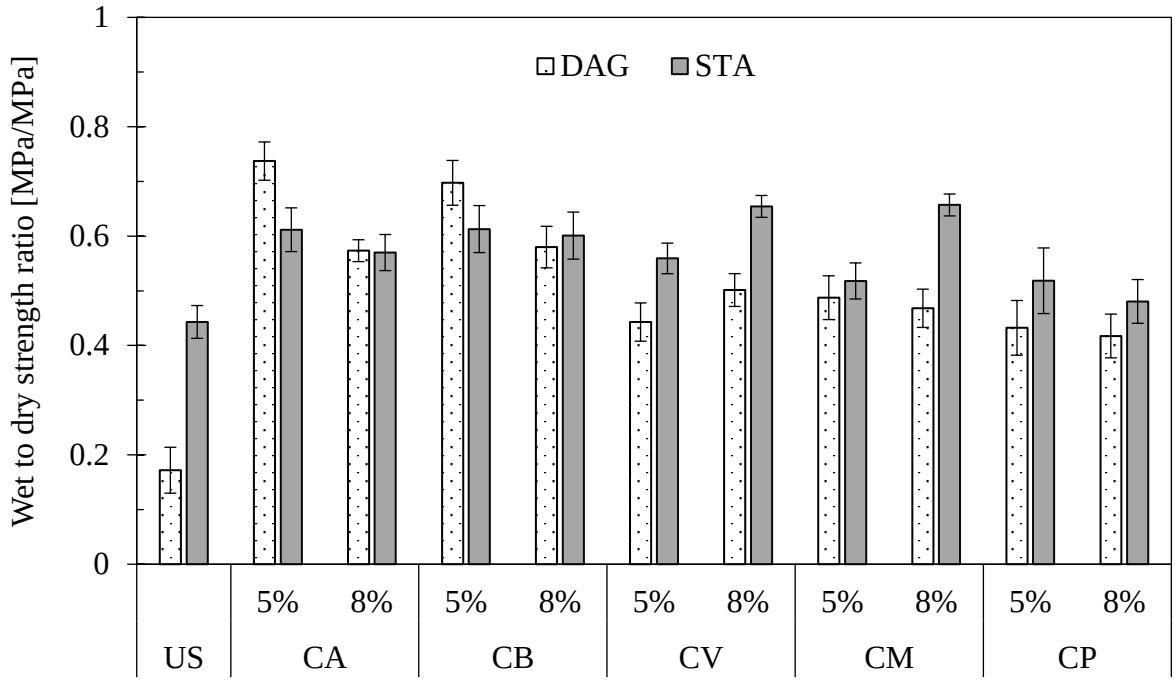

Figure 3.4. Wet to dry strength ratio [MPa/MPa]

3.2.2 Hygroscopicity

3.2.2.1 Introduction

Since the hygroscopic character is an important asset of earthen materials, the question of its preservation after stabilization is crucial. For that purpose, the impact of stabilization on key parameters that drive the hygroscopic behavior, namely sorption-desorption isotherms and water vapor permeability (cf. chapter 1) were determined.

3.2.2.2 Sorption-desorption curves

a. Measurement method

The dynamic gravimetric sorption DVS method was used to estimate the isothermal sorption-desorption curves of the materials of the study. Measurements were made on a part sawn from samples used for compressive strength testing dried following solvent replacement method (cf. D).

b. Results

Sorption-desorption isotherms of DUS and SUS and corresponding stabilized formulations with 8% cement are displayed in Figure 3.5 and Figure 3.6. As expected, the sorption isotherms have a S-shape corresponding to the type II in the IUPAC classification, which is generally the case of building materials [301]. This type of isotherm is characterized by a progressive increase of the adsorbed water layer [302] with the final sharp increase corresponding to pore filling through capillary condensation.

Isotherm curves show that stabilized formulations adsorb considerably less water in comparison with the unstabilized ones. The impact of the stabilization is more important for the DAG earth than the STA earth. The addition of cement reduces the equilibrium moisture

content over the whole range of relative humidity. But the most remarkable difference in the absorbed water between stabilized formulations of the two earths can be seen at relative humidity levels higher than 90%. In this range, the absorbed water by DAG formulations after stabilization is reduced by about a half. While stabilized formulations made with STA present an average reduction of 15% only.

All formulations exhibited a very similar behavior with a relatively small shift between sorption and desorption curves, called hysteresis. This effect is more or less important depending on the materials and it is commonly observed for building materials like wood [303], [304], hemp concrete [305], [306], concrete [307]. The obtained curves are consistent with which is commonly observed in the literature for earthen materials [221], [308], [309].

The hysteresis between adsorbed and desorbed water content is plotted in function of the average relative humidity of DAG and STA formulations in Figure 3.7 and Figure 3.8, respectively. For DAG earth, it appears clearly that the hysteresis is higher for stabilized formulations than the unstabilized in the range of relative humidity lower than 60%. Between 60 and 80%, the hysteresis of DUS becomes higher than DA8 and DB8 but it remains lower than that of DV8 and DM8. Beyond this range, the hysteresis of DUS becomes higher than all stabilized formulations. In addition, the hysteresis of DUS increase linearly with the relative humidity in the range 30%-80%. In the same range, the hysteresis of stabilized formulations is quite stable.

For STA earth, the hysteresis of stabilized and unstabilized formulations are relatively similar. A remarkable difference can be noticed at high relative humidity (88%) where SUS recorded higher hysteresis than SA8 and SB8. In addition, the hysteresis increases with increasing the relative humidity in the range 30%-80% for all formulations and reach its maximum at high relative humidity (88%).

Now let look at the hygric capacity (ξ) that could be calculated from the average slope between 30% and 80%RH, given that the realistic hygrometry cycles in buildings commonly do not exceed 80% RH and do not go below 30% RH. We recall that de definition of ξ is given by the relation (1-6) in Chapter 1.

The calculated values of DAG formulations from the sorption and desorption isotherms curves presented in Figure 3.9 show that samples lost approximately half of their hygric capacity after stabilization. The gap between $\xi_{sorption}$ (hygric capacity calculated from the adsorption curve) and $\xi_{desorption}$ (hygric capacity calculated from the desorption curve) of DUS (23 kg/m^3) is more important than that of stabilized formulations (5-9 kg/m^3). Results show also that DV8 and DM8 have a slightly higher capacity to absorb relative humidity than DA8 and DB8.

The reduction in the hygric capacity after stabilization is less important in case of STA. Figure 3.10 show a reduction between 30 and 40% between SUS and stabilized formulations. In addition, the variation between hygric capacities calculated form the sorption and desorption curves are of the order of 12-15 kg/m^3 for all formulations. These results give information about the action of cement on the two earths, that appear to be more important on DAG earth.

To explain the difference in hygric capacity between DUS and SUS, the cation exchange capacity was measured with the cobaltihexamine chloride method. It was found equal to 11.5 meq./100g for DUS and 4.8 meq./100g for SUS, which could explain the highest hygric capacity calculated for DUS. As for stabilized formulations, it appears that mixtures made with both, DAG and STA, range in the same interval. It seems that the decrease in hygroscopicity

of the mixture in the middle range of isotherm curves becomes representative of the binder rather than the earth.

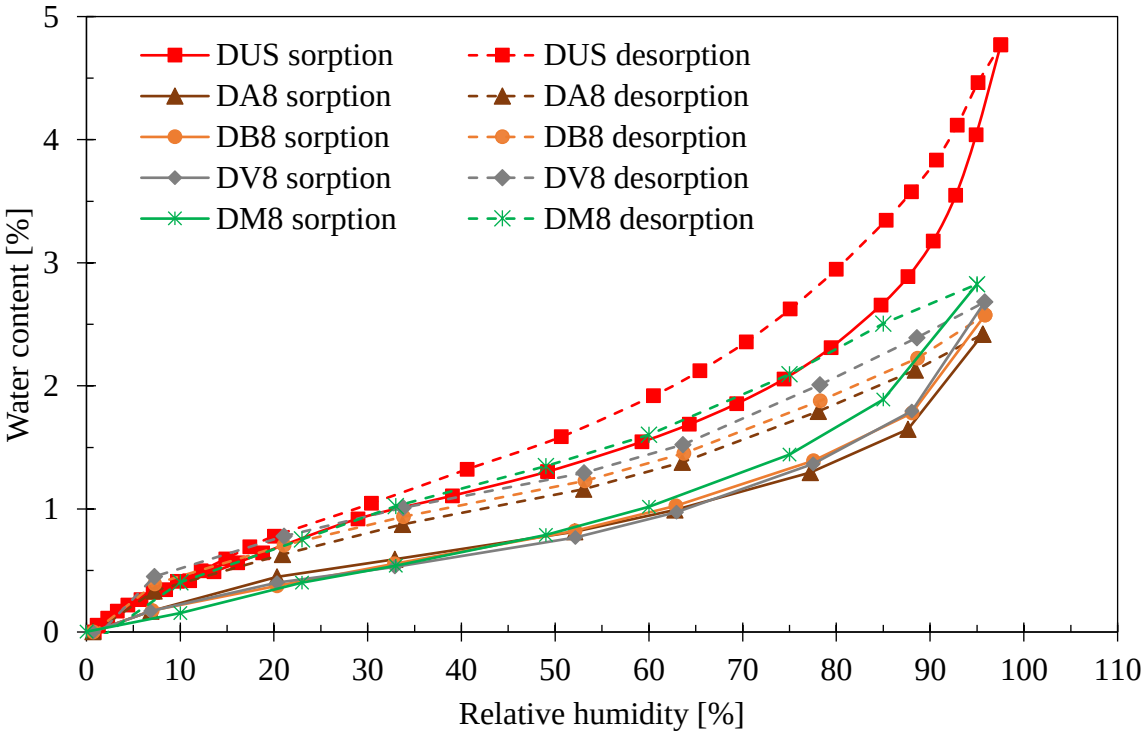

Figure 3.5. Sorption-desorption isotherms of DAG formulations

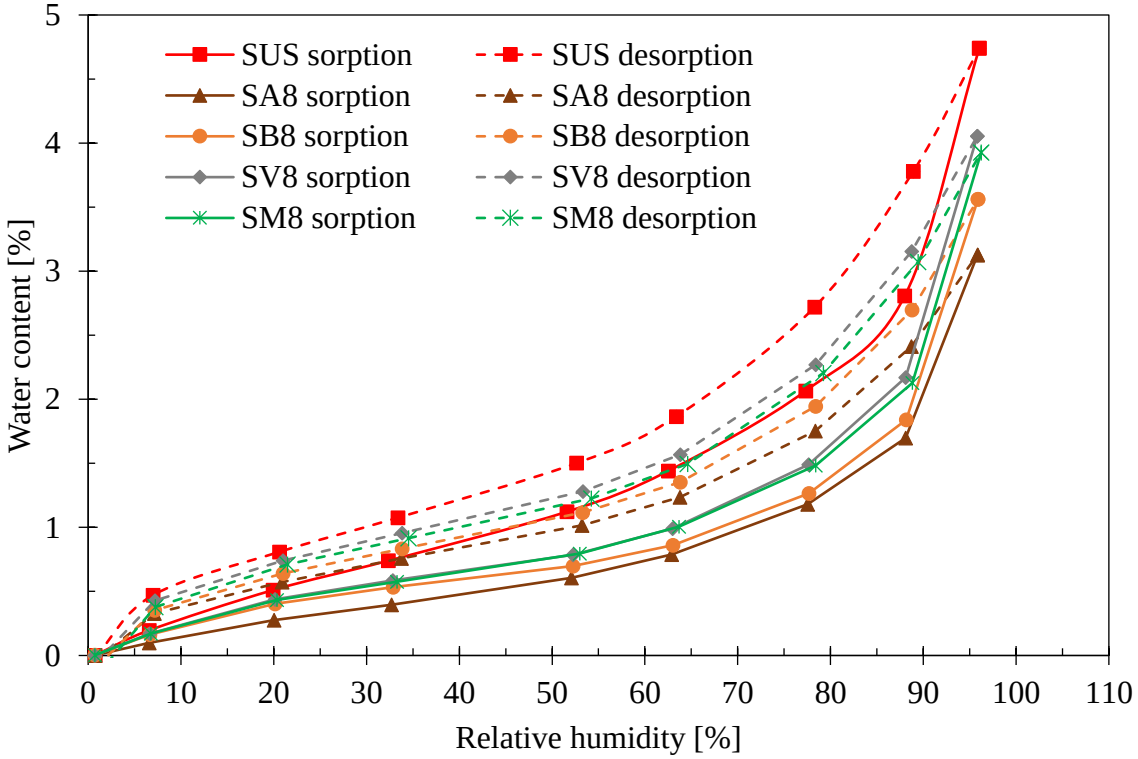

Figure 3.6. Sorption-desorption isotherms of STA formulations

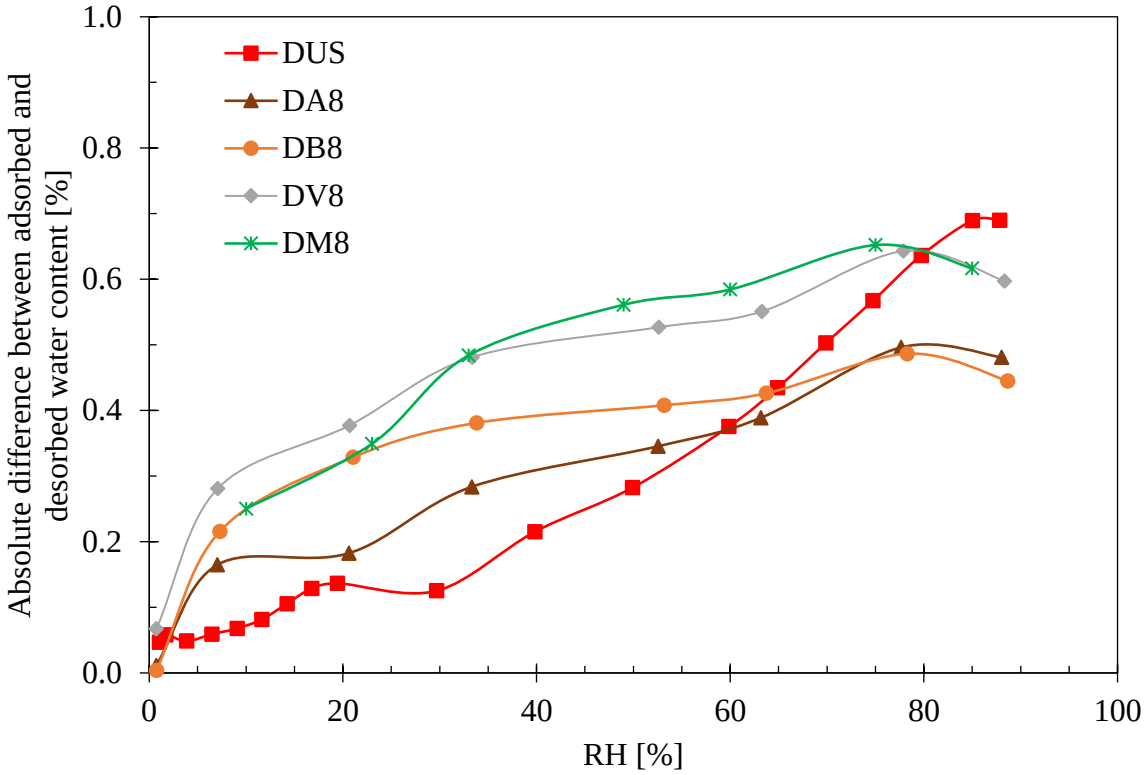

Figure 3.7. Hysteresis between adsorbed and desorbed water content in function of relative humidity of DAG formulations

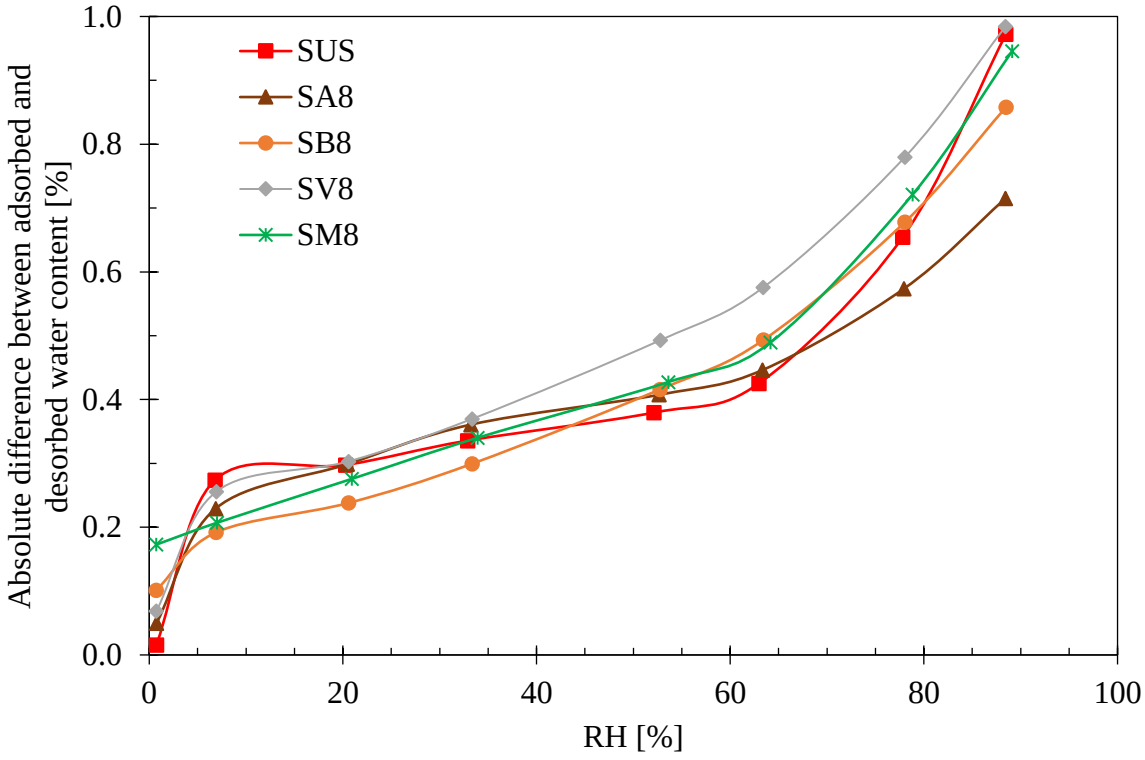

Figure 3.8. Hysteresis between adsorbed and desorbed water content in function of relative humidity of STA formulations

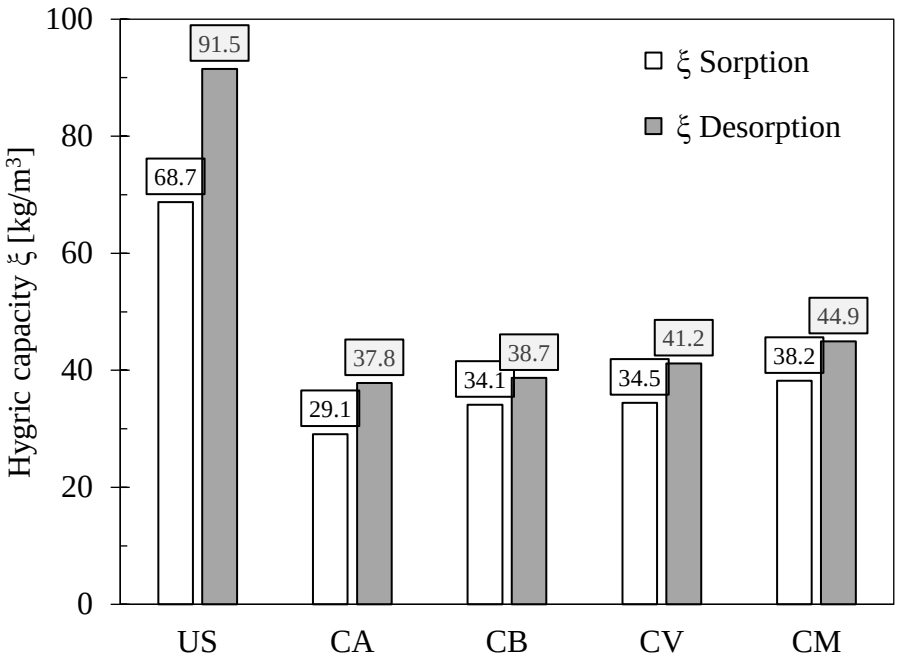

Figure 3.9. Average hygric capacity calculated between 30% and 80%RH of DAG formulations

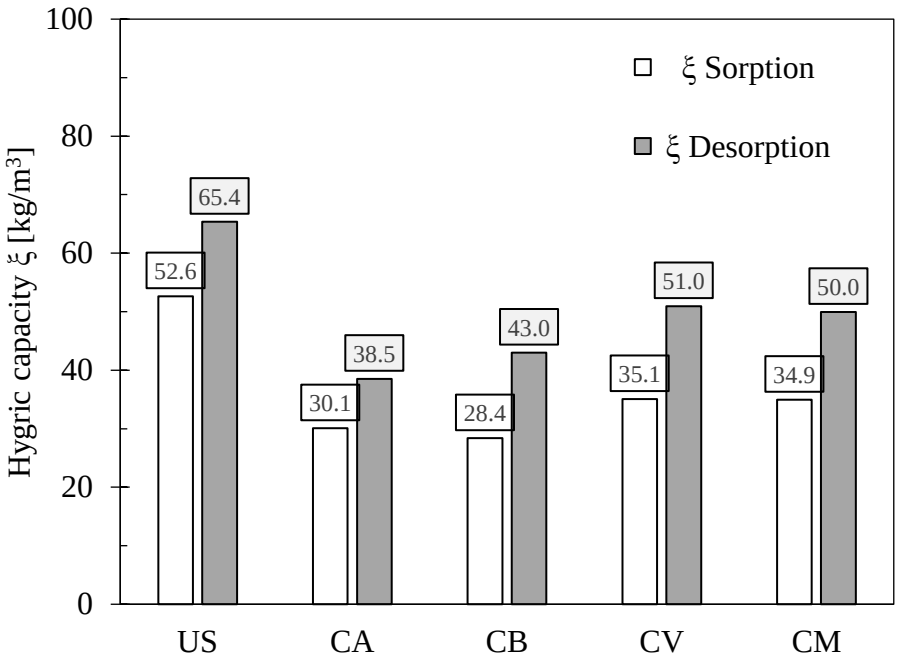

Figure 3.10. Average hygric capacity calculated between 30% and 80%RH of STA formulations

3.2.2.3 Water vapor permeability

a. Measurement method

The water vapor permeability was measured here according to the standard EN ISO-12572 [310] with the "wet cup" method. It involves generating a vapor pressure gradient across the sample by maintaining the relative humidity at 85% inside the cup and 50% outside it.

Tests were made in a temperature-controlled room at 21°C. The cup design was done according to the procedure followed by McGregor et al. [311]. Potassium chloride solution was used to maintain relative humidity in the cup at 85%. A thin bed of silicon was applied to seal the samples to the plastic cup. A vapor-tight aluminum tape was used to seal the sides of the sample with the side of the cup because it is impermeable and does not adsorb moisture itself [312]. The space between the saline solution and the bottom of the sample is called the air layer and was about 20mm for all samples as recommended by the ISO 12572 standard (15mm±5mm). The samples with the cup were stored in hermetic glove boxes where the relative humidity was maintained at 50% with saturated potassium carbonate solution. The design of the hermetic box enables weighting samples inside the box (Figure 3.11). Measurements were taken periodically (once a day) until a constant decrease of mass was observed for each test specimen, denoted by G in $kg/m^2/s$. For the tested materials, the equilibrium was reached after 3 days only but the test was run for 2 weeks to verify the linear relationship of mass loss with time.

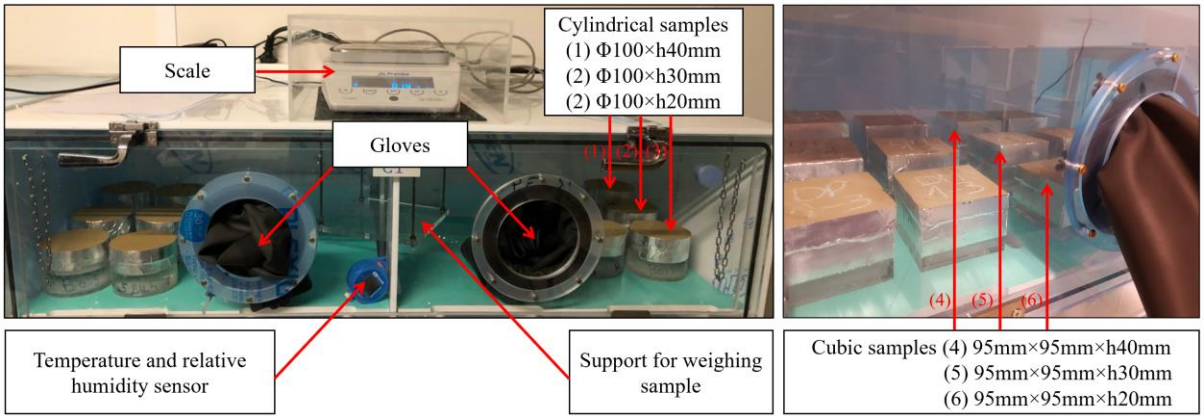

Figure 3.11. Hermetic gloves box

Two sample geometries were tested, cylindrical samples of 100mm in diameter and cubical samples of 95mm edge length. Three different thicknesses (40, 30 and 20mm) were tested to take into account the surface resistance effect, as it was recommended by [43]. Cubical samples were sawn from compacted earth blocks to verify if there is a difference between the values measured on individual compacted cylindrical samples and compacted earth blocks. It was decided to saw samples because it was not feasible to undertake tests on an entire block (295mm×140mm×95mm) Indeed, not only is the preparation of the block far more time consuming but also, weighing and conditioning the entire block would have been unrealistic because of its mass and size. The time required to reach a steady state would also have been very long.

b. Results

Results of permeability test undertaken on cylindrical samples presented in Figure 3.12 show that DUS present lower vapor resistance factor than SUS, and thus a higher permeability. It is

known that the permeability of soil is affected by different factors like dry density, porosity, size and shape of particles, specific surface area, etc. However, the differences between the two earths are a combination of different physical and chemical properties. Firstly, the difference in dry density between the two earths is of the order of 5% so its effect was supposed negligible with respect to other factors that could affect permeability. Anyway, an explanation based on dry density in our case lead to contradictions because the dry density of DUS is higher than that of SUS. The same issue could be said about the apparent porosity. At this stage it appears that the obtained results could be connected to the Atterberg limits. Indeed, liquid limit and plasticity index of STA are higher than those of DAG by 30% and 38%, respectively. And typically, when the ratio of plastic clay increases in soil, a lower permeability is expected [313], and therefore a higher water resistance.

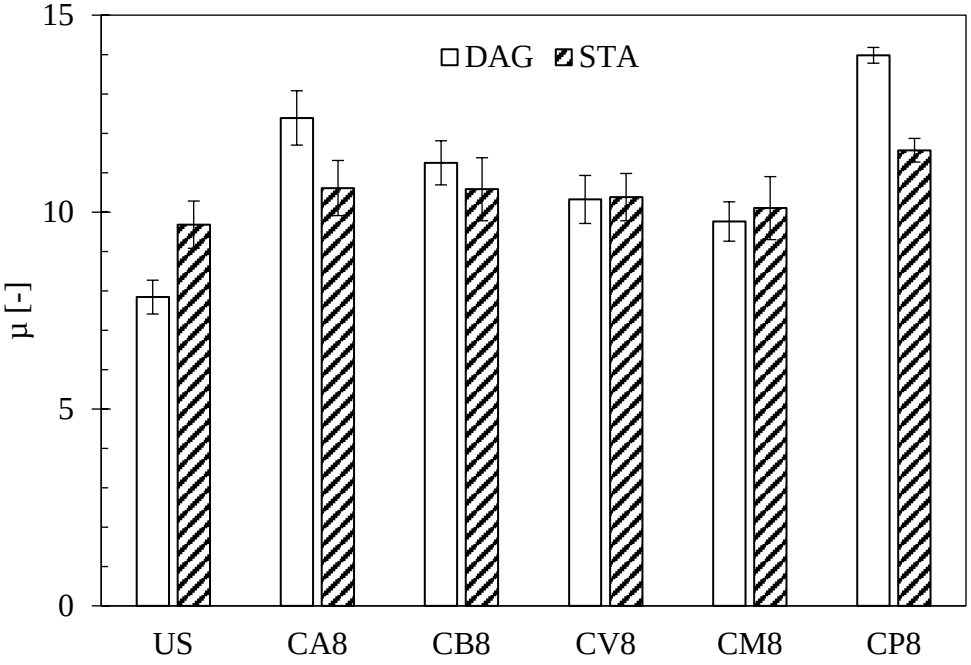

Figure 3.12. Results of corrected water resistance factors of cylindrical samples

Another issue to be noticed in these results is the increase in the vapor resistance factor after stabilization, which appears more important for formulations made with DAG earth. For DAG earth, CP shows the highest μ factor that corresponds to an increase by 78% when compared to DUS, followed by CA with an increment of 58%. While CM shows the lowest increase in μ by about 25%. CB and CV lie between the two extremes. On the other side, μ factor of STA earth was increased with about 10% only with all cements except CP, which shows an average increase of 20% with respect to SUS. These results prove again that DAG is more impacted with cement action than STA. The recorded μ factors are in accordance with what is usually found in literature, given that vapor resistance factors vary between 5 and 15 for uncompressed stabilized earth blocks.

Concerning the difference between cements, results show that μ factor decreases with increasing limestone filler from CA to CM. In addition, the relatively high μ factors of formulations stabilized with CP could be referred to its fineness. In fact, CP have a fineness approximately two times higher than CA and CB (see Table 2-3). In analogy with concrete, increasing cement fineness decreases its permeability [314]. Thus, results with CP seem logical.

The permeability test was executed on cubical samples sawn from blocks as mentioned above to verify the values obtained on cylindrical samples. Four formulations were tested only, DUS, DB8, DM8 and DP8. It appears that μ factors corresponding to measurements made on cubical samples sawn from blocks are slightly lower than those made on cylindrical samples compacted individually (Figure 3.13). It is worth mentioning that samples were sawn with precaution in such a way that the parallel faces are normal to the direction of vapor flow to avoid any cutting effects. The slightly lower vapor resistance factors could be attributed to the fact that the block is more heterogeneous than the small cylindrical sample. Figure 3.14 indicates that the structural arrangement of soil particles is slightly more dispersed in the block than in the cylindrical sample. Therefore, the permeability will be lower in this latter. Nonetheless, values of the two samples follow the same trend with respect to formulations.

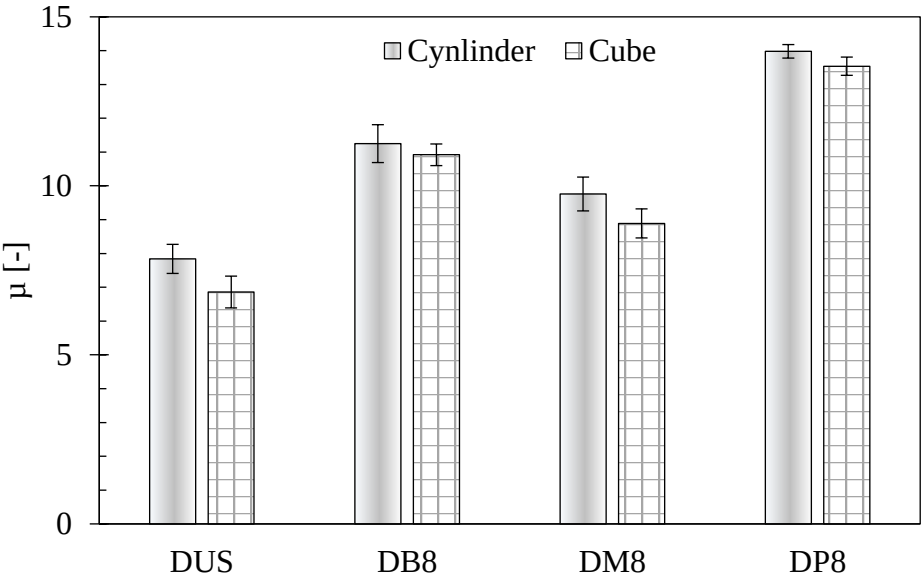

Figure 3.13. Comparison between results of corrected water resistance factors on cylindrical and cubical samples

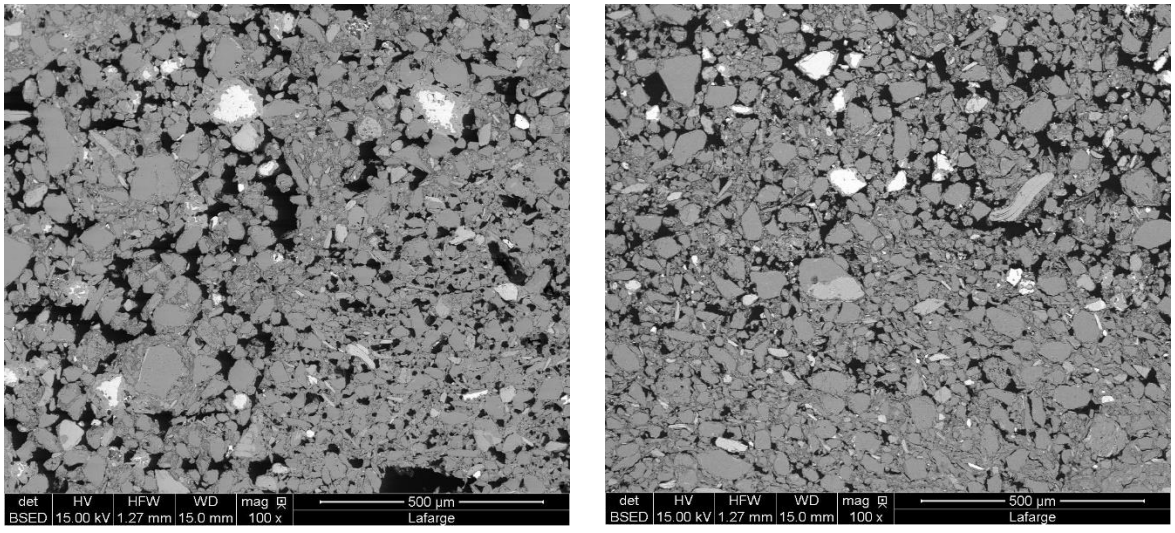

(a) SEM of stabilized block (b) SEM of stabilized cylindrical sample

Figure 3.14. Example on the difference between microstructure of compacted block DB8 (a) and compacted cylindrical sample (b)

3.2.3 Durability toward water

To quantify cement action on DAG and STA earth, one method of each category of those introduced in §1.4.3 was selected. From the first category, the spray erosion test was chosen because it was too easy for all stabilized materials to pass the drip test without any noticeable damage or change, so no difference could be noticed between formulations. From the second category the immersion test was chosen for its simplicity.

3.2.3.1 Resistance to spray erosion

a. Testing method

The method was performed according to the specifications of the Australian earth building handbook (HB-195). It consists in submitting sample's surface to a horizontal water spray at 50kPa for 60 minutes. The area of application is of 70mm in diameter from a distance of 470mm as shown in Figure 3.15. This test was applied on cylindrical samples having 40mm in thickness and 100mm in diameter. The maximum depth of erosion should be measured at the end of the test with 10mm flat ended rod, but here it was measured with the help of digital sliding caliper accurate to 0.01mm.

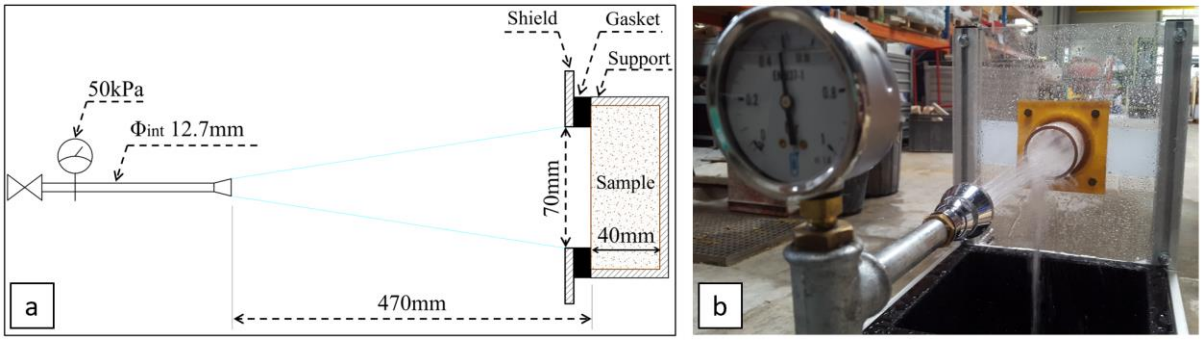

Figure 3.15. Schematic representation of the spray erosion test (a), setup of the test (b)

The performance of the sample is judged based on the erosion rate and the mass loss calculated as follow:

$$\text{Erosion rate [mm/min]} = \frac{d}{t} \qquad (3\text{-}1)$$

Where:
d [mm] is the maximum eroded depth, and
t [min] is the spraying duration, or the duration that corresponds to sample's perforation.

$$\text{Mass loss [\%]} = \frac{M_{i\,50\%} - M_{f\,50\%}}{M_{i\,50\%}} \qquad (3\text{-}2)$$

Where $M_{i\,50\%}$ [g] and $M_{f\,50\%}$ are the dried masses at 50%RH/21°C before and after the test, respectively.

b. Results

Figure 3.16 shows examples of the state of the sample's surface subjected to the water spray erosion test. Important improvement in the sample's resistance after stabilization could be seen

clearly. Average erosion's rates and mass loss of the formulations are presented in Figure 3.17 and Figure 3.18, respectively. Let mention that the erosion rate of SUS formulation was determined at the time at which water penetrates the opposite face of the sample, since it happened before the end of the test.

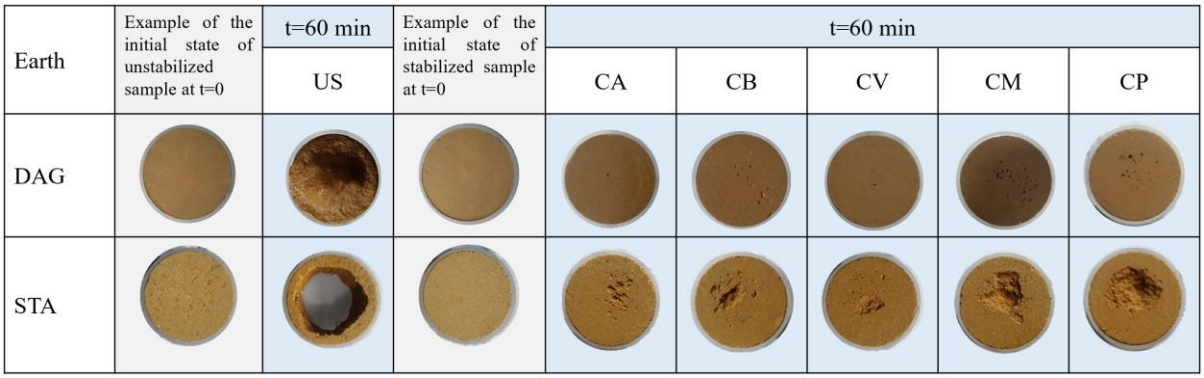

Figure 3.16. Examples of the state of the exposed surface of the samples before and after the spray erosion test

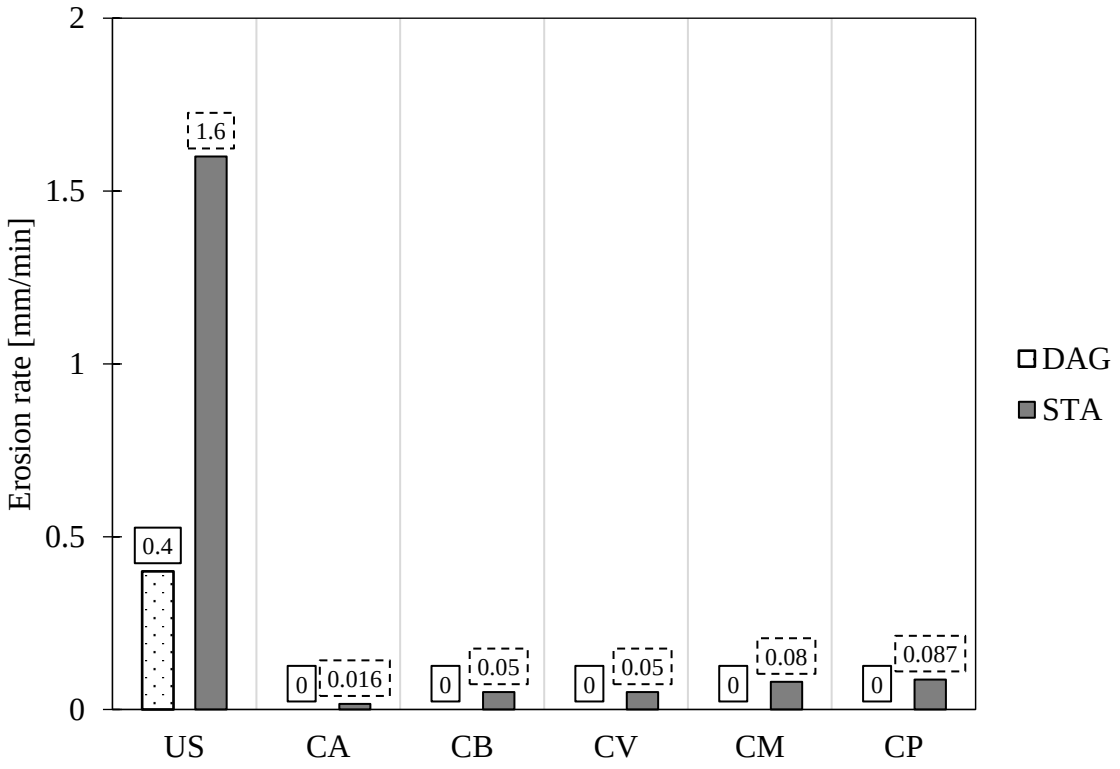

Figure 3.17. Erosion rate of DAG and STA formulations

The erosion rate of unstabilized formulations indicate that SUS is prone to more erosion than DUS. Important decrease in the erosion rate and mass loss is manifested with the 5 types of cements used without significant difference between them for DAG earth. As for STA, it appears that there is an important improvement in its performance after stabilization, which was not seen on strength outcomes.

Based on the average calculated erosion rate, all formulations passed this test except SUS because in this latter, erosion progressed at a rate higher than 1mm/min. It's worth mentioning that the conditions of this test are more severe than actual climatic conditions [315], [316] and the performance of unstabilized materials against this test cannot be used as an indicator of their durability since they are not supposed to be exposed to water. Here the test was performed on unstabilized samples to put in context the effectiveness of cement stabilization.

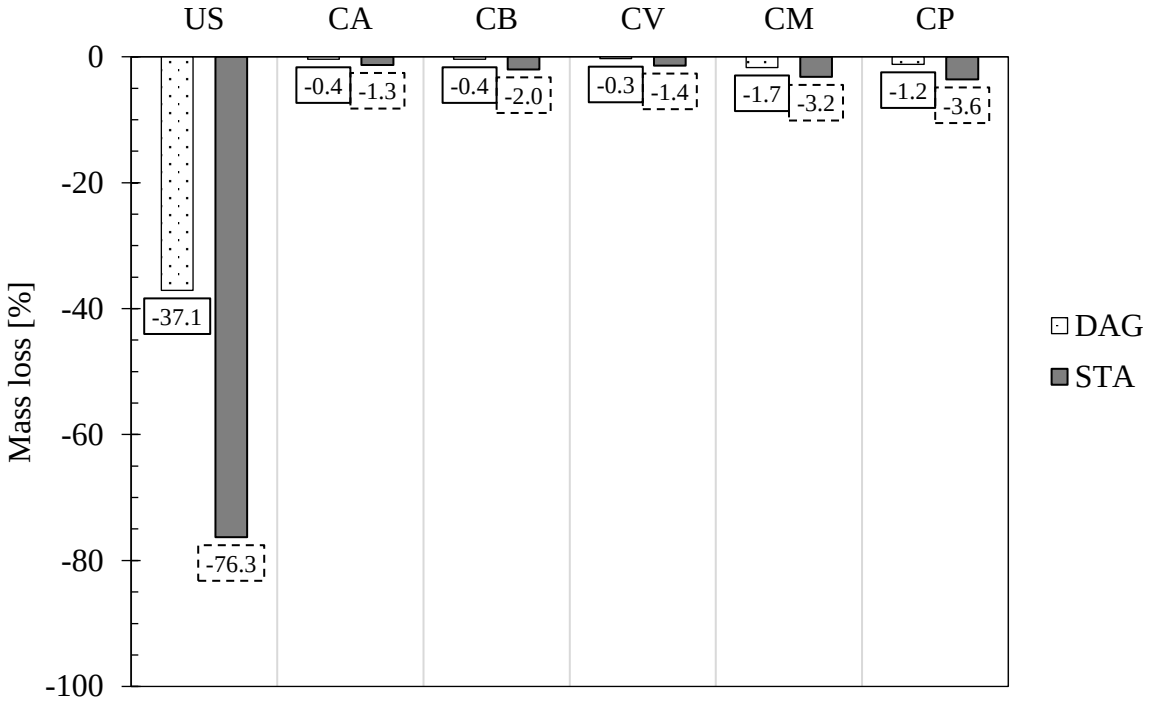

Figure 3.18. Mass loss at the end of the spray erosion test

3.2.3.2 Resistance to water immersion

a. Testing method

The procedure consists in immerging samples under 10cm of water for 10 minutes in room temperature at 21°C±2°C (Figure 3.19).

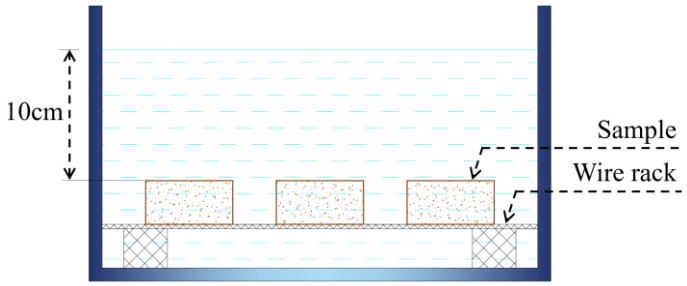

Figure 3.19. Schematic representation of the water immersion test

The performance of samples is evaluated in function of the mass loss calculated as follow:

$$\text{Mass loss [g/min]} = \frac{M_{di} - M_{df}}{t} \quad (3\text{-}3)$$

Where:
M_{di} [g] and M_{df} [g] are the dry masses at 50%RH/21°C of the sample before and after immersion, respectively, and
t [min] is the immersion duration.

b. Results

The average mass losses of the tested samples are shown in Figure 3.20. After stabilization with CA, the mass loss of DAG and STA earths was reduced by 98% and 90% respectively. While a treatment with CM or CP have reduced the mass loss of DAG and STA by about 80% and 50% respectively. It appears form the obtained results that the higher is the strength class of the cement, the lower is the mass loss of samples at the end of the test. Moreover, this assessment tool confirms again that cement stabilization is more effective with DAG than STA.

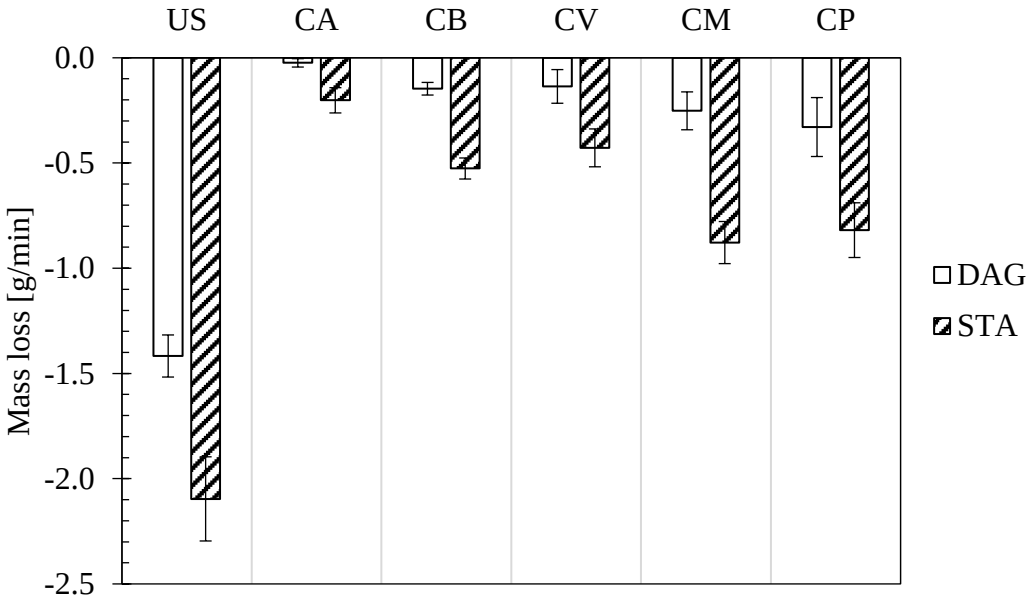

Figure 3.20. Mass loss of unstabilized and stabilized formulations at 8% cement at the end of the immersion test

3.2.3.3 Conclusion based on durability indicator

The obtained results demonstrated that the two methods give information on the stabilizer efficacy rather than the material durability. However, similarly to the wet to dry strengths ratio, it was not evident to make a clear distinction between the action of different cements and to establish a relation between the outcomes of the two methods. For instance, DUS reported a wet to dry strength ratio two times lower than SUS but it shows at the same time a much better resistance to AET and water immersion test. The same issue happened with stabilized formulations made with STA earth. SA8, SV8 and SM8 have similar wet to dry strength ratio, but the degradation of SV8 and SM8 against AET and immersion test is more important than SA8. Thus, results from one method cannot be used to predict those of another. But in term of cement stabilization efficacy, the two performance indicators demonstrated that cement action on DAG was much more important than that on STA.

3.2.4 Essential points to remember from the performance assessment of the compacted cement-earth mixtures

All results converge to the conclusion that the performance of DAG earth was impacted by cement treatment more than that of STA and the essential points to remember could be summarized as follow:

- The difference between the action of the tested cements is remarkable on the wet compressive strength rather than the dry one.
- Increasing cement dosage from 5 to 8% did not improved the wet and dry compressive strengths of STA earth.
- No considerable difference in the hygroscopicity between formulations made with DAG and STA and stabilized with CB, CV, and CM.
- The resistance toward water of all stabilized formulations was improved considerably with respect to the unstabilized ones.
- The results of spray erosion test and water immersion test could not be pre-estimated from the wet to dry strength ratio.

3.3 Microstructural analysis of cement-earth mixtures

To investigate chemical impact of cement on the two earths we attempt to identify the reaction products by using and X-ray diffraction (XRD) and thermogravimetric analysis (TGA).

3.3.1 X-ray diffraction analysis

XRD analyses were made to identify the main phases present in unstabilized and stabilized formulations and they could help in the interpretation of the TGA curves. Analyses were made in two different laboratories for verification purposes. The main identified phases in the analyzed samples are presented in Table 3-2 and Table 3-3 and the corresponding spectrum are presented in Appendix G and Appendix H.

The two analyses show that the two earths are mainly composed of quartz as expected. Despite their granulometric differences, the two earths are mainly composed of silt, sand, and gravels (about 70-80% of the total earth). These grains have in general the same physicochemical characteristics and they are essentially composed of quartz structured in the same way [317], [318].

Other common minerals between the two earths are muscovite, microcline, clinochlore and kaolinite as identified in the first analysis. Muscovite is the most common dioctahedral mica, microcline is a potassium-rich alkali feldspar and clinochlore is a mineral of the chlorite family. The minerals that were identified only in DAG samples by the first analyses are albite and actinolite (or cordierite). Albite is a plagioclase mineral, and the second analyses show that DAG contains much more plagioclase than STA. While actinolite is an amphibole silicate mineral and the second analyses show that amphibole was not detected in STA. Further, goethite was detected by the first analyses in STA only, and it was detected in STA with higher percentage than DAG by the second analysis. Thus, it appears that there is good correlation between phases identified in the two XRD analyses.

	DAG			STA		
	DUS	DB8	DM8	SUS	SB8	SM8
Phase	Intensity [counts per second]					
Quartz	2574	2232	2281	2211	1983	1847
Muscovite	42	38	35	35	30	30
Microcline	57	52	52	35	35	32
Clinochlore	38	47	44	36	26	27
Goethite	ND	ND	ND	55	49	50
Halloysite or Kaolinite	ND	17	15	32	34	33
Albite	152	142	212	ND	ND	ND
Calcite	ND	68	86	ND	56	68
Ettringite	ND	22	19	ND	ND	ND
Actinolite or Cordierite	17	15	16	ND	ND	ND
C_2S and/or C_3S	ND	18	16	ND	18	15

ND: Non detected

Table 3-2. Main identified minerals by the first XRD analyses (@LafargeHolcim - Saint Quentin Fallavier)

	DUS	DB8	SUS
Phase	Proportion [%]		
Quartz	47.3	42.0	49.6
Swelling clay minerals	17.5	18.0	5.2
Chlorite	1.0	0.8	0.2
Mica + Illite (I/S >90% Illite)	8.3	6.8	8.7
Plagioclase	9.9	8.6	1.0
Goethite/hematite	1.8	1.4	5.3
Kaolinite	10.1	9.1	28.1
Calcite	1.2	6.0	0.3
Ettringite	ND	3.9	ND
Potassium feldspar (K-spar)	1.8	2.2	1.0
TiO_2 (rutile or anatase)	0.7	0.6	0.4
Amphibole	0.3	0.4	ND

Table 3-3. Main identified minerals by the second XRD analyses (@ ERM - Poitiers)

The two analyses show that the two earths are mainly composed of quartz as expected. Despite their granulometric differences, the two earths are mainly composed of silt, sand, and gravels (about 70-80% of the total earth). These grains have in general the same physicochemical characteristics and they are essentially composed of quartz structured in the same way [317], [318].

Other common minerals between the two earths are muscovite, microcline, clinochlore and kaolinite as identified in the first analysis. Muscovite is the most common dioctahedral mica, microcline is a potassium-rich alkali feldspar and clinochlore is a mineral of the chlorite family. The minerals that were identified only in DAG samples by the first analyses are albite and actinolite (or cordierite). Albite is a plagioclase mineral, and the second analyses show that DAG contains much more plagioclase than STA. While actinolite is an amphibole silicate mineral and the second analyses show that amphibole was not detected in STA. Further, goethite was detected by the first analyses in STA only, and it was detected in STA with higher

percentage than DAG by the second analysis. Thus, it appears that there is good correlation between phases identified in the two XRD analyses.

Swelling clay minerals were detected in DAG earth with concentrations more than three times higher than those detected in STA. This issue seems in accordance with the measured clay activity index (Table 2-2), which is 9.33 for DAG and 3.11 for STA. The detected swelling clay minerals characterize interlayered illite/smectite minerals.

On the other side, calcite was detected in stabilized formulations made with both earths. Its presence could be attributed to the addition of cement. For the two earths, its concentration is higher in DM8 and SM8 than in DB8 and SB8 since the mineralogical composition of masonry cement is richer in calcite than that of CB (see Appendix E). However, ettringite was detected only in DB8 and DM8. This issue could be explained by the higher concentration of sulfates in DAG earth compared to STA (see Appendix F), knowing that sulfate is normally consumed to form ettringite at early ages.

3.3.2 Thermogravimetric analysis

Prior to the thermogravimetric analysis, unstabilized formulations and stabilized formulations at 8% were dried following the solvent exchange method prescribed earlier. Then they were heated in the heating analyzer NETZSCH STA 449F3 Jupiter® with the following temperature process: (1) heated to 35°C at 10°C/min from room temperature; (2) held for 30 min; (3) heated to 1010°C at 10°C/min. These analyses were done in the laboratories of Technodes S.A.S Calcia. The obtained mass loss and DTA curves of DAG and STA formulations are presented in Figure 3.21 and Figure 3.22, respectively, while the corresponding mass variations in each range of temperature are summarized in Table 3-4 and Table 3-5. The TGA analysis was repeated in the ENTPE laboratory with the ATG-DSC SETARAM Sensys Evo, where samples were heated from temperature room (21°C) to 600°C at 7°C/min under an oxygen purge. The obtained results in the two different laboratories shows that curves were reproduced with a good repeatability in the common range of temperature (see Appendix I and Appendix J). To facilitate the interpretation of results, the TGA temperature's peaks of various phases present in concrete were summarized in Appendix K as found in the literature. The correspondence between the obtained results and possible reactions is based on the Handbook of thermogravimetric system of minerals and its use in geological practice [319].

In general, the thermogravimetric peaks of soil show four characteristic regions in the interval from 35°C to 640°C. In the region < 110°C, mass loss is mainly due to the volatilization of water vapors. In the second region (200–400°C), the mass loss is caused due to the thermal degradation of organic matter, mainly carboxylic and phenolic functional groups and hydrocarbon compounds. It might also be due to the release of low molecular weight organic compounds. In the third region (400–580°C), the mass loss is primarily due to the decomposition of the recalcitrant organic compounds. In the fourth region (580–640 °C), the mass loss is mainly due to dehydroxylation of metallic hydroxides and carbonate derived components.

In our study, we are interested in the differences between the thermal analyses of stabilized and unstabilized formulations for the two earths. Results show that there is hardly any difference between stabilized and unstabilized formulations of the same earth, except some peaks that will be addressed in what follow.

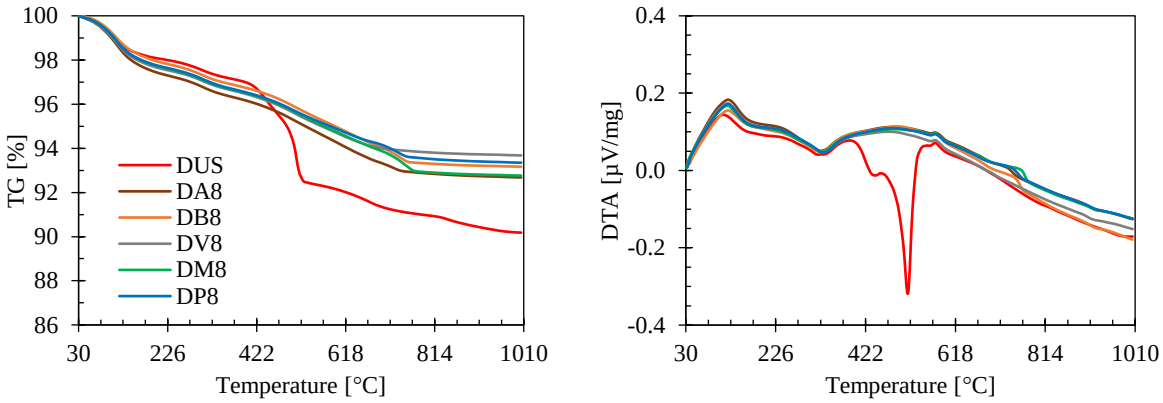

(a) Mass loss curves (b) DTA curves

Figure 3.21. TG and DTA curves of DAG formulations

Variation [%]	DUS	DA8	DB8	DV8	DM8	DP8
35-110°C	-1.07	-1.17	-0.91	-1.09	-1.01	-1.01
110-200°C	-0.83	-1.35	-1.14	-1.43	-1.21	-1.19
200-650°C	-6.32	-3.72	-3.50	-3.42	-3.47	-3.32
650-1000°C	-1.58	-1.04	-1.28	-0.58	-1.50	-1.10
35-1000°C	-9.80	-7.28	-6.83	-6.52	-7.19	-6.62

Table 3-4. Mass variation of DAG formulations in different temperature ranges

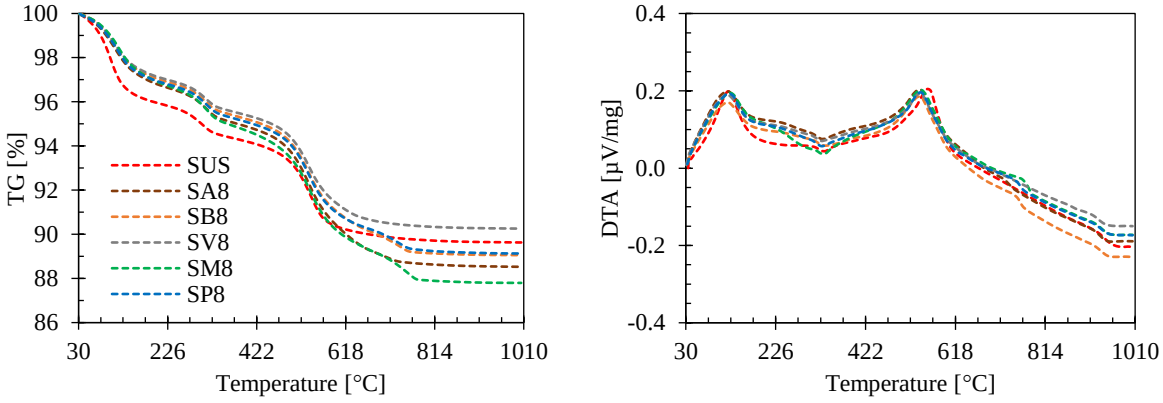

(a) Mass loss curves (b) DTA curves

Figure 3.22. TG and DTG curves of STA formulations

Variation [%]	SUS	SA8	SB8	SV8	SM8	SP8
35-110°C	-2.58	-1.52	-1.41	-1.33	-1.24	-1.42
110-200°C	-1.45	-1.60	-1.50	-1.45	-1.78	-1.57
200-650°C	-5.90	-7.31	-6.73	-6.38	-7.44	-6.57
650-1000°C	-0.44	-0.98	-1.27	-0.52	-1.70	-1.26
35-1000°C	-10.37	-11.41	-10.91	-9.68	-12.16	-10.82

Table 3-5. Mass variation of STA formulations in different temperature ranges

The small endothermal peak at ~574°C detected for all DAG formulations correspond to the transition of trigonal α-quartz to hexagonal β-quartz. It appears that it was not possible to detected it in STA formulations because usually this peak is overlapped by other reactions that happened in the same range of temperature.

For all STA formulations, there is an endothermal peak in the range 530-590°C that could correspond to the dehydroxylation of kaolinite following the reaction: $Al_2Si_2O_5(OH)_4 \rightarrow Al2O_3.2SiO_2$ (amorphous metakaolinite) + H_2O. Knowing that STA earth has high proportions of this mineral.

A small flat peak is detected between 600 and 750°C in all stabilized formulations except DV8 and SV8. A peak in this range of temperature correspond usually to the decarbonation of calcite present in cement. It was not detected for DV8 and SV8 because CV does not contain limestone. This observation is in accordance with results of the XRD analyses since calcite was detected only in stabilized formulations.

As for DUS, a small exothermic peak was detected at ~450°C followed by another sharp exothermic peak at 514°C. Usually, in the range 400-600°C, an exothermic effect could take place due to the oxidation of iron beared by actinolite (or amphibole) and chlorite present in DAG. Otherwise, it could be a signal for organic materials. Maybe a combination of the three effects was taken place. To verify that it has oxidation reaction, the thermal analysis was repeated in nitrogen purge. As shown in Figure 3.23, exothermic peaks disappeared in the latter conditions. Thus, the reaction type was verified.

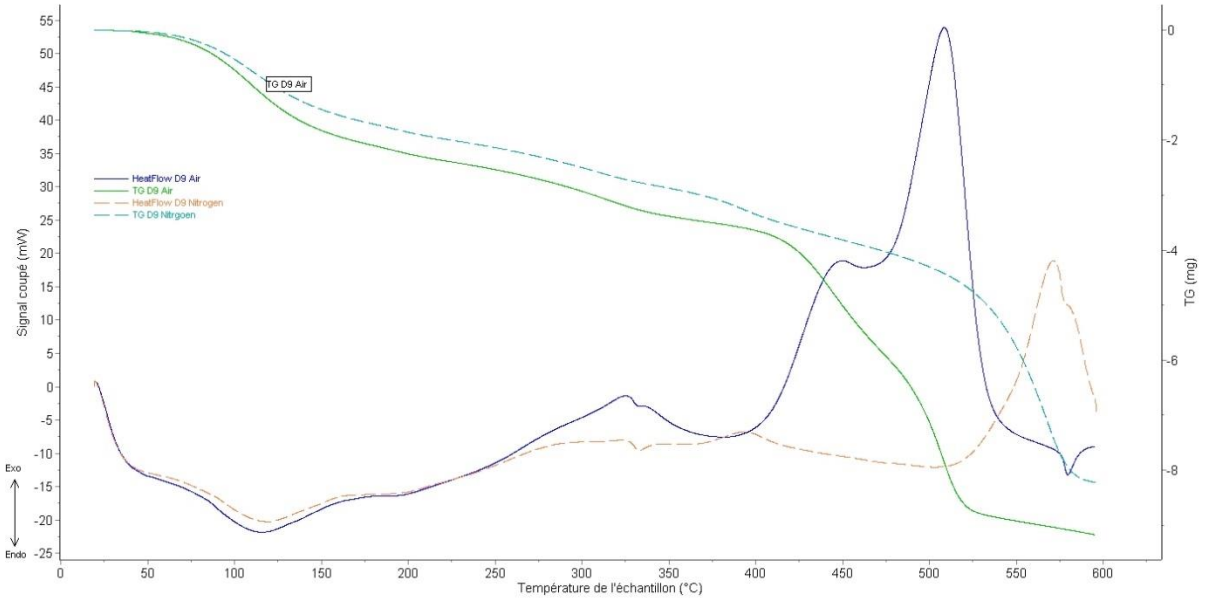

Figure 3.23. Results of the thermal analyses of DUS in oxygen (air) and nitrogen

The exothermic peaks were not detected in the corresponding stabilized formulations of DAG. It had been assumed that they were maybe overlapped by other endothermic reactions of cementitious products that take place in the same range of temperature. For example, the dehydration of calcium hydroxide and the decarbonation of calcium carbonate.

On the other hand, an average decrease of 30% in the total mass loss at 1000°C was registered in DAG formulations after stabilization. While the opposite happened for STA formulations.

The major difference in mass loss between stabilized and unstabilized DAG formulations appears in the region corresponding to the sharp exothermic reactions. Otherwise, the differences remain negligible.

3.3.3 Conclusion

The microstructural analyses made showed that it was difficult to detect the action of cementitious products in STA samples. Which could explain to some extent the lower efficacy of cement in the latter case when compared to DAG as provided by the performance analyses.

3.4 Discussion on stabilization efficiency

3.4.1 Impact of cement characteristics

3.4.1.1 Cement dosage

It had been shown that increasing cement dosage from 5 to 8% did not improve the UCS of stabilized samples made with STA. Addedly, samples stabilized at 5% of CB registered slightly higher UCS than those stabilized at 8% in wet conditions. The first comment is that the chosen cement dosages were possibly not sufficient to show their best action on the two earths. Especially that the acceptance of the two earths to treatments with different cements was not similar.

In practical engineering, it is desirable to know the amount of cement required for the improvement of a particular soil/earth before implementing the treatment process. Thus, an interesting issue that could be made here is to determine an “optimum” dosage of cement for each cement-earth mixture that gives – for example – the maximum possible strength, while fixing a cement dosage interval. Probably, this optimum cement dosage will vary from cement to another, and it will depend on the characteristics of earth. In this study, higher cement dosages were not considered because increasing cement dosage imply increasing the environmental impact, and the starting idea was to select cements more ecological than OPC with moderate cement dosages. If future work will be made, we propose optimizing cement dosage for each cement type and with earth characteristics.

3.4.1.2 Cement composition

Figure 3.24 shows that no proportional correlation exists between the relative strength of stabilized compacted earth samples and clinker content of the corresponding cement used for stabilization. It appears that increasing clinker content between 57 and 77% does not increase strength in both wet and dry conditions for the two earths, and that compressive strength decreases with clinker dosage higher than 88%. The first look on such graph gives the impression that there is optimal clinker content that corresponds to higher compressive strength of the compacted sample. This comparison is obviously incorrect since cement’s composition is not identical and it is clear that parameters other than clinker content are involved.

Indeed, cement hydration involves a collection of coupled chemical processes that may operate in series, in parallel, or in some more complex combinations. The main phases involved in cement hydration process and that have significant effect on the strength of the final mortar are alite (C_3S), belite (C_2S), aluminate (C_3A) and ferrite (C_4AF). In addition, the presence of ettringite in the cement system depends on the ratio between calcium sulfate (gypsum) and

aluminate. Each phase has generally accepted characteristics in the reaction of cement with water to produce durable and resistant product [320], [321]. However, the analysis of chemical kinetics in cement-earth mixtures is complex due to the number of components of earth that could influence the hydration of cement. But if we consider that cement phases perform similar functions in the cement-earth mixtures, and by restricting attention to these four phases, a simple correlation between the sum of these minerals in the composition of cements used in this study (cf. Appendix E for cement compositions) and the corresponding relative strength of the final product could be made.

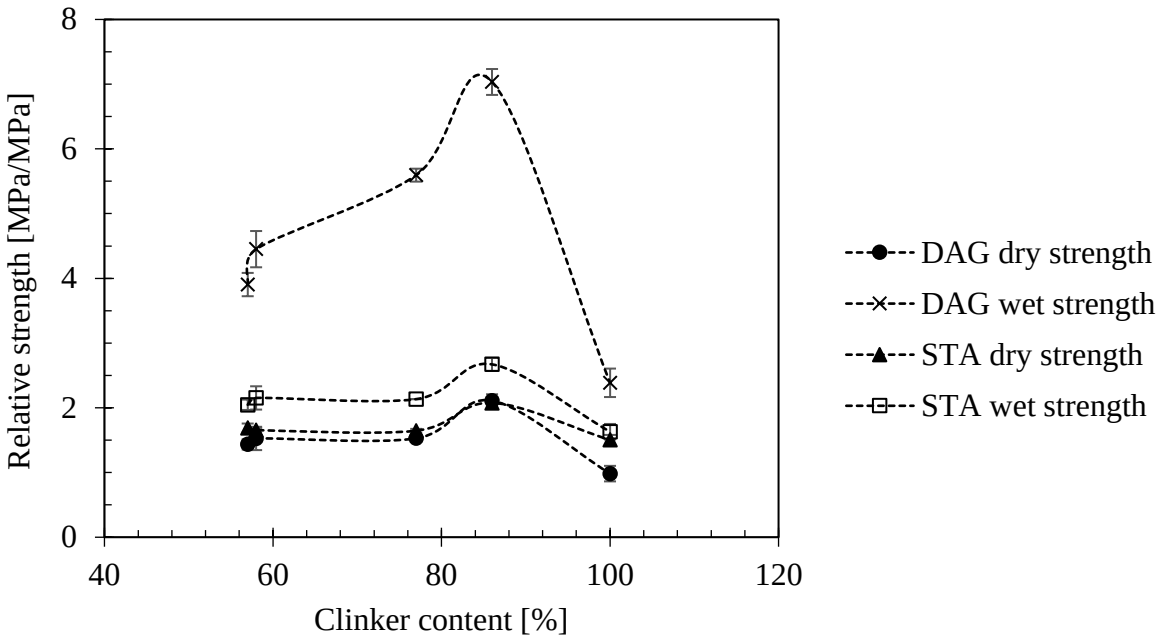

Figure 3.24. Relative strength of stabilized compacted samples at 8% versus clinker content of the corresponding cement used for stabilization

As shown in Figure 3.25, the relative strength seems to vary linearly with the proportion of these four cement phases. This visualization of results make sense. It's well known that models developed to predict strength of cement paste after 7 and 28 days are mainly based on the mineralogical composition of cement, while early age strength is mainly affected by fineness characteristics [322]–[327]. However, most of equations proposed to estimate strength of cement treated clays considers other factors like clay content, water to cement ratio, liquid limit (or liquidity index), age, etc. [328]–[333]. The applicability of exiting strength prediction models for soil-cement mixtures and clay-cement mixtures was justified by authors only in specific conditions of samples preparation, in particular testing conditions and in limited interval of water content and clay content. In additions, when components other than clay are incorporated in the physical structure of the mixture, the convergence of proposed models becomes more complicated.

It was not programmed here to orient the study in this direction, but it will be interesting to invest in the development of models that are able to predict strength of compacted earth in function of the mixture composition. To facilitate this task, extensive experimental studies on the effect of each of the characteristics of cement composition, earth properties and samples

characteristics should be made to establish a benchmark for identifying the combined effect of different parameters in earth-cement structure. Further, the compressive strength testing methodology should be unified to enable a wider application of such models.

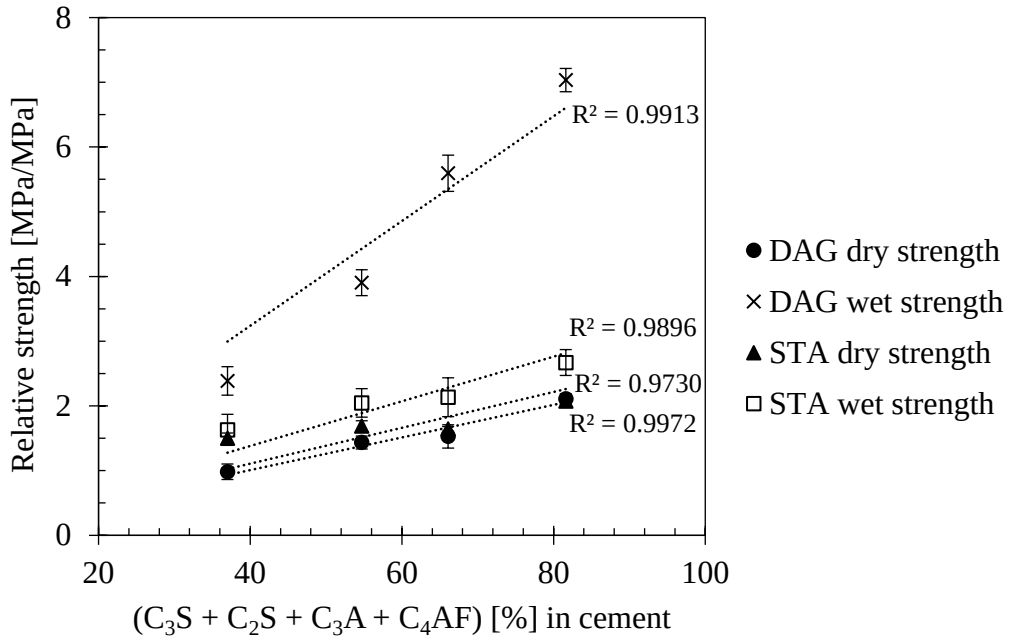

Figure 3.25. Correlation between UCS of stabilized compacted samples at 8% and percentage of phases (Alite + Belite + Aluminate + Ferrite) in the corresponding cement used for stabilization.

3.4.2 Optimum manufacturing properties

In this thesis, as it is the case of all studies made on stabilized and unstabilized compacted earth, the optimum manufacturing properties are determined based on the optimum water content that deliver the highest dry strength of the material which corresponds as well to the minimum porosity. This procedure is admitted based on the soil compaction theory, where the strength is inversely related to the porosity. In concrete, the strength does not depend only on the porosity, but it is controlled by the water to cement ratio as well. For example, in the ACI code, the water to cement ratio could be selected based on desired 28-days compressive strength, then the required cement content for the concrete mixture could be calculated. However, almost all studies on cement stabilized compacted earth (or stabilized earthen materials in general) focused on the optimum water content and not on the water-to-cement ratio.

The question that may arise is, are we really optimizing the manufacturing properties of cement stabilized earth if we follow the same procedure of unstabilized earth?

To provide insight into this question, we will firstly consider the variation of dry UCS of all stabilized samples with respect to their corresponding water to cement ratio. Let recall that the optimum water content (OWC) is the percentage of water mass with respect to the total mass of the dried sample and the cement content (cc) is the dosage of cement with respect to the dry mass of earth in the sample. Thus, assuming that the water is distributed in proportional manner

between cement and earth, the water-to-cement ratio ($\frac{w}{c}$) could be expressed in function of OWC [%] and cc [%] as follow:

$$\frac{w}{c} = \frac{OWC \times (1 + cc)}{cc} \quad (3\text{-}4)$$

Dry UCS of stabilized formulations made with DAG and STA are presented in Figure 3.26 in function of the water to cement ratio of the mixture. It shows that for the same cement type, the compressive strength tends to decrease with the increase of water to cement ratio. In addition, it appears that all water to cement ratios are relatively high (between 2 and 6). An interesting issue that could be made is to determine the water content of each formulation based on the water to cement ratio that deliver the maximum dry compressive strength. Of course, in this case, the corresponding dry density will vary, and it will not be equal to the maximal one. Anyway, it is possible that the maximum dry density will not ensure the maximum USC in cement stabilized earth as it was found in a recent study concerned by optimizing water content of cement-soil mixtures for geotechnical applications [334]. However, this issue should be verified depending on earth characteristics.

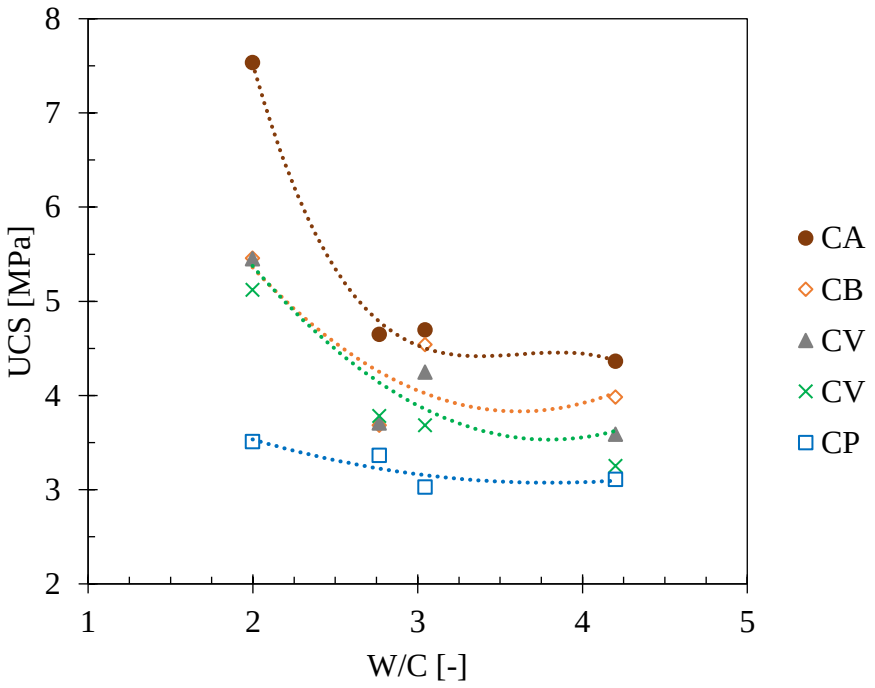

Figure 3.26. Variation of dry UCS with water to cement ratio

3.4.3 Impact of earth characteristics

It was not evident to connect the performance of the tested earth-cement mixtures to one factor because DAG and STA differ in all these properties. It was decided firstly to consider physical properties because they were determined before launching the experimental campaign.

Firstly, the granular distribution was considered. Since the gain in performance achieved with DAG was more important than STA, and that DAG is finer than STA, it was decided to increase the fineness of STA while maintaining its chemical properties. The advantage of this choice is to verify if increasing the fineness of STA only could improve the action of cement on it. The

difficulty of this task is that we need to maintain the clay content of STA earth and its chemical composition while decreasing the percentage of grain higher than 80µm, because about 90% of DAG's grains are lower than this diameter. The solution proposed consists firstly of crushing the entire original STA earth at 80µm, which means that its chemical composition is conserved. This earth is named as STAcrush. The second step is to prepare a mixture from the original STA and STAcrush in such a way to approach as near as possible the granular distribution of DAG. After different trials, a mixture named STAmix was fixed. It is composed of 20% of STA and 80% of STAcrush. The granular distribution of STAmix is presented in Figure 3.27 – a.

The second idea is to look at the impact of clay content and chemical composition of the earth. For that, a third earth named Lim, having a fineness close to that of DAG and a clay content higher than STAmix was introduced. The advantage of the comparison between the performance of DAG, Lim and STAmix (Figure 3.27 – b) is to put stress on the effect of chemical composition at constant, rather close, granulometry. Let recall that geotechnical properties of Lim are given in section 2.2.1.

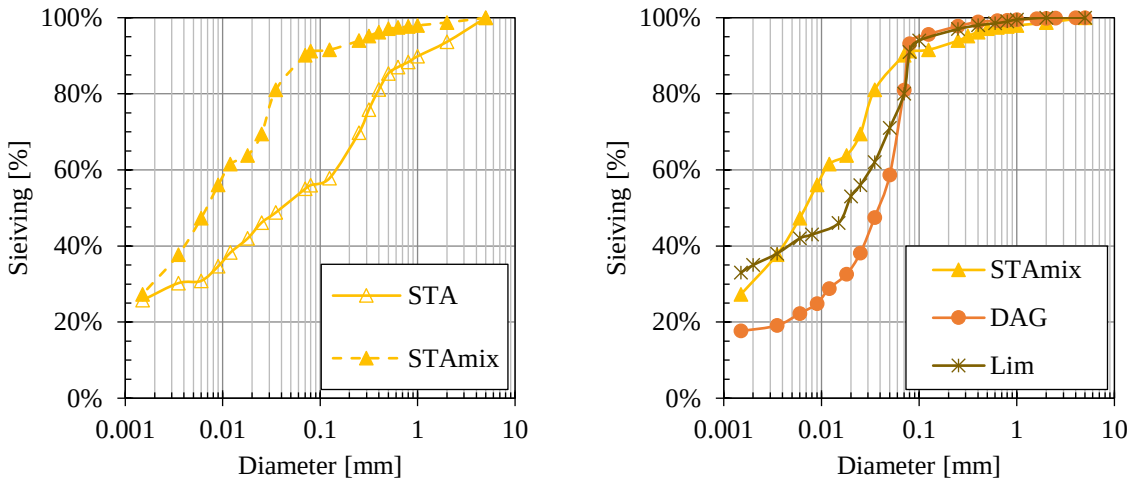

(a) Similar chemistry and different granulometry (b) Similar granulometry and different chemistry

Figure 3.27. Granular distribution of the two considered cases

The optimum manufacturing properties of STAmix were determined following the same procedure described in section 2.3.1. It was not possible to produce unstabilized samples made with STAmix (referenced as SxU in what follow) having the same manufacturing properties of unstabilized STA samples (SUS) with the same fixed compaction energy of the press. The main difference between the manufacturing properties of SUS and SxU and corresponding stabilized formulations manifested in their water content, while the difference in their dry density was of the order of 4% only (Table 3-6). The difference in manufacturing properties could lead to additional variable factors between the two earths. However, fixing a manufacturing dry density and water content for all formulations made with different earths was not considered in this study. Anyway, for construction applications, blocks are produced depending on the optimum manufacturing properties that could be obtained with the available block press. So, we tried to follow the same logic of what it is the case in practice.

In what follows, the wet and dry compressive strengths at 28 days will be used as indicators of the performance of mixtures. Since the focus was made here on earth properties, only one cement will be considered for stabilization. CB was chosen because it showed average impact between the cements of the study.

	DAG	STA	STAmix	Lim
MDD [g/cm^3]	1.85	1.73	1.66	1.90
OWC [%]	14	19	22	16

Table 3-6. Summary of the optimum manufacturing properties of different earths at their unstabilized state

3.4.3.1 Earth fineness

Figure 3.28 (a) shows that stabilized and unstabilized samples made with STAmix recorded higher wet UCS than those made with STA. Hence, increasing the fineness of STA was accompanied by an increase in the wet strength by about 60% and 50% for unstabilized and stabilized formulations, respectively.

On the opposite, dry compressive strengths of samples made with STAmix are, slightly lower than, or relatively close to those made with STA (Figure 3.28 – b). The slight lower dry UCS of STAmix formulations could be due to their lower dry density.

When it comes to the gain in strength, (i.e., relative strength between stabilized and corresponding unstabilized formulation), the differences between STA and STAmix becomes negligible, in both, wet and dry conditions (Figure 3.28 – c). In consequence, it seems that the increase of soil fineness does not significantly modify the efficiency of cement action.

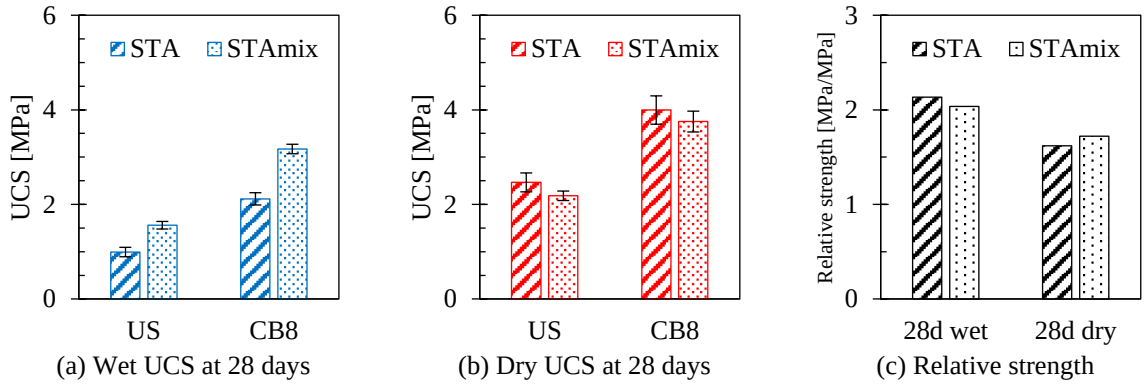

(a) Wet UCS at 28 days (b) Dry UCS at 28 days (c) Relative strength

Figure 3.28. Wet (a) and Dry (b) UCS at 28 days of STA and STAmix - unstabilized (US) and stabilized with 8% of CB (CB8)

3.4.3.2 Earth chemistry

Results displayed in Figure 3.29 (a) show that unstabilized samples made with STAmix recorded higher wet UCS than those made with DAG and Lim. After stabilization, samples made with Lim recorded lower wet strength than those made with DAG and STAmix.

In term of dry compressive strength (Figure 3.29 – b), Lim recorded the highest values and STAmix the lowest ones. And this for stabilized and unstabilized formulations. This result is not surprising given that dry compressive strength increases with increasing dry density.

If we look now on the relative wet strength (Figure 3.29 – c), we can see that DAG derives the highest gain, followed by Lim than STAmix.

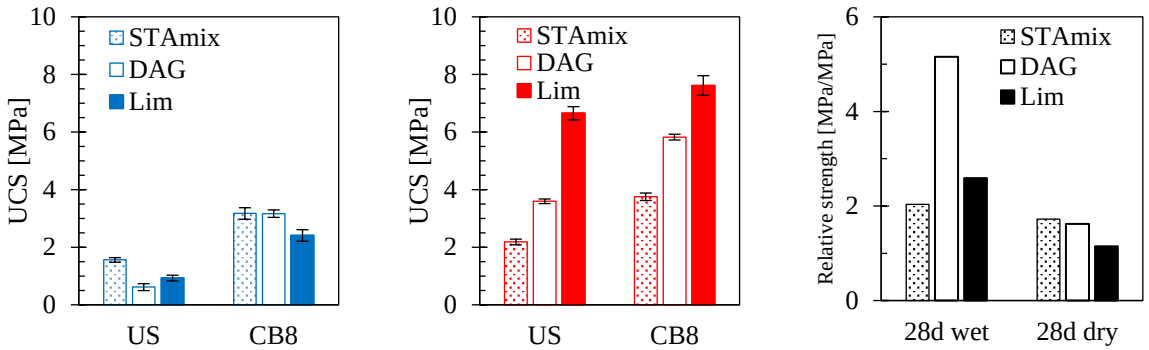

Figure 3.29. Wet (a) and Dry (b) UCS of STAmix, DAG and Lim – unstabilized (US) and stabilized with 8% of CB (CB8)

a. Major chemical potential disruptors elements

To explain these results, chemical analysis of the three earths was made and the concentration of sulphates, phosphates and nitrates was determined as summarized in Table 3-7. It shows some differences in the concentration of these main chemical potential disruptors contained in the three earths. Firstly, the concentration of sulfates in DAG and Lim are similar and higher than that in STA, given that the presence of high concentrations of sulfates boosted the formation of ettringite.

Secondly, the concentration of phosphates and nitrates are higher in DAG than STA and Lim. However, all these concentrations are considered low with respect to concentrations that could have negative impact on the hydration of cement. Thus, it does not appear that a direct correlation between the performance of the sample and the concentration of these compounds could be established.

Element	DAG	STA (&STAmix)	Lim
Sulphates (SO_4) [mg/kg DM]	160	<100	160
Phosphates (PO_4) [mg/kg DM]	1.5	<0.4	<0.4
Nitrates (NO_3) [mg/kg DM]	190	<100	<100

DM: Dried material

Table 3-7. Main potential disruptors of cement hydration contained in the three earths

b. pH and organic matters contents

Now let us look on the organic matter and the pH of the earths presented in Table 3-8. As it can be seen, the highest concentration of organic matters is found in STA and the lowest in DAG. In addition, the pH of DAG indicates that it is an alkaline soil, while the pH of STA denotes that it is very acidic (<5.5) while Lim is slightly acidic. These two indicators prove that chemical characteristics of DAG are more favorable for cement hydration than those of STA. Which explain why DAG's performance was improved with cement stabilization more than STA and Lim's one.

In Figure 3.30, the correlation between wet relative strength at 28days of samples DB8, SxB8 and LB8 and pH and organic matter content of the corresponding earths is drawn. It appears clearly that wet strength increases with increasing pH and decreases with increasing organic matter content of the earth.

	DAG	STA (&STAmix)	Lim
Organic matter [%]	3.65	5.35	4.70
pH	7.63	5.23	6.54

Table 3-8. pH and organic matter content of the three earths

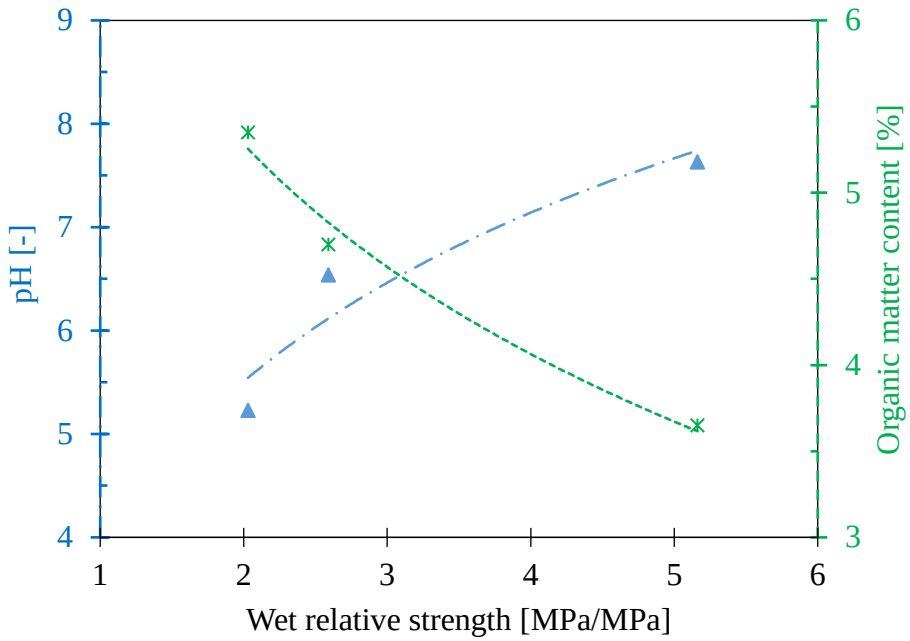

Figure 3.30. Correlation between wet relative strength at 28days of samples DB8, SxB8 and LB8 and pH and organic matter content of the corresponding earths

3.5 Conclusions

In this chapter, the performance of different cement-earth mixtures made with DAG and STA earths and stabilized with five types of cement (CA, CB, CV, CM and CP) at 5 and 8% was studied. The performance analysis was based on the evaluation of the wet and dry compressive strengths, wet to dry strength ratio, water permeability, sorption-desorption isotherms, resistance to spray erosion and resistance to water immersion.

Compressive strength displays a distinction between cements action on the two tested earths. On one hand, the total gain in wet strength was more important for DAG earth than STA. On the other hand, compressive strength of stabilized formulations made with STA earth varies slightly with cement type and do not show improvement with cement dosage between 5 and 8%. As expected, a reduction in the hygroscopic character of the two earths was observed after stabilization. Besides, the hygroscopic characterization of cement-earth mixtures prove that DAG earth was more influenced by the action of cement than STA. Concerning the durability toward water, the obtained results demonstrated that spray erosion test and water immersion test give information on the stabilizer efficacy rather than the material durability. However, it was not evident to make a clear distinction between the action of different cements and to establish a relation between the outcomes of the two methods. Thus, results from one method cannot be used to predict those of another. But in term of cement stabilization efficacy, the two

performance indicators demonstrated that cement action on DAG was much more important than that on STA.

To investigate chemical impact of cement on the two earths, the reaction products were identified by using X-ray diffraction (XRD) and thermogravimetric analysis (TGA). The microstructural analyses made showed that it was difficult to detect cementitious products in STA samples. Which could explain to some extent the lower efficacy of cement in the latter case when compared to DAG as provided by the performance analyses.

In a second stage, results were discussed in function of cements characteristics (dosage, composition, and water to cement ratio). The discussion made call for further investigations of the optimum manufacturing properties based on the water to cement ratio that deliver the maximum compressive strength. This strategy is not usually applied for the determination of the optimum manufacturing properties of CSEB. Then a discussion was made based on the earth characteristics (fineness and chemistry). It was demonstrated that the efficacy of cement stabilization could be connected to the pH and the organic matter contents of the earth. Thus, these parameters seem to be important pre-characterization parameters of natural earth destined for cement stabilization.

Chapter 4. Cyclic erosion test

4.1 Introduction

Results of the durability tests indicates that no coherent relation could be drawn between the three tests. Let us begin with the unstabilized formulations. DUS reported a wet to dry strength ratio two times lower than SUS but it shows at the same time a much better resistance to AET and water immersion test. The same issue happened with stabilized formulations made with STA earth. SA8, SV8 and SM8 have similar wet to dry strength ratio, but the degradation of SV8 and SM8 against AET and immersion test is much more important than SA8. Thus, results from one method cannot be used to predict those of another. Nonetheless, the common point between the three assessment methods is that they tend to provide information about the short-term effectiveness of cement stabilization rather than the durability toward realistic long-term aggression conditions.

Another problematic issue is that tests like AET and immersion tests and other durability tests prescribed in Chapter 1 could not be considered as realistic tools to evaluate the durability of unstabilized materials since they impose unrealistic environmental conditions. They thus induce to a biased assessment of the durability (in particular of unstabilized earths, but not only) that may lead to conclude that some products have good to exceptional resistances and can withstand the normal operating conditions of the building without problem, which is not necessarily true [224]. Therefore, it's essential to develop laboratory methods more convenient to evaluate the durability of stabilized earth blocks.

The first key durability factor that should be the subject of interest in future assessment methods is the way or the rate in which the solicitation is applied. For instance, it's not because samples have resisted to harsh conditions like water sprayed at 50kPa during 60min that it will resist to a - *a priori* - less severe prolonged wind-driven rainfall. Indeed, the latter situation could be more harmful for the same amount of water because in this case water will have more time to penetrate the material and, thus, to reduce its core resistance [300].

The second factor that should be considered is the cyclic drying/wetting effect which inevitably occurs during the lifetime of the material. It follows that the use of a sole wetting experiment should lead to misestimate the durability. However, here again, the way in which the stabilized material is humidified and dried during the test must remain realistic in order to reach proper results. To explain this point let consider the wire brush test which is the only normalized method that consists of wetting/drying cycles to evaluate the durability of earthen materials. It consists of immersing sample 5 hours in water then drying it at 72°C for 42 hours. Thereafter sample's surface is brushed with a wire brush and the sequence is repeated 12 times [335], [336]. The performance of the sample is connected to its total mass loss at the end. Although the cyclic effect of water, the test lacks correlation with realistic wetting/drying conditions. Indeed, there is no proof yet that this kind of extreme cycles will lead to the same deterioration mechanisms as the ones that should be engenders by cycling wind-driven drying and rainfall driven wetting processes. It follows that, as it is, this test should be rather used to estimate the stabilizer efficacy.

In order to bridge this lack of test to accurately assess blocks durability to water erosion, attempt was made in this thesis to develop a novel experimental set-up. This latter aims at simulating the combined effect of wind-driven drying and rainfall. The test was then applied on limited formulations and methods for quantification of the results are suggested and discussed.

4.2 Mechanism of water erosion by wind-driven rainfall (WDR)

4.2.1 Erosivity of rainfall

The erosivity of rainfall is defined as the ability of rain to cause erosion and it is essentially related to the kinetic energy of the raindrop which depends on the rainfall intensity (the volume of water falling on a unit horizontal surface during a unit time) and the angle of the rainfall [337], [338]. The erosivity is influenced also by the physical rainfall characteristics, like the height and the size of the drop and the terminal fall velocity [339]. According to Morgan (1995) [340] the most appropriate expression of the erosivity is the kinetic energy defined as the available energy for detachment and transport by splashing rain [341], [342]. Sophisticated and costly instruments are required to measure the rainfall kinetic energy. For this reason, it is usually estimated from the rainfall intensity which can be easily measured in most countries. Existing empirical relationships between kinetic energy of the raindrop and the rainfall intensity varies from author to another but they could be applicable in specific regions only [343]–[345].

4.2.2 Erodibility of the material

The erodibility of a construction material is defined as its ability of to resist to erosion. In case of CSEB, the erodibility will depend on its water content. If water can evaporate then rainfall will not be damaging [346]. Thus, it is necessary that moisture build up to cause material deterioration that happen due to the internal cohesion reduction and hydromechanical weakness of the material [347]–[349].

The conditions that should exist simultaneously before that water penetrate the material are as follow [350]:

- Presence of water on the material,
- Existence of route for travel of water in the material,
- Presence of a force to move the water.

For non-protected CSEB wall exposed to WDR, the route for moisture is mainly the open microstructure of the earth block and the force that move water is the wind pressure.

Another important factor affecting the erodibility of the material is its surface roughness. The effect of erosion is supposed to be greater on rough surface than on smooth one. In a rough surface, the material removal mechanism is referred to the shear failure of the asperities on the surface [351]–[354]. A crucial point here is that the surface roughness evolves with the successive impact of water, which may make the material more susceptible to erosion.

4.3 Cyclic wetting/drying erosion test

4.3.1 Aim of the test

According to Heathcote (1995) [239], a prolonged rainfall could be more erosive than strong but short rainfall for the same amount of water. In prolonged rainfall, the erodibility of the material decreases because water will have more time to penetrate it. Hence, the effect of prolonging and repeating the action of water on the surface of the material is more harmful

than increasing the kinetic energy of droplets. Therefore, the erosion test proposed focuses on the repetitive prolonged action of water droplet on the surface of CSEB.

4.3.2 Experimental setup description

The proposed method is based on the drip erosion test prescribed earlier in section 1.4.3.2. It consists of submitting earth block to a continuous stream of water generated by a glass tube of 5mm in internal diameter suspended 400mm above the block. The block itself is inclined at 27° from the horizontal. The water level in the reservoir is maintained at 100mm during the test with a tube of water closed on the top. A fan is placed at the same level of the exposed surface of the block at 70mm from the center of the sample as shown in Figure 4.1. The ventilation speed was adjusted at 2m/s. The wetting/drying process is automated and controlled with Labview interface, which allows regulating wetting duration, ventilation duration and cycles number.

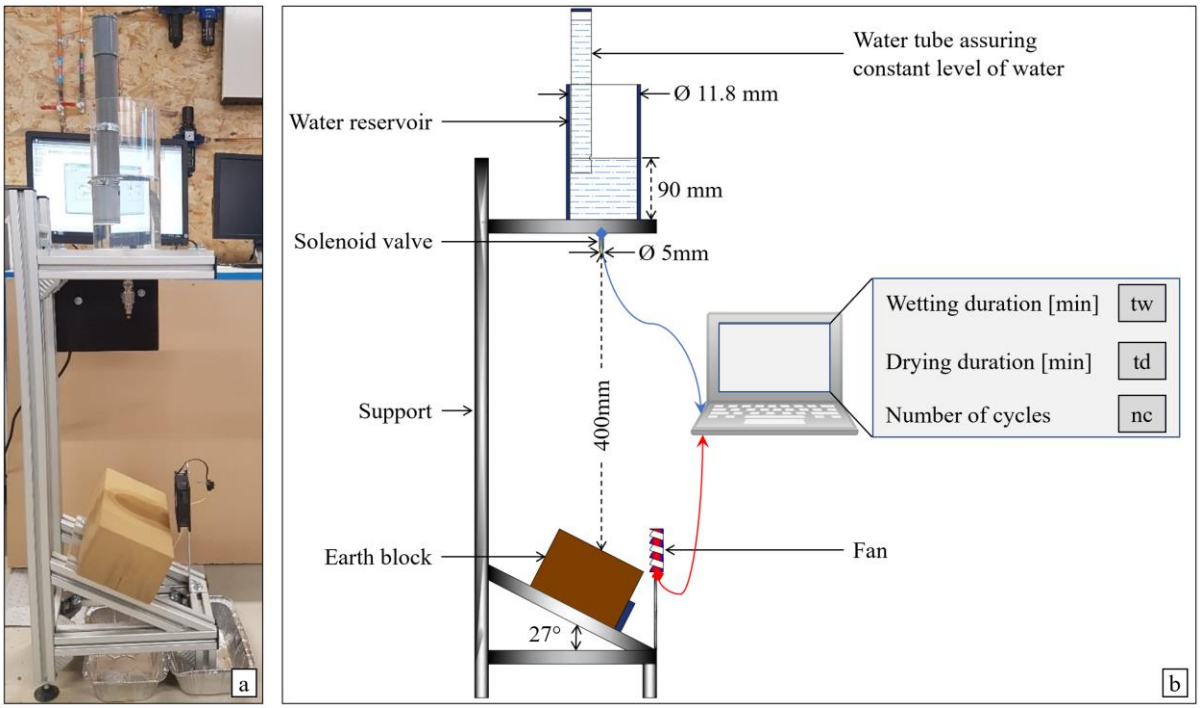

Figure 4.1. Setup of test (a) Schematic representation of the cyclic wetting/drying test (b)

4.3.3 Test parameters

The parameters that could be regulated are the volume flow rate, the wetting and drying duration, and the number of cycles.

The calibration of the water volume flow rate, which correspond in what follow to the number of drops per minute, was chosen based on the average dripping duration suggested in the Geelong drip erosion test. According to the specifications of this test, 100 ml of water should be released within 20 to 60 minutes. The corresponding experimental dripping speeds obtained with the manufactured device are 75 and 25 drops per minute, respectively.

The wetting duration was fixed to 30 minutes. The drying duration was calibrated based on the average duration required for the drying of the block after 30 minutes of wetting at 25 drops per minute.

Stabilized wetted blocks were left to dry in laboratory-controlled conditions of temperature and relative humidity while ventilating the surface. To fix the drying time, a first attempt has consisted in checking the mass decrease several times per day to verify when the block reached a constant mass. It was found that this state was not attained before at least three days, which would lead to unacceptable test duration. It was thus decided to restrict the dried state to the surface of the block only. This latter was considered to be reached when a homogenized color of the surface is obtained (Figure 4.2). It was found to be about 90 minutes for stabilized blocks DB8, DM8, SB8 and SM8.

In conclusion, the chosen cycle consists of 30 minutes of wetting and 90 minutes of drying.

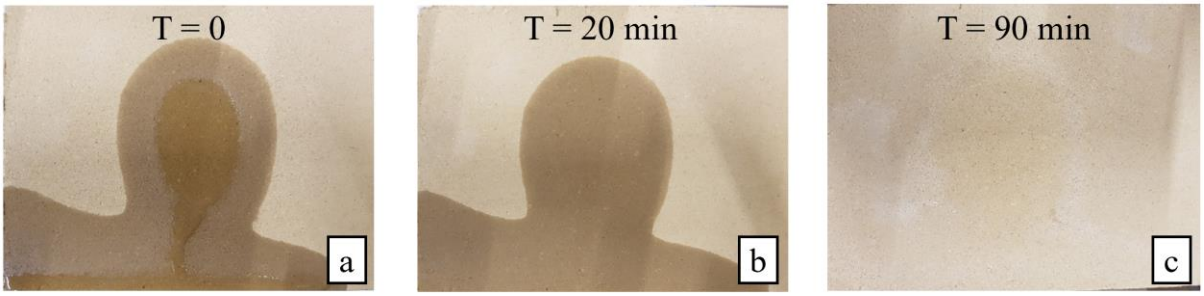

Figure 4.2. Example of the state of the surface of stabilized earth block at the end of the wetting stage (a), during the drying stage (b) and at the end of the drying (c)

4.3.4 Test conditions

All tests were performed in laboratory conditions of 21°±2°C in temperature and 50%RH±5%RH in relative humidity. The tested blocks were cured for 7 days at 21˚C/100%RH then dried in laboratory-controlled conditions at 21˚C±2˚C/50%RH±5%RH until reaching a constant mass.

4.4 Test of the proposed experimental setup

4.4.1 Resistance of DUS and DB8 to uncycled test

The first trial was to perform the drip test on DUS and DB8 to evaluate their performance according to the specifications of the Geelong drip test.

As it is underlined in the introduction of this chapter, even if evidence is limited in existing publications, the drip test cannot indicate long term performance of stabilized earth blocks, but it can give an idea on the short-term resilience to erosion of unstabilized materials. However, to undertake the original test as it is, was found to be necessary to verify how the material of the study behave toward it and to identify the differences that will be induced by wetting-drying cycles.

Blocks were wetted with 100 ml of water with a dripping speed of 75 drops per minute, which corresponds to the most unfavorable condition of this test.

Examples of the state of the exposed surface of the block are presented in Figure 4.3. The pitting depth in the unstabilized block DUS was measured with a digital sliding caliper accurate

to 0.01mm and it was found to be equal to 10.2mm. Thus, DUS could be classified as very erosive according to the specifications of this test. The moisture penetration at the impact point should be lower than 120mm to pass this test. Since the block thickness in the direction of wetting application is 95mm only, and that at the end of the test there was no sign of water on the opposite side of the block, it was evident that the moisture penetration was lower than 120mm. Thus, DUS passed that test.

For its part, the stabilized block DB8 did not show any visible signs of deformation at the end of the test. It could be classified as non-erosive according to the specifications of this test. These observations are in accordance with existing finding of the literature presented in §1.4.3.2.

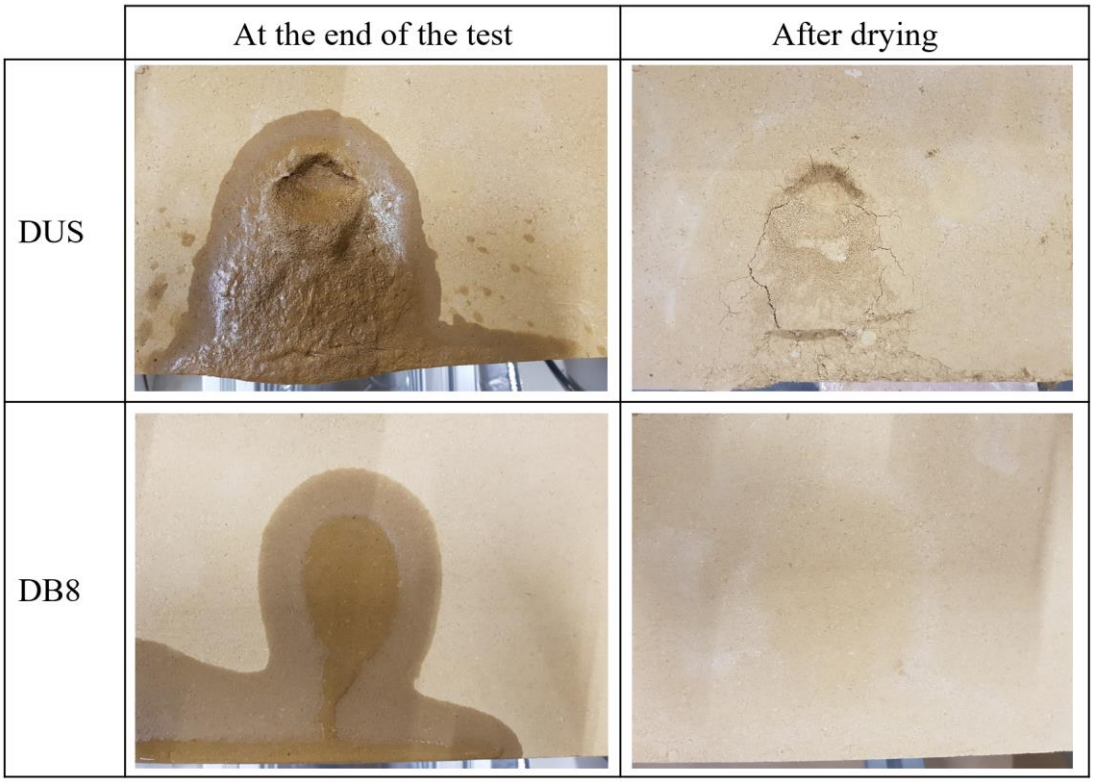

Figure 4.3. State of the exposed surface of DUS and DB8 at the end of the drip test

4.4.2 Resistance of DB8 to cycled test

Since DB8 passed the drip test without degradation, we proposed to test its resistance to wetting/drying cycles. Each cycle consisted of 30 min wetting with a dripping speed of 25 drops per minute followed by a drying (ventilation) stage for 90 minutes. 100 cycles were performed. The corresponding total volume of water used for all cycles is 5 litters. A recipient was putted under the setup to recuperate the water that fall during the test (see Figure 4.1– a). It requires 8.5 days to finish testing one block.

The evolution of the exposed surface of the block is presented in Figure 4.4. No degradation was visualized, nor mass loss was recorded after 100 cycles. However, there is a formation of permanent modification of the surface color on the periphery of the impact point, which remain even after drying the sample in oven at 105°C (Figure 4.4 – d). This could be formed due to the ventilation that is concentrated on the central zone only, which accelerated water

evaporation from this zone before the absorption of water at its surface. While the periphery is less ventilated and thus water has more time to penetrate. If we represent the thickness of the periphery between the dry zone of the block and the central zone by α as shown on Figure 4.4, we can remark that α increases with increasing cycles numbers. But since no degradation was detected, it could be said that erosion was not initiated.

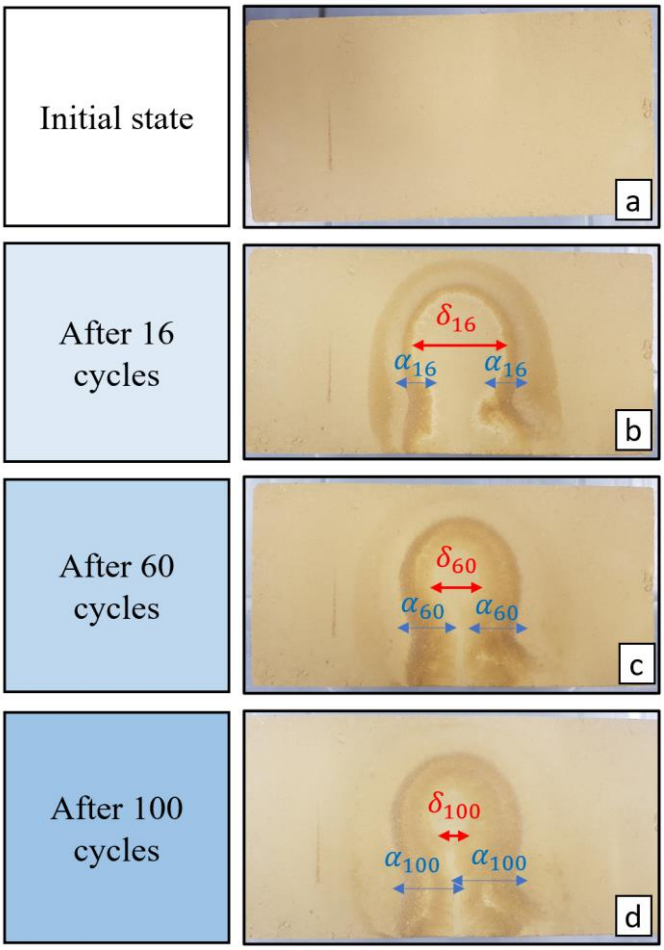

Figure 4.4. Evolution of the surface of block DB8 exposed to the cyclic action of wetting and drying

The high resistance of DB8 (and all stabilized sample made with DAG) to water erosion was already observed in the spray erosion test, where samples did not show a degradation after 60 minutes of continuous exposure to water flow sprayed with a pressure of 50kPa. During the latter test, the kinetic energy of water was significantly higher than that of the drip test. In addition, the total water volume measured with a flowmeter placed at the entrance of water in the spray erosion test was about 500 litters, while the total water volume in the drip test after 100 cycles is 5 litters only. However, prolonged wetting through cycles seems to have impacted the sample more than continuous wetting with higher kinetic energy, since the permanent modification of the surface color was only observed in the former. To make a better comparison, it will be interesting to continue cycles until reaching a total amount of water equal to that one of the spray tests (it corresponds to 10 000 cycles!) or to perform a spray erosion test using a lower water quantity. Due to a lack of time, this comparison could not be made, and we rather decided to continue the test on stabilized blocks made with STA earth which seems to undergo a lower water resistance.

4.4.3 Comparison between cycled and uncycled resistances of SB8 and SM8

In this section, two conditions were tested: cyclic wetting/drying and continuous wetting. Cyclic wetting/drying was performed in the same conditions prescribed in the above section. The continuous wetting consists of submitting the block to the same total amount of water of the cyclic wetting/drying (i.e., 5 litters) with the same dripping speed (25 drops per minute). Each block requires about 2 days to finish the continuous wetting test (uncycled test).

Figure 4.5 presents examples of the initial and finale surface state of the tested blocks in the two conditions. No deformation was detected on the exposed surface of SB8 (Figure 4.5 – b) and SM8 (Figure 4.5 – e) under uncycled test, neither swelling on the edge on which water runoff (Figure 4.5 – c & f). Thus, based on the results of this test, it appears that SB8 and SM8 have similar resistance. But results of the cycled test indicate that SM8 (Figure 4.5 – k & l) is more prone to surface erosion than SB8 (Figure 4.5 – h & i).

We propose to define three parameters could for the evaluation of the state of the blocks surface at the end of the cyclic test: the limits of the shallow surface absorption, the limits of the impact point and the width of edge erosion. The first parameter indicates the borders between the surface that remained dry and the that one that was wetted during the test. As shown on Figure 4.6, this limit is wider for SB8 than SM8.

The second parameter is used to verify the state of the zone directly subjected to the dripping action, which could result in the formation of a marked eroded hole like the case of SM8 (Figure 4.6 – b). While SB8 was not eroded within the limits of the impact point (Figure 4.6 – a). The diameter of the eroded hole on SM8 measured in the perpendicular and parallel direction to that one of the water movement direction is 20 and 28mm, respectively. It is worth noting that the pitting depth is shallow, and it did not result in stagnant water inside the hole. Knowing that stagnant water phenomenon disrupts the study of erosion of earth-based materials as highlighted by Beckett *et al.* (2020) [355].

The third parameter is the eroded width of the material from the lower edge of the block that experiences water runoff during the test, and it is denoted by Δ. Here it was measured with digital sliding caliper on the dried block at the end of all cycles after passing a metallic brush on the edge of the block two times (going and coming) without pressure (e.g., see the difference between the edge state on Figure 4.5 – h before and Figure 4.6 – a after brushing). The measured Δ is 126.4mm for SM8 and 84.1mm for SB8.

To connect the three parameters, it seems that the local absorption of water by block SM8 under the impact point is higher than that of SB8. This issue was traduced with noticeable erosion of materials in block SM8 and a concentration of the water absorption in a limited periphery of the impact point. Therefore, the edge erosion was accelerated in the latter block. Thus, it will be interesting to follow the variation of these three parameters with respect to cycle's numbers to know the time from which different formulations start to exhibit different behaviors.

Another interesting issue is to cut the block in the middle into 4 parts passing in perpendicular and parallel direction to the water movement to measure the depth of moisture penetration at the end of the latest wetting stage. Here it was not done because we planned to quantify the erosion of the block as it will be presented in the following sections.

Finally, the observed differences in these three parameters between the two blocks indicate that the resistance of block made with STA earth and stabilized with cement type CB has a higher

resistance to the repetitive action of water than that one stabilized with CM. Whereas, it was not possible to detect this difference in the behavior of the formulations from the uncycled test.

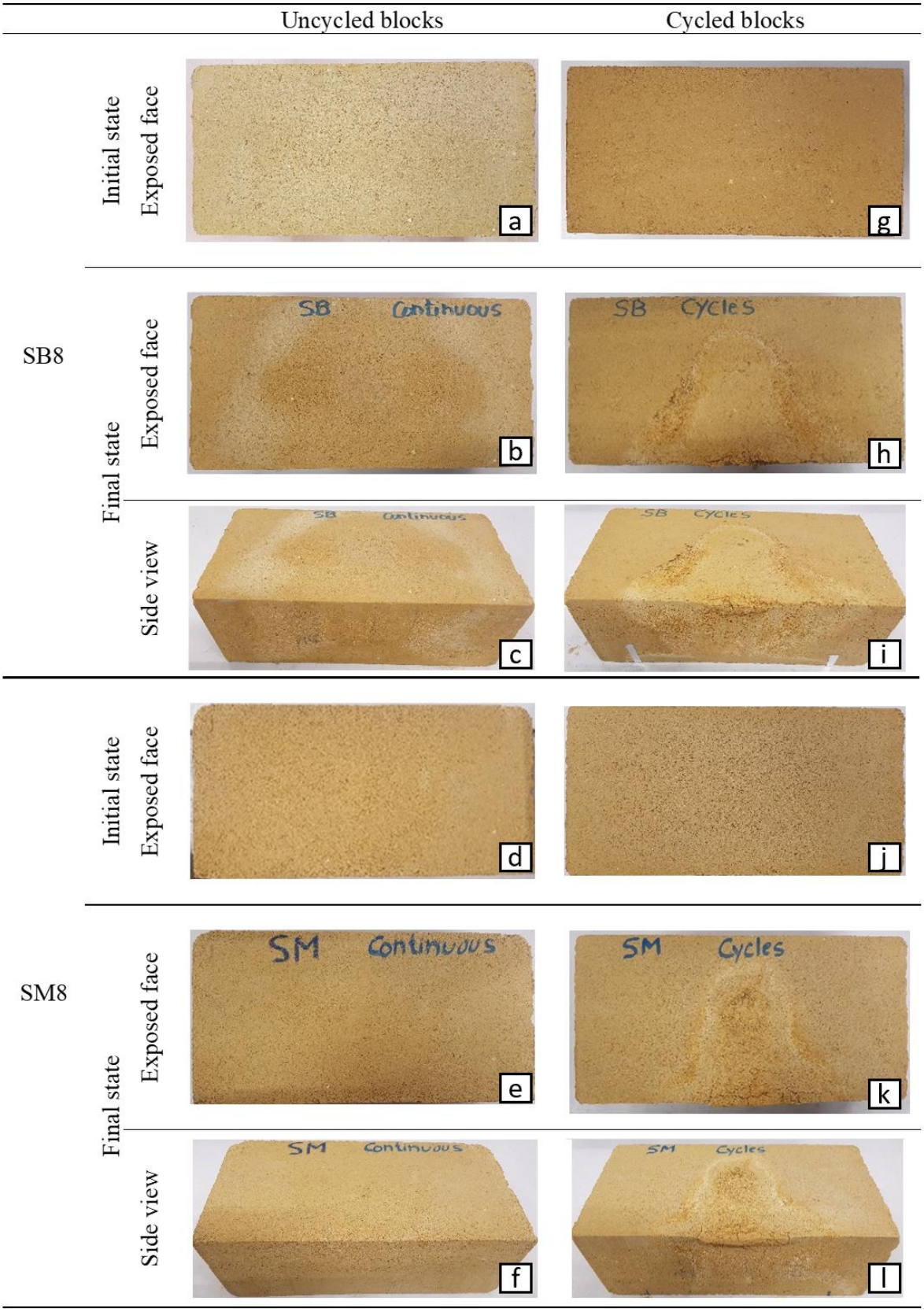

Figure 4.5. blocks states before and after uncycled and cycled erosion test

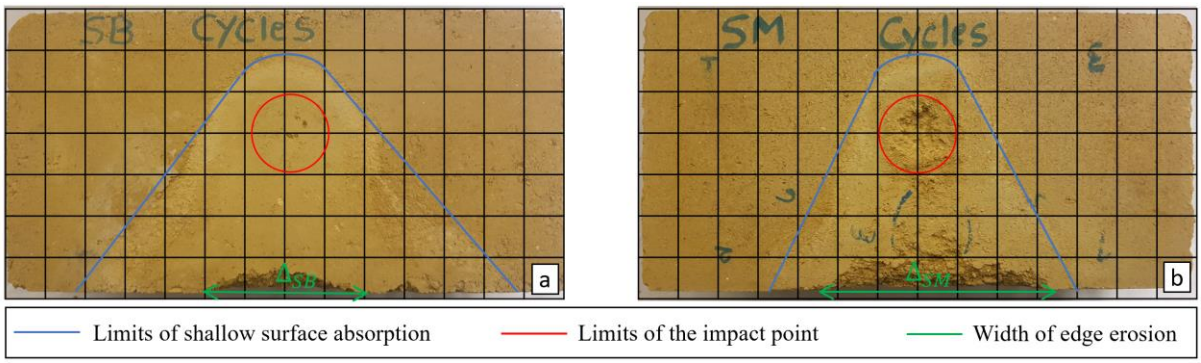

Figure 4.6. Visualization of different parameters used to evaluate the surface erosion of SB8 (a) and SM8 (b)

4.5 New tools for the quantification of the results

Despite their simplicity of implementation, on the basis of our personal experience, the data analysis presented in the previous section were found to be quite complex to carry out in cases where the degradations appear to be too low, too high or heterogeneous. In order to correct this issue, new approaches to quantify the test results are proposed in this section. They are based on measurement of ultrasonic wave propagation in the block and on the mass loss after abrasion.

4.5.1 By ultrasonic testing

Ultrasonic testing is a well-known non-destructive method used for the evaluation of material properties in civil engineering. The measurement of ultrasound pulse velocity is one of the standard tests for concrete properties determination defined by the standard EN 12504-4 [356]. The concrete quality could be estimated from the ultrasonic pulse velocity (UPV) that is used as an indicator of strength with 95% confidence limits of about ±20% on predicted strength [357]. In [358], the UPV was used as indicator of density and compressive strength of a mixture of cement, fly ash and sand. UPV is also employed for the characterization of non-visible subsurface damage in concrete because the propagation of ultrasonic wave have the potential to give information about the depth of the crack as it is the case in studies made in [359] and [360]. Further, examining the ultrasonic method is beneficial for predicting the fatigue lives of the asphalt concrete specimens non-destructively [360].

It follows that quantifying the results of the erosion test through the ultrasonic testing seems to be very interesting for many reasons. Firstly, it is a non-destructive method, thus it could be applied between cycles to follow the evolution of the block's properties with cycle's number (Young modulus, compressive strength, etc.). Secondly, it an easy and simple method that does not requires sophisticated or expensive equipment. Thirdly, it is a well-known method for material characterization in civil engineering. Thus, it could benefit from existing models and empirical relations that enables estimating the materials properties from the measured transmission time. Or at least it could benefit from existing models to develop other more adapted to earth-based materials. Fourthly, it enables characterizing the block in many directions and in different modes, which provide more information on the characteristic's evolution of the block. Especially that during the developed erosion test the block is expected to be deformed in all directions.

Here the ultrasonic testing was adopted to verify its potential to quantify the results of the erosion test on CSEB. The ultrasonic measurements were done in direct transmission mode as shown in Figure 4.7 – b. Knowing that ultrasonic probes could be arranged in three configurations: on opposite faces for direct transmission, on adjacent faces for semi-direct transmission and on the same face for indirect or surface transmission (Figure 4.8).

The device used measures the wave propagation time with accuracy of 0.1µs. The pulse transmission frequency was set to 4 Hz and the voltage was set to 1000V. Prior to measurements, the device was calibrated with a standard calibration bar provided with it. The diameter of transducers is 45mm. Ultrasound gel was applied on the surface of the two probes for each measurement. The measurements could be made in three directions as schematized in Figure 4.9. It was not possible to make measurements in direction 3 because the time required to travel the distance in this direction was out of the range of measurements of the device used.

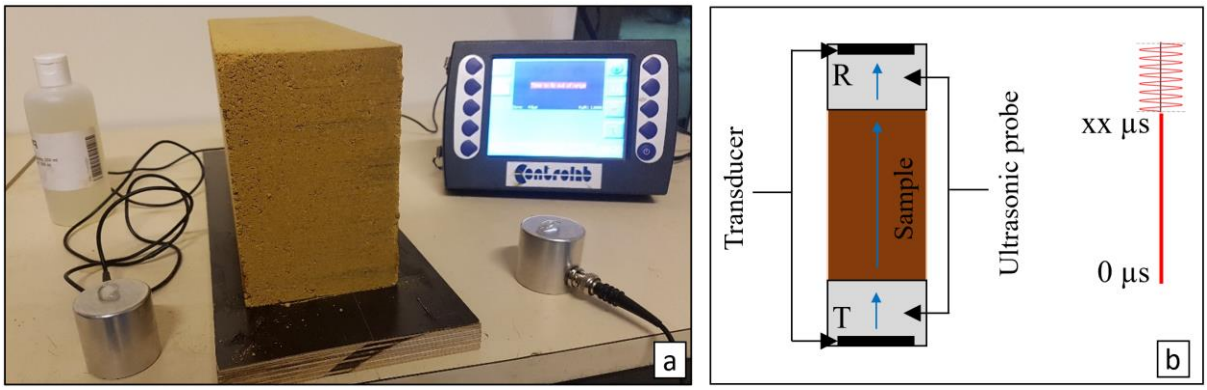

Figure 4.7. Visualization of the ultrasonic device (a), ultrasonic wave travel in direct transmission mode (b)

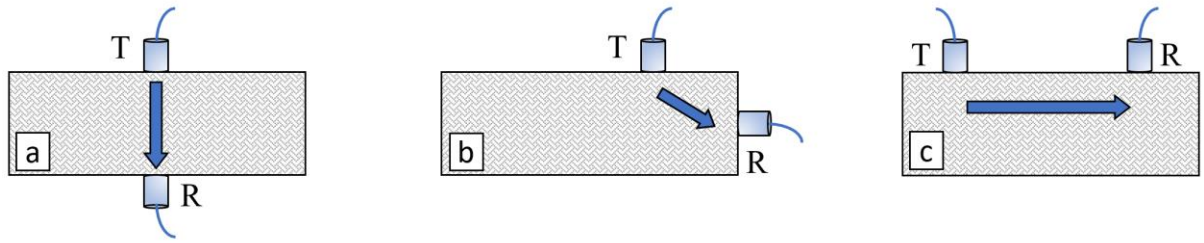

Figure 4.8. Possible arrangement of probes: direct transmission (a), semi-direct transmission (b) and surface transmission (c)

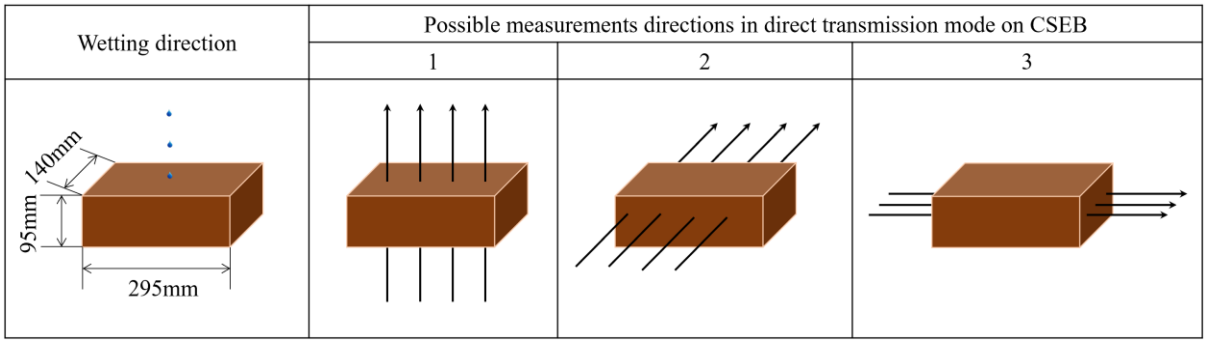

Figure 4.9. Possible measurement directions in direct transmission mode on CSEB

Finally, since water content impact the wave propagation velocity, all the measurements were made on blocks dried at 21˚C ± 2˚C/50%RH ± 2%RH until reaching a constant mass.

To verify the accuracy of the measured values, measurements were made firstly in direction 1 on block that was not tested in erosion. A grid guide was applied on opposite surfaces of the block as shown in Figure 4.10 to facilitate the measurements. On each position, between 4 and 10 measurements were done, and the ultrasonic probes of the device were permuted between two measurements as recommended in the manual of the device. Results of the measured propagation time are presented in Table 4-1.

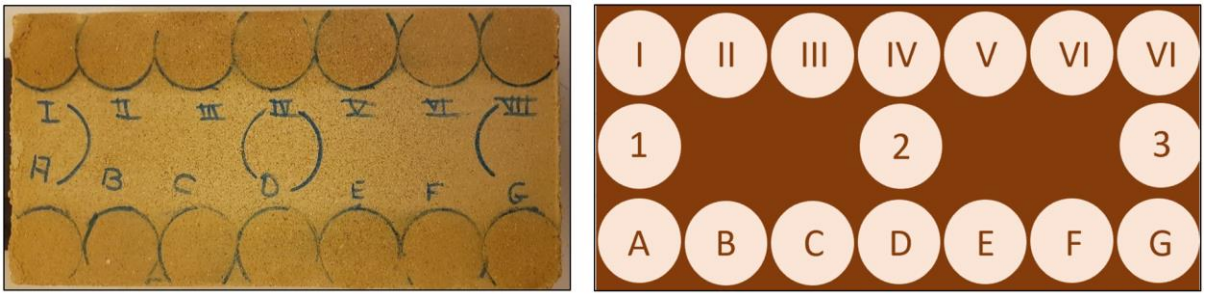

Figure 4.10. location of probe placement on the surface of non-tested block – first trial

The ultrasound propagation velocity (V) in km/s was deduced from the average values of transmission time in each position as follow:

$$V = \frac{L}{T} \tag{4-1}$$

Where L is the transmission distance, which is in our case the thickness of the sample between the two transducers. It was measured with a digital sliding caliper in the middle of each position on the block (i.e., I, II, etc., A, B, etc., 1, 2, 3, see Figure 4.10). For position 2, it was not possible to measure the thickness with the sliding caliper, thus it was taken as the average between thicknesses on positions IV and D.

Results made on untested block are visualized as a velocity map (V-map) in Figure 4.11. The obtained values are in the range of 1 km/s. To get an idea, the propagation velocity in concrete mixtures made of gravel, slag, and cement (2 to 6%) prepared in [361] at their optimum water content and dry density ranged from 1.5 to 3.5 km/s. In [362], the propagation velocity in light weight concrete ranged between 3.5 and 4.5 km/s. The reported velocity in [363] in concrete for different aggregates ranged from 3.2 to 4.6 km/s for compressive strength between 18.3 and 42.8 MPa. Thus, it appears that the obtained values are in harmony with what is found in literature data, given that compressive strength of CSEB tested here are of the order of 5 – 6 MPa and knowing that higher ultrasound propagation velocity indicates higher compressive strength resistance [362], [364].

A variation in the transmission velocity of the order of 0.14 km/s between the corners of the block and other positions. This small variation is expected since there are slight differences in densities of outer and central parts of the produced blocks (see Figure 2.10). Although these differences, the transmission velocities are uniformly distributed far from the corners.

After the verification of the setup, the number of measurement points was reduced to 5 in directions 1 and 2 as shown Figure 4.12 and Figure 4.13, respectively.

The ultrasound propagation velocity calculated from the transmission time was measured in direction 1 and 2 in cycled and uncycled blocks. We recall that for uncycled and cycled tests, the same total amount of water was drop in the sample (5 litters), with the same dripping speed (25 drops per minute). Results are summarized in Table 4-2 (direction 1) and Table 4-3 (direction 2). They show that the calculated ultrasonic pulse velocity values range from 0.5 to 1.35 km/s.

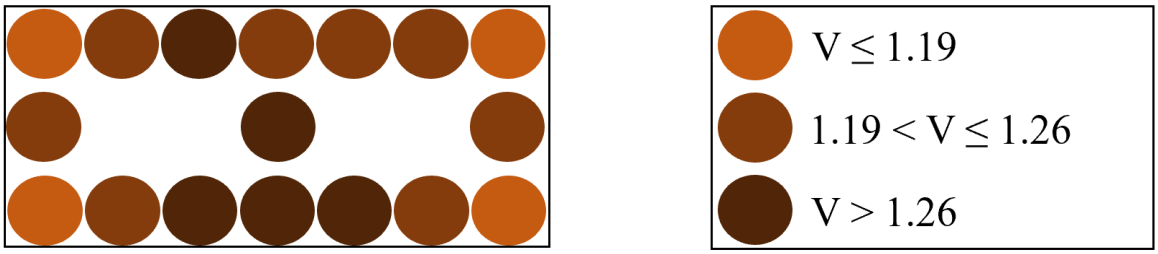

Figure 4.11. V-map [km/s] in non-tested block SM8

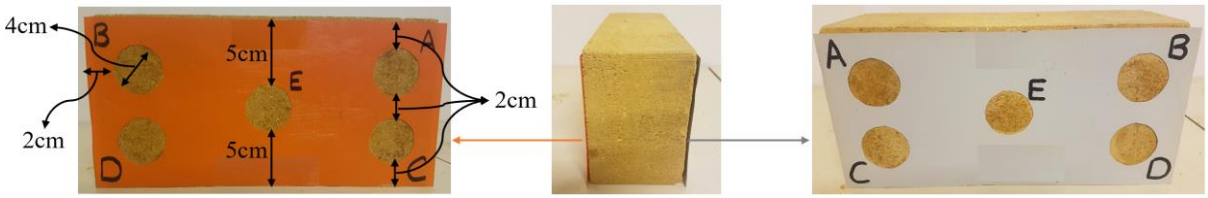

Figure 4.12. Grid guide adopted for measurements in direction 1 (parallel to direction of the water drops)

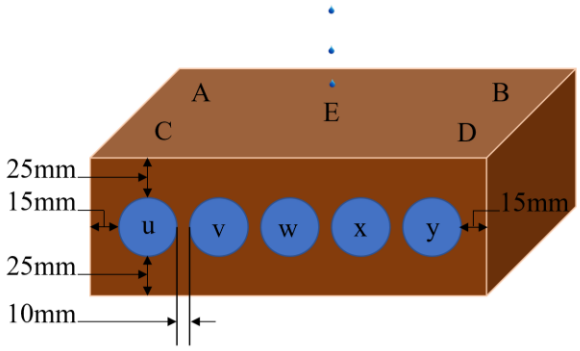

Figure 4.13. Schematic representation of the location of measurement points on the block in direction 2 (perpendicular to the direction of the water drops)

The V-maps that correspond to measurements in direction 1 are presented in Figure 4.14 while those in direction 2 are presented in Figure 4.15. At first, whatever the direction, lower velocities values are observed for SM8 than for SB8. It is consistent with the higher stiffness of SB8.

Measurements on direction 1 showed that for both blocks, the velocity maps remain quite close untested sample, when they are under uncycled conditions. In particular, the highest velocity value is obtained under the impact point (E), while the opposite should have been observed if

damage had occurred. For their part, blocks submitted to cycled conditions showed lower velocities, in particular under the impact point, which tend to indicate the occurrence of damage.

Top			Middle			Bottom		
	t [µs]			t [µs]			t [µs]	
Position	Measured	Average	Position	Measured	Average	Position	Measured	Average
A	81.2 81.4 81.0 81.1 81.6 81.1 80.9 81.8 81.8 81.5	81.3±0.31	1	76.1 76.5 76.6 77.2	76.6±0.39	I	81.8 82.2 82.6 81.9	82.1±0.31
B	76.0 77.0 76.0 77.0 76.3 77.4 77.4 77.4 77.8 78.3	77.1±0.73				II	76.4 77.5 77.3 77.2	77.1±0.42
C	73.0 73.9 73.4 73.7 74.4	73.7±0.47				III	73.9 75.0 74.6	74.5±0.46
D	73.4 73.6 73.6 73.6 73.9	73.6±0.16	2	70.8 70.5 71.6 71.1	71.0±0.41	IV	76.0 76.5 76.9 76.0	76.4±0.38
E	72.5 73.0 72.9 72.7	72.8±0.19				V	77.6 77.6 77.8	77.7±0.09
F	76.0 76.0 76.6 76.7	76.3±0.33				VI	78.8 78.6 79.2	78.9±0.25
G	79.4 79.1 80.1 80.2 80.5 80.5	80.0±0.53	3	79.9 79.5 79.4 79.5	79.6±0.19	VII	81.1 81.8 81.3	81.4±0.29

Table 4-1. Summary of wave propagation time (t) in block SM8 (initial state)

The V-maps that corresponds to measurements in direction 2 are presented in Figure 4.15. Consistently to what happened in direction 1, lower velocities values are measured for cycled than for uncycled conditions.

Let us mention here that some problems were encountered during the measurements in direction 1 on cycled blocks. Indeed, particles were torn off from the exposed surface of the block by the action of the application of ultrasonic gel. Thus, measurements in the same point were not repeatable like untested and uncycled blocks. This problem was not faced in testing surfaces in direction 2.

Anyway, even if some interesting tendencies where found, this method struggles to give a precise quantification of the damage induced by both cycled and uncycled tests. In particular, it was not possible to detect apparent distinction between SB8 and SM8 tested in uncycled conditions. Actually, the main disadvantage of this method is that it requires the use of ultrasonic gel. Since this latter could be absorbed by the block and/or remove some materials form rough surfaces it is not possible to realize an initial V-map of the sample in the direction 1 before testing. On the other side, the accuracy in the direction 2 was found to be too small in order to detect significant differences between undamaged and damaged samples. Another problem is the time it requires to test one block if measurements in different directions will be carried out, while at least 3 measurements per point should be made, adding to that the measurements of the transmission distance.

However, here measurements were made only in two directions and in one transmission mode. Depending on the device used, its characteristics and its accuracy, more measurements could be made to make robust conclusions. Thus, even if the results obtained in this former study were not conclusive, some additional research on that measurement protocol might not be worthless.

Block	SB8					SM8				
Point	A	B	C	D	E	A	B	C	D	E
Uncycled	1.28	1.28	1.26	1.26	1.34	1.10	1.11	1.11	1.08	1.30
Cycled	1.24	1.15	1.24	1.11	1.25	1.21	1.19	1.14	1.19	1.12

Table 4-2. Summary of ultrasound propagation velocities [km/s] measured in direction 1

Block	SB8					SM8				
Point	u	v	w	x	y	u	v	w	x	y
Uncycled	1.20	1.27	1.28	1.32	1.29	0.87	1.14	1.23	1.19	0.64
Cycled	1.16	1.09	1.13	1.25	1.26	1.16	1.15	0.95	0.96	1.08

Table 4-3. Summary of ultrasound propagation velocities [km/s] measured in direction 2

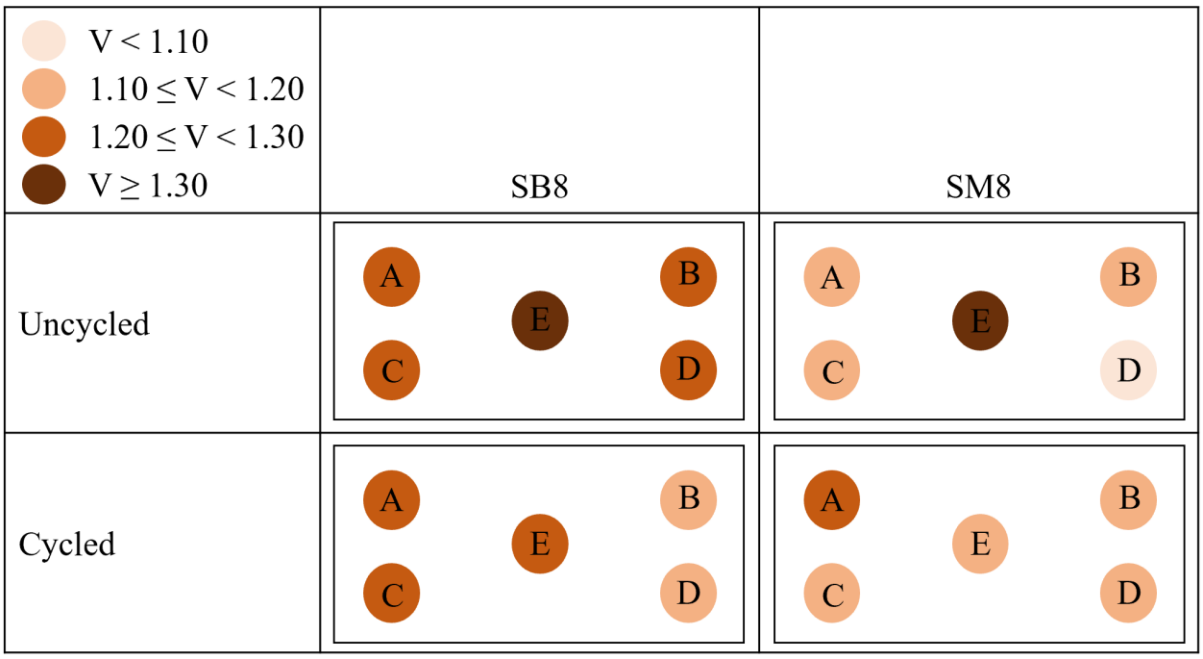

Figure 4.14. V-map [km/s] of block SB8 and SM8 (direction 1)

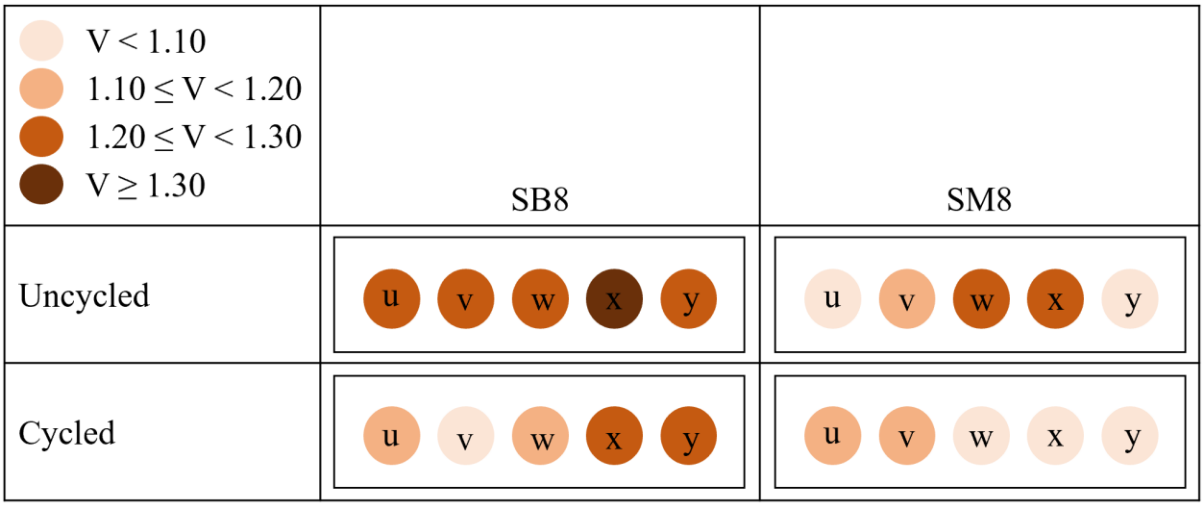

Figure 4.15. V-map [km/s] of block SB8 and SM8 (direction 2)

4.5.2 By abrasion testing

The second method that we proposed to quantify the results of the developed erosion test is the abrasion test. To do so, the dried blocks were brushed with a wire brush having the characteristics shown in Figure 4.16 according to the French standard XP P13-901 [190].

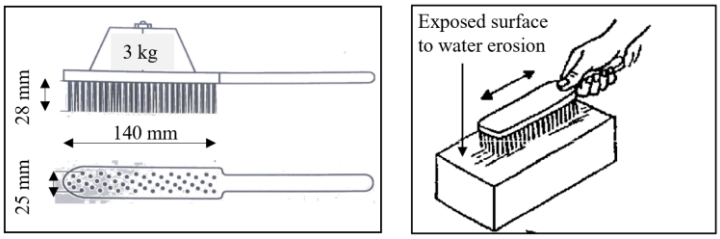

Figure 4.16. Schematic visualization of the abrasion test

The exposed surface of the blocks was split into 5 strips as shown in Figure 4.17. One going and coming per second for 1 minute was done on each strip. The abrasion test was performed on cycled and uncycled block tested with the erosion test. Figure 4.18 present the state of the surface of blocks before and after the abrasion test.

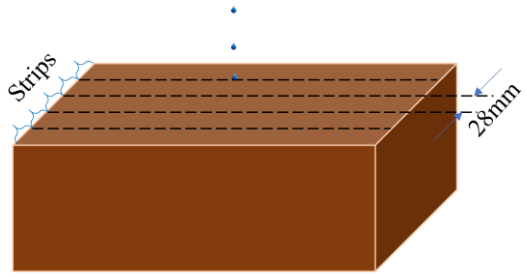

Figure 4.17. Strips distribution on the exposed surface of the block

The abrasion coefficient of blocks was calculated as shown in eq. (4-2).

$$\text{Abrasion coefficient} = \frac{M_{ab}}{A} \tag{4-2}$$

Where:

- M_{ab} [g] is the total mass loss of a sample tested in cycled or uncycled erosion test (sum of the mass loss after the erosion test and the mass loss after the abrasion test).
- A [cm^2] is the area of the brushed surface (here 413 cm^2).

The mass loss after the erosion test was calculated from difference between the air-dried masses of the block after the erosion test and that one before the test. It is worth noting that usually the mass loss after the abrasion test in the French standard requires weighting the mass of the recuperated material quantity from the block. However, it was easier here to weigh the block before and after the abrasion test to deduce this mass loss.

Results are summarized in Figure 4.19. It shows two interesting points. Firstly, the uncycled block SM8 has an abrasion coefficient higher than SB8 by 60% approximately. Logically, this difference becomes even more important for cyclic conditions, for which SM8 have an abrasion coefficient 3 times higher than that of SB8.

This quantification through the abrasion coefficient seems to be interesting for different reasons. Firstly, the test is already normalized in many standards and it could be done in most of laboratories that work on the characterization of earth-based and geo-based materials. Secondly, it is a rapid test that takes only 1 minute per block for brushing, then the block is simply weighted.

The sole problem is that measurements depend on the operator since brushing is done manually. To automatize the test, the metallic brush could be fixed on a support connected to a motor that enable moving the support with fixed pressure and defined speed without the intervention of an operator.

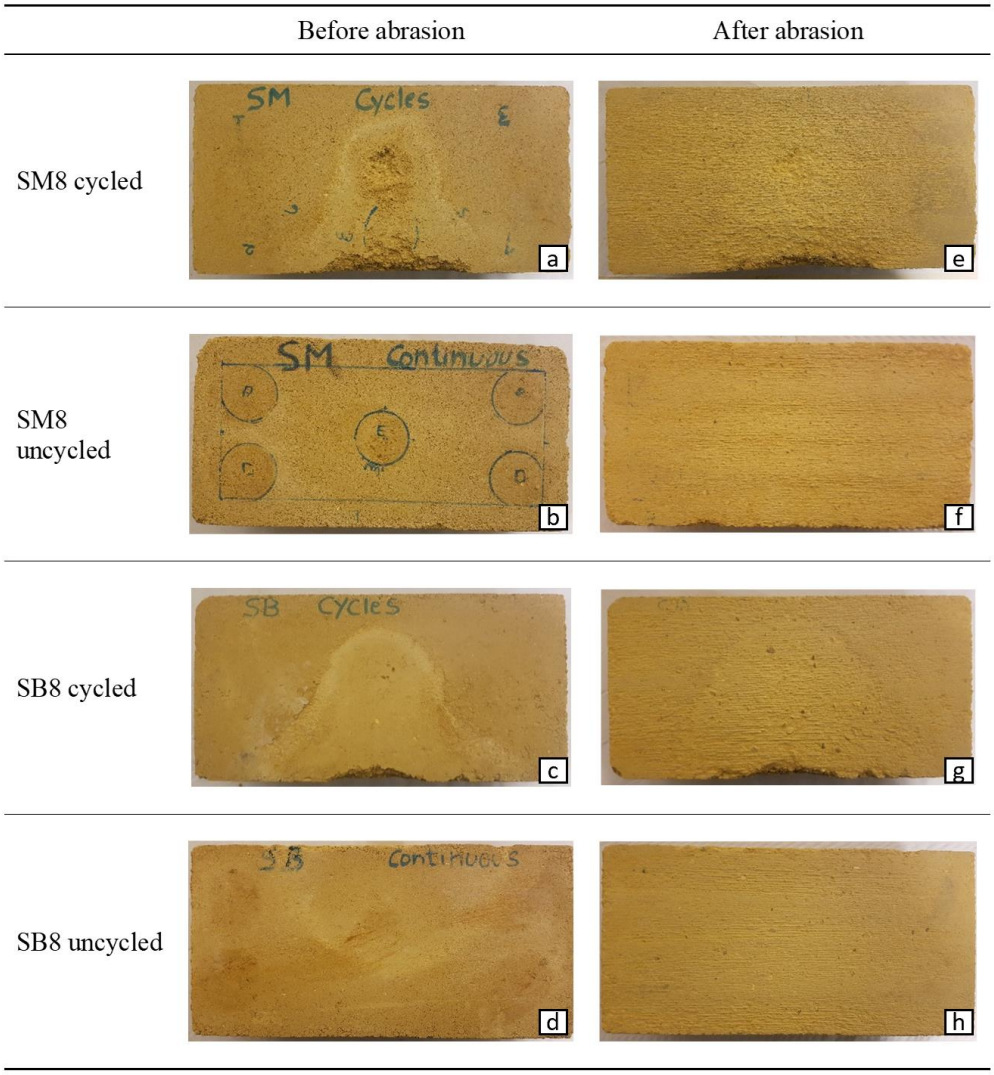

Figure 4.18. Examples of block surface's state before and after abrasion

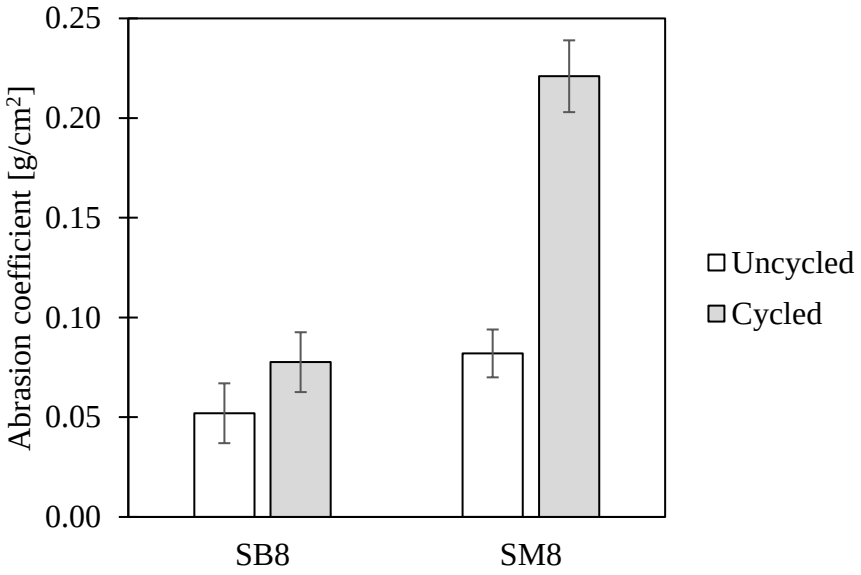

Figure 4.19. Results of abrasion coefficient

4.6 Conclusions and future trend

In this chapter, a novel cycled wetting drying test was developed to mimics the effect of wind-driven rainfall on the surface of CSEB. Each cycle consists of submitting the inclined surface of a block to the action of water droplets released with a constant dripping speed and followed by a ventilation stage. The wetting and drying duration, the number of cycles and the dripping speed could be controlled as desired. As a first choice, the dripping speed was fixed at 25 drops per minutes based on the recommendations of Geelong drip test. Firstly, the test was applied on DUS and DB8 in continuous mode by submitting the surface of blocks to 100ml of water. The two formulations passed the test, but DB8 did not show any degradation or deformation at the end of test. Then, the wetting and drying duration were putted at 30 and 90 minutes, respectively. After 100 cycles, DB8 did not show any visible degradation or deformation, but a color modification of the surface of the block was detected on the periphery of the impact point.

In a second stage, the cycled and uncycled test was applied on SB8 and SM8 with the same conditions. Results show that both formulations passed the uncycled test without any visible degradation or deformation. While results of the cycled test highlighted a lower resistance of SM8 in comparison with SB8.

Two methods were proposed to quantify the results of the erosion test, the ultrasound propagation velocity, and the abrasion test. Both methods enable identifying differences in the performance of SB8 and SM8 toward uncycled test that were not possible to be visually detected on the blocks, even if we managed to produce quantified results of degradation only for the abrasion test.

The results presented in this chapter will be completed by further studies including the effect of varying the parameters of the test and the evolution of the block characteristics with cycle's number to improve the understanding of degradation of stabilized earth block with respect to the formulations properties.

In this context, CSEB wallets were prepared and placed in an exposed open space in the laboratory as shown in Figure 4.20 to follow their degradation in real conditions and then trying to connect their performance to the results of laboratory testing. This work will be continued in another study after the present thesis.

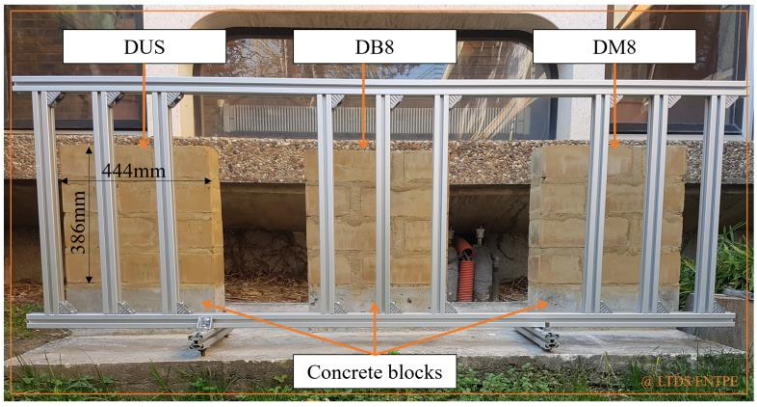

Figure 4.20. Examples of wallets exposed to real environmental conditions at the LTDS/ENTPE

Chapter 5. Bond development and moisture transfers in block-mortar interface

As introduced in Chapter 1, the mechanical performance of masonry does not depend only on the quality of the block. The past literature reveals that bond in masonry is function of mortar composition, water quantity in the fresh mortar, and the water content of the block at the time of masoning. However, studies on the moisture transport phenomenon and their influence on the bond strength development in the stabilized earth block masonry are limited. In this chapter, the bond strength development is investigated though the RILEM method and triplet test in function of block and mortar properties. Since the inclusion of mortar joint in mechanical tests makes strength determination under saturated conditions difficult, water absorption test is used to estimate the quality of the block-mortar interface in saturated conditions.

5.1 Materials

5.1.1 Blocks

Blocks that will be tested belongs to the formulations DUS, DB5 and DM5. To simplify the designation of assemblies in what follow, DUS will be referenced as BU (for **B**lock **U**nstabilized), DA5 will be referenced as BA (for **B**lock stabilized with CEM II/**A**) and DM5 will be referenced as BM (for **B**lock stabilized with **M**asonry cement). All blocks were cured 7 days at 21˚C±2˚C/~100%RH then dried at 21˚C±2˚C/50%RH±5%RH for two months[5] until reaching a constant mass (Figure 5.1).

Figure 5.1. Blocks stored in controlled conditions of temperature and relative humidity

[5] It was planned to undertake tests at the age of 28 days, but due to the process of laboratory closure at the beginning of the COVID-19 pandemic, it was not possible to perform tests as planned.

5.1.2 Mortar

5.1.2.1 Formulation and designation

Two families of mortar were designed to be tested in this study, earth-based mortar and cement-sand mortar. A well graded sand sieved at 2mm, having a coefficient of uniformity (Cu) equal to 3 and a coefficient of curvature (Cc) equal to 1.15, was used in formulating all mortar mixtures.

The designation of the mortar is made in lowercase letter. The first letter denotes the main component (**d** for DAG, **s** for STA and **c** for cement) and the second letter is for the cement type that is used (**u** if no cement is used, **a** if CEM II/A is used and **m** if masonry cement is used). The summary of the mortar formulation is presented in Table 5-1. Cement:earth:sand ratios were chosen based on ratios recommended in [283] without optimization of the ratios in function of the earth properties.

Concerning earth-based mortars, the prime focus was put on mortars made with DAG (same earth than the studied blocks). But mortars made with STA earth were introduced to discuss de possibility to use some kind of "generic" earth-based mortars, composed with a different earth than block's one. Note that the two earths were sieved at 2mm before being incorporated in mortar's mixtures.

Mortar type	Designation	Earth	Cement type	Cement:Earth: Sand ratio	Water content by dry mass of solid W/S [%]	Water to cement ratio W/C
Earth-based mortars	**du**	DAG	-	0:4:8	17.6	-
	da		CA	1:4:8	22.7	2.95
	dc		CM			
	su	STA	-	0:4:8	21.2	
	sa		CA	1:4:8	25.1	3.26
Cement-sand mortars	**ca**	-	CA	1:0:3	18.7	0.75
	cm	-	CM			

Table 5-1. Mortar's properties

5.1.2.1 Optimal manufacture water content

A first attempt to ascertain the manufacture water content of earth-based mortars was based on the modified slump test notably defined and used in [365]. This test was performed using a downscaled Abrams cone geometry of 10.5cm in height, 7cm in bottom diameter and 3.5cm in top diameter (Figure 5.2). The cone was filled-up with three layers of mortar, each layer was pricked by 10 strokes using a plexiglass rod of 5mm in diameter. The excess of mortar was removed from the top surface of the cone, which was lifted immediately, vertically, and carefully by turning it a little to unmold it.

It was however found a significant earth's nature-dependency on slump value leading to a workable material. For example, a slump between 5 and 6cm was found optimal of stabilized earth-based mortar made with DAG earth, while in case of STA optimal slump rather lies between 1 and 3.

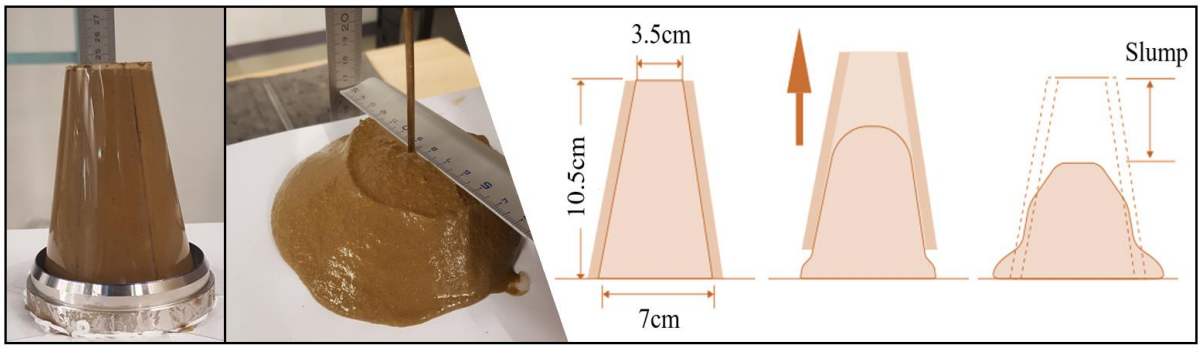

Figure 5.2. Testing the consistency of the mortar - slump test

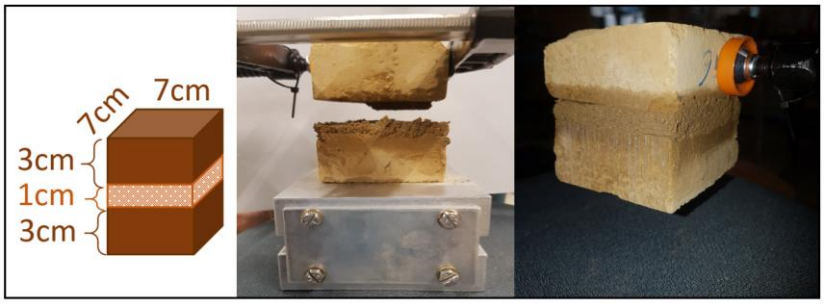

Figure 5.3. Fresh-sticking test

Mortar type	W/S [%]	W/C	Workability	Slump [cm]
du	16.0	-	Too dry	0.7
	17.6	-	Workable	1.2
	19.1	-	Too wet	3.0
da and dc	18.9	2.46	Too dry	1.6
	21.1	2.74	Dry	2.7
	22.0	2.86	Min. Workable	5.4
	22.7	2.95	Workable	5.9
	23.9	3.11	Max. workability	6.4
	25.0	3.25	Too wet	8.3
su	19.7	-	Too dry	0.5
	21.2	-	Workable	1.3
	23.1	-	Too wet	2.0
sa	21.2	2.76	Too dry	0.9
	22.5	2.92	Dry	1.2
	23.5	3.06	Min. workability	1.4
	25.1	3.26	Workable	2.1
	26.5	3.45	Max. workability	2.7
	28.4	3.69	Wet	5.6
	30.0	3.90	Too wet	6.2

Table 5-2. Results of slump test

To avoid this earth's nature-dependency issue, we proposed another test named fresh-sticking test for verification purposes. It allows verifying mortar mixtures that enable sticking two

pieces of blocks together. It consists of verifying if two part of block stuck together with a mortar mixture for 3 minutes under the self-weight of the assembly (Figure 5.3). If so, the corresponding water to solid ratio could be selected. All workable mortars passed the test, while dry and wet mortar failed. When different water contents are possible, the average is taken.

The obtained results are listed in Table 5-2. They show that in case of unstabilized earth-based mortar, the water to solid ratio ensuring a good workability is approximately equal to the plastic limit of the corresponding earth. After stabilization, this ratio was increased by 4% approximately. Further, cement mortars need less water to cement ratio when compared to the corresponding value for stabilized earth mortar. This observation is in accordance with results found in [366].

5.2 Methods

5.2.1 Measurement of the uniaxial compressive strength

Simple compressive strength was measured following the procedure recommended by the French standard XP P13-901 [190], which is introduced in Chapter 1. Compression tests were carried out using a hydraulic press with a capacity of 250kN and were run at a constant rate of 1.2mm/min until failure. Blocks were tested in the direction in which they were compacted, which is the direction in which they are generally used in walls.

The preparation of each assembly consists firstly of sawing a single block into two equal parts using a saw machine. A homemade formwork was used to facilitate the application of a uniform mortar bed of 10mm thickness and to ensure its good distribution. Prior to the application of the mortar layer, the surface of the two halves in contact with mortar were humidified with a sponge soaked in water. This practice is recommended by skilled bricklayers and it is one of the block lying principles for walls to avoid the quick migration of water from the mortar to the dry block [283]. Joints were fully bedded over a 140mm×145mm bed face area and the formwork was removed quickly after assembling the two halves. Finally, the assembly was adjusted using a spirit level to confirm an even thickness of the mortar. All samples were cured for 7 days under plastic sheeting and placed in laboratory-controlled conditions of 21˚C in temperature and 50% in relative humidity.

5.2.2 Measurement of the shear strength at the block-mortar interface

A shear test inspired from the triplet test defined in the European Standard NF EN 1052-3 [367] was realized in this work to investigate the influence of mortar composition on the shearing behavior of masonry. The testing apparatus consists of a rigid frame composed of steel plates connected through threaded rods as detailed in Figure 5.4 – a. The masonry triplet is positioned between a system of thin plates (3) separated with ball joints (4), except plates (3e) where a rode joint (5) is positioned. A temporary platen element was installed on each system of plates as illustrated in Figure 5.4 – b to facilitate the triplet's positioning before starting the test. A system consisted in a frame that held in place a pressure jack (6) was used to apply the pre-compressive load in horizontal position perpendicularly to the shear surface. Figure 5.5 – d shows the assembled equipment used to perform the shear tests on triplets.

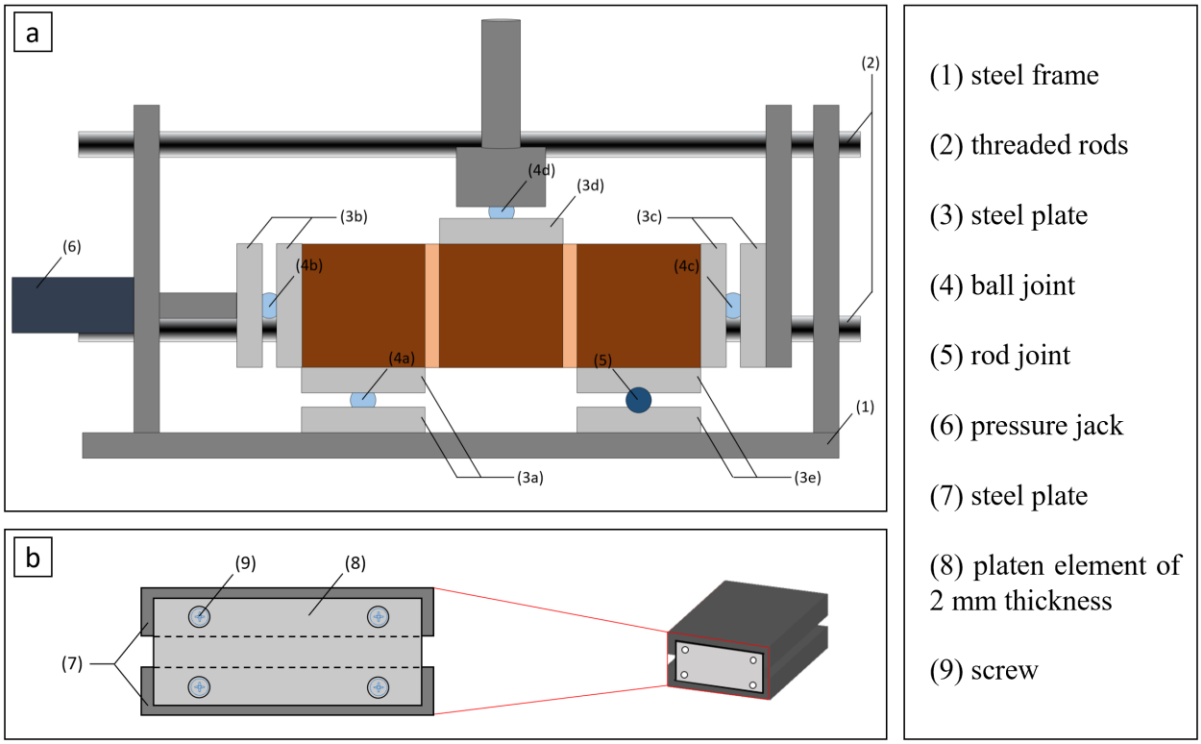

Figure 5.4. Front view of the testing equipment apparatus used to perform shear test (a), Details of the temporary platen element (b)

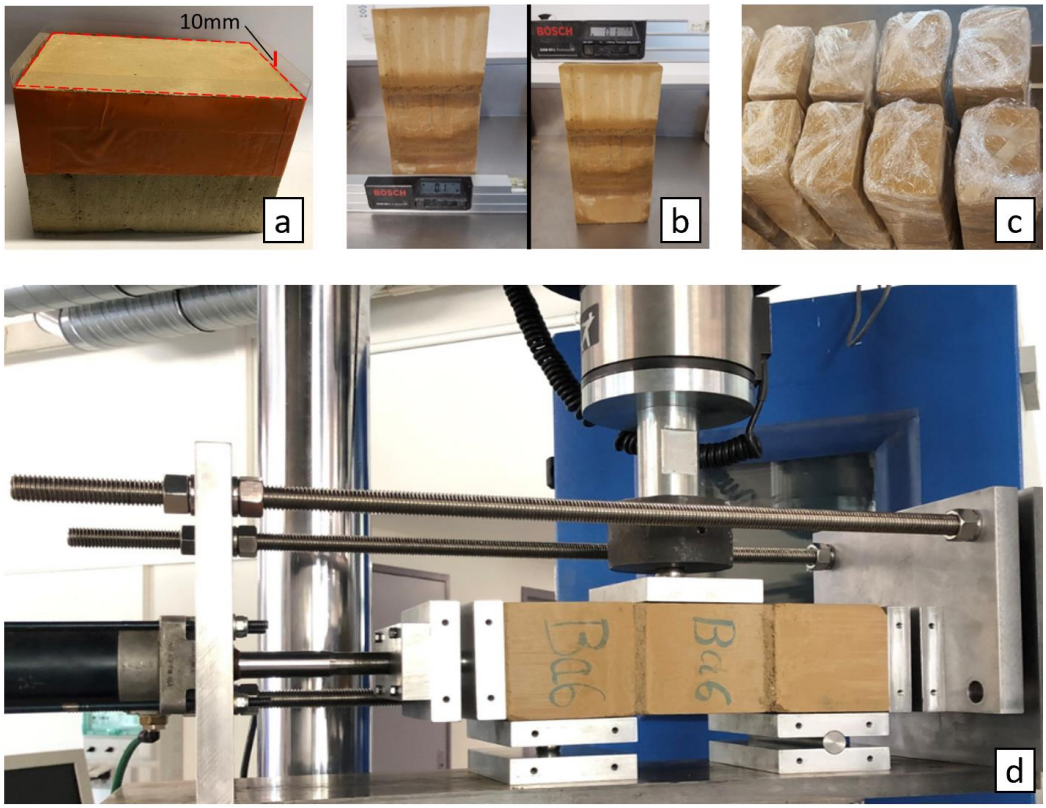

Figure 5.5. Temporary framework used to facilitate the application of the mortar bed (a), checking the straightness of the assembly (b), curing under plastic sheet (c), assembled equipment of the shear test (d)

Concerning the preparation of masonry triplets, the same steps described in §5.2.1 were followed as shown in Figure 5.5 (a, b & c), but here each block was sawn in three equal parts of 145mm×95mm×95mm in dimension. Tests were performed by means of the computer-controlled hydraulic press with a maximum load capacity of 10kN. The shear loading was applied with a constant displacement rate of 1.2 mm/min. A constant level of pre-compression horizontal loading of 0.05 MPa was maintained during tests.

5.2.3 Measurement of moisture adsorption rate and capacity

5.2.3.1 Test set-up

Water adsorption test is the most widespread procedure to assess the behavior of the material in highly saturated states. It was performed according to the French standard NF EN 1015-18 [368]. The method consists of monitoring the mass of the sample, initially dry, and submerged in 5mm of water for 90 minutes. This protocol allows calculating the adsorption coefficient or the so-called "A-value", defined as the quantity of adsorbed water per unit area per square root of time. This simple assessment tool was selected because the bond strength development in masonry element can be influenced by the water adsorption rate of the earth block.

In this study, the testing device is composed of a water tank equipped by a water tube that aims at maintaining a constant level of water during the test and a metallic grid submerged 5mm under the water surface (Figure 5.6). All samples were conditioned at 21˚C±2˚C/50%RH±5%RH for 7 days before the test. Samples were weighted using a scale accurate to 0.01g every 5 minutes during the first 30 minutes, then every 10 minutes until the 100th minute, then once a day until the 7th day. Blocks were characterized by performing the test on sawed prismatic samples having a size of 95mm×70mm×70mm.

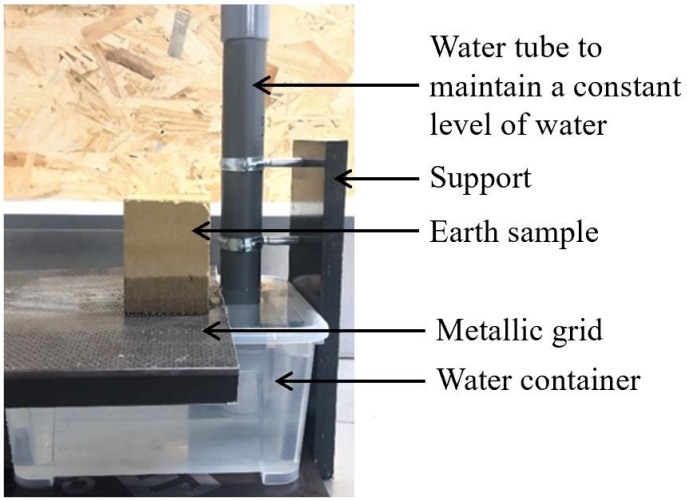

Figure 5.6. Water absorption test setup

5.2.3.2 Hydro-thermal analysis

Since water absorption and heat flux through the sample cause changes of the surface temperature, it had been decided to measure hygrothermal couplings by analyzing the thermographic measurements. Thus, temperature measurements were performed with the use of a thermal imaging CEDIP camera (Figure 5.7) to monitor the variation of surface temperature during the liquid and heat transfer caused by water at the bottom of the specimen. Images were treated through the software Altair.

Two different boundary conditions listed below were applied to the sample to reveal the impact of the conduction phenomenon on the variation of surface temperature:

- Case i: the lateral surfaces and the top are covered with foil (bottom open).
- Case ii: the lateral surfaces, the top and the bottom are covered with foil (all close).

The difference between the surface temperature of these two boundary conditions could be linked to the quantity of absorbed water thanks to an approximated calculation, which is developed in the next section.

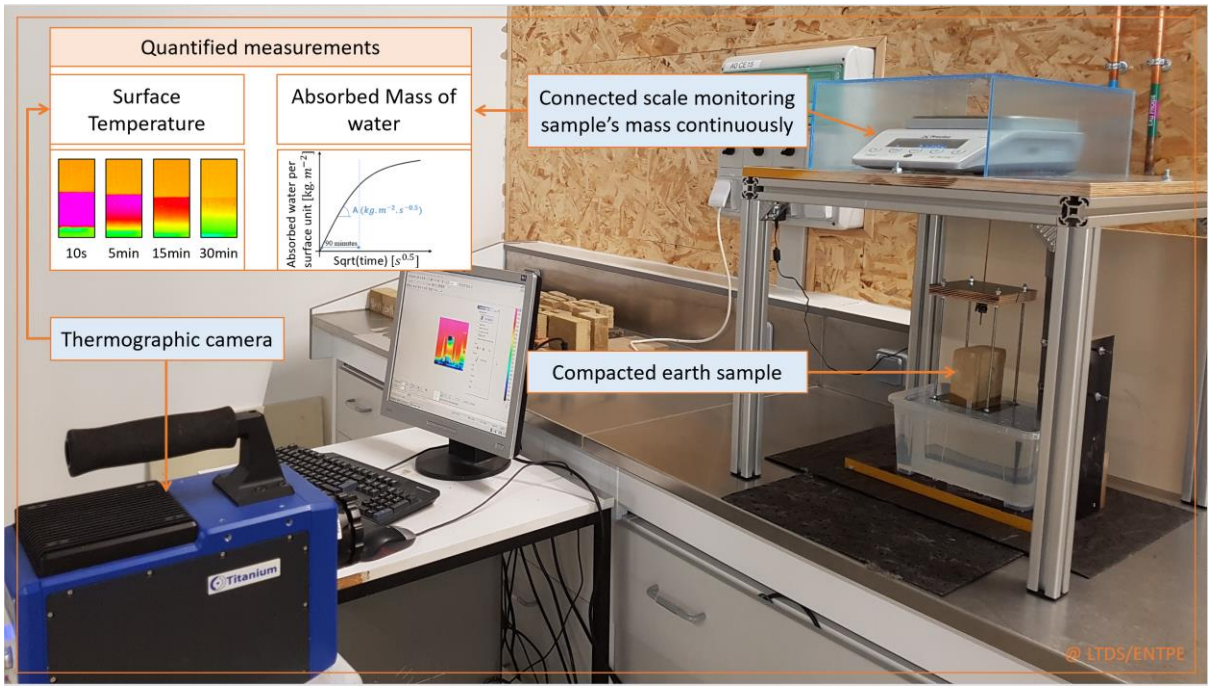

Figure 5.7. Measurement of surface temperature and mass of earth sample during adsorption test

5.2.3.3 Design of samples for the assessment of the interface effect

Moisture transport in block-mortar interface was investigated by performing the test on block-mortar assemblies. The goal was to connect the observed mechanism to the mechanical performance of the assemblies. To do so, two assemblies' configurations were considered as shown in Figure 5.8.

In the first configuration (a), a 10mm thick mortar bed was applied on one face of the block. In this case, mortar surface will be in contact with water that penetrate the block through the mortar layer. In the second one (b), two-block prisms of 30mm×70mm×70mm in dimension were sandwiched with a mortar joint of 10mm, then another 10mm-thick mortar bed was lied at the top surface of the upper prism. The top mortar bed was used to visually detect mortar swelling and/or cracking at the end of the test. In this case, block surface will be in contact with water that penetrate firstly from the block element to the mortar layer.

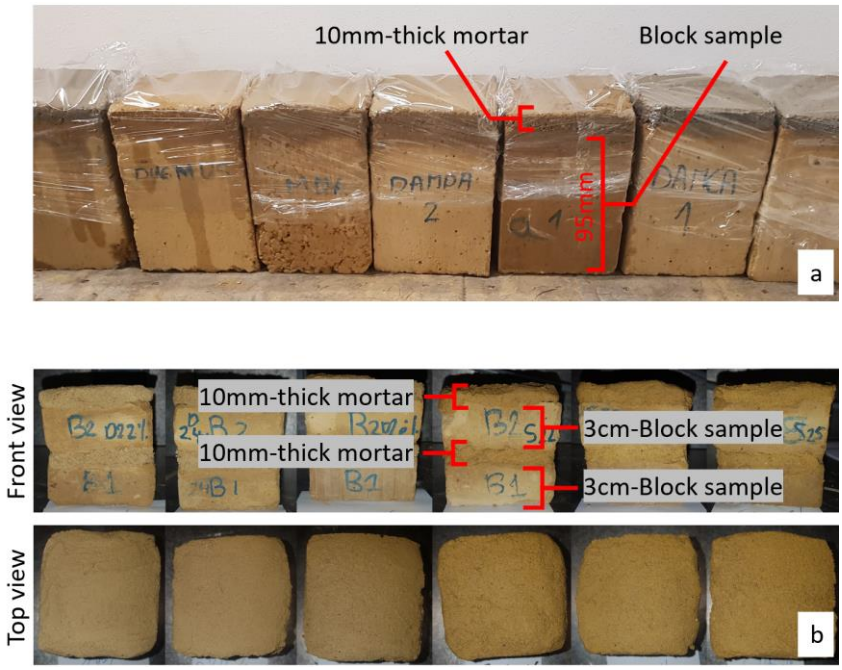

Figure 5.8. Examples of samples used for the measurement of the A-value on assemblies

5.3 Results

5.3.1 Uniaxial compressive strength (UCS)

Blocks BU and BA were tested in compression with plaster joint and with two different types of mortar. The first one is of a similar composition of each type of block and the second one is a sand-cement mortar as recommended by the French standard. Plaster joint used respected a water:solid ratio of 1:2 as usually prepared for partition walls work. Each test was made on triplicate. The compressive strength presented in Table 5-3, and denoted by Av UCS, is the average value of the three tests.

In case of plaster joint, all tested samples show vertical cracks in the two halves of the block and horizontal cracks propagation near the interface (Figure 5.9 – a). The recorded compressive strengths of stabilized formulations are slightly higher than the unstabilized ones. When a mortar of similar composition of the block is used, the difference in the UCS becomes more important between unstabilized and stabilized blocks with vertical cracks developing at failure (Figure 5.9 – b). The highest strengths were registered in case of cement-sand mortar, which increased again the increment in the UCS between stabilized and unstabilized formulations as well. In the latter condition, stabilized assemblies failed by block crushing near the interface (Figure 5.9 – c) while unstabilized blocks showed vertical cracks at failure.

These outcomes could be viewed from different perspectives. Firstly, the high initial water content (50%) of the plaster joint has led to softening of the material near the interface due to the significant quantity of water that migrated from the joint to the two halves of the block. This may explain the weakness of the block-joint interface confirmed by the mode of failure of the assemblies, whether blocks were stabilized or not. Another interesting point to consider is the mechanical inter-locking of mortar into the surface pores of the block, which was

traduced by vertical cracks traversing assemblies made with mortar of similar composition of the corresponding block. Regarding cement-sand joint, the stiffest zone of the assemblies was at the interface and the good adhesion was revealed by recording the highest “strength” values.

These results highlight the high sensitivity of the testing method to the nature of the joint, which was not a surprising issue. In what follows, the results of a shear test adapted to examine the bond interface will be presented.

Block type	Mortar Type	W/S of the mortar [%]	Av. UCS [MPa]	Failure mode
BU	Plaster	50	2.1 ± 0.14	Vertical cracks in the block then failure near the interface
	du	17.6	1.7 ± 0.09	Vertical cracks
	ca	18.7	2.3 ± 0.05	Vertical cracks
BA	Plaster	50	2.3 ± 0.11	Vertical cracks in the block then failure near the interface
	da	22.7	2.4 ± 0.07	Vertical cracks
	ca	18.7	3.6 ± 0.04	Block crushing

Table 5-3. Results of compressive strength test

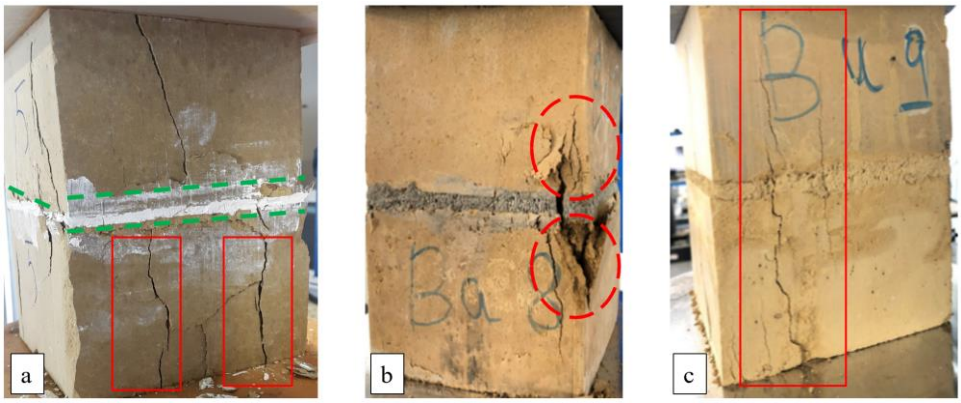

Figure 5.9. Examples of failure patterns of masonry; vertical cracks in the block then sliding at the interface (a); block crushing (b); vertical cracks (c)

5.3.2 Interface shear strength (ISS)

The shear bond strength at the interface (ISS) was calculated when the bond between the block and the mortar joint failed as follow:

$$\text{ISS [kPa]} = \frac{\text{F [kN]}}{\text{2S [m}^2\text{]}} \tag{5-1}$$

Where F is the ultimate load and S is the vertical cross-section passing through the mortar joints.

The expected failure modes for this kind of test are illustrated in Figure 5.10. Results of the shearing test conducted on triplet samples are given in Table 5-4. Apparently, assemblies tested in shearing behaved in a comparable way to those tested in compression. The highest shear

strength values were recorded by assemblies made with cement-sand mortar. In this specific case, stabilized assemblies failed following mode C (Figure 5.10 – c). This latter expresses a good adhesion between the block and the mortar, but at the same time, it indicates that the mortar is of a high strength with respect to the block elements. This is not the case for unstabilized assemblies that failed in mode A1, which revealed a weakness at the interface level. On the other hand, when a mortar of similar composition of the block is employed, assemblies failed following a joint failure mode on a face (A1) or divided between two faces (A2) as displayed in Figure 5.10 a&b.

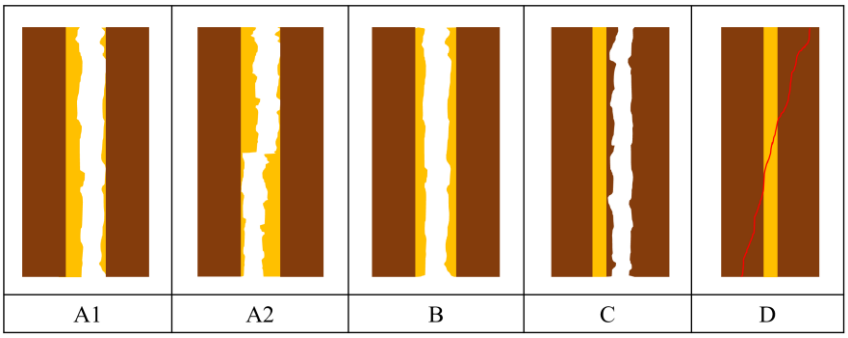

Figure 5.10. Expected failure modes of triplet test according to (EN 1052-3, 2007); A1 and A2: joint failure on a face or divided between two faces; B: shear mortar failure; C: shear block failure and D: crushing and/or splitting in blocks.

Another interesting feature in these results is that hierarchical relationship in strength between BA, BM and BU is respected only when a mortar of similar composition of the block is used: in this case, the highest shear strengths were recorded by BA triplets and the lowest by the unstabilized ones (BU).

This hierarchical relationship between the shear resistance and the block strength was not more observed when different mortar compositions are used. Indeed, the shear strengths recorded by unstabilized triplets made with stabilized earth-based mortar (da) and cement-sand mortar (ca) are higher than those recorded by stabilized triplets BM made with stabilized earth-based mortar (dm) and cement-sand mortar (cm). Along the same line, unstabilized triplets bonded with cement-sand mortar (ca) showed a higher shear strength than BA triplets bonded with stabilized earth mortar (da).

Bock type	Mortar type	Av. ISS [kPa]	Failure mode
BU	du	47.6	A2
	da	86.9	A1
	ca	131.3	A1
	su	49.2	A1
BA	da	128.8	A1
	ca	211.5	C
	sa	124.1	A1
BM	dm	54.8	A1
	cm	81.7	C

Table 5-4. Results of triplet test

Thus, it appears that the resistance at the interface depends on mortar quality rather than block properties. A mortar of higher quality ensures better interlocking with block, whether stabilized or not.

Finally, BA and BU tested with mortar sa and su, respectively, show a shear resistance similar to that one tested with da and du, respectively. It seems that varying the earth used in earth-based mortars does not affect the bond shear strength of the masonry, at least in the condition of the present study.

Figure 5.11. Examples of the three observed failure modes, A1 (a), A2 (b) and C (c)

5.3.3 Water adsorption

5.3.3.1 Absorbed water and surface temperature variations

The objective of this section is to connect the differences between the two boundary conditions in terms of moisture ingress, with their respective surface temperature variation and the corresponding evaporation/condensation process of water. The calculation described enables a first evaluation of the link between these two phenomena.

For each boundary condition, the hygrothermal coupling transfer can be written based on heat and mass conservation equations showen below. The variable associated to the hydric state of the material is the liquid pressure P_L.

a. Test condition (i) – bottom open

In this case, water that migrates through the porous medium is present in liquid and vapor phase. In the following development, the impact of evaporation-condensation processes on the heat balance are neglected, as well as the impact of water vapor transfers on the water mass balance. Under these assumptions, the total mass conservation occurring within the porous media, neglecting the transfer due to gravity, is given by:

$$\rho_d \frac{\partial u}{\partial P_L}\frac{\partial P_L}{\partial t} = -\mathrm{div}(\overrightarrow{J_L}) = \mathrm{div}(D_L \overrightarrow{\mathrm{grad}}(P_L)) \tag{5-2}$$

Where $\overrightarrow{J_L} = -D_L \overrightarrow{\mathrm{grad}}(T)$ is the liquid flux density, D_L is the hydraulic conductivity (in kg/(m.Pa.s)) and $\frac{\partial u}{\partial P_L}$ can be determined from the suction curves through the relation:

$$\frac{\partial u}{\partial P_L} \approx \frac{\partial \varphi}{\partial P_L}\frac{\partial u}{\partial \varphi} = \frac{M_L}{\rho_L RT}\exp\left(\frac{P_L M_L}{\rho_L RT}\right)\frac{\partial u}{\partial \varphi} \tag{5-3}$$

where M_L is the molar mass of water, ρ_L is its density, R is the perfect gaz constant and T is the temperature (in K).

The energy conservation equation is given below by considering the heat transfer by conduction and convection by water in the pores:

$$(C_p^0 + \rho_d u c_L)\frac{\partial T}{\partial t} = \mathrm{div}(\lambda\overrightarrow{\mathrm{grad}}(T)) - c_L\overrightarrow{J_L}\cdot\overrightarrow{\mathrm{grad}}(\mathrm{T}) \quad (5\text{-}4)$$

Where C_p^0 [J. m^{-3}. K^{-1}] is the volumetric heat capacity of the dry material, T is the temperature of the material [K], λ [W. m^{-1}. K^{-1}] is the thermal conductivity, c_L [J. kg^{-1}. K^{-1}] is the specific heat capacity of water.

b. Test condition (ii) – all close

In this condition where all the faces of the sample are covered, only the heat transfer by conduction occurs and is given by:

$$(C_p^0)\frac{\partial T}{\partial t} = div(\lambda\overrightarrow{grad}(T)) \quad (5\text{-}5)$$

c. Comparison of « bottom open » and « all closed » boundary conditions

Equations (5-4) and (5-5) differ from the term $-c_L\overrightarrow{J_L}\cdot\overrightarrow{\mathrm{grad}}(\mathrm{T})$ which denote the heat flow advected by water and from $\rho_d u c_L\frac{\partial T}{\partial t}$ which denote the variation of heat capacity due to the variation in water content. Since these two contributions are caused by the migration of water within the material, the analysis of the difference in temperature profiles between test conditions (i) and (ii) would allow to estimate, by inverse analysis, the water ingress within the material.

Figure 5.12 illustrates the images of thermographic camera corresponding to both test conditions at different times. These data can be used to draw the temperature profiles reported in the Figure 5.13.

Unfortunately, no significant differences were observed between the two test conditions. This means that the variation of temperature due to water and heat transfer in case (i) is approximately the same in case (ii) due to the heat transfer by conduction only. This is due to the too high thermal conductivity of the material with respect to its hydraulic conductivity. Thus, for the tested samples, surface temperature measurements could not be used to estimate the moisture intake profiles of samples. Therefore, this methodology will not be used to analyze the liquid water ingress in the block in the following of this manuscript. However, this methodology may remain interesting for material with a lower thermal conductivity and/or a higher hydraulic conductivity.

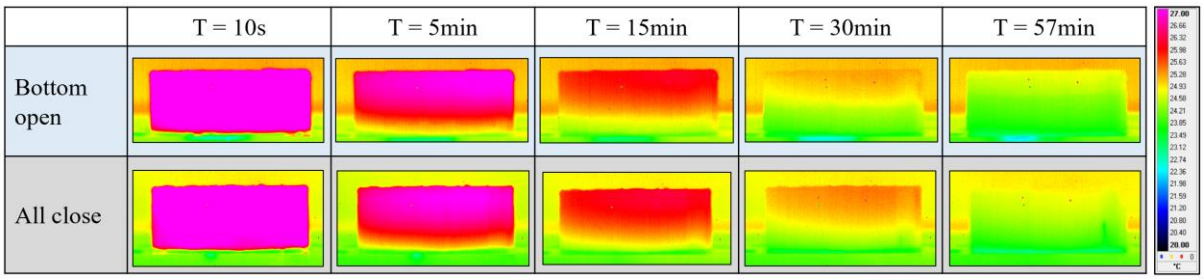

Figure 5.12. Thermographic measurements of moisture ingress for sample DB5

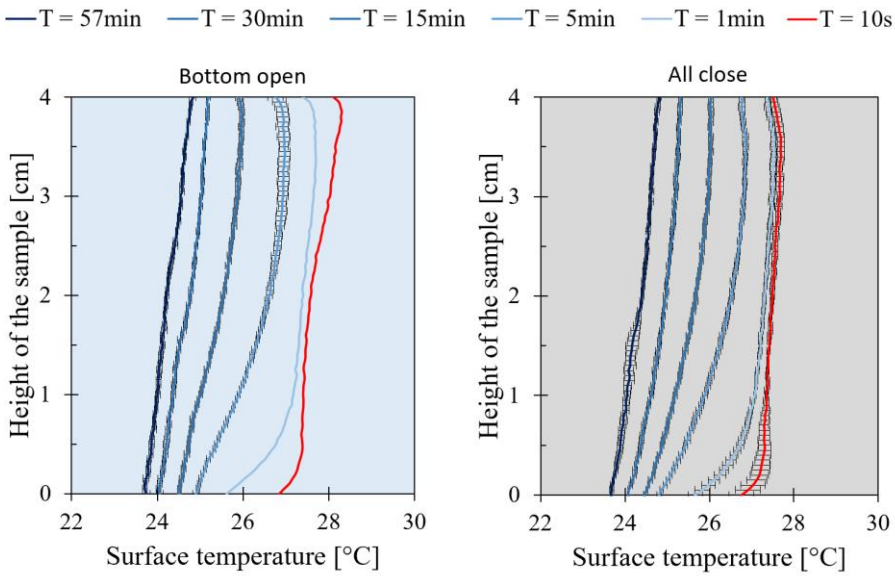

Figure 5.13. Surface temperature of the samples DB5 for the two boundary conditions during moisture ingress process

5.3.3.2 A-value measured on block prisms

Absorbed water quantity versus square root of time for the block samples used in the experiment are plotted in Figure 5.14. It shows that beyond 24 hours the change in the water absorption values becomes negligible. The liquid water adsorption coefficient (A-value) was calculated from the slope of the linear relation that can be noticed between absorbed water quantity and square root of time during the first 90 minutes. Not surprisingly, BA and BM samples have absorbed less water with an adsorption rate lower than BU by 28% and 14% respectively. The decrease in these parameters is a normal consequence of cement stabilization [369], [370].

To analyze further these results, it can be interesting to compare the theoretical water content at saturation of the samples, denoted by u_{sat_theo}, to the one measured at the end of the absorption test, denoted by u_{sat_exp}. Theoretical water content at saturation can be deduced from the dry and solid grains densities through the relation:

$$u_{sat\_theo}=\rho_L\left(\frac{1}{\rho_d}-\frac{1}{\rho_s}\right) \quad (5\text{-}6)$$

Where ρ_L is the liquid density at 21°C (0.998 g.cm^{-3}), ρ_d is the dry density of the sample and ρ_s is the density of solid grains (2.7 g. cm^{-3}).

The experimental water content could be calculated as follow:

$$u_{sat\_exp} = \frac{m_{sat} - m_s}{m_s} \quad (5\text{-}7)$$

Where m_{sat} is the saturated mass of the sample and m_s is the dry mass of the sample.

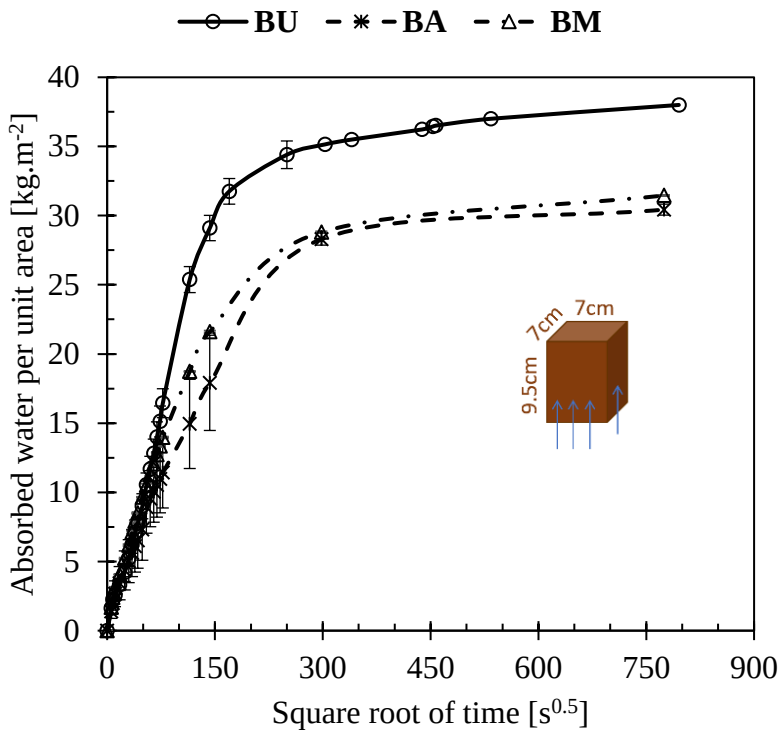

Figure 5.14. Variation of adsorbed water quantity in function of square root of time of block prisms

The calculated values summarized in Table 5-5 indicate that the water adsorbed by BU exceeded its theoretic maximum value by 28% approximately. On the contrary, the experimental water content of BA and BM remained lower, although close to the theoretical one. This issue could be explained by the high sensitivity of unstabilized samples toward water, which is strongly reduced after stabilization. Indeed, the high sensitivity to water enhances swelling of the material which expand its porous network, resulting in an increase of the capacity of the material to adsorb water.

Formulation	Av. A-value [kg.m^{-2}.s$^{-0.5}$]	u_{sat_exp}[%]	u_{sat_theo}[%]
BU	0.21 ± 0.08	21.78	16.98
BA	0.15 ± 0.03	18.96	19.42
BM	0.18 ± 0.05	18.81	19.42

Table 5-5. Results of the water adsorption test performed on block prisms

5.4 Discussion

5.4.1 Role of the mortar joint in the compressive and shear tests

The direct comparison between interface shear strength (ISS) and uniaxial compressive strength (UCS) obtained for the assemblies BU-du, BU-ca, BA-da and BA-ca is reported in Figure 5.15. This comparison seems to underline a quite good linear correlation between UCS and ISS. This indicates a strong impact of the interface on the unconfined compressive strength results of the block assembly.

On the other side, it would be interesting to look at the effect that could have the interface on the relative UCS of assemblies using stabilized blocks with reference to the unstabilized ones. To do so, relative UCS with the different tested interface conditions will be confronted with the relative UCS measured on samples without interface (i.e., made on cylindrical samples). Let recall that the three tested interfaces are cement-sand mortar, earth-based mortar, and plaster joint. As presented in Figure 5.16, it seems that the relative UCS with a cement-sand mortar correspond most closely to the relative UCS measured on the block samples without interface. This interface type may thus be recommended rather than the others in order to perform UCS tests on blocks assemblies.

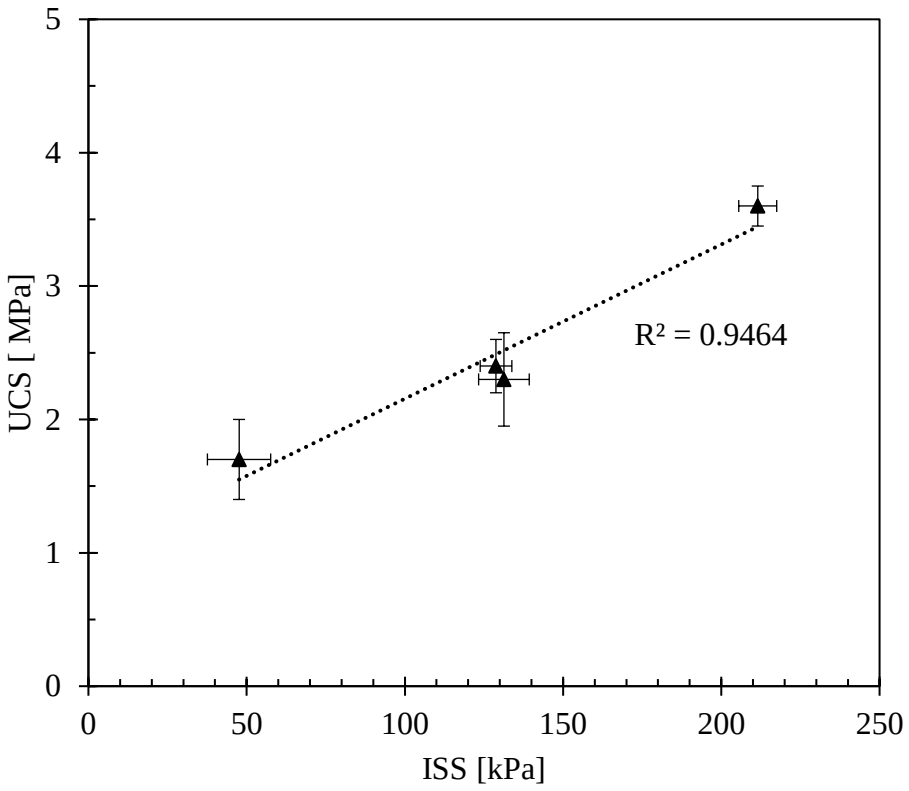

Figure 5.15. UCS versus ISS

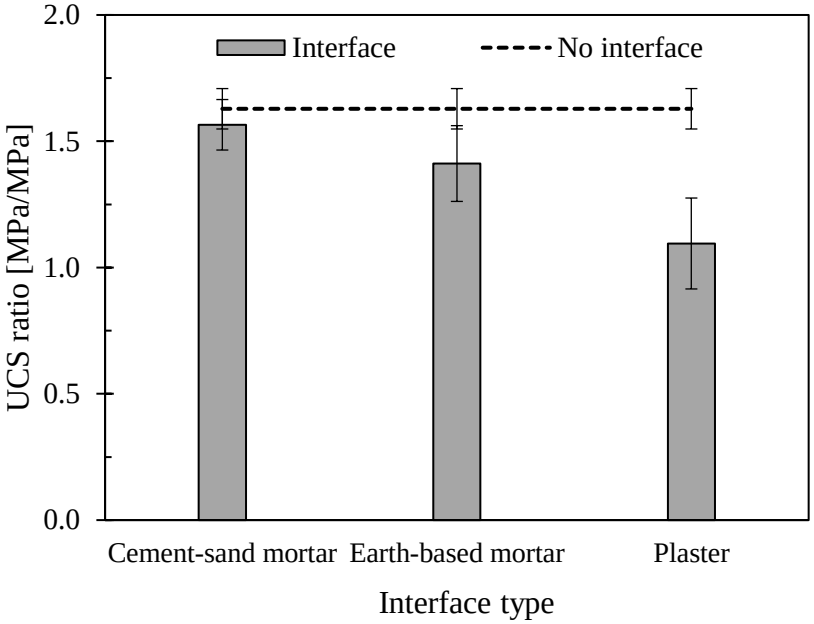

Figure 5.16. Relative UCS of assembled stabilized blocks BA (The relative UCS is defined as the ratio between UCS of stabilized and unstabilized blocks with the same interface type)

5.4.2 Influence of the interface on the transport properties

Performing triplet test on saturated assemblies was not feasible. Thus, water adsorption test performed on block-mortar assemblies was used as a tool to investigate the quality of the interlocking between block and mortar. The focus was made on two points:

- Verifying the compatibility between unstabilized blocks and cement-sand mortar.
- Verifying the compatibility between stabilized blocks and earth-based mortar made with different earths.

Mechanical tests show that unstabilized assemblies BU sticked with cement-sand mortar resist to higher strengths than those sticked with earth-based mortar. But Figure 5.17 shows that in less than 3 hours of water absorption test, the block BU lifted off from the cement-sand mortar (ca) while it remains assembled with earth-based mortar (da) throughout the test for more than 7 days. This issue could be explained by the differential swelling between unstabilized block BU and cement-sand mortar. BU is expected to swell more than cement-based mortar (ca) during the water ingress as it was manifested in the difference between the theoretical and experimental saturation water content (section 5.3.3.2). This de-bounding problem was not noticed between stabilized block BA and either cement-based or earth-based mortar. This should be due to its significantly lower swelling.

Another remarkable outcome of the mechanical investigations was the similar behavior of triplets made with earth-based mortars made with DAG and STA. However, water absorption test performed on block-mortar assemblies (Figure 5.18) show a sort of discontinuity in the water adsorption curve after 40min when the middle mortar layer starts to lift off from the bottom block prism saturated with water. This deviation in moisture transport underlined the imperfect hydraulic contact between the two elements and could be attributed to an interface resistance that describes bond development between mortar and block.

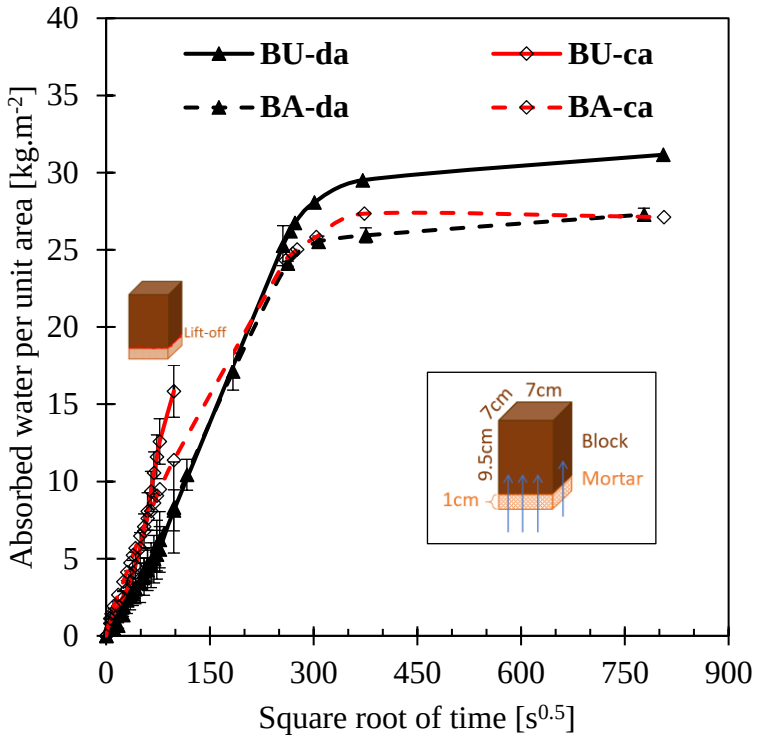

Figure 5.17. Variation of adsorbed water quantity in function of square root of time of mortar-block assemblies (configuration a)

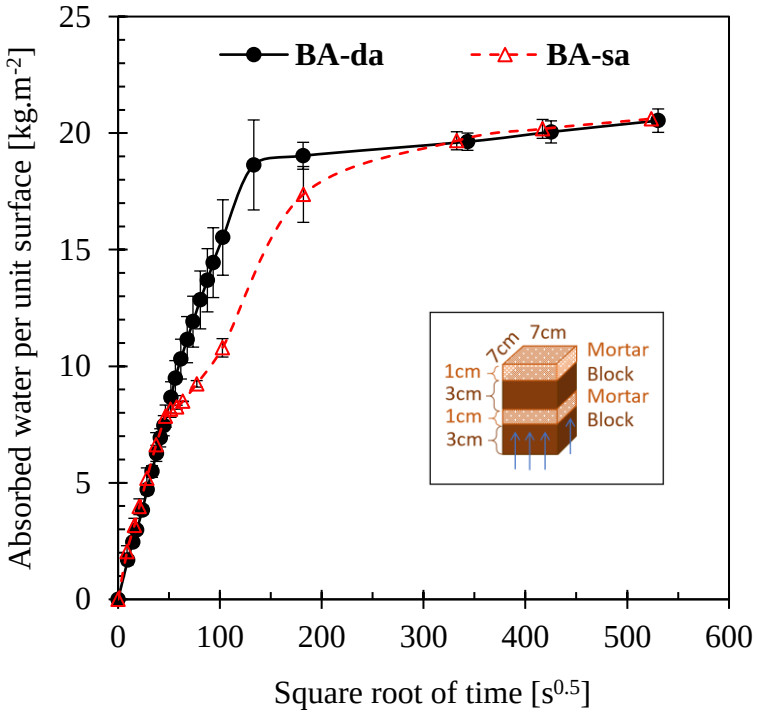

Figure 5.18. Variation of adsorbed water quantity in function of square root of time of mortar-block assemblies (configuration b)

These investigations mean that mechanical strength is not sufficient to judge the quality of the block-mortar interface because interlocking problems usually happen in structures due to variation in the water content of the masonry elements rather than in dry conditions.

5.5 Conclusion

In this chapter, the uniaxial compressive strength and interface shear resistance were measured on different block-mortar assemblies. It had been shown that cement-sand mortar gives the highest mechanical characteristics for both stabilized and unstabilized blocks. Then water adsorption test was used as indicator of their interlocking quality due to water ingress through the sample. The behavior of assemblies toward water adsorption indicates a lack of compatibility between unstabilized block and cement-sand mortar due to differential swelling during the test. In addition, blocks assembled with earth-based mortar made with DAG and STA earths resisted to mechanical tests in dry conditions with similar strength. However, DAG blocks assembled with STA earth-based mortar failed during water absorption test.

Thus, it appears that performing mechanical tests on air-dried block-mortar assemblies is necessary but not sufficient for the investigation of the interlocking between masonry elements. In addition, more attention should be given to the type of mortar used to stick blocks, especially in norms and standards. More details about the characteristics (w/c ratio, composition, etc.) of mortar in function of the block composition must be specified clearly.

The analyses made in this chapter requires further tests on blocks and mortar assemblies made with different earths to verify the possibility of generalizing results.

General conclusions and perspectives

This Ph.D. thesis is a contribution to the optimization of earth's treatment with hydraulic binders for construction with CSEB. It aims at producing tools for quantification of impacts of cement composition and raw earth nature, as well as their dosages, on the performance of the earth block at the material scale.

The state of the art presented in Chapter 1 showed to what extent each characteristic of earth could influence the performance of the resulting stabilized block with OPC. While some characteristics are always determined in publication that deals with earth stabilization, other important characteristics like the mineralogical and chemical composition are less aborded. At the same time, essential stages like manufacturing properties and curing conditions are still questionable. In addition, not only the materials characteristics influence the quality of the block, but the way in which this quality is assessed play an important role in the delivered result as well. No unified method for the determination of the most studied mechanical parameter (i.e., compressive strength) of CSEB exists and no consensus on a durability testing procedure of this material.

Therefore, this work aimed at assessing the efficacy of cement stabilization of earths in their natural states using different cements other than OPC by focusing on four main subjects.

Firstly, particular attention was addressed to the curing conditions of stabilized blocks in Chapter 2, where the compressive strength was used as an indicator of the curing effectiveness. It had been demonstrated that in the tested conditions the curing period could be reduced to 7 days based on the results of 8 different formulations made with two different earths and 4 cements. Secondly, the performance of 20 cement-earth mixtures was assessed in chapter 3 based on a multi-criteria approach that take into consideration the mechanical, hygroscopic and durability property. It had been shown that optimizing stabilized mixtures is not as easy as it may look, and one should analyze all possible factors affecting stabilization before delivering an explication of the performance of the block. Those factors are a combination of earth and cement properties, samples properties, and testing conditions and method. In case of water durability, existing tests are rather destined for the evaluation of the stabilizer efficacy rather than the analysis of the long-term durability of CSEB. Thus, a new cyclic wetting-drying method was developed in Chapter 4 in the aim of investigating the resistance of CSEB to the repetitive action of wind-driven rainfall. The developed method and the proposed procedure to quantify the results of the test demonstrated their ability to distinguish formulations stabilized with different cements. Finally, brief investigations were made in Chapter 5 on the mechanical and transport properties in block-mortar interface with the intention of opening discussion on the influence of mortar composition on the mechanical interlocking of the assembly. Knowing that bound development between block and mortar is crucial for a durable masonry structure made of CSEB, this study appears to be of first importance.

Several aspects of the work presented in this thesis drive to further investigations. Paving the way to the optimization of cement usage in CSEB requires testing new possibilities like the relation between compressive strength and water to cement ratio to determine the optimum manufacturing properties instead of the dry density and the optimum water content. Another issue is to add pH and organic matter content of earth to the pre-characterization list required before conducting studies on cement stabilization. In particular, these latter were found to be more impacting than the soil grading and the methylene blue value, which are however the most recommended parameters that examine the possibility of a soil to be stabilized with cement.

On the other hand, the broadening of the developed erosion test would be to make a link between the resistance of exposed CSEB's wallets to real weathering conditions and the accelerated erosion in the laboratory. The test parameters could be calibrated after monitoring and analyzing the real degradation scenarios of the material. It will be very interesting to fully automatize the quantification method of the results to enable testing large number of formulations, which could contribute to a deeper understanding of the degradation of CSEB in function of their characteristics.

Finally, the investigations made on different blocks-mortar interfaces underline that estimating the quality of the bound between the two elements would require different assessment of the assemblies in both dry and wet conditions. The hydric exchange was found to be quite complex. Thus, further analysis of this latter by varying the properties of mortar and block are necessary for the quantification of durability of earthen masonry walls made with CSEB.

Résumé du mémoire

Introduction

Dans le contexte actuel de la mutation des pratiques constructives en accompagnement de la transition énergétique, le développement de matériaux limitant les impacts environnementaux - dont notamment l'empreinte carbone et l'énergie grise - relève d'un enjeu stratégique. Ainsi, les matériaux à base de terre crue sont particulièrement étudiés comme réponse à ces problématiques. Toutefois, ils présentent une résistance mécanique plus faible que les matériaux de construction habituels et une grande sensibilité à l'eau liquide. Pour améliorer ces deux dernières faiblesses, une stabilisation chimique par liants hydrauliques est fréquemment pratiquée. Pourtant, celle-ci repose plus sur des pratiques empiriques que scientifiques.

L'objectif de ce travail de doctorat est de déterminer des indicateurs de la performance, actuellement essentiellement considérée au travers de la résistance mécanique dont la pertinence est remise en question, au regard des différentes fonctions attendues. Dans ce but, sont étudiés les effets de la stabilisation au ciment (cure et nature du ciment) sur différents indicateurs : résistance mécanique, échanges hygroscopiques et durabilité vis-à-vis de l'eau liquide, afin d'optimiser la formulation, les conditions de cure, et de lever certains freins à la dissémination de cette pratique constructive.

Bien que de nombreuses études aient été menées pour évaluer l'influence de la stabilisation au ciment sur les propriétés mécaniques et hygrothermiques du bloc de terre compactée, l'efficacité de la stabilisation au ciment n'est pas encore maitrisée. Des études ont montré par exemple que la résistance mécanique dépend de nombreux facteurs comme le dosage du ciment, la fraction argileuse de la terre, la densité de l'échantillon et sa teneur en eau. Mais des questions se posent sur les indicateurs nécessaires pour juger de l'efficacité de la stabilisation du ciment pour les applications de construction de bâtiments. Et sur la pré-caractérisation nécessaire de la terre avant de procéder à la stabilisation des blocs de terre compactée avec du ciment.

Deuxièmement, les performances mécaniques de la maçonnerie ne dépendent pas uniquement de la qualité du bloc. La littérature révèle que l'adhérence dans la zone de contact entre la maçonnerie et le mortier est fonction de la composition du mortier, de la quantité d'eau dans le mortier frais et de la teneur en eau du bloc au moment de l'application du mortier. Cependant, les études sur le phénomène de transport d'humidité et leur influence sur le développement de d'adhérence sont limitées.

Enfin, même si la stabilisation augmente la durabilité des matériaux, l'utilisation de liant hydraulique peut générer de nouveaux problèmes de durabilité, alors qu'il n'existe pas d'expression uniformément acceptée pour la durabilité des terres stabilisées. De plus, des méthodes de laboratoire pour évaluer la durabilité du bloc stabilisé sont toujours nécessaires pour étudier cette caractéristique dans des conditions réalistes.

En réponse à ces questions, mes travaux de thèse s'organisent autour de trois grandes parties :

- Analyse des performances du bloc de terre stabilisé au ciment par rapport aux caractéristiques du ciment et de la terre.
- Développement d'un test d'évaluation en laboratoire pour évaluer la durabilité du bloc de terre stabilisée au ciment vis-à-vis de l'érosion à l'eau.
- Évaluation du transport de l'humidité et du développement de l'adhérence entre le bloc de terre stabilisée et le mortier.

Pour la première partie, une approche basée sur la performance a été suivie. Deux terres naturelles (nommées DAG et STA) ont été choisies sur la base des types de terre déjà étudiés dans notre laboratoire. Cinq types de ciment ont été proposés par les cimentiers intervenus dans le comité de pilotage de cette thèse. Ces ciments diffèrent principalement par leur composition et leurs propriétés physiques et chimiques. Les performances des formulations ciment-terre ont été analysées à la lumière de la composition physique et minéralogique de la terre et du type de ciment utilisé dans chaque cas. Le terme performance comprend la résistance mécanique, les capacités hygroscopiques et la durabilité vis-à-vis de l'eau.

En ce qui concerne la deuxième partie, un test de mouillage et de séchage cyclique inspiré du test d'érosion au goutte-à-goutte a été développé pour imiter l'effet couplé des précipitations et du vent sur la surface des blocs de terre stabilisée.

Enfin, le transport de l'humidité dans l'assemblage bloc-mortier et leurs influences sur le comportement mécanique de l'assemblage ont été évalués expérimentalement.

Matériaux, échantillonnage et conditions de cure

Pour pouvoir évaluer les effets de la stabilisation par la comparaison des matériaux, certains paramètres doivent être fixés. La figure 2.1 résume le choix des paramètres fixes et variables, de même pour les indicateurs de performances mécaniques, hygrothermiques et de durabilité, résumés synthétiquement dans la figure 2.2. Le Tableau 2.1 permet d'avoir une vue d'ensemble de l'ambitieux programme expérimental. La détermination de la quantité d'eau à ajouter dans le mélange terre-ciment est calculée d'après l'optimum BTC.

Ensuite, le sujet de l'optimisation des conditions de cure des échantillons a été abordé. L'accent a été mis sur l'évaluation de l'efficacité de la durée de cure humide, consistant à conditionner des échantillons en environnement humide (~100% HR) à température ambiante (21˚C). La durée de cure humide a été variée entre 0 (sans cure) et 21 jours. Les résultats obtenus mettent en évidence l'importance des conditions de cure (durée, humidité) dont l'optimisation contribue à la diminution des impacts environnementaux.

L'effet de la cure sur l'hydratation est abordé par l'examen d'images obtenues par MEB. Pour parachever l'étude des conditions de cure, l'effet de l'élévation de la température est regardé : il est confirmé que l'humidité est le facteur prépondérant pour l'augmentation de la résistance mécanique. Cette étude originale ouvre d'intéressantes perspectives pour changer les pratiques actuelles en matière de fabrication des blocs de terre stabilisée.

La conclusion de ce chapitre à l'aulne des résultats obtenus présente les conditions de cure des échantillons faisant l'objet des travaux. Il a été démontré que la cure humide à température ambiante est bénéfique pour le développement de la résistance mécanique jusqu'à 7 jours, et ce pour les deux terres DAG et STA stabilisées à 8% avec 4 types de ciments différents.

Performance des mélanges ciment-terre

Dans ce chapitre est abordée l'influence de la nature des ciments sur les performances en terme de la résistance mécanique, des propriétés hygroscopiques et de la résistance vis-à-vis de l'eau liquide. Ces essais sont interprétés d'un point de vue microstructural pour comprendre l'impact chimique des ciments sur les deux terres, avant de conclure sur les facteurs affectant la stabilisation. La résistance mécanique est mesurée par des tests de compression uniaxiale sur des échantillons saturés (équilibrés à 99,8% d'humidité relative) et secs. La stabilisation de la

terre DAG s'avère plus effective que celle de la terre STA, bien que la terre STA non stabilisée sèche présente une meilleure résistance en compression. Pour approfondir la compréhension de l'influence de la cure sur les effets de la stabilisation d'un point de vue mécanique, un indicateur est proposé : le rapport des résistances en compression des matériaux saturés et secs. Il permet de conclure que la teneur en ciment peut être diminuée si l'objectif est d'améliorer les résistances à l'état saturé.

L'hygroscopicité est ensuite analysée au travers des courbes de sorption-désorption des matériaux, obtenues par la méthode de sorption gravimétrique dynamique (DVS). La stabilisation diminue les capacités hygroscopiques des terres, l'effet est plus marqué pour DAG que STA. Le comportement des deux terres est similaire jusqu'à 90% d'humidité relative, après la capacité d'adsorption de STA diminue de 15% alors que DAG de 90%. Ce résultat parait essentiel pour appréhender les phénomènes de stabilisation. Pour compléter l'interprétation, des hystérésis sont tracés et la capacité hydrique ξ calculée. Puis, la perméabilité à la vapeur d'eau est mesurée.

Pour finir, la durabilité par rapport à l'eau liquide est investiguée. Les deux méthodes d'évaluation sélectionnées d'après celles répertoriées dans la littérature sont détaillées : érosion par pulvérisation d'eau et immersion dans l'eau. La terre DAG non stabilisée s'érode peu par aspersion, et une fois stabilisée elle est inaltérée. La terre STA s'avère très sensible à l'érosion, sa stabilisation permet de significativement diminuer cette sensibilité. Les mêmes conclusions sont formulées pour le test d'immersion. La considération de ces résultats ne permet pas de distinguer clairement l'effet de la stabilisation par les différents types de ciments.

Pour comprendre les effets de la stabilisation, une étude des phases minérales est conduite par diffraction des rayons-X et analyses thermogravimétriques. L'analyse minéralogique souligne les difficultés à détecter l'action des produits cimentaires, essentiellement dans STA à cause de la plus faible réactivité du ciment dans cette terre.

Dans un deuxième temps, les résultats ont été discutés en fonction des caractéristiques des ciments (dosage, composition et rapport eau/ciment). La discussion a appelé à d'autres recherches sur les propriétés de fabrication optimales basées sur le rapport eau/ciment qui offrent la résistance à la compression maximale. Cette stratégie n'est généralement pas appliquée pour la détermination des propriétés de fabrication optimales du bloc de terre stabilisée. Ensuite, une discussion a été faite sur la base des caractéristiques de la terre (finesse et chimie). Il a été démontré que l'efficacité de la stabilisation du ciment pouvait être liée au pH et aux teneurs en matière organique de la terre. Ainsi, ces paramètres semblent être des paramètres de pré-caractérisation importants des terres naturelles destinées à la stabilisation du ciment.

Test d'érosion cyclique

Dans ce chapitre, une méthode d'évaluation de la durabilité des blocs de terre stabilisée dans des conditions plus réalistes d'utilisation est développée, les méthodes exposées au chapitre précèdent n'ayant pas permis de statuer sur l'efficacité de la stabilisation et les tests de durabilité à l'eau liquide n'étant pas représentatifs des conditions d'usage. Dans ce but, le dispositif expérimental mis au point simule l'érosion induite par les effets cycliques et couplés du vent et des précipitations. Chaque cycle consiste à soumettre la surface inclinée d'un bloc à l'action de gouttelettes d'eau libérées avec une vitesse d'égouttage constante et suivie d'une étape de séchage (ventilation). La durée de mouillage et de séchage, le nombre de cycles et la vitesse d'égouttage peuvent être contrôlés à volonté.

Des indicateurs spécifiques sont proposés pour supporter l'analyse des résultats obtenus et d'autres outils sont utilisés pour approfondir l'interprétation : méthodes ultrasonores non-destructive pour analyser les modifications de vitesse de propagation des ondes, et abrasivité des surfaces exposées par une brosse.

Dans une première étape, une cartographie de la vitesse de propagation des ondes à la surface des blocs est tracée. Malgré le soin apporter à cette étude, cette méthode de caractérisation ne se révèle pas assez discriminante. Le coefficient d'abrasion quant à lui différencie la résistance des blocs à l'érosion, cyclique et non cyclique des formulations testées.

Les résultats présentés dans ce chapitre seront complétés par des études complémentaires incluant l'effet de la variation des paramètres de l'essai et l'évolution des caractéristiques du bloc avec le nombre de cycle pour améliorer la compréhension de la dégradation du bloc de terre stabilisée par rapport aux propriétés des formulations.

Ainsi, des murets ont été préparés et placés dans un espace ouvert exposé dans le laboratoire comme le montre la figure 4.20 pour suivre leur dégradation en conditions réelles puis essayer de connecter leurs performances aux résultats des tests de laboratoire. Ce travail sera poursuivi dans le cadre d'une autre étude après la présente thèse.

Développement de la liaison et transferts d'humidité à l'interface bloc-mortier

Ce dernier chapitre propose d'étudier le développement des mortiers liant les blocs, et les transferts d'humidité à ces interfaces. Ce chapitre s'appuie sur les résultats précédents acquis à l'échelle des matériaux pour interpréter le comportement à l'échelle de la paroi, donc de l'élément dans la structure réelle.

Tout d'abord, l'ouvrabilité de différentes formulations de mortiers à base de terre et de ciment est testée pour choisir les plus adéquates. Puis, les performances mécaniques, résistances à la compression et au cisaillement, sont évaluées sur respectivement des blocs et des assemblages de trois blocs.

Concernant les transferts hydriques, ils sont abordés par la vitesse et la capacité d'adsorption des échantillons. La quantification choisie est originale, elle utilise une caméra thermographique qui détermine les températures de surfaces à partir desquelles les flux hydriques dans les échantillons sont calculés. Il est mis en avant que le mortier ciment-sable offre les meilleures performances mécaniques pour les blocs, stabilisées et non-stabilisées. Cependant, le test d'adsorption d'eau montre que pour les blocs non stabilisés des problèmes d'adhésion au niveau du joint se posent lorsque de l'eau est adsorbée, lié à un gonflement différentiel.

En conclusion, les essais sur des blocs ou leurs assemblages à l'état sec ne sont pas suffisants pour prédire le comportement en présence d'humidité (i.e., en conditions réels). De plus, la nature du joint est à adapter en fonction de la composition du bloc. Ce transfert de connaissances ouvre pour ces travaux des perspectives d'application très intéressantes et pourrait contribuer à enrichir les pratiques de la profession.

Conclusion

Cette thèse est une contribution à l'optimisation de la stabilisation des terres crues aux liants hydrauliques pour la construction avec le bloc de terre stabilisée. Elle vise à produire des outils de quantification des impacts de la composition du ciment et de la nature des terres brutes, ainsi que leurs dosages, sur les performances du bloc de terre à l'échelle du matériau.

Premièrement, une attention particulière a été portée aux conditions de cure des blocs stabilisés, où la résistance à la compression a été utilisée comme indicateur de l'efficacité de la cure. Il a été démontré que dans les conditions testées, la durée de cure pouvait être réduite à 7 jours sur la base des résultats de 8 formulations différentes réalisées avec deux terres différentes et 4 ciments. Dans un deuxième temps, les performances de 20 mélanges ciment-terre ont été évaluées sur la base d'une approche multicritères prenant en compte les propriétés mécaniques, hygroscopiques et de durabilité à l'eau liquide. Il a été démontré que l'optimisation des mélanges stabilisés n'est pas aussi simple qu'il y paraît, et il faut analyser tous les facteurs possibles affectant la stabilisation avant de livrer une explication des performances du bloc.

Concernant de la durabilité à l'eau liquide, les résultats obtenues ont montré que les essais sélectionnés sont destinés à l'évaluation de l'efficacité du stabilisant plutôt qu'à l'analyse de la durabilité à long terme du bloc. Ainsi, une nouvelle méthode d'humidification-séchage a été développée dans le but d'étudier la résistance du bloc stabilisé à l'action répétitive des précipitations et du vent. La méthode développée et la procédure proposée pour quantifier les résultats du test ont démontré leur capacité à distinguer des formulations stabilisées avec différents ciments.

Enfin, de brèves investigations ont été faites sur les propriétés mécaniques et le transport d'humidité au niveau de l'interface bloc-mortier avec l'intention d'ouvrir la discussion sur l'influence de la composition du mortier sur l'adhésion de l'assemblage.

Par conséquent, plusieurs pistes de recherche sont ouvertes à la suite de ce travail de thèse. D'une part, les résultats obtenus ont montrés que la résistance à la compression uniaxiale a une tendance à diminuer fortement avec le rapport eau/ciment. Une étude sur l'influence du rapport eau/ciment sur les performances du produit finale serait nécessaire pour optimiser la production des blocs de terre stabilisée.

D'autre part, les résultats de l'essai cyclique de mouillage et de séchage nécessitent une confrontation à des résultats expérimentaux dans des conditions climatiques réelles. Ainsi, les paramètres d'essai pourraient être calibrés après avoir suivi et analysé les scénarios réels de dégradation du matériau.

Appendices

Appendix A Portland cement classification according to the BSI 2000

Main types	Notation of the 27 products (types of common cement)		Composition (percentage by mass[a])											
			Main Constituents											
			Clincker K	Balast furnace slag S	Silica fume D[b]	Pozzolana		Fly ash		Burnt shale T	Limestone		Minor additional constituents
						Natural P	Natural calcined Q	Siliceous V	Calcareous W		L	LL	
CEM I	Portland cement	CEM I	95-100	-	-	-	-	-	-	-	-	-	0-5
CEM II	Portland- slag cement	CEM II/A-S	80-94	6-20	-	-	-	-	-	-	-	-	0-5
		CEM II/B-S	65-79	21-35	-	-	-	-	-	-	-	-	0-5
	Portland-silica fume cement	CEM II/A-D	90-94	-	6-10	-	-	-	-	-	-	-	0-5
	Portland-pozzolana cement	CEM II/A-P	80-94	-	-	6-20	-	-	-	-	-	-	0-5
		CEM II/B-P	65-79	-	-	21-35	-	-	-	-	-	-	0-5
		CEM II/A-Q	80-94	-	-	-	6-20	-	-	-	-	-	0-5
		CEM II/B-Q	65-79	-	-	-	21-35	-	-	-	-	-	0-5
	Portland-fly ash cement	CEM II/A-V	80-94	-	-	-	-	6-20	-	-	-	-	0-5
		CEM II/B-V	65-79	-	-	-	-	21-35	-	-	-	-	0-5
		CEM II/A-W	80-94	-	-	-	-	-	6-20	-	-	-	0-5
		CEM II/B-W	65-79	-	-	-	-	-	21-35	-	-	-	0-5
	Portland-burnt shale cement	CEM II/A-T	80-94	-	-	-	-	-	-	6-20	-	-	0-5
		CEM II/B-T	65-79	-	-	-	-	-	-	21-35	-	-	0-5
	Portland-limestone cement	CEM II/A-L	80-94	-	-	-	-	-	-	-	6-20	-	0-5
		CEM II/B-L	65-79	-	-	-	-	-	-	-	21-35	-	0-5
		CEM II/A-LL	80-94	-	-	-	-	-	-	-	-	6-20	0-5
	Portland-composite cement[c]	CEM II/B-LL	65-79	-	-	-	-	-	-	-	-	21-35	0-5
		CEM II/A-M	80-94	-	-	-	-	6-20	-	-	-	-	0-5
		CEM II/B-M	65-79	-	-	-	-	21-35	-	-	-	-	0-5
CEM III	Blast Surnace cement	CEM III/A	35-64	36-65	-	-	-	-	-	-	-	-	0-5
		CEM III/B	20-34	66-80	-	-	-	-	-	-	-	-	0-5
		CEM III/C	5-19	81-95	-	-	-	-	-	-	-	-	0-5
CEM IV	Pozzolanic cement[c]	CEM IV/A	65-89	-	-	-	11-35	-	-	-	-	-	0-5
		CEM IV/B	45-64	-	-	-	36-55	-	-	-	-	-	0-5
CEM V	Composite cement[c]	CEM V/A	40-64	18-30	-	-	18-30	-	-	-	-	-	0-5
		CEM V/B	21-38	31-50	-	-	31-50	-	-	-	-	-	0-5

[a] The values in the table refer to the sum of the main and minor additional constituents

[b] The proportion of silica fume is limited to 10%

[c] In Portland-composite cements CEM II/A-M and CEM II/B-M, in pozzolanic cements CEM IV/A and CEM IV/B and in composite cements CEM V/A and CEM V/B the main constituents other than clinker are declared by designation of the cement.

Appendix B Measurement of the air relative permeability of compacted earth in the hygroscopic regime of saturation

Measurement of the air relative permeability of compacted earth in the hygroscopic regime of saturation

Antonin Fabbri[a,*], Noha Al Haffar[a], Fionn McGragor[a]

[a]*LTDS, UMR 5513 CNRS, ENTPE, 69100 Vaulx-en-Velin, France*

Abstract

The hygroscopic behavior of earthen materials has been extensively studied in the past decades. However, while air flow within their porous network may significantly affect the kinetic of vapor transfer and thus their hygroscopic performances, few studies have focused on its assessment. For that purpose, a key parameter would be the gas permeability of the material, and its evolution with the air relative humidity. Indeed, due to the sorption properties of earthen material, an evolution of the water content, and thus of the relative permeability, are foreseeable if the humidity of in-pore air changes. To fill this gap, this paper presents the measurement of relative permeabilities of a compacted earth sample with a new experimental set-up. The air flow through the sample is induced with an air generator at controlled flow rate, temperature and humidity. The sample geometry was chosen in order to reduce, as much as possible, its heterogeneity in water content and the tests were realized for several flow rates. The results, which show the evolution of gas permeability with the relative humidity of the injected air and with the water content of the material, either in adsorption or in desorption, were eventually successfully compared to predictions of the well known Corey's law.

Keywords: Earthen materials; Relative permeability; Steady-state; Darcy's law; Vapor advection

*Corresponding author

1. Introduction

In the general context of global warming, earthen constructions are regaining interest mainly due to their attractiveness in terms of their low embodied energy [26, 1] and for their high potential to contribute to a passive regulation of the interior climate of dwellings and other buildings [18, 30, 21, 6]. Each construction can potentially be built with a different material and cannot be totally included in an industrial process. Therefore, several constructions techniques have been invented adapting them to the nature of the soil used. Among these techniques the three most common ones are adobe blocks, cob and rammed earth [19]. But, whatever the construction technique, strong similarities exist in the soils used. For instance, all earthen materials used are described as a porous media with a relatively high permeability with a solid matrix composed of non-negligible amount of clays, therefore, allowing good vapor sorption properties [24]. The affinity of earthen materials to water also induces substantial complexity in their mechanical behavior. Indeed, in addition to the drop in strength commonly observed at high water content values [4], recent studies have underlined that significant changes in the mechanical behavior (strength variations, shrinkage, swelling) may be observed under normal operating conditions due to the modification of air relative humidity [8, 31, 3]. In consequence, a first step to correctly assess the behavior of earthen walls is the precise quantification of the humidity field within the in-pore air and within the material. [13].

For that purpose, the main equations which describe the hygroscopic couplings are nowadays quite well known by the scientific community (cf. [22, 29] for example). But, one of the main challenges remains the proper estimation of the material parameters which drive these mass transports equations, such as the vapor transfer coefficient [23], the isothermal sorption-desorption curve [12, 5], as well as the liquid and gas relative permeabilities [14].

In particular, the increasing development of research activities on mass transfer through earthen materials has highlighted the strong lack in literature of mea-

surements of gas relative permeability in the hygroscopic range of saturation. This can be explained by the fact that advection of vapor due to gas transport is almost always neglected. But this quite common simplification has not got any consensus since some authors have already underlined that air flows may have a significant impact on the hygroscopic behavior of porous material like concrete [**?**], textiles [16], or even earthen and bio-based materials [2].

In this context, this paper presents the development of an experimental set up to measure the relative permeabilities of a compacted earth sample. The air flow through the sample was induced with a humid air generator at controlled flow rate, temperature and humidity. The testing protocol, including the definition of the sample geometry, is presented in the first part. Then, the results of gas permeability in function of relative humidity of the injected air and water content, either in adsorption or in desorption, are presented and compared to predictions of the well known Corey's law.

2. Material characterization and preparation

2.1. Raw earth material and sample realization

The earthen material presented in this study is sampled from rammed earth walls of an existing construction located in the South-East of France during operations of opening new doors and windows. This choice ensures that the studied material is suitable for building sustainable earth constructions. Particle size distribution, Atterberg limits and methylene blue value were measured. It shows a mass content of clay (particles with a diameter lower than 2 μm) equal to 16%, a plasticity index of 14% and a blue value of 2.7.

Cylindrical samples of 3.5 cm in diameter and 7 cm high were manufactured at the optimum moisture content resulting in maximum dry density (11% and 1.97 g/cm^3). Those parameters were previously determined using a manual CEB press. More details on the sample realization protocol are given in [8]. Just after their production, the samples were dried at 23°C in a desiccator with

silica gel until a constant mass was reached. The relative humidity within the desiccator was checked with a portable sensor (Rotronic HygroLog HL-NT), and it was found to be consistently lower than 5% RH. After this drying period, the cylinders were weighed and measured in order to estimate their dry density. A value of 1.97 g/cm^3 $\pm$ 0.02 g/cm^3 was found.

2.2. Porous and hygroscopic properties

The adsorption-desorption curves of the material were measured using the dynamic gravimetric sorption method, commonly called the DVS (dynamic vapor sorption) method. It consists in measuring uptake and loss of moisture by flowing a carrier gas at a specified relative humidity (or partial pressure) over a small sample (from several milligrams to several grams depending on the device used) suspended from the weighing mechanism of an ultrasensitive recording microbalance. Variations in the gas's relative humidity are automatically calculated by the device when the target condition in mass stability is reached. Density and porosity measurements are reported in the Table 1 and the adsorption-desorption loop is reported in the Figure 1.

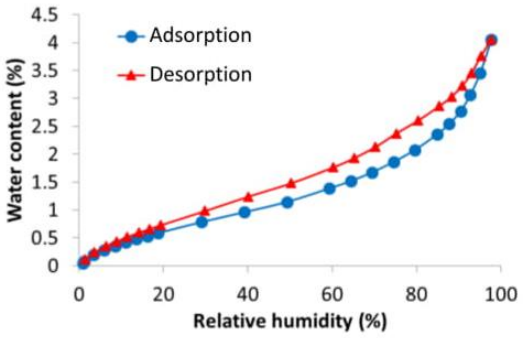

Figure 1: Adsorption and desorption curves at 23°C of the tested material obtained with the DVS method.

The water vapor permeability was measured using the wet cup method following the procedure described in [23]. The vapor pressure gradient is created for the wet cup by setting the RH at 60% in the chamber and 85% in the cup.

It leads to the values reported in the Table 1.

Symbol	Description	Value [unity]
ϕ	Porosity	0.26
ρ_d	Dry density	1.97 [g/cm^3]
ρ_s	Specific density	2.7 [g/cm^3]
δ_p	diffusion coefficient of vapor	4.2×10^{-11} [kg/m/Pa/s]

Table 1: Hygroscopic parameters of the samples.

Since this study focuses on the hygroscopic regime of saturation (saturation degree lower than 20%) the impact of liquid water transport was neglected and the liquid permeability was not measured.

3. Experimental method to measure the gas permeability

3.1. Intrinsic and relative permeability

The gas permeability, denoted by κ_G, characterizes the ability of a fluid mass to move through the porosity of a material. For an isotropic medium, and neglecting the influence of gravity, mass flow of gas writes in the form:

$$\underline{\omega_G} = -\rho_G \frac{\kappa_G}{\eta_G} \underline{\nabla} P_G \tag{1}$$

where $\underline{\omega_G}$ is the mass flow vector, η_G is the viscosity of the gas, P_G its pressure and ρ_G its density, which is assumed to satisfy the perfect gas relation:

$$\rho_G = \frac{M_G}{RT} P_G \tag{2}$$

The value of the gas permeability depends on the geometry of the porous network, which may change when the material deforms, and on the volumetric proportion of the pore space occupied by adsorbed and/or condensed water molecules [25]. The present study is limited to unloaded materials, which remain in the hygroscopic range of saturation. Thus the impact of the material

deformation can reasonably be neglected and, for an isotropic medium, the gas permeability can be written in the form:

$$\kappa_G = \kappa_G^0 \kappa_G^r(w) \tag{3}$$

where κ_G^0 is the intrinsic permeability, that is the gas permeability for a totally dried sample, and $\kappa_G^r(w)$ is the relative permeability, which is function of the water content, denoted by w. For the record, the water content is defined as the mass of water divided by the dry mass of the solid.

3.2. Set up of experimental device

Several methods exist to estimate the intrinsic permeability. Mainly transient methods [10] or steady-states methods [27]. Indirect estimation methods, based on the upscaling of the transfers within the interconnected pores at several levels have also been developed [7].

In this paper, an steady-state approach is chosen. When low saturation ratios are considered, the main difficulty of this method is to be able to generate flows of gas and/or liquid while keeping a constant and homogeneous saturation state through the tested sample. To overcome this problem, one method, already used to assess the liquid relative permeability of cement based materials [32] and gas relative permeability of textiles [15], consists in fixing the water content of the material through the relative humidity of the incoming air. Indeed, as it is depicted by the sorption curves (cf. Figure 1), any increase of air relative humidity will increase its water content.

For that purpose, we develop in this study and experimental set up quite similar to the one used by Gibson et al. [15] for textiles applications. The gas at controlled relative humidity was injected at constant flow rate within the material. Difference between inlet and outlet pressures, respectively denoted by $P_{G,i}$ and $P_{G,o}$, was recorded. When this latter became constant, the steady state was assumed to be reached. The apparatus is made of a static triaxial cell (GDS/CEL/STA/100) with drainage systems on its cap and base pedestal.

They are linked to a wet air generator (WETSYS S60/59105) at constant flow rate, varying between 5mL/min to 200mL/min depending on the relative humidity, which varies between 0% and 95% and a temperature between ambient and 50°C. A special climatic chamber was built to contain the cell and regulate its temperature (accuracy of 0.1°C). The wet air can be injected in the sample through its bottom side or its top side, while the other side is kept at atmospheric pressure. The inlet/outlet pressures, temperatures and relative humidity are monitored during the whole test. A diagram of the experimental device is reported in the Figure 2.

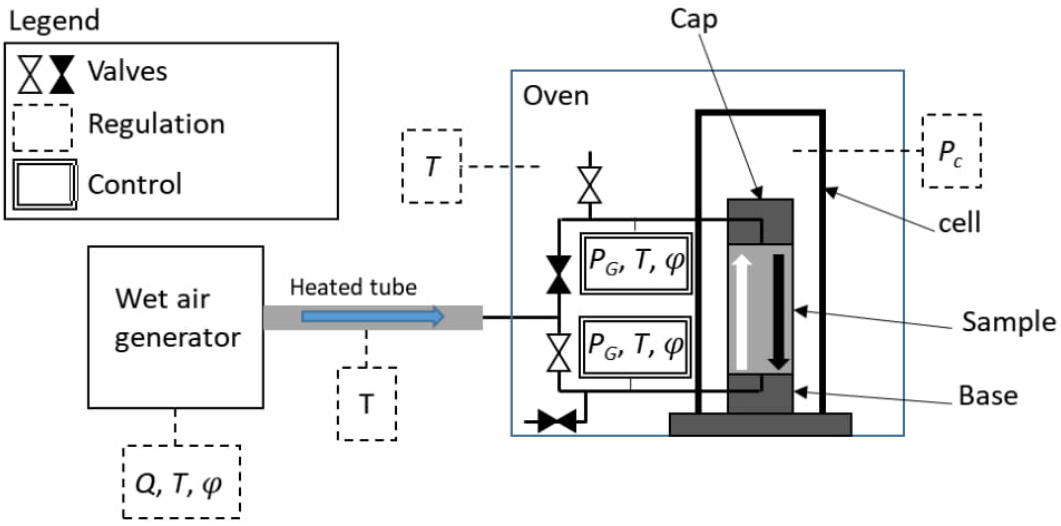

Figure 2: Schematic diagram of the experimental device. The black arrow through the sample represent the direction of the gas flow when the black valves are open and the white valves are closed, and reciprocally for the white arrow. P_c is the confinment pressure in the cell, T the temperature, Q the volumetric flow rate, φ the relative humidity and P_G the gas pressure.

To ensure an unidirectional flow and to avoid leakage at the interfaces with the base and the cap, the sample was jacketed in an impermeable latex membrane, and a confinement pressure of 1bar is applied, which remains at least twice the inlet overpressure. Given the bulk modulus of the materials, which is higher than 300 MPa even for a relative humidity of 97%, the volumetric

strain induced by the confinement pressure is in the order of 10^{-4}, therefore the impact on transport properties is assumed to be negligible.

3.3. Principle of measurement

Under steady-state condition, if the water content is homogeneous through the sample, the mass conservation of the gas phase (that is $\underline{\nabla} \cdot \underline{\omega_G} = 0$), combined with (1-2) leads to:

$$\kappa_G = \kappa_0 \kappa_G^r(w) = Q \ \eta_G \ \frac{2HP_{G,i}}{A(P_{G,i}^2 - P_{G,o}^2)} \tag{4}$$

where H is the sample thickness, A its cross surface and Q is the incoming volumetric gas flow rate ($Q = \rho_{G,i}\underline{\omega_G} \cdot \underline{n}$, with $\rho_{G,i}$ is the gas density of incoming gas and $\underline{n}$ the outgoing normal vector).

On the other side, if the water content is not homogeneous though the sample, the mass conservation of the air does not directly provides the permeability, but its average value.

3.4. Definition of the sample geometry and of the maximum flow rate

A good control of the heterogeneity in water content, and thus of the air relative humidity, through the sample is necessary for an accurate measurement of the gas permeability. For that purpose, the flow of vapor mass within the sample, which is denoted by $\underline{\omega_V}$, must be assessed precisely. Considering both vapor advection and diffusion processes, $\underline{\omega_V}$ satisfies:

$$\underline{\omega_V} = \frac{\rho_V}{\rho_G}\underline{\omega_G} - P_G \delta_p \underline{\nabla}\left(\frac{\varphi p_V^s}{P_G}\right) \tag{5}$$

where φ is the relative humidity of the in-pore air, p_V^s the vapor pressure at saturation and ρ_V its apparent density, which is assumed to satisfy the perfect

gas relation:

$$\rho_V = \frac{M_w}{RT}\varphi p_V^s \tag{6}$$

In (5), the term $(\rho_V/\rho_G)\underline{\omega_G}$ represents the mass of vapor advected by the gas phase, while $-P_G\delta_p\underline{\nabla}(p_V/P_G)$ is the diffusion of vapor within the gas phase. If the incoming flow of air is in the order of 10mL/min, the order of magnitude of the mass of vapor advected by the gas phase within the sample of cross section $A = 10\text{cm}^2$ is 10^{-5}kg/s/m^2. On the other side, considering the material parameters of the table 1, the diffusive flow for a variation of relative humidity of 0.1 within a 1cm thick sample is in the order of 10^{-6}kg/s/m^2. At first, order, this latter can thus be neglected.

Under this assumption, the combined use of the relations (1-6), the mass conservation equations ($\underline{\nabla}\cdot\underline{\omega_G} = 0$ and $\underline{\nabla}\cdot\underline{\omega_V} = 0$), and the relation (4) allows to express the relative difference between outlet and inlet relative humidity at constant temperature, denoted by r_φ, in the form:

$$r_\varphi = \frac{\varphi_o - \varphi_i}{\varphi_i} = \frac{1}{\xi}\left(\sqrt{1+\xi^2}+1\right) - 1 \tag{7}$$

where φ_o and φ_i are respectively the outlet and the inlet relative humidity while ξ is a dimensionless number, which is a function of the permeability of the material, its geometry (thickness and cross section), of the flow rate and of the outlet pore pressure. It is equal to:

$$\xi = \frac{\kappa_0 < \kappa_G^r >}{\eta_G}\frac{AP_{G,o}}{QH} \tag{8}$$

The evolution of r_φ with ξ is reported in the Figure 3. To insure a good homogeneity in water content through the sample, r_φ must be as low as possible, and thus ξ must be as high as possible.

Since the outlet pressure and the sample surface are fixed, the only parameters on which it is possible to act to increase ξ are the gas flow and the sample thickness, which should be both as small as possible. The lower flow rate that

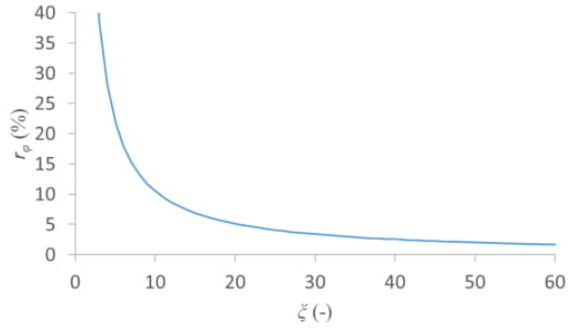

Figure 3: Evolution of r_φ with ξ.

can be reached while keeping a good regulation with our system is 10mL/min. On the other side, in order to avoid too important inlet overpressure, Q will be limited at 25mL/min.

Under these conditions, and assuming permeability values higher than 1×10^{-14} m^2, a sample thickness of 1cm would lead to values of ξ higher than 12.7 and r_φ lower than 8%. This relative variation, which is range of uncertainties of the relative humidity sensors, is considered as acceptable.

3.5. Test protocol

The first stage consist in applying through the sample a flow of dry air at 25mL/min. When the permanent state is reached (stable relative humidity and pressure at inlet and outlet), the flow is progressively reduced to 10mL/min by steps of 5mL/min. For each step, the inlet and outlet pressures were recorded and the permeability coefficient was estimated using the equation (4) as long as the permanent state was reached. Even if permeability measurements were made at different flows, the outlet overpressure remained equal to 0, while the inlet overpressure was limited to 0.5 bar. Due to these technical constrains, the mean pressure variations remained quite limited and it was not possible to study the Klinkenberg's effect [20]. In consequence, only the apparent gas permeability was measured in this study.

4. Results of gas permeability measurements

Gas permeabilities measured for all testing configurations are summarized in the Table 2. At first, the tests performed at the several flow rates underline its limited impact in the range of values considered in this study (that are between 10mL/min and 25mL/min). This result gives some confidence on the accuracy of measurements, particularly with regard to those of inlet and outlet pressures. Whatever the relative humidity of the injected air, permeabilities in the range of 10mD (10^{-14}m^2) were observed. It emphasizes the permeable nature of the tested material. Indeed, it is in the range of gas permeability of permeable rocks like Voges sandstones [28], while being at least three orders of magnitude higher than that of cement based materials [11].

This result is interesting by itself. Indeed, given this high value of gas permeability, the mass transfer of vapor through the material by air advection process might not be negligible if gas pressure variations, caused by wind effect for example, are considered. Anyway, it underlines that this point deserve be analyzed.

Nonetheless, even if they remained in the same order of magnitude, a noticeable reduction of the gas permeability was observed when the relative humidity of the injected air increases. For the record, injection of dry air led to permeabilities 35% higher than injection of wet air at 90%HR. This variation may not be negligible if in-pore vapor advection need to be considered to have a correct estimation of the humidity field within the material, especially since it is in the range of relative humidity that may be observed during the lifetime of an earthen wall.

To analyze further these results, the average relative humidity, defined as the arithmetic mean between the inlet and outlet relative humidity, was rather considered. It is supposed to be representative of the average humidity within the sample. Indeed, due to the quite limited gradient of relative humidity within the sample, this approach, though simplified, is considered sufficient.

The variation of gas permeability with the average relative humidity is reported in the Figure 4A. Interestingly, a difference is observed between the permeabilities which were measured during adsorption and desorption stages. Because gas permeability should rather be driven by the water content than by air relative humidity (cf. eq. (3)), this may be a consequence of the hysteresis between adsorption and desorption curves as it is depicted in the Figure 1. This assumption seems verified by the results presented in the Figure 4B, in which almost no more difference was observed between adsorption and desorption stages if the gas permeability is expressed in function of the water content instead of the relative humidity. For this graph, the water content was not directly measured, but it was calculated from the average relative humidity and using either the adsorption or the desorption curves in function of the stage which is considered.

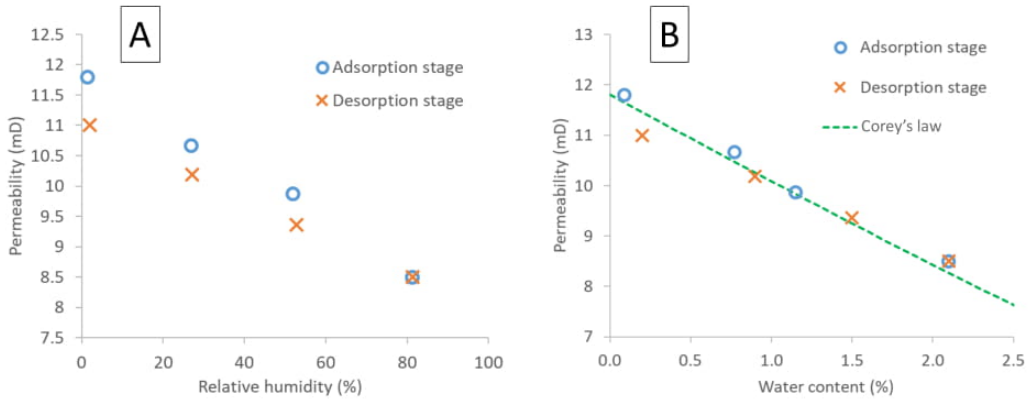

Figure 4: Evolution of the gas permeability with relative humidity (A) and water content (B). The permeability is expressed in mD (1mD $\approx$ 1.0 10^{-15} m^2)

5. Discussion on the evolution of air relative permeability with liquid saturation

The variation of gas permeability with water saturation can be attributed to several phenomena A first one, which was already observed in textile material by [17], can be the modification of the microstructure due to swelling processes.

However, this explanation might not be consistent with the quite limited volumetric swelling, lower than 0.005%/%rh, which was measured in [**?**] for similar compacted earth samples (same earth, similar dry density, same compaction procedure).

A second explanation can rise up from the analysis of the porous network structure of the material. As it was discussed in [14], it should be composed by large pores connected to each others by narrow throats. Adsoprtion of water molecules at the pore walls when the air relative humidity increases may thus fill some of these narrow throats. As a consequence, the number of percolation pathways through the material for the gas phase would be reduced, which translates, at the macroscopic scale, by a reduction of the gas permeability. To go further on that point, it could be interesting to analyses more in detail the shape of the relation between the gas permeability and the liquid ratio. For that purpose, several theoretical and empirical laws have been already developed [10]. Among them, on of the most used is the Corey's law [9], which writes in the form:

$$\kappa_G = \kappa_G^0 (1 - S_r)^2 (1 - S_r^2) \tag{9}$$

where S_r is the reduced saturation ratio, which can take into account the impact of both liquid and gas residual saturation. If these two terms are considered to be null and, if the deformation of the material is neglected, S_r can be linked to the water content, denoted by w, through the relation:

$$S_r = w \frac{\rho_d \rho_s}{\rho_s - \rho_d} \tag{10}$$

The comparison between the predictions obtained with the relations (9-10) and the experimental results is reported in the Figure 4B. A good consistency is observed even though no calibration parameters were used since both residual liquid and gas saturation were assumed to be null.

Even if it is not a formal proof, the fact that Corey's law was intially established from experimental data of non-swelling porous materials and for oil

and gas in-pore phases (instead water and air) tends to give some confidence on the assumption that the variation of permeability is rather induced by filling of some narrow pores with liquid water than by swelling phenomena.

Finally, to interpret properly this result it is important to underline that, for a given hydric state, water content value depends on the method which is used to reach the reference dry state of the sample (that is for which $w = 0$). For example, it was shown in [12] that earthen samples will have a lower mass after being dried in an oven at 105°C than after being dried by a flow of dry air at 23°C. In this study, a flow of dry air at 23°C was used to determine the dry mass of the samples. In consequence, to obtain same results while considering a dry mass from oven-drying at 105°C, it would be necessary to take into account a residual saturation in the expression of S_r. In view of the definition of a standardized method to estimate a consistent dry mass of earthen materials, this results, although it needs to be further investigated, may be quite interesting.

6. Conclusion

In this paper, a novel apparatus to measure the evolution of the gas permeability of earthen material in the hygroscopic range of saturation was presented. From the analysis of the water vapor transport within the porous network of the material, limits on sample thickness and flow rate of the injected wet air were determined. The obtained results were analyzed in terms of water content and relative humidity. The Corey's law was found to fit accurately the experimental results, without the needs of any calibration parameters. In consequence, at least for the same kind of sample than the one studied here (compacted fine earth with no gravels, quite high dry density), a single measurement of the intrinsic gas permeability can be sufficient to estimate the variation of the gas permeability with water content in the hygroscopic range of saturation.

References

[1] Arrigoni A, Beckett C, Ciancio D and Dotelli G (2017) Life cycle analysis of environmental impact vs. durability of stabilised rammed earth. *Construction and Building Materials* **142**: 128–136.

[2] Berger J, Gasparin S, Dutykh D and Mendes N (2018) On the solution of coupled heat and moisture transport in porous material. *Transport in Porous Media* **121**: 665–702.

[3] Bruno A, Perlot C, Mendes J and Gallipoli D (2018) A microstructural insight into the hygro-mechanical behaviour of a stabilised hypercompacted earth. *Materials and Structures* **51**: 32.

[4] Bui QB, Morel JC, Hans S and Walker P (2014) Effect of moisture content on the mechanical characteristics of rammed earth. *Construction and Building Materials* **54**: 163–169.

[5] Bui R, Labat M and Aubert J (2017) Comparison of the saturated salt solution and the dynamic vapor sorption techniques based on the measured sorption isotherm of straw. *Construction and Building Materials* **141**: 140–151.

[6] Busser T, Pailha M, Piot A and Woloszyn M (2019) Simultaneous hygrothermal performance assessment of an air volume and surrounding highly hygroscopic walls. *Building and Environment* **148**: 677–688.

[7] Carmeliet J, Descamps F and Houvenaghel G (1999) A mutliscale network model for simulating moisture transfer properties of porous media. *Transport in porous media* **35**: 67–88.

[8] Champiré F, Fabbri A, Morel J, Wong H and McGregor F (2016) Impact of hygrometry on mechanical behavior of compacted earth for building constructions. *Construction and Building Materials* **110**: 70–78.

[9] Corey A (1954) The interrelation between gas and oil relative permeability. *Producers Monthly* **19**: 38–41.

[10] Dana E and Skoczylas F (1999) Gas and stones permeability and pore structure of sandstones. *International Journal of Rock Mechanics and Mining Science* **36**: 613–625.

[11] Fabbri A, Corvisier J, Schubnel A, Brunet F, Goffé B, Rimmele G and Barlet-Gouédard V (2009) Effect of carbonation on the hydro-mechanical properties of portland cements. *Cement and Concrete Research* **39**: 1156–1163.

[12] Fabbri A, McGregor F, Costa I and Faria P (2017) Effect of temperature on the sorption curves of earthen materials. *Materials and Structures* **50**: 253.

[13] Fabbri A, Morel J and Gallipoli D (2018) Assessing the performance of earth building materials: a review of recent developments. *RILEM Technical Letters* **3**: 46–58.

[14] Fabbri A, Soudani L, McGregor F and Morel J (2019) Analysis of the water absorption test to assess the intrinsic permeability of earthen materials. *Construction and Building Materials* **199**: 154–162.

[15] Gibson P and Charmchi M (1997) Modeling convection/diffusion processes in porous textiles with inclusion of humidity-dependent air permeability. *International Communications in Heat and Mass Transfer* **24**: 709–724.

[16] Gibson P, Elsaiid A, Rivin CKD and Charmchi M (1997) A test method to determine the relative humidity dependence of the air permeability of textile materials. *Journal of Testing and Evaluation* .

[17] Gibson P, Rivin D, Kendrick C and Schreuder-Gibson H (1999) Humidity-dependent air permeability of textile materials. *Textile Research Journal* **69**: 311–317.

[18] Hall M and Allinson D (2009) Analysis of the hygrothermal functional properties of stabilised rammed earth materials. *Building and Environment* **44**: 1935–1942.

[19] Hall M and andM. Krayenhoff RL (2012) *Modern earth buildings*. Woodhead.

[20] Klinkenberg J (1941) The permeability of porous media to liquids and gases. *Drilling and Production Practice* .

[21] Labat M, Magniont C, Oudhof N and Aubert J (2016) From the experimental characterisation of the hygrothermal properties of straw-clay mixtures to the numerical assessment of its buffering potential. *Building and environment* **97**: 69–81.

[22] Labat M and Woloszyn M (2016) Moisture balance assessment at room scale for four cases based on numerical simulations of heat?air?moisture transfers for a realistic occupancy scenario. *Journal of Building Performance Simulation* **9**: 487–509.

[23] McGregor F, Fabbri A, Ferreira J, Simoes T, Faria P and Morel JC (2017) Procedure to determine the impact of the surface film resistance on the hygric properties of composite clay/fibre plasters. *Materials and Structures* **50**.

[24] McGregor F, Heath A and Shea A (2014) The moisture buffering capacity of unfiered clay masonry. *Building and Environment* **82**: 599–207.

[25] Monfared M, Sulem J, Delage P and Mohajerani M (2014) Temperature and damage impact on the permeability of opalinus clay. *Rock Mechanics and Rock Engineering* **47**: 101–110.

[26] Morel J, Mesbah A, Oggero M and Walker P (2011) Building houses with local materials: means to drastically reduce the environmental impact of construction. *Buildings and Environment* **36**: 1119–1126.

[27] Osselin F, Fabbri A, Fen-Chong T, Pereira J, Lassin A and Dangla P (2015) Experimental investigation of the influence of supercritical state on the relative permeability of vosges sandstone. *Comptes Rendus Mecanique* **343**: 495–502.

[28] Osselin F, Fen-Chong T, Fabbri A, Lassin A, Pereira J and Dangla P (2013) Dependence on injection temperature and on aquifer's petrophysical properties of the local stress applying on the pore wall of a crystallized pore in the context of co_2 storage in deep saline aquifers. *The European Physical Journal Applied Physics* **64**: 21101.

[29] Soudani L, Fabbri A, Morel J, Woloszyn M, Chabriac P, Wong H and Grillet A (2016) A coupled hygrothermal model for earthen materials. *Energy and Buildings* **116**: 498–511.

[30] Woloszyn M, Kalamees T, Abadie M, Steeman M and Kalagasidis AS (2009) The effect of combining a relative-humidity-sensituve ventilation system with the moisture buffering capacity of materials on indoor climate and energy efficiency of buildings. *Building and Environment* **44**: 515–524.

[31] Xu L, Wong K, Fabbri A, Champir F and Branque D (2018) Loading-unloading shear behavior of rammed earth upon varying clay content and relative humidity conditions. *Soils and Foundations* **58**: 1001–1015.

[32] Zamani S, Kowalczyk R and McDonald P (2014) The relative humidity dependence of the permeability of cement paste measured using nmr profiling. *Cement and Concrete Research* **57**: 88–94.

φ_i [%]	Q [mL/min]	φ_{moy} [%]	$\Delta\varphi$ [%]	κ_G [mD]
Adsorption stage				
0.5	24.88	1.1	1.3	11.74
0.5	19.97	1.2	1.4	11.76
0.8	14.64	1.4	1.2	11.6
1.8	9.80	2.3	0.4	12.1
29.1	24.67	26.7	4.8	10.68
29.2	19.75	26.8	4.8	10.61
30.0	14.76	27.2	5.6	10.64
29.5	9.78	27.2	4.7	10.77
57.0	24.67	52.0	10.0	9.94
56.8	19.46	52.0	9.6	9.83
56.7	14.67	51.9	9.6	9.80
56.4	9.66	51.6	9.6	9.90
90.9	24.62	81.5	18.8	8.61
88.9	19.46	80.6	16.7	8.49
91.4	14.67	81.7	19.3	8.42
91.3	9.66	81.5	19.7	8.49
Desorption stage				
57.3	24.67	52.8	9.0	9.41
57.8	19.75	53.0	9.6	9.37
58.5	14.71	53.3	10.5	9.29
57.4	9.69	52.4	9.9	9.38
29.6	24.96	27.3	4.7	10.24
29.2	19.61	27.2	4.1	10.03
29.2	14.67	27.2	4.1	10.01
29.2	9.71	27.2	4.0	10.50
0.3	24.85	1.1	1.5	11.02
0.7	19.84	2.0	2.5	10.91
1.2	14.92	2.3	2.1	10.93
1.9	9.91	2.7	1.7	11.12

Table 2: Summary of the results obtained for the several relative humidity and air flow. φ_{in} is the relative humidity of the injected air, φ_{moy} is the average between the inlet and outlet relative humidity while $\Delta\varphi$ denotes the difference between the inlet and outlet relative humidity.

Appendix C Variation of sample's mass during conditioning

No moist curing

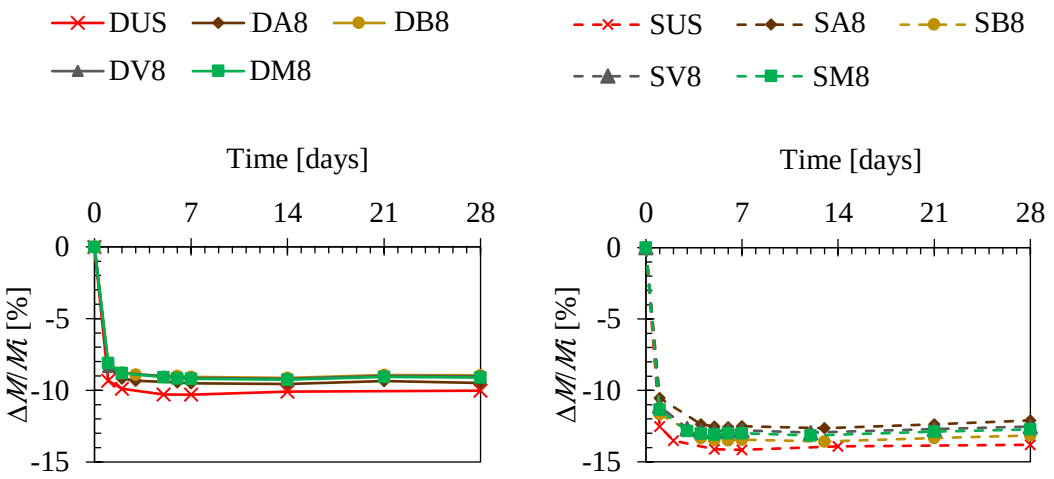

1 day of moist curing

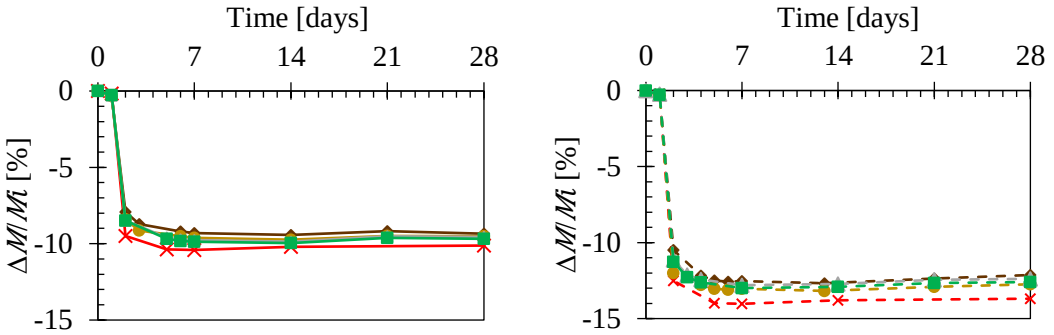

3 days of moist curing

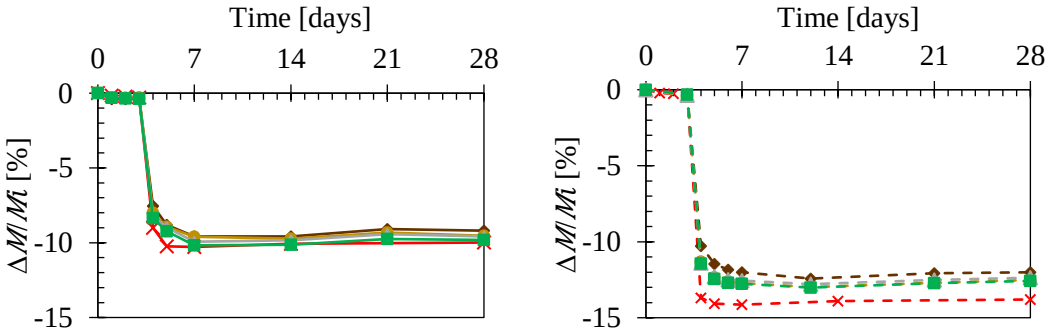

5 days of moist curing

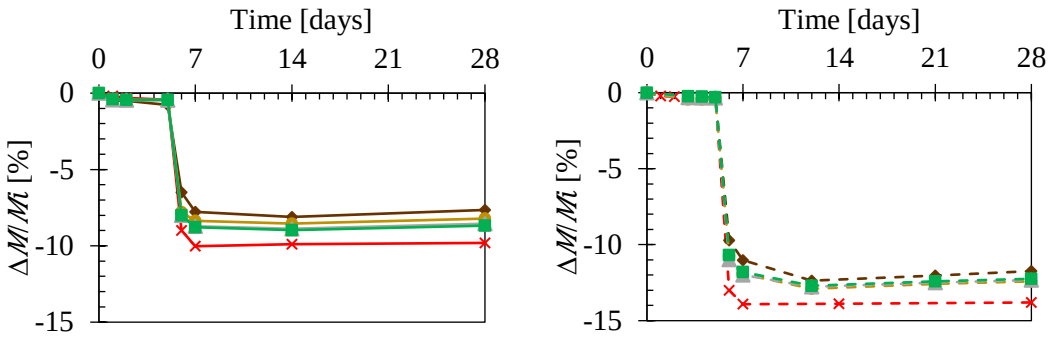

7 days of moist curing

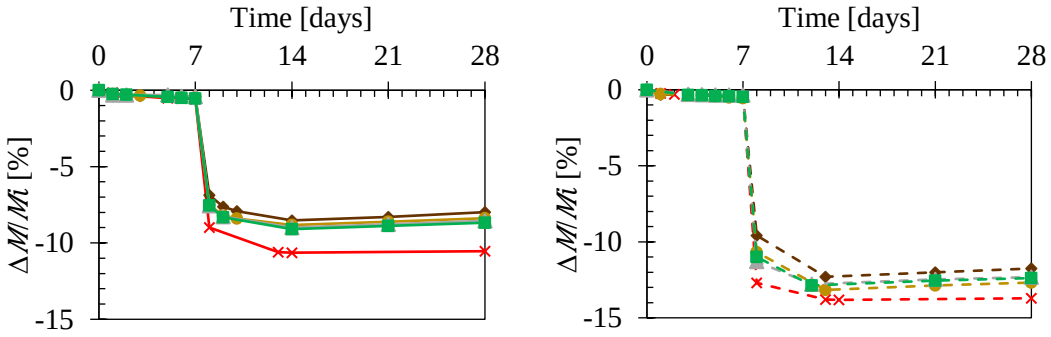

Appendix D Solvent exchange method

The solvent replacement method, also named solvent exchange method, was used because it is considered to be gentle to the cement paste microstructure [371], [372]. Organic solvent tend to naturally replace the pore solution in a hydrated cement paste by a simple counter-diffusion process due to their significant lower specific gravity in comparison with water [373], [374].

Directly after the compression tests, a part of the samples was entirely crushed and immerged in acetone to arrest cement hydration in stabilized formulations. The unstabilized samples were dried following the same procedure as the unstabilized ones. In this way, we were sure that all samples were tested at their 28th day-hydrated state.

The drying procedure followed here was proposed by industrial partners and it consists of immersing the crushed specimen in acetone solution, placing it on magnetic stirrer, and stir for 24 hours. Acetone is supposed to immediately penetrates the pores and replace the cement paste pore solution. Thereafter, sample is filtrated and dried under fume hood than immersed in di-ether solution, placed on magnetic stirrer again and stir for 40 minutes. Finally, sample is dried under fume hood to accelerate drying, and the resulting sample is conserved in small hermetic bottles at 21°C/50%RH until the tests (Figure 0.1).

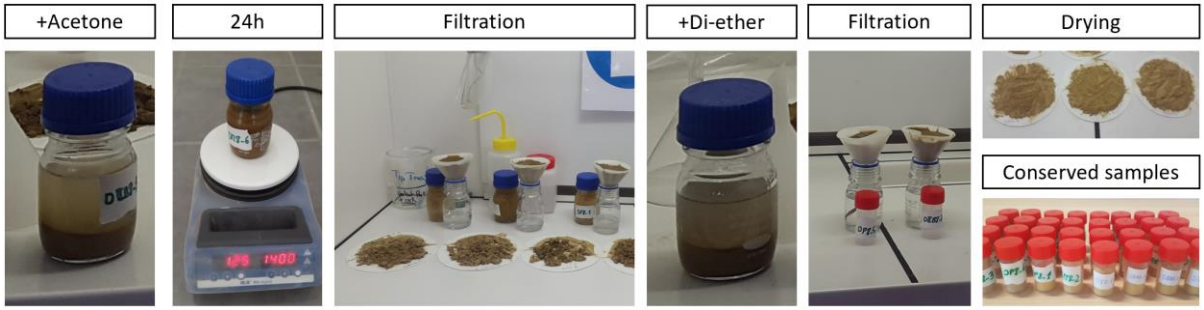

Figure 0.1. Sample's preparation steps by solvent replacement method

Appendix E Chemical and mineralogical composition of cements (@Vicat)

Qualité du ciment		CEM II/A LL 42.5 R CE NF	CEM II/B-LL 32.5 R CE NF	MC 12.5 NF POLYCIM	Ciment Naturel Prompt*
Usine productrice		MONTALIEU	MONTALIEU	MONTALIEU	La Pérelle / Voreppe
Date du prélèvement		02/05/2018	02/05/2018	02/05/2018	26/04/2018
Numéro d'échantillon		28670	28639	28640	23238
Utilisation prévue		THESE ATILH	THESE ATILH	THESE ATILH	THESE ATILH
Bénéficiaire		ENTPE	ENTPE	ENTPE	ENTPE
Date d'émission de la demande		23/04/2018	23/04/2018	23/04/2018	23/04/2018
Composition chimique (FX) - % massique	PF 975°C	5,60	10,65	15,95	10,0
	SiO2(%)	18,34	15,97	14,79	18,02
	Al2O3(%)	4,16	3,63	3,54	7,32
	Fe2O3(%)	2,95	2,60	2,38	3,03
	CaO(%)	61,64	59,92	58,41	54,06
	MgO(%)	1,99	1,65	1,41	3,39
	SO3(%)	3,16	3,14	2,37	3,94
	K2O(%)	0,97	0,82	0,76	1,2
	Na2O(%)	0,24	0,17	0,13	0,12
	P2O5(%)	0,23	0,19	0,14	
	Cl(%)	0,07	0,07	0,02	0,01
	Total(%)	99,36	98,80	99,89	101,09
Composition minéralogique (DRX) - % massique	Alite	60,6	45,0	40,0	1,3
	Belite	8,5	10,7	5,5	27,7
	Aluminate tricalcique	3,6	2,9	2,7	1,8
	Ferrite	8,9	7,5	6,5	6,2
	Mayenite				2,3
	Yeelemite				2,1
	Spurrite				15,4
	Gehlenite				4,2
	Gypse	1,3	1,2	0,6	
	Bassanite	0,9	1,1	0,7	
	anhydrite	1,3	1,4	1,7	2,7
	Calcite	9,1	23,8	36,5	21,0
	chaux libre/Portlandite	2,0	1,7	1,2	5,5
	Sulfate alcalin (Arcanite, Langbeinite, Aphthitalite)	1,4	1,6	0,9	2,3
	Autres (quartz, periclase, dolomite, sylvite, magnesite)	2,2	3,1	3,6	7,6
	Total (%)	99,9	100,0	100,0	100,1
Finesse	Blaine (cm²/g)	4176	4123	5241	7950
	Médian (µm)	11,1	12,8	7,92	13,6
Composition (% massique)	Clinker(%)	83%	70%	59%	100%
	Additions calcaire	12%	24%	37%	
	Gypse (%)	6%	6%	4%	

*produit naturel dépendant des variations de la roche exploitée

EQIOM A CRH COMPANY Le L.A.B

Eqiom Le L.A.B
Parc Vendôme - CRT1
460, Allée de l'innovation
59810 Lesquin

T + 33 3 20 66 30 41
F + 33 3 20 66 31 49
www.eqiom.com

Demande :	20-CF-115 220 21/12/2020 348
Titre :	ATILH - Analyses de terres
Client :	EQIOM FedPro: Fédération Professionnelle-220

Référence échantillon			201395	201396	201397
Nature			TERRE DAG ENTPE	TERRE STA ENTPE	TERRE LIM ENTPE
Origine			TERRE DE DAGNEUX	TERRE DE ST. ANTOINE L ABBAYE	TERRE DE LIMONEST
			NB : analyses sur matières séchées à 40°C		
	protocole		résultats	résultats	résultats
SiO_2	EN 196-2 FX	%	73,44	69,25	69,34
Al_2O_3	EN 196-2 FX	%	11,7	14,89	13,69
Fe_2O_3	EN 196-2 FX	%	4,66	6,78	5,96
CaO	EN 196-2 FX	%	0,60	<0,78	<0,78
MgO	EN 196-2 FX	%	1,00	0,37	0,91
Na_2O	EN 196-2 FX	%	1,42	<0,10	0,87
K_2O	EN 196-2 FX	%	1,66	1,31	2,06
$S\ SO_{3\ total}$	EN 196-2 FX	%	**<0,12**	**<0,12**	**<0,12**
TiO_2	EN 196-2 FX	%	0,72	0,47	0,71
P_2O_5	EN 196-2 FX	%	0,16	0,12	0,14
Mn_2O_3	EN 196-2 FX	%	0,12	0,02	0,18
Perte au feu	PAF 950°C 1h	%	4,59	6,92	5,80
Somme		%	100,07	100,13	99,66
dont Matières Organique	selon P94-047	%	3,65	5,35	4,70
SO3 total	interne LECO IR	%	**0,10**	**0,09**	**0,09**
pH	avec eau osmosée labo mortier	-	7,63	5,23	6,54
	avec eau ultra-pure labo chimie	-	7,76	5,14	-

ppm = mg/kg Matière Sèche

Rapport d'essai n°. : ULI21-000100-1
Projet : *ANALYSES SUR LIMONS*

WESSLING
Quality of Life

WESSLING France S.A.R.L.
Z.I. de Chesnes Tharabie · 40 rue du Ruisseau
BP 50705 · 38297 Saint-Quentin-Fallavier
Tél. +33 (0)4 74 99 96 20 · Fax +33 (0)9 72 53 90 56
labo@wessling.fr · www.wessling.fr

Le 19.01.2021

N° d'échantillon		**21-001232-02**	**21-001232-03**	**21-001232-04**
Désignation d'échantillon	**Unité**	***201395***	***201396***	***201397***
		DAG	STA	Lim
o-Phosphate (P) - NF EN ISO 6878 - Réalisé par WESSLING Lyon (France)				
o-Phosphate (PO4)	mg/l E/L	0,15	<0,04	<0,04
Analyse physique				
Matières sèches - NF ISO 11465 - Réalisé par WESSLING Lyon (France)				
Matière sèche (A)	% mass MB	97,6	97,7	96,2
Lixiviation				
Lixiviation à l'eau - DIN 38414-4 (1984-10) - Réalisé par WESSLING Lyon (France)				
Sur lixiviat	MB	12/01/2021	12/01/2021	12/01/2021
Sur lixiviat filtré				
Anions dissous (filtration à 0,2 µm) - Méthode interne : ANIONS - IC - Réalisé par WESSLING Lyon (France)				
Nitrates (NO3) (A)	mg/l E/L	19	<10	<10
Nitrates (NO3-N)	mg/l E/L	4,3	<2,3	<2,3
Sulfates (SO4) (A)	mg/l E/L	16	<10	16
Fraction solubilisée				
Sulfates (SO4) - (calculé d'éluat à solide (1:10)) - Réalisé par WESSLING Lyon (France)				
Sulfates (SO4)	mg/kg MS	160	<100	160
ortho-Phosphates (o-PO4) - (calculé d'éluat à solide (1:10)) - Réalisé par WESSLING Lyon (France)				
o-Phosphate (PO4)	mg/kg MS	1,5	<0,4	<0,4
Anions dissous - (calculé d'éluat à solide (1:10)) - Réalisé par WESSLING Lyon (France)				
Nitrates (NO3)	mg/kg MS	190	<100	<100
Nitrates (NO3-N)	mg/kg MS	43	<23	<23

MB : Matières brutes
E/L : Eau/lixiviat
MS : Matières sèches

Informations sur les échantillons

Date de réception :	07.01.2021	07.01.2021	07.01.2021
Type d'échantillon :	*Sol*	*Sol*	*Sol*
Récipient :	2x250VB	2x250VB	2x250VB
Température à réception (C°) :	15	15	15
Début des analyses :	07.01.2021	07.01.2021	07.01.2021
Fin des analyses :	19.01.2021	19.01.2021	19.01.2021
Préleveur :	*CLIENT*	*CLIENT*	*CLIENT*

Appendix G XRD spectrums of unstabilized and stabilized mixtures (@Lafarge)

DUS (Unstabilized DAG earth)

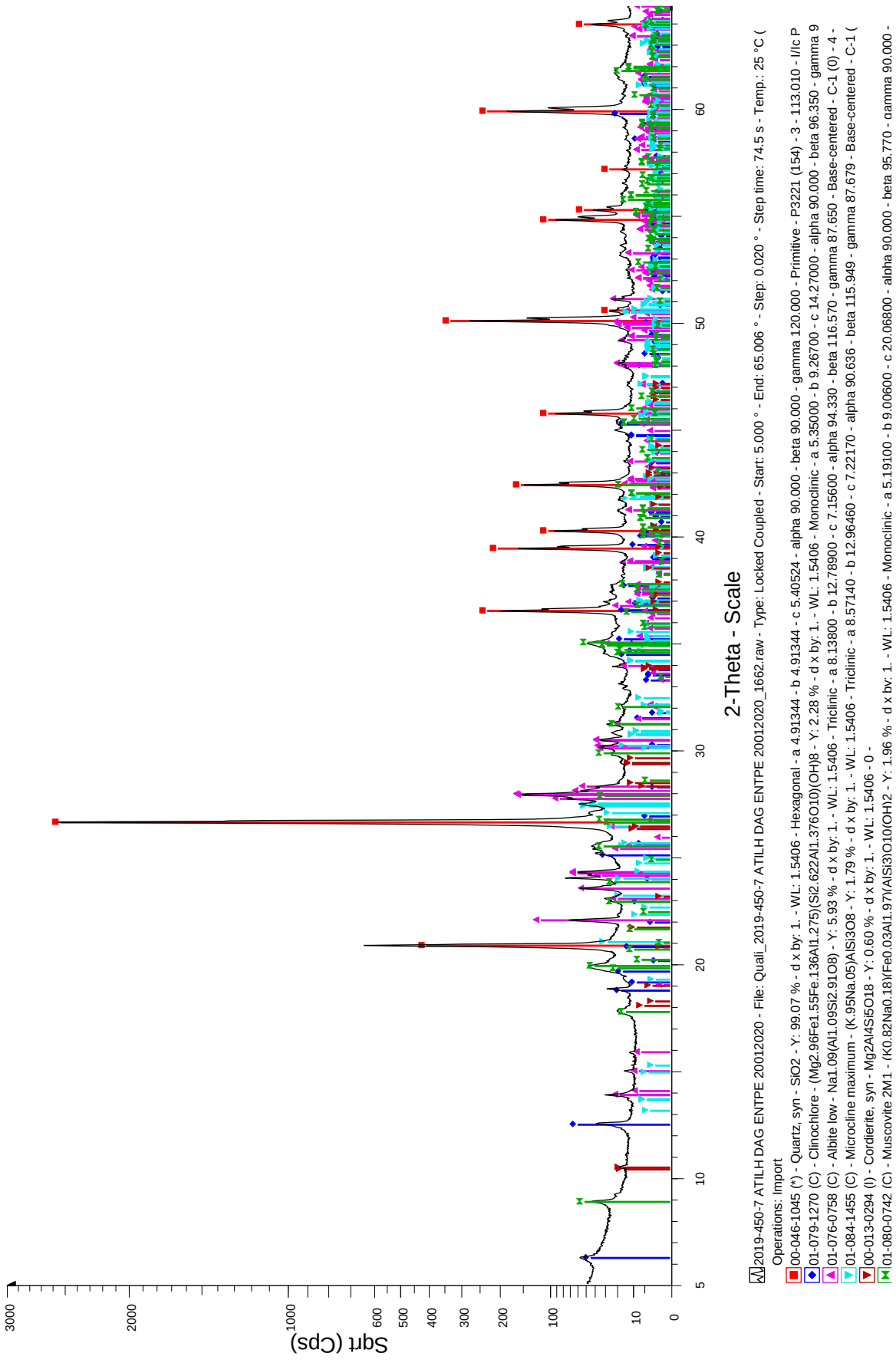

DB8 (Stabilized DAG earth with 8% of CEM II-B/LL 32.5R)

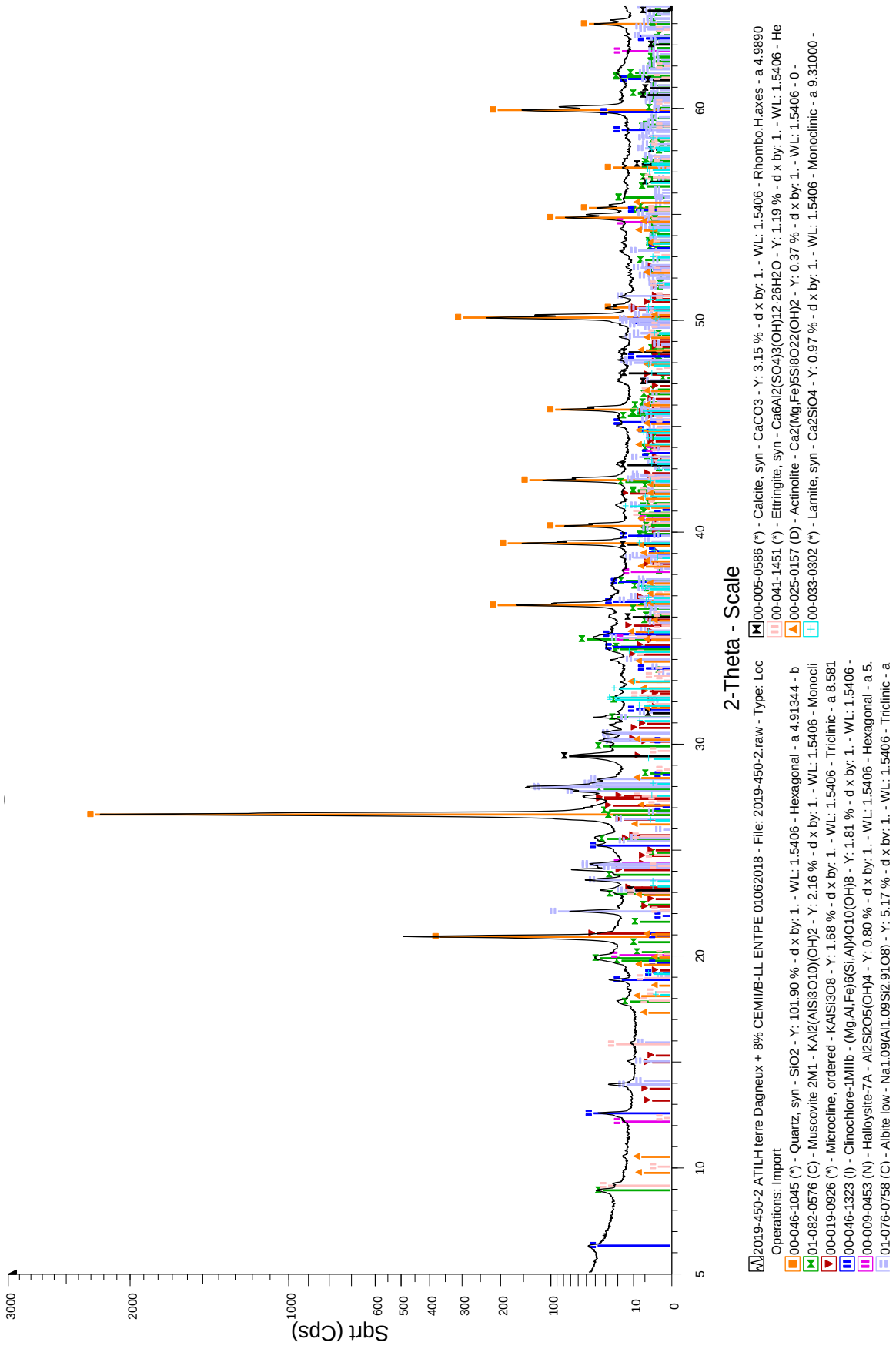

DM8 (Stabilized DAG earth with 8% of Masonry cement CM 12.5)

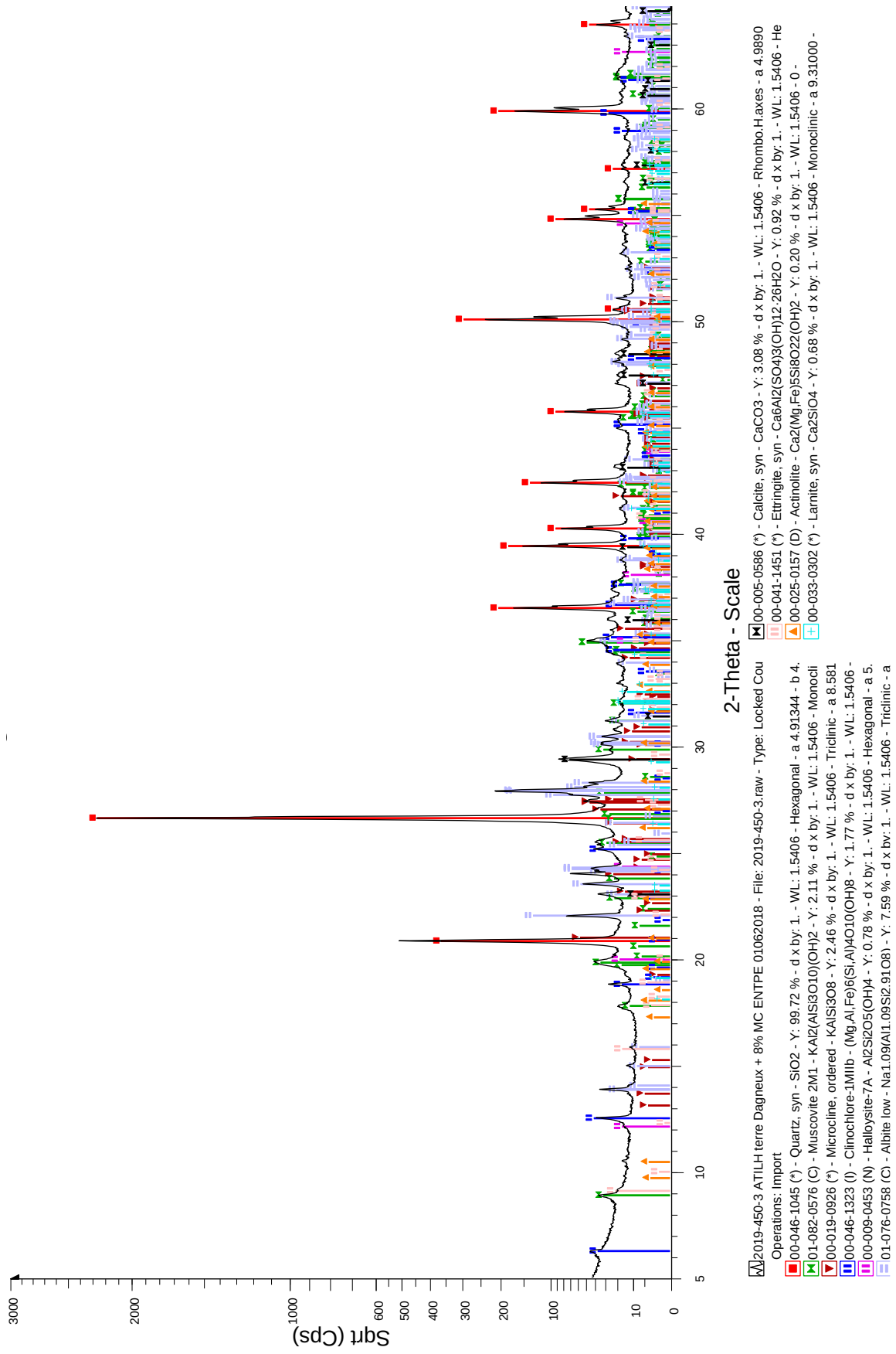

SUS (Unstabilized STA earth)

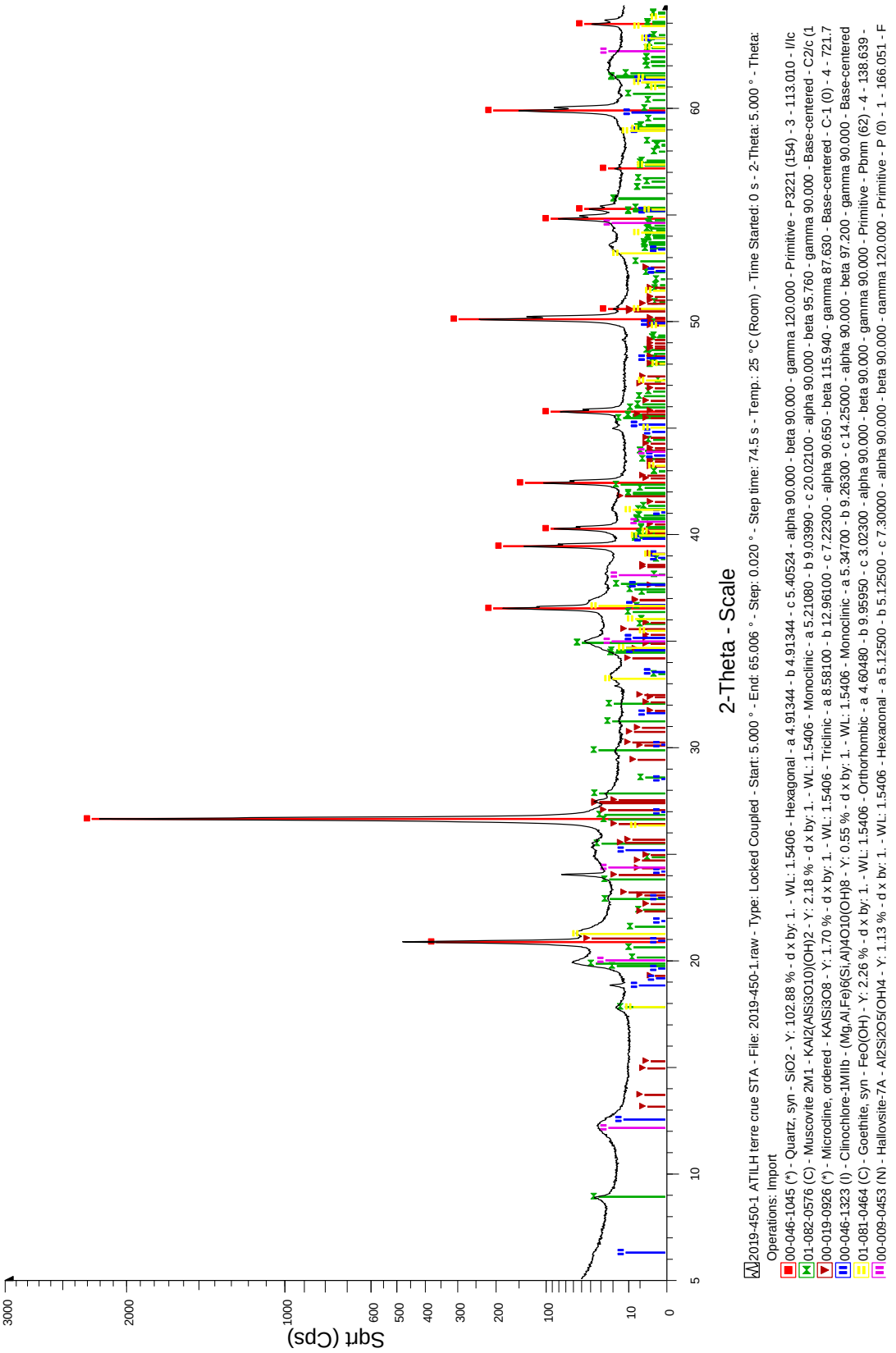

SB8 (Stabilized STA earth with 8% of CEM II-B/LL 32.5R)

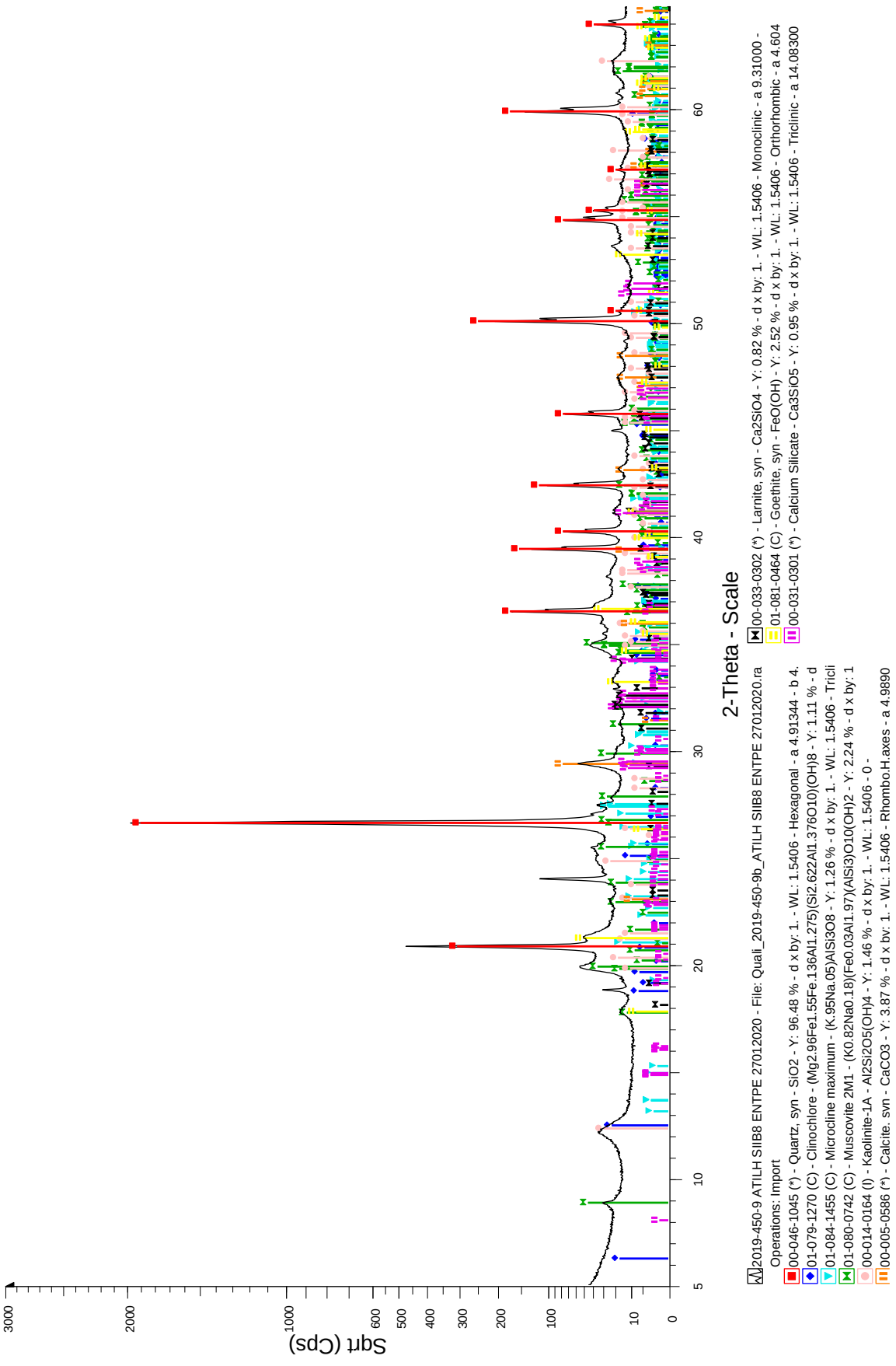

SM8 (Stabilized STA earth with 8% of Masonry cement CM 12.5)

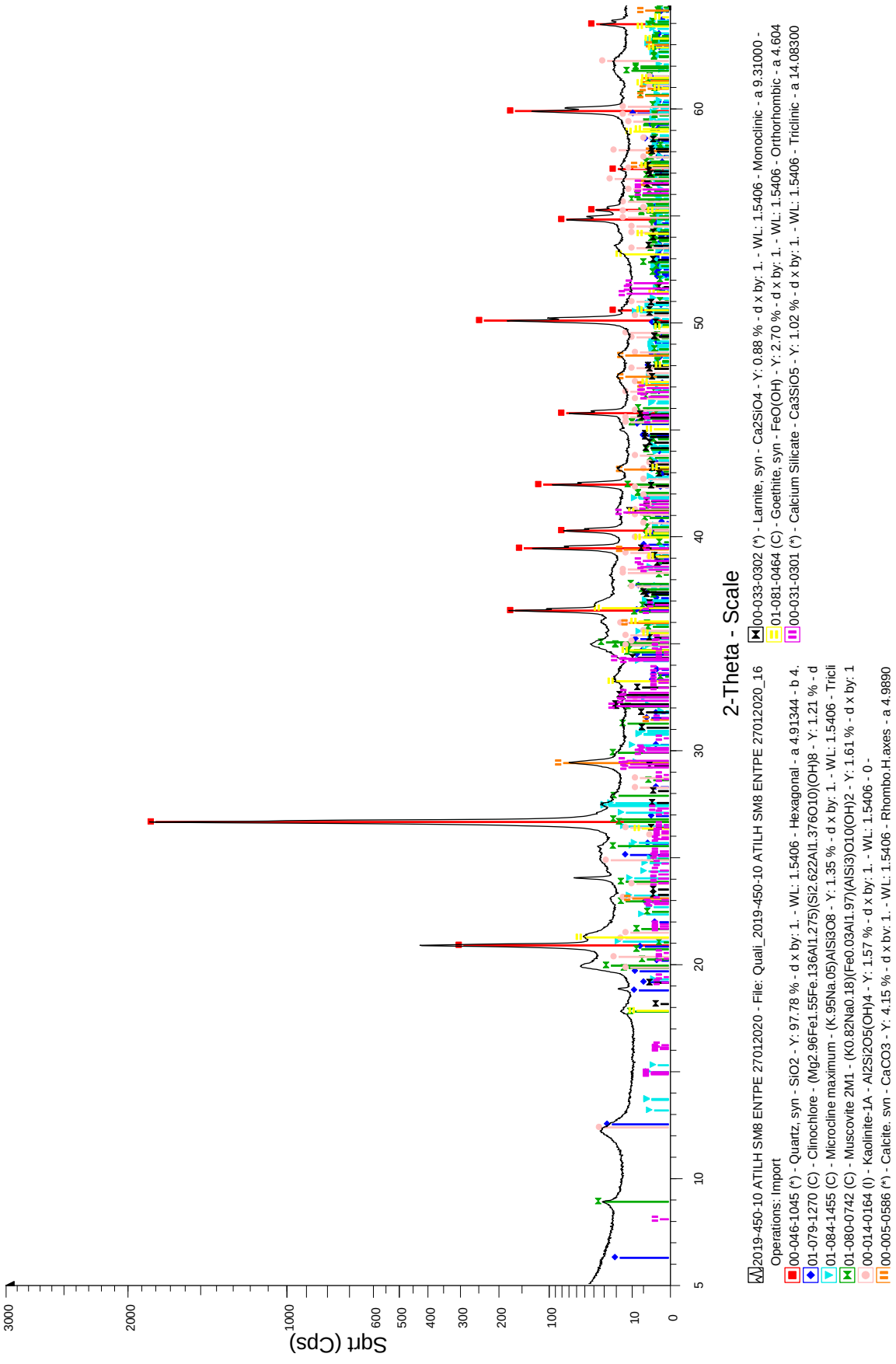

Appendix H XRD spectrums of unstabilized and stabilized mixtures (@ERM Poitier)

DUS (Unstabilized DAG earth) - on crushed powder

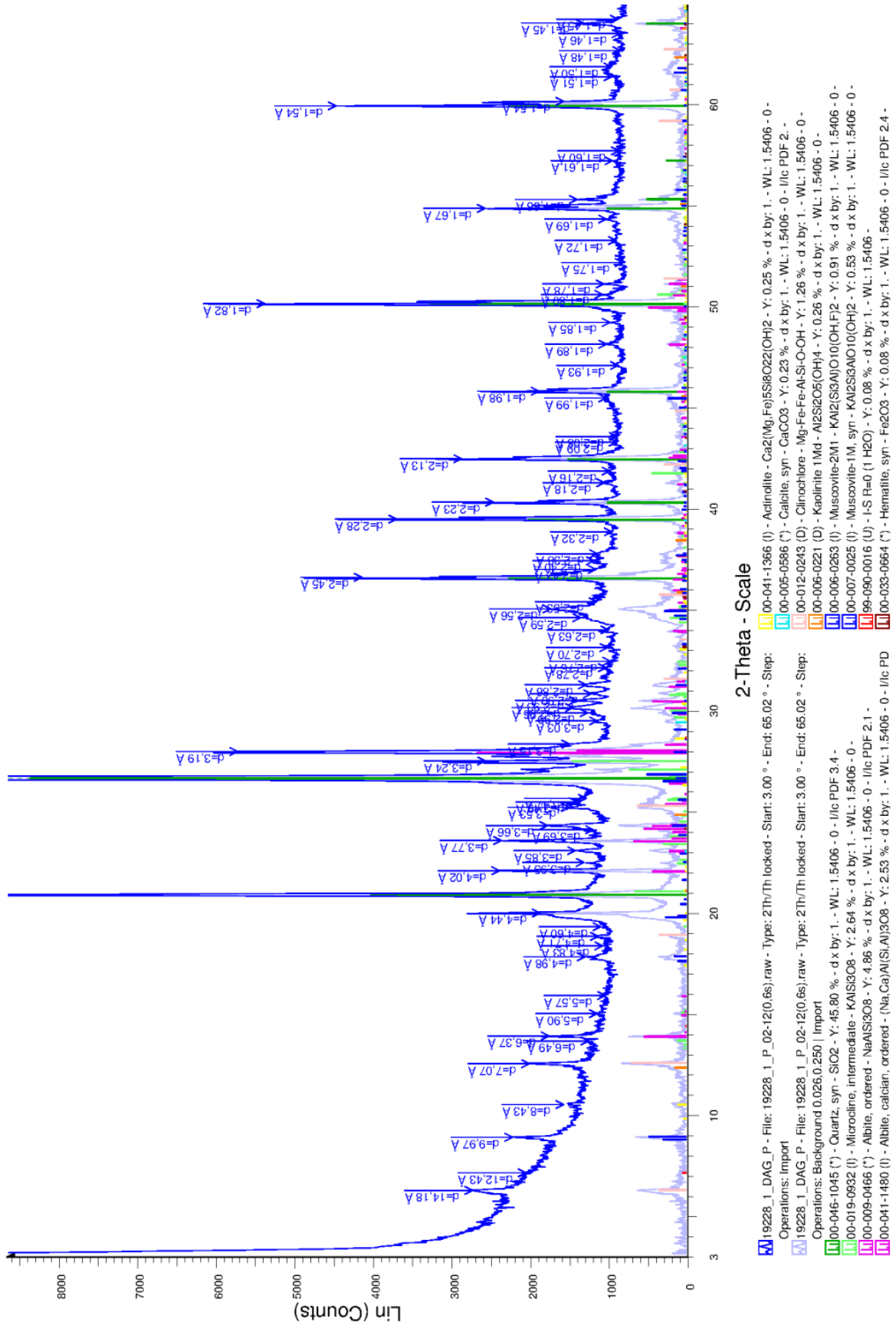

DUS (Unstabilized DAG earth) – on oriented aggregate

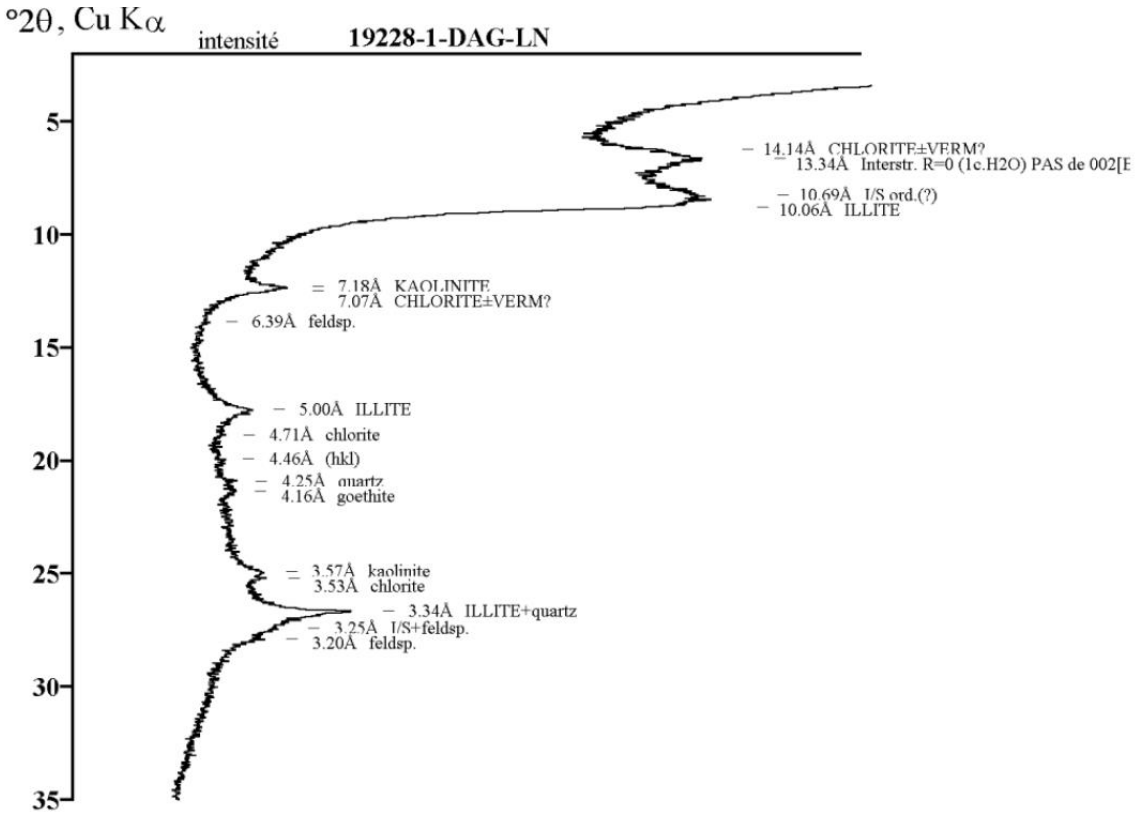

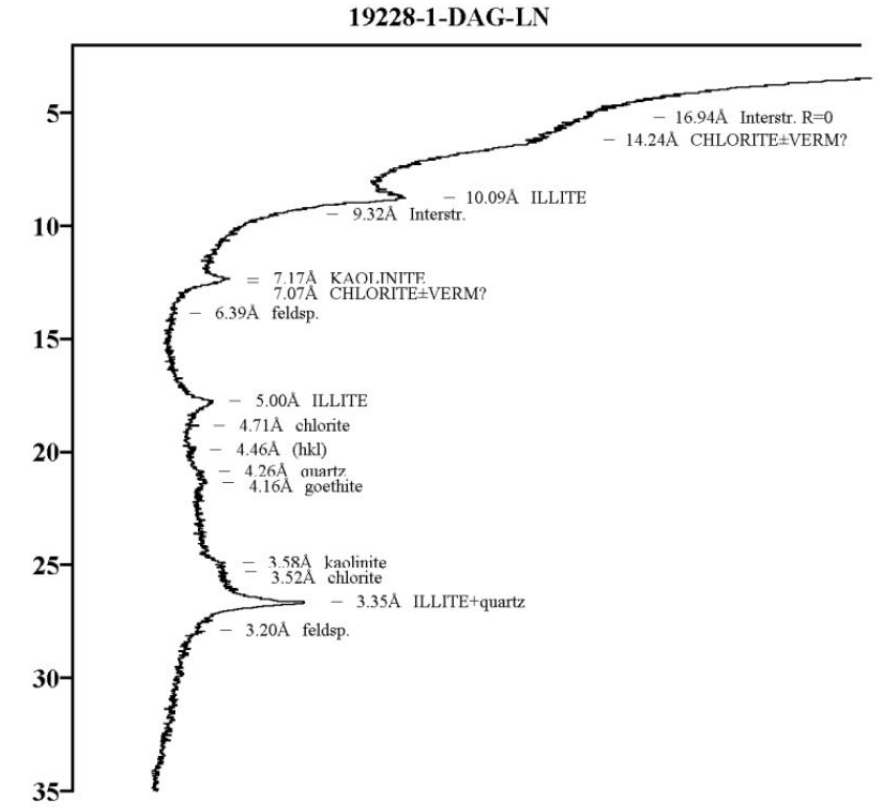

DB8 (Stabilized DAG earth with 8% of CEM II-B/LL 32.5R) - on crushed powder

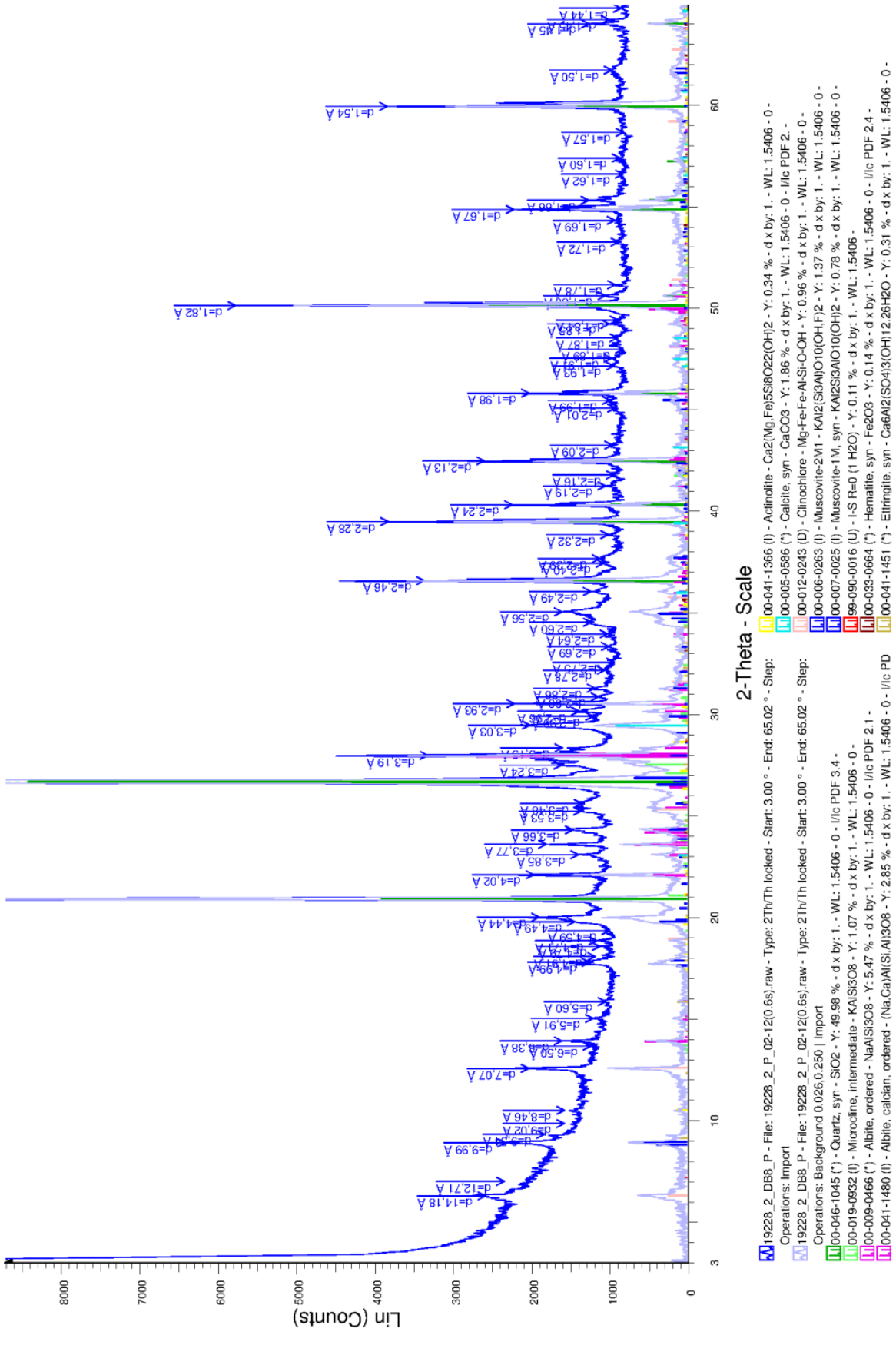

DB8 (Stabilized DAG earth with 8% of CEM II-B/LL 32.5R) – on oriented aggregate

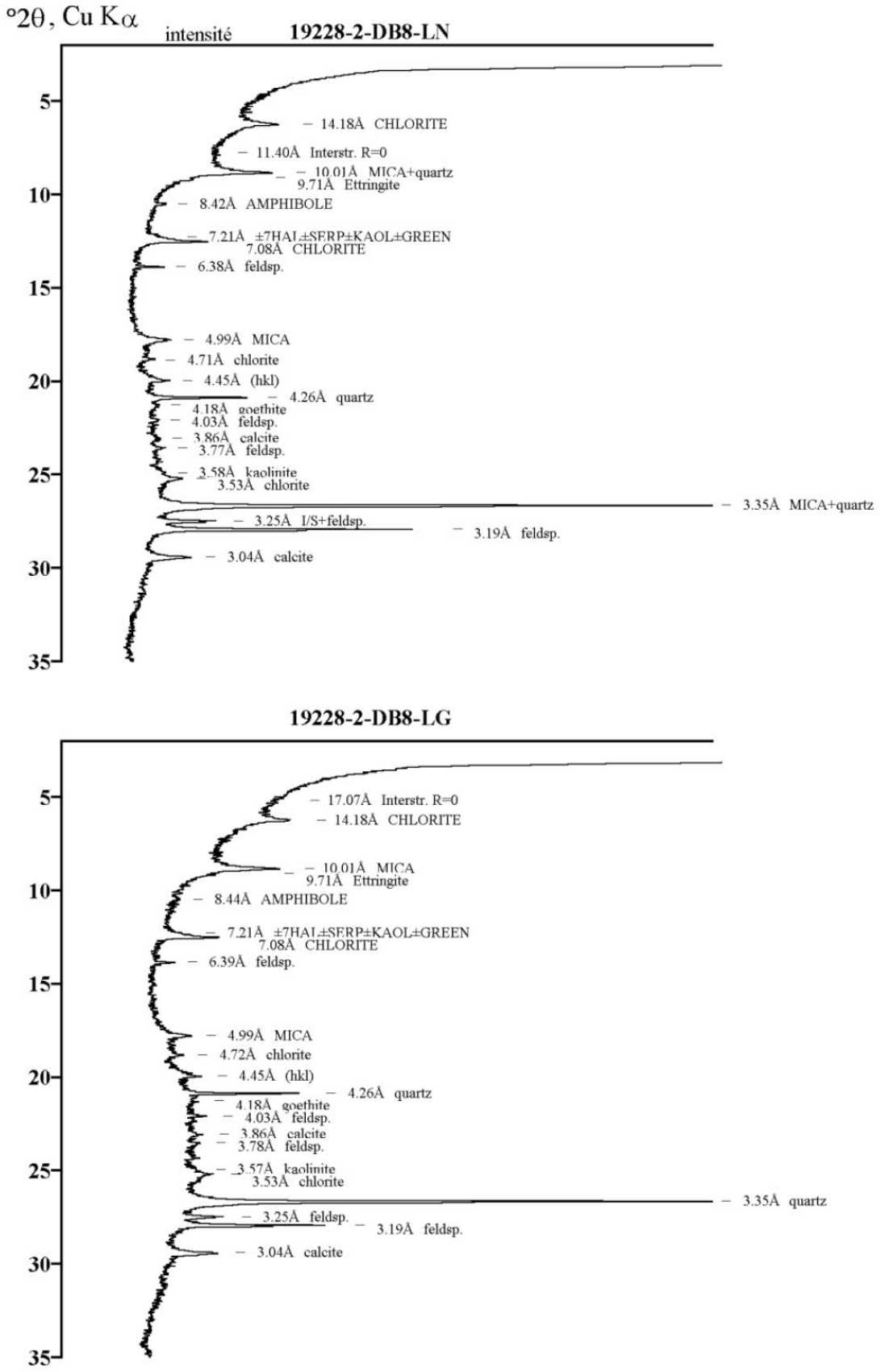

SUS (Unstabilized STA earth) - on crushed powder

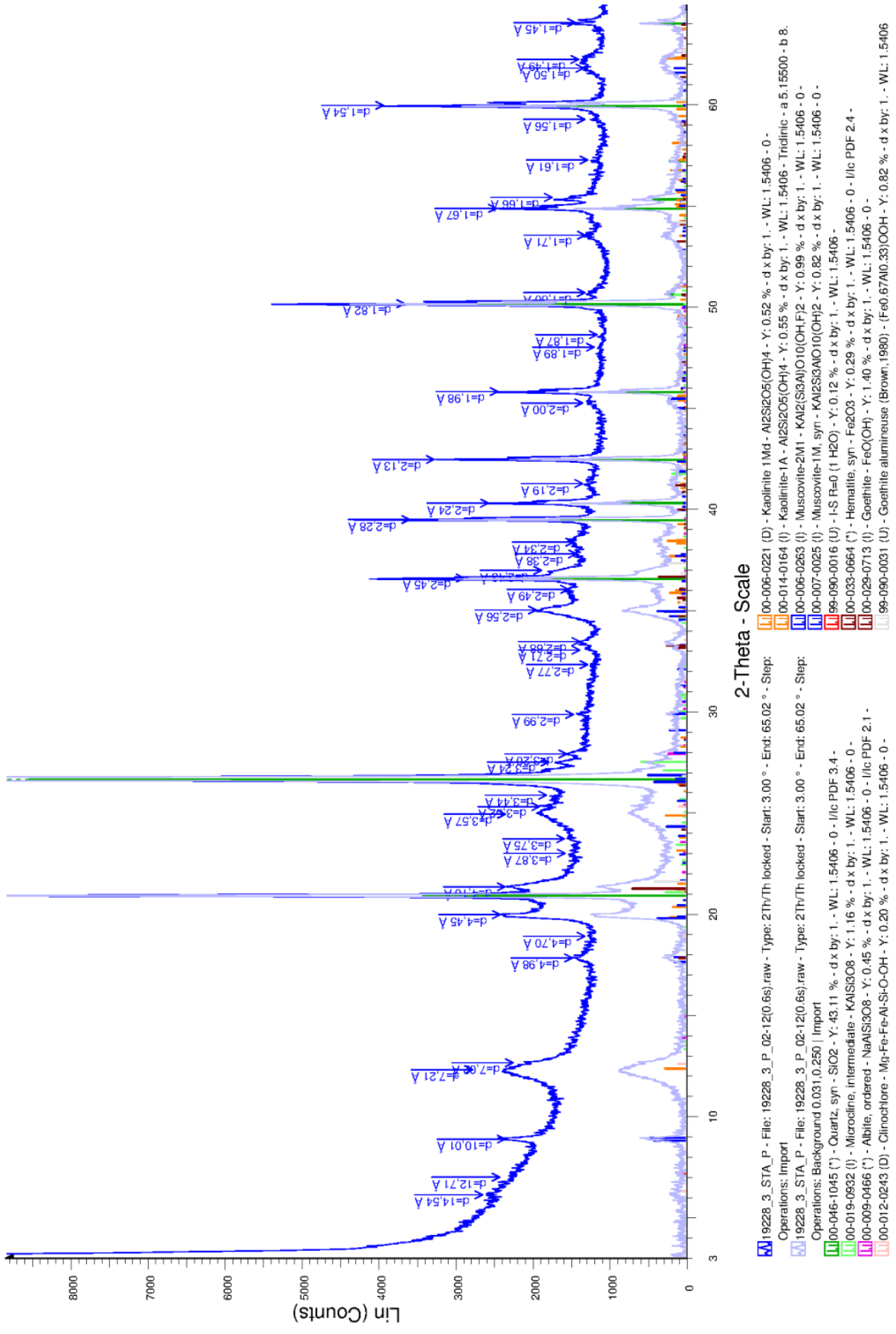

SUS (Unstabilized STA earth) – on oriented aggregate

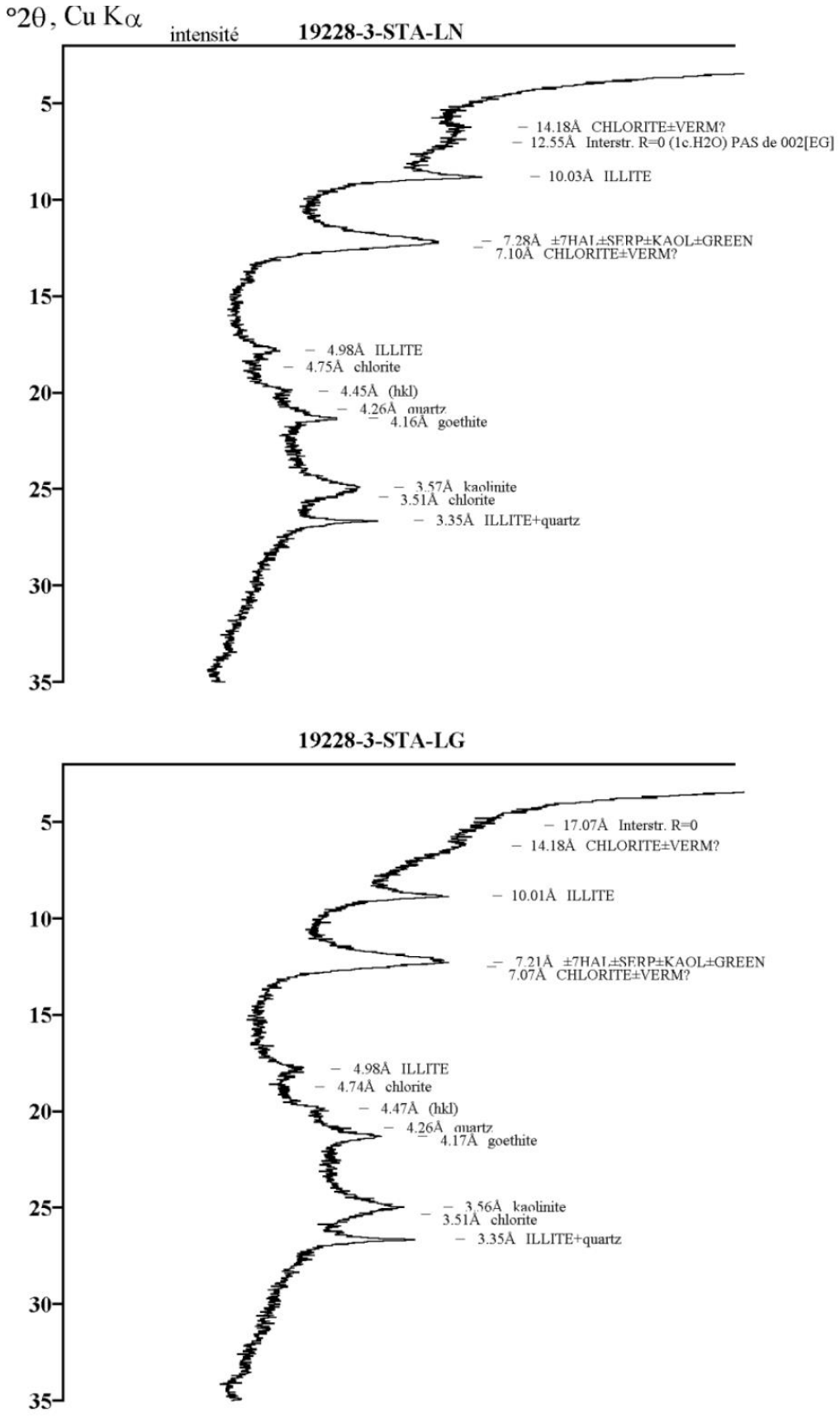

Appendix I DTA/TG/DTG curves of unstabilized and stabilized mixtures (@Technodes S.A.S Calcia)

DUS

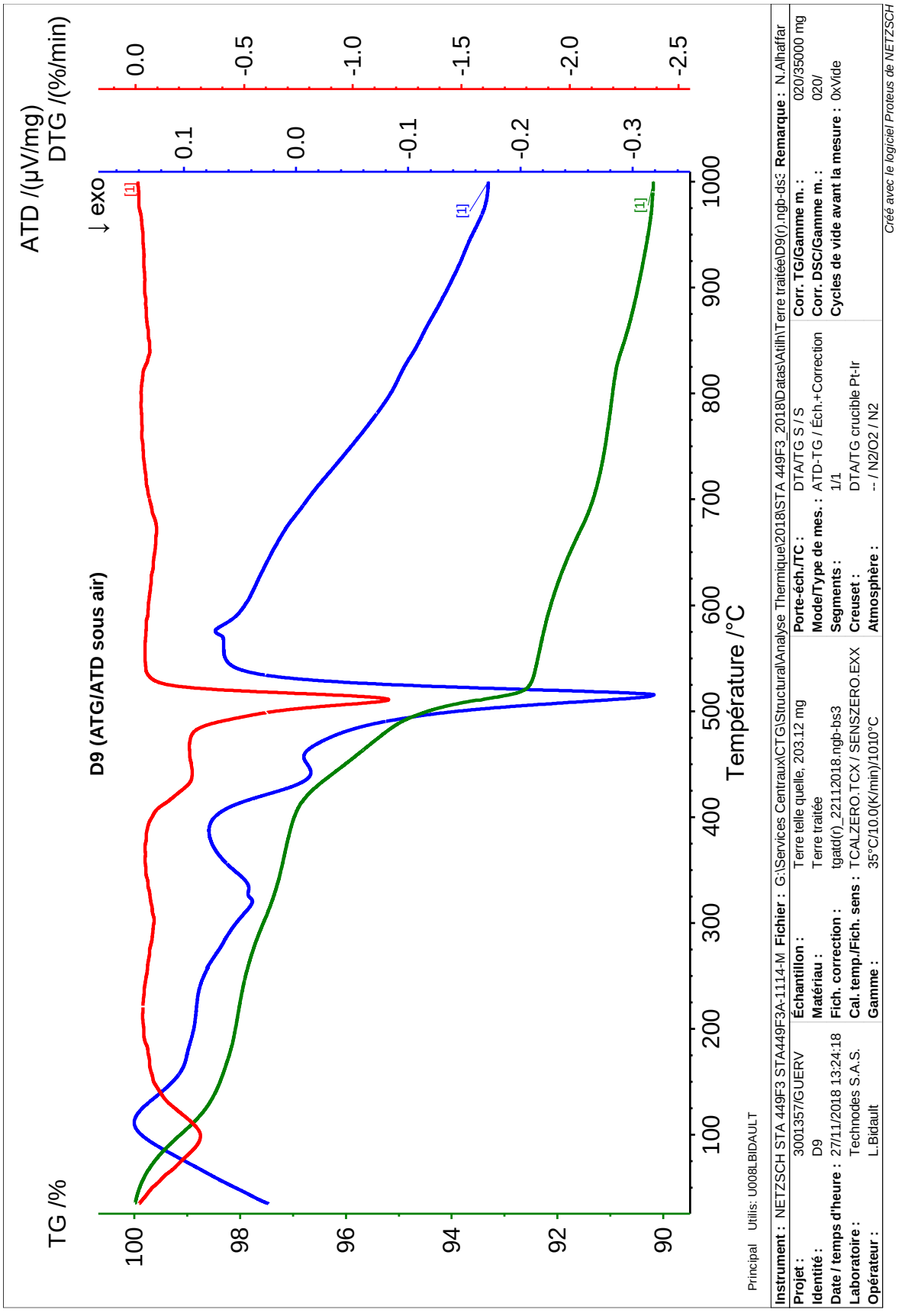
TG /%
ATD /(µV/mg)
DTG /(%/min)
↓ exo
D9 (ATG/ATD sous air)
Température /°C
Principal Utilis: U008LBIDAULT
Instrument : NETZSCH STA 449F3 STA449F3A-1114-M Fichier : G:\Services Centraux\CTG\StructuralAnalyse Thermique\2018\STA 449F3_2018\Datas\Atilh\Terre traitée\D9(r).ngb-ds
Remarque : N.Alhaffar
Projet : 3001357/GUERV
Identité : D9
Date / temps d'heure : 27/11/2018 13:24:18
Laboratoire : Technodes S.A.S.
Opérateur : L.Bidault
Échantillon : Terre telle quelle, 203.12 mg
Matériau : Terre traitée
Fich. correction : tgatd(r)_22112018.ngb-bs3
Cal. temp./Fich. sens : TCALZERO.TCX / SENSZERO.EXX
Gamme : 35°C/10.0(K/min)/1010°C
Porte-éch./TC : DTA/TG S / S
Mode/Type de mes. : ATD-TG / Éch.+Correction
Segments : 1/1
Creuset : DTA/TG crucible Pt-Ir
Atmosphère : -- / N2/O2 / N2
Corr. TG/Gamme m. : 020/35000 mg
Corr. DSC/Gamme m. : 020/
Cycles de vide avant la mesure : 0xVide
Créé avec le logiciel Proteus de NETZSCH

DUS vs DA8

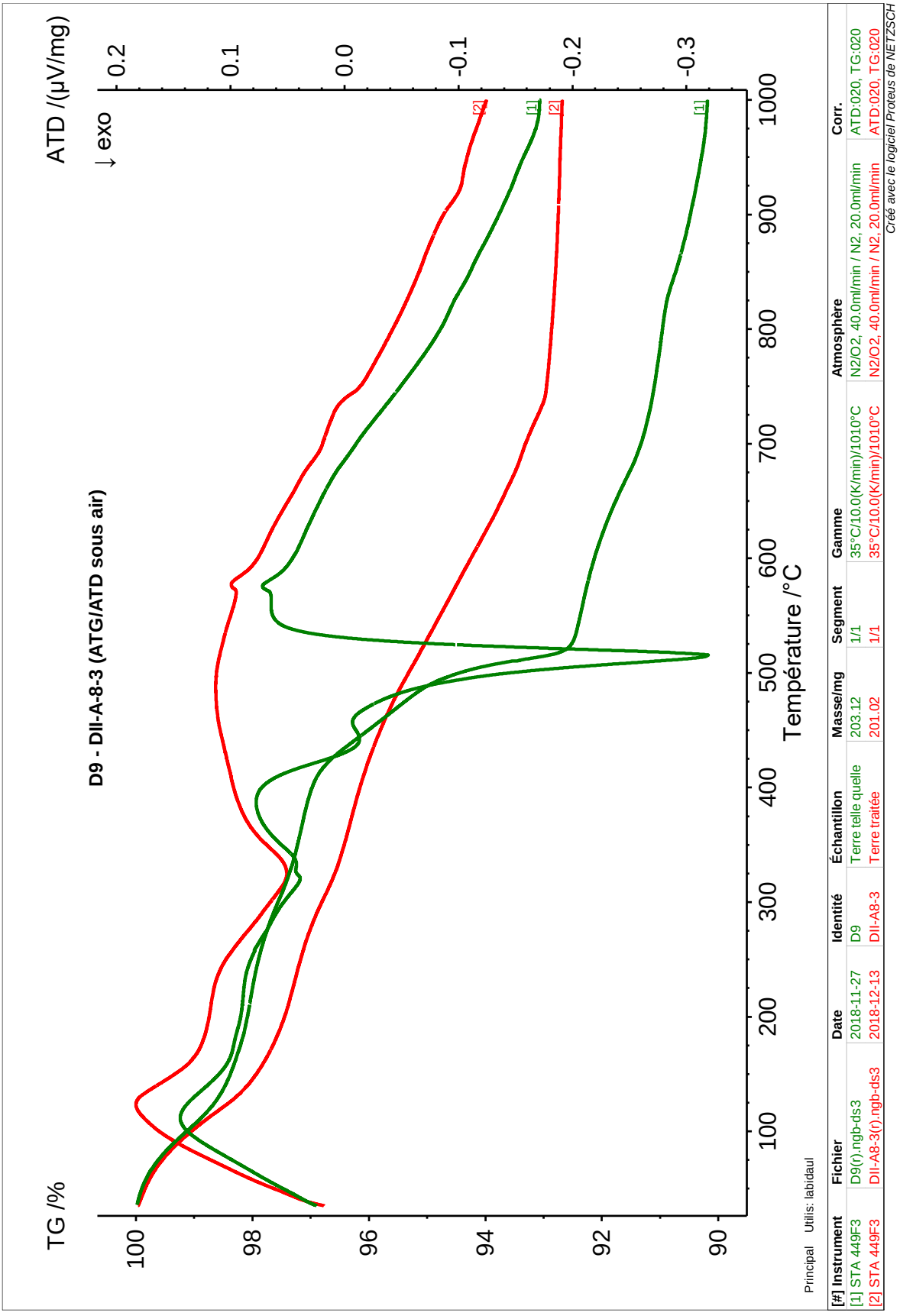

[#]	Instrument	Fichier	Date	Identité	Échantillon	Masse/mg	Segment	Gamme	Atmosphère	Corr.
[1]	STA 449F3	D9(r).ngb-ds3	2018-11-27	D9	Terre telle quelle	203.12	1/1	35°C/10.0(K/min)/1010°C	N2/O2, 40.0ml/min / N2, 20.0ml/min	ATD:020, TG:020
[2]	STA 449F3	DII-A8-3(r).ngb-ds3	2018-12-13	DII-A8-3	Terre traitée	201.02	1/1	35°C/10.0(K/min)/1010°C	N2/O2, 40.0ml/min / N2, 20.0ml/min	ATD:020, TG:020

DUS vs DB8

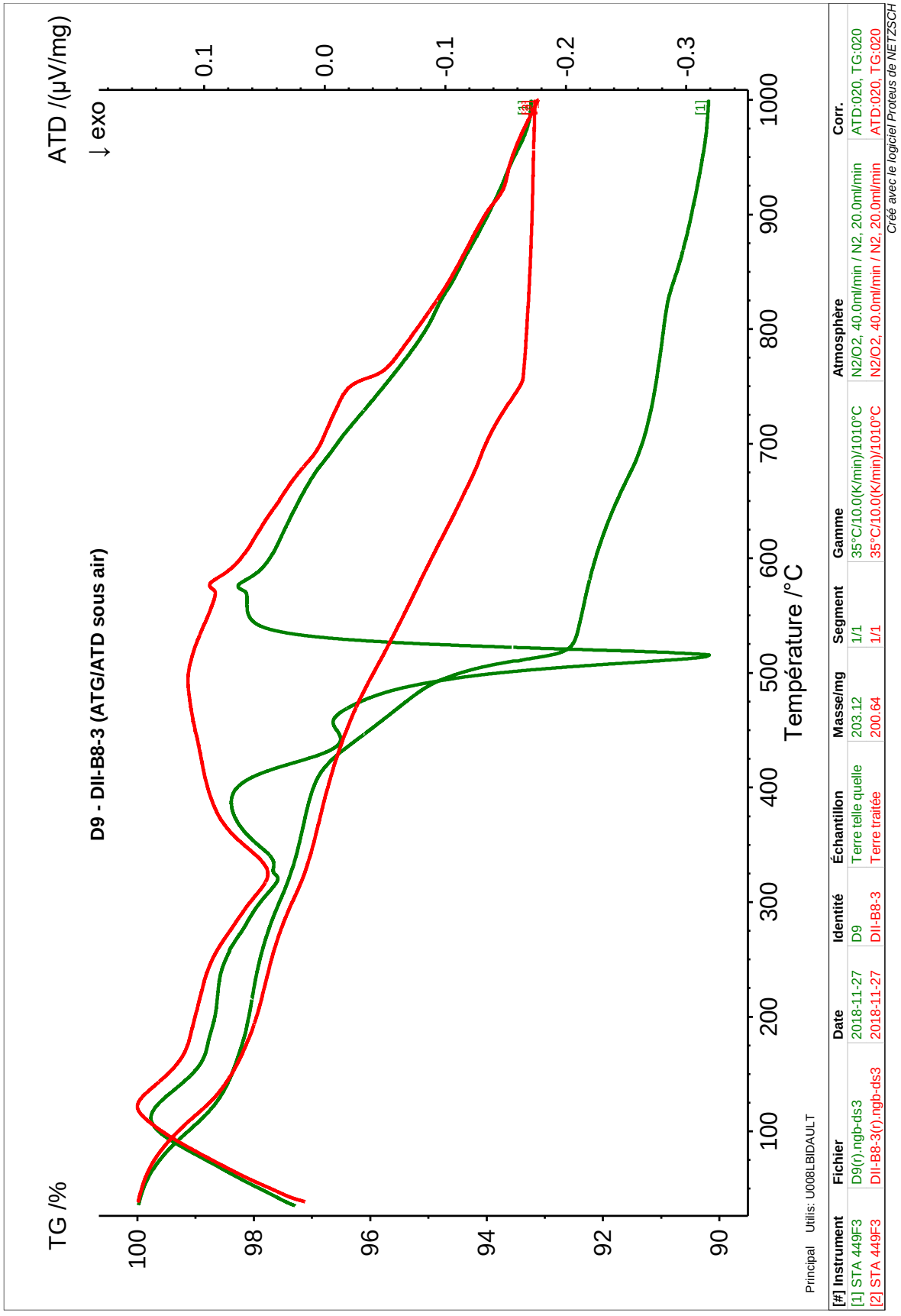

[#]	Instrument	Fichier	Date	Identité	Échantillon	Masse/mg	Segment	Gamme	Atmosphère	Corr.
[1]	STA 449F3	D9(r).ngb-ds3	2018-11-27	D9	Terre telle quelle	203.12	1/1	35°C/10.0(K/min)/1010°C	N2/O2, 40.0ml/min / N2, 20.0ml/min	ATD:020, TG:020
[2]	STA 449F3	DII-B8-3(r).ngb-ds3	2018-11-27	DII-B8-3	Terre traitée	200.64	1/1	35°C/10.0(K/min)/1010°C	N2/O2, 40.0ml/min / N2, 20.0ml/min	ATD:020, TG:020

DUS vs DV8

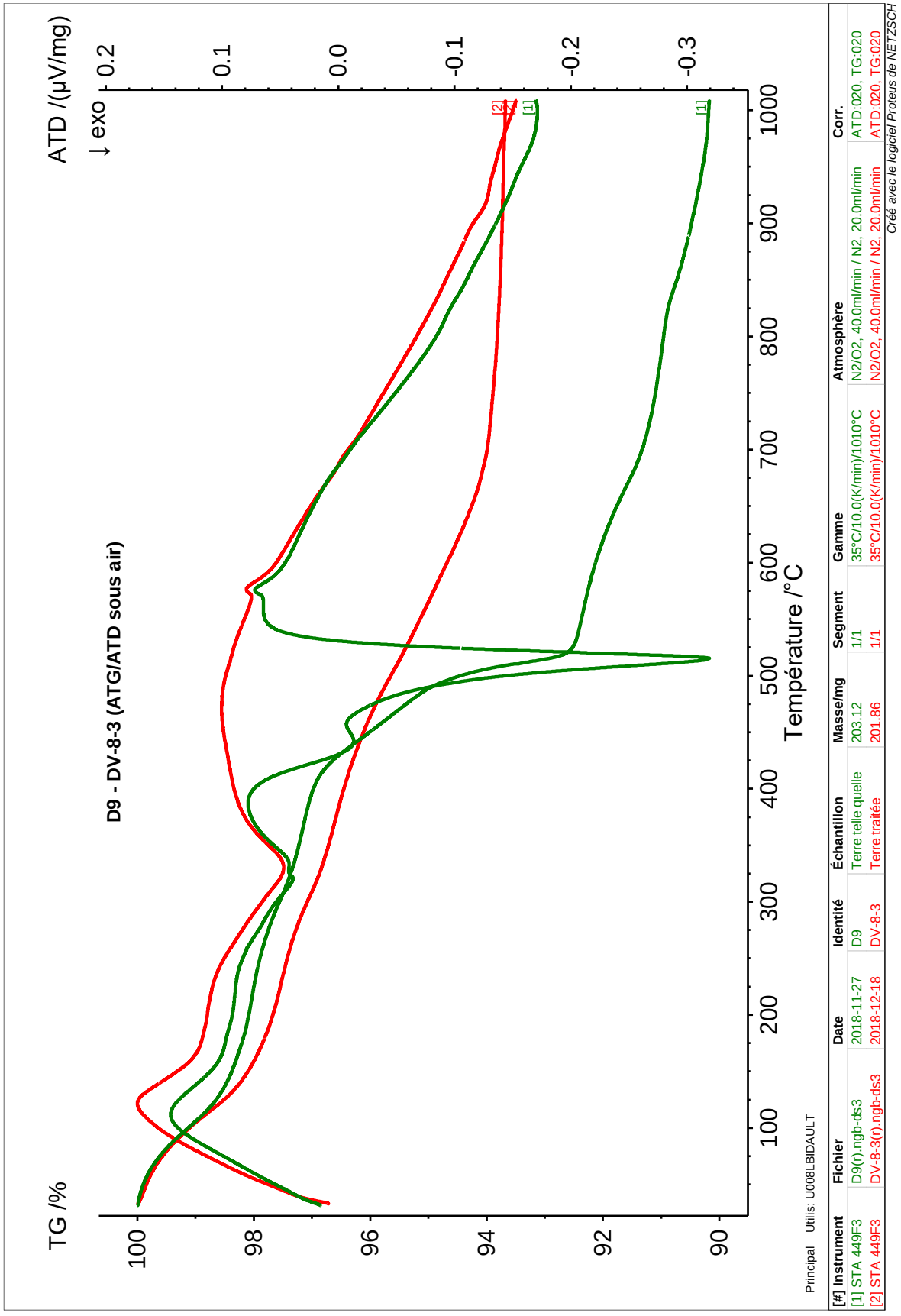
D9 - DV-8-3 (ATG/ATD sous air)
TG /%
ATD /(µV/mg)
↓ exo
Température /°C
100
98
96
94
92
90
0.2
0.1
0.0
-0.1
-0.2
-0.3
100
200
300
400
500
600
700
800
900
1000
[1]
[2]
Principal Utilis: U008LBIDAULT
[#] Instrument | Fichier | Date | Identité | Échantillon | Masse/mg | Segment | Gamme | Atmosphère | Corr.
[1] STA 449F3 | D9(r).ngb-ds3 | 2018-11-27 | D9 | Terre telle quelle | 203.12 | 1/1 | 35°C/10.0(K/min)/1010°C | N2/O2, 40.0ml/min / N2, 20.0ml/min | ATD:020, TG:020
[2] STA 449F3 | DV-8-3(r).ngb-ds3 | 2018-12-18 | DV-8-3 | Terre traitée | 201.86 | 1/1 | 35°C/10.0(K/min)/1010°C | N2/O2, 40.0ml/min / N2, 20.0ml/min | ATD:020, TG:020
Créé avec le logiciel Proteus de NETZSCH

DUS vs DM8

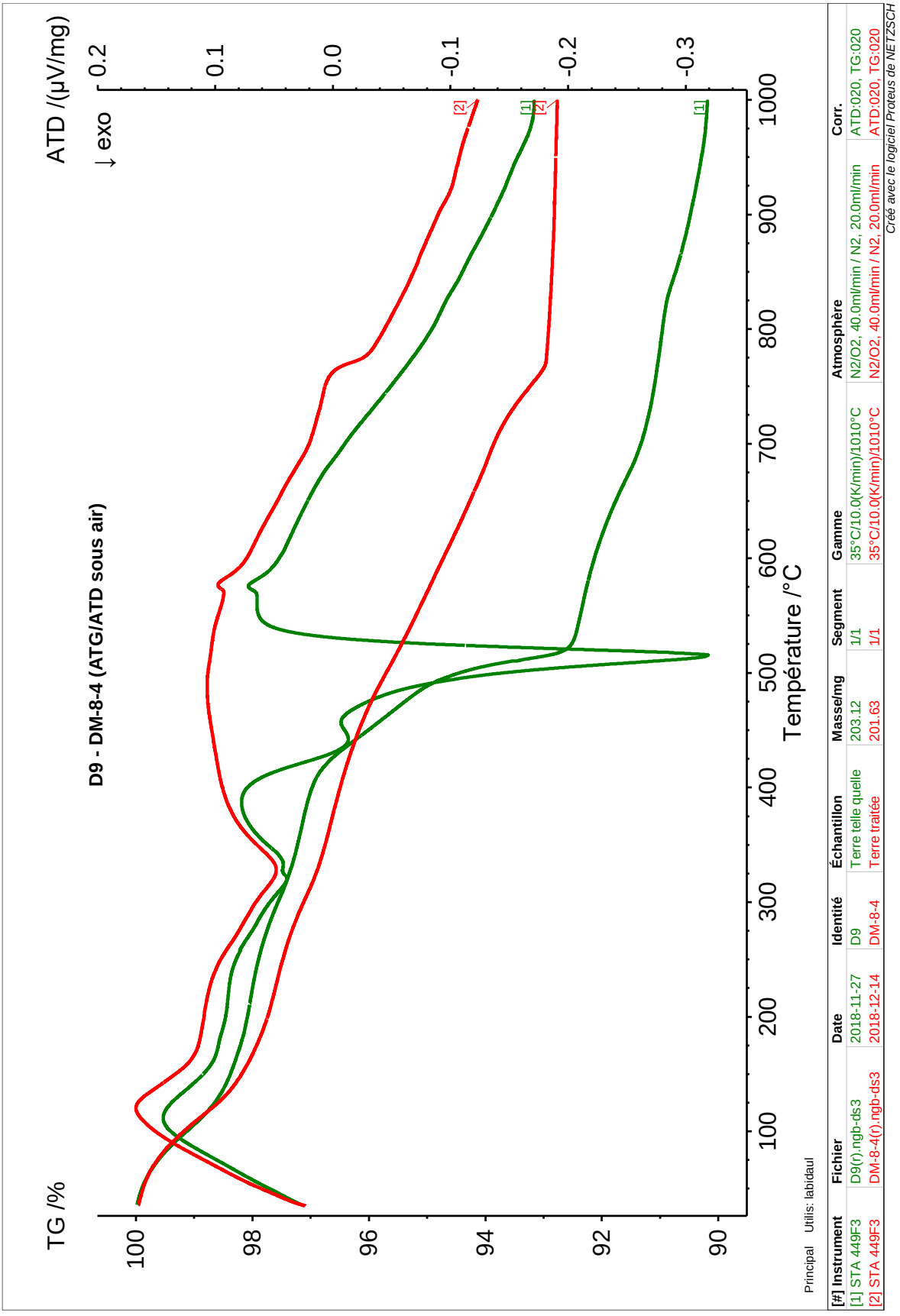
D9 - DM-8-4 (ATG/ATD sous air)
TG /%
ATD /(µV/mg)
↓ exo
Température /°C
100
98
96
94
92
90
0.2
0.1
0.0
-0.1
-0.2
-0.3
100
200
300
400
500
600
700
800
900
1000
[1]
[2]
Principal Utilis: labidaul
[#] Instrument Fichier Date Identité Échantillon Masse/mg Segment Gamme Atmosphère Corr.
[1] STA 449F3 D9(r).ngb-ds3 2018-11-27 D9 Terre telle quelle 203.12 1/1 35°C/10.0(K/min)/1010°C N2/O2, 40.0ml/min / N2, 20.0ml/min ATD:020, TG:020
[2] STA 449F3 DM-8-4(r).ngb-ds3 2018-12-14 DM-8-4 Terre traitée 201.63 1/1 35°C/10.0(K/min)/1010°C N2/O2, 40.0ml/min / N2, 20.0ml/min ATD:020, TG:020
Créé avec le logiciel Proteus de NETZSCH

DUS vs DP8

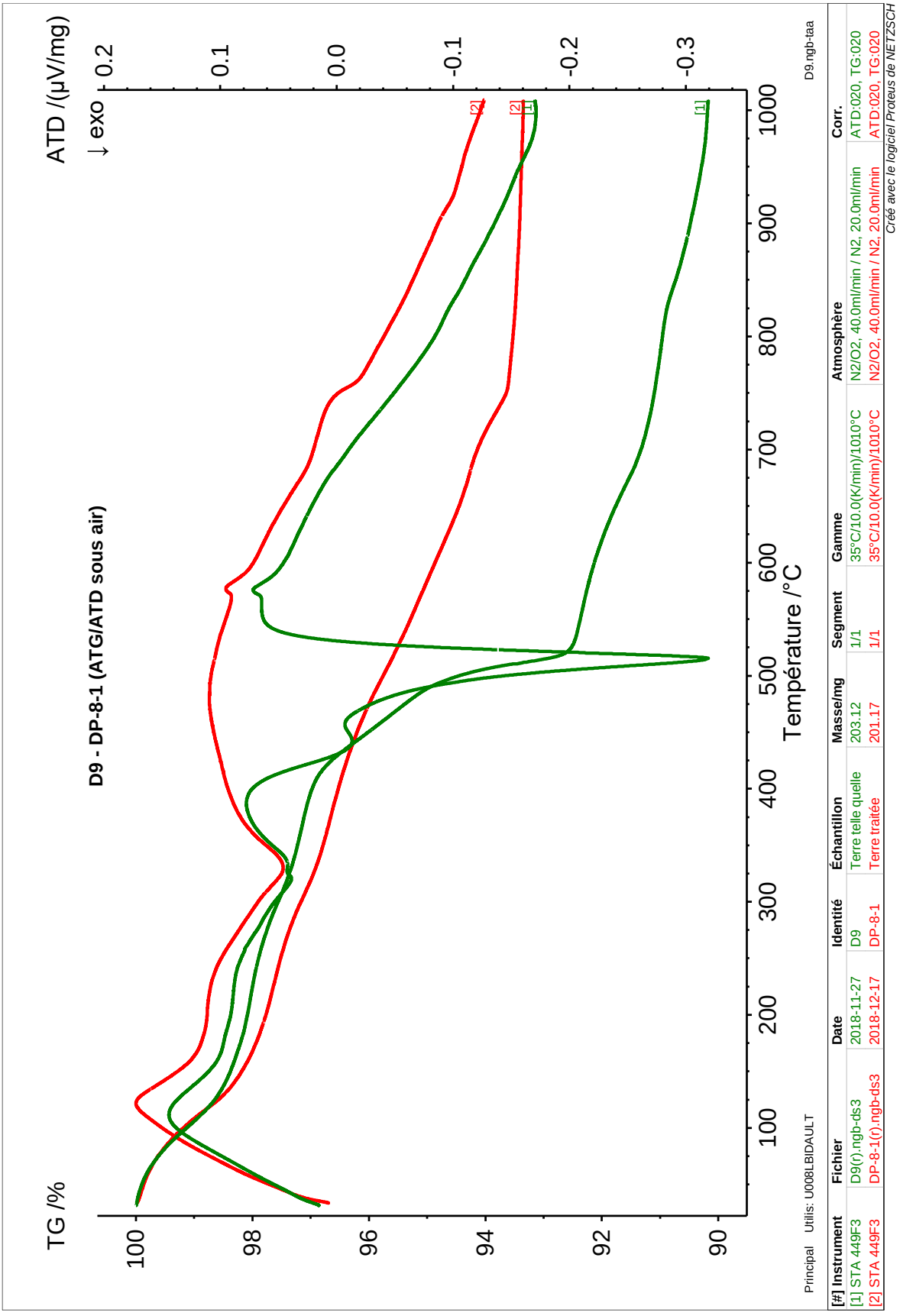

[#] Instrument	Fichier	Date	Identité	Échantillon	Masse/mg	Segment	Gamme	Atmosphère	Corr.
[1] STA 449F3	D9(r).ngb-ds3	2018-11-27	D9	Terre telle quelle	203.12	1/1	35°C/10.0(K/min)/1010°C	N2/O2, 40.0ml/min / N2, 20.0ml/min	ATD:020, TG:020
[2] STA 449F3	DP-8-1(r).ngb-ds3	2018-12-17	DP-8-1	Terre traitée	201.17	1/1	35°C/10.0(K/min)/1010°C	N2/O2, 40.0ml/min / N2, 20.0ml/min	ATD:020, TG:020

SUS

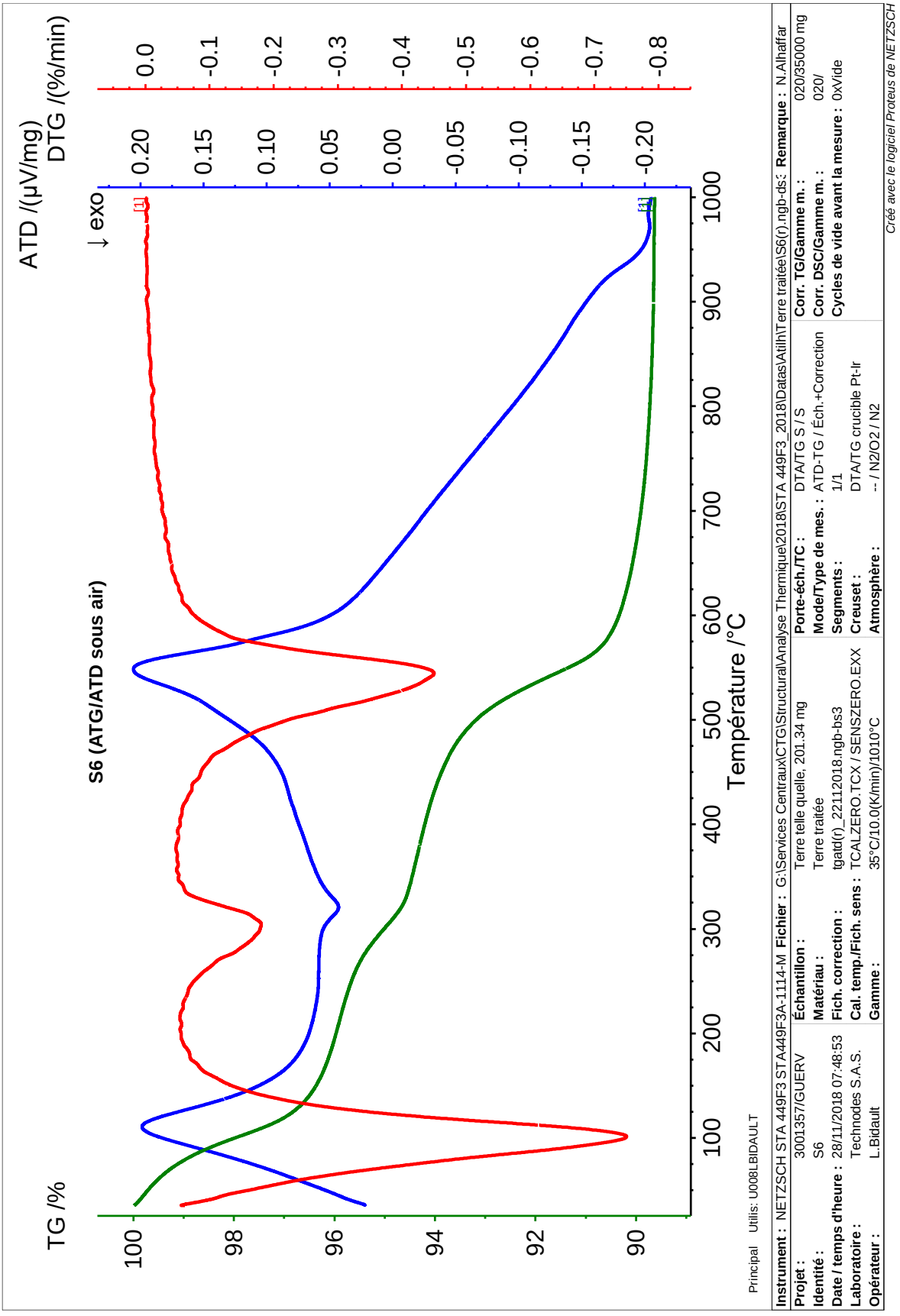
S6 (ATG/ATD sous air)
TG /%
ATD /(µV/mg)
DTG /(%/min)
↓ exo
Température /°C
Principal Utilis: U008LBIDAULT
Instrument : NETZSCH STA 449F3 STA449F3A-1114-M Fichier : G:\Services Centraux\CTG\Structural\Analyse Thermique\2018\STA 449F3_2018\Datas\Atilh\Terre traitée\S6(r).ngb-ds3 Remarque : N.Alhaffar
Projet : 3001357/GUERV
Identité : S6
Date / temps d'heure : 28/11/2018 07:48:53
Laboratoire : Technodes S.A.S.
Opérateur : L.Bidault
Échantillon : Terre telle quelle, 201.34 mg
Matériau : Terre traitée
Fich. correction : tgatd(r)_22112018.ngb-bs3
Cal. temp./Fich. sens : TCALZERO.TCX / SENSZERO.EXX
Gamme : 35°C/10.0(K/min)/1010°C
Porte-éch./TC : DTA/TG S / S
Mode/Type de mes. : ATD-TG / Éch.+Correction
Segments : 1/1
Creuset : DTA/TG crucible Pt-Ir
Atmosphère : -- / N2/O2 / N2
Corr. TG/Gamme m. : 020/35000 mg
Corr. DSC/Gamme m. : 020/
Cycles de vide avant la mesure : 0xVide
Créé avec le logiciel Proteus de NETZSCH

SUS vs SA8

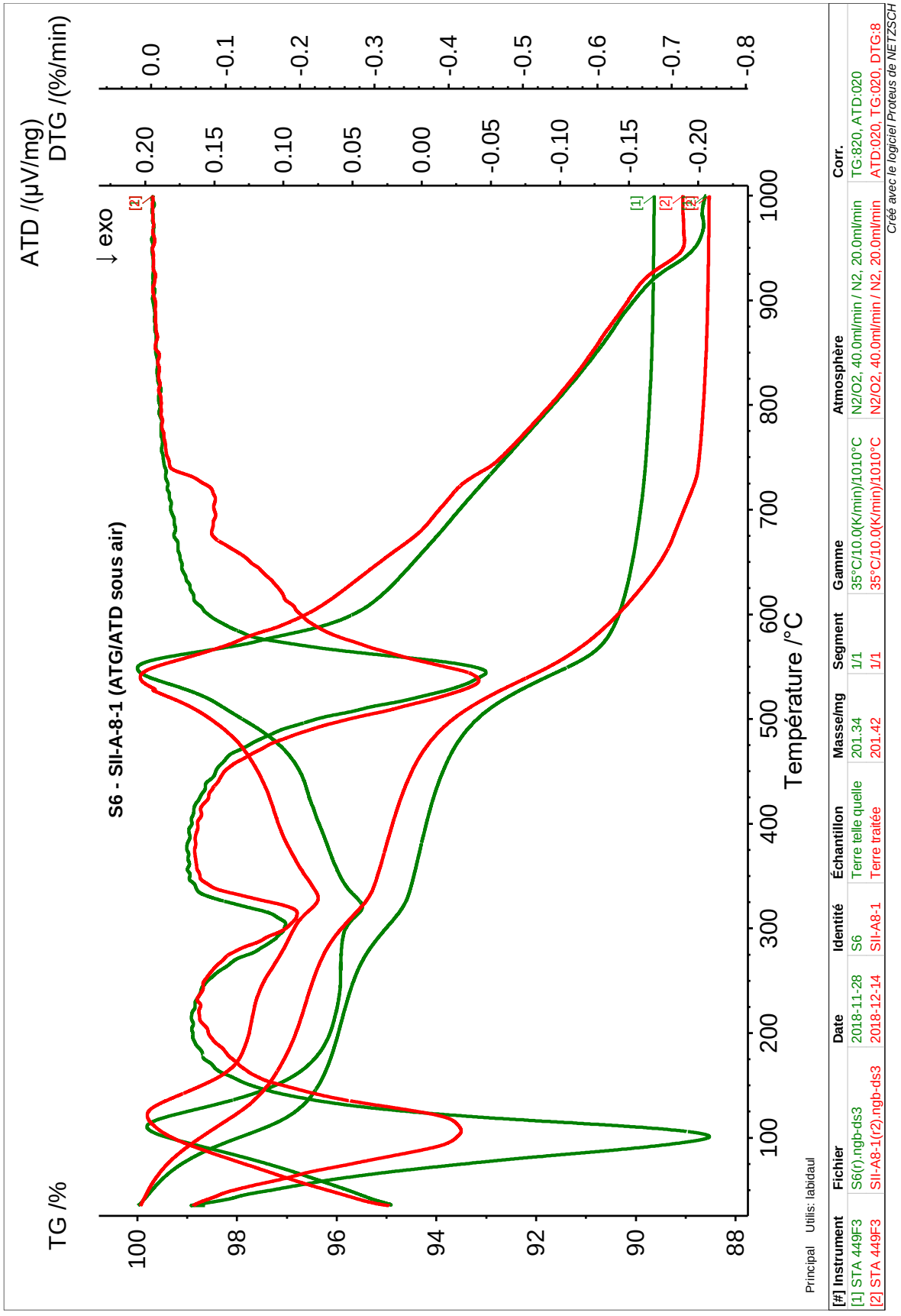

[#]	Instrument	Fichier	Date	Identité	Échantillon	Masse/mg	Segment	Gamme	Atmosphère	Corr.
[1]	STA 449F3	S6(r).ngb-ds3	2018-11-28	S6	Terre telle quelle	201.34	1/1	35°C/10.0(K/min)/1010°C	N2/O2, 40.0ml/min / N2, 20.0ml/min	TG:820, ATD:020
[2]	STA 449F3	SII-A8-1(r2).ngb-ds3	2018-12-14	SII-A8-1	Terre traitée	201.42	1/1	35°C/10.0(K/min)/1010°C	N2/O2, 40.0ml/min / N2, 20.0ml/min	ATD:020, TG:020, DTG:8

SUS vs SB8

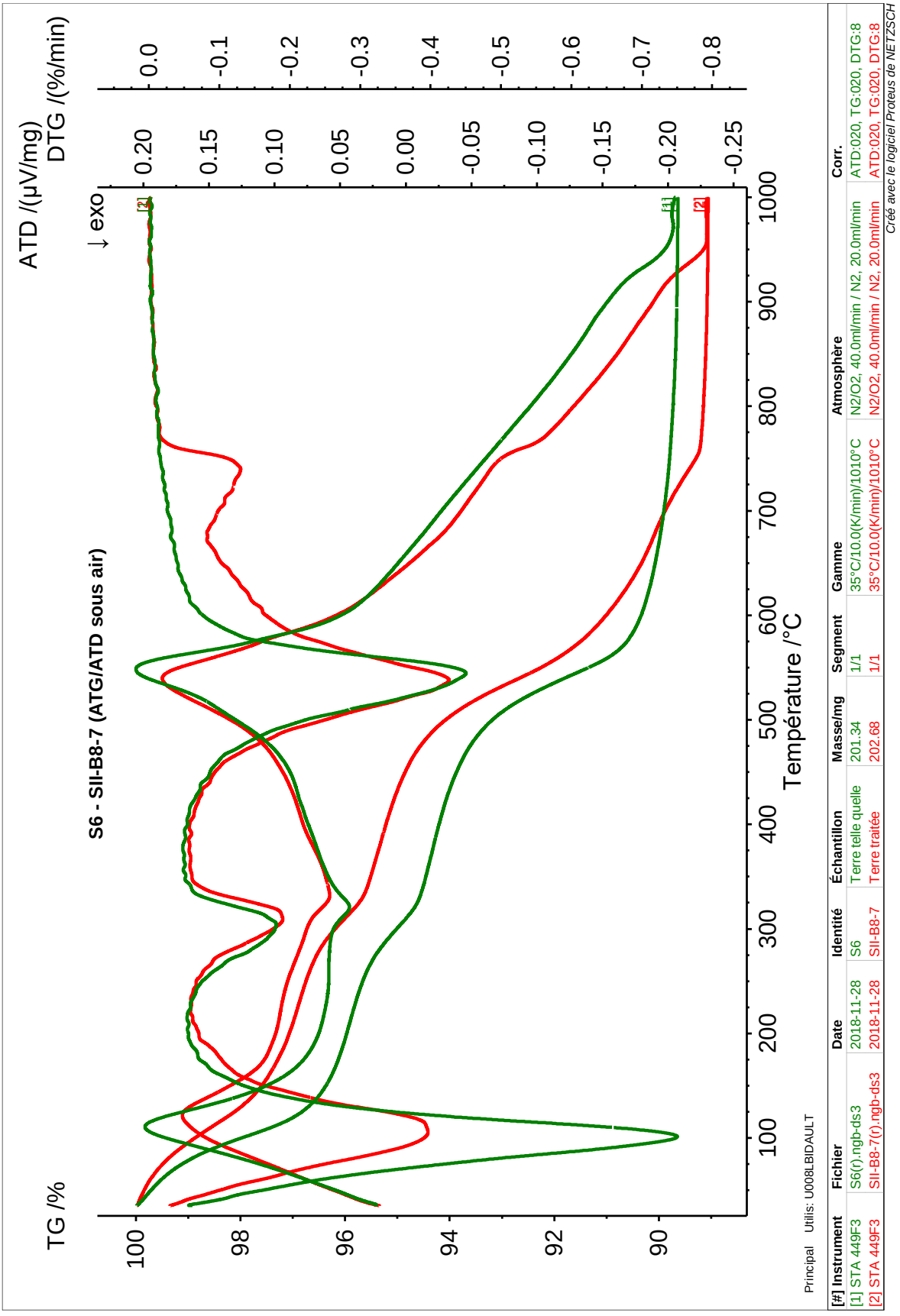

[#]	Instrument	Fichier	Date	Identité	Échantillon	Masse/mg	Segment	Gamme	Atmosphère	Corr.
[1]	STA 449F3	S6(r).ngb-ds3	2018-11-28	S6	Terre telle quelle	201.34	1/1	35°C/10.0(K/min)/1010°C	N2/O2, 40.0ml/min / N2, 20.0ml/min	ATD:020, TG:020, DTG:8
[2]	STA 449F3	SII-B8-7(r).ngb-ds3	2018-11-28	SII-B8-7	Terre traitée	202.68	1/1	35°C/10.0(K/min)/1010°C	N2/O2, 40.0ml/min / N2, 20.0ml/min	ATD:020, TG:020, DTG:8

SUS vs SV8

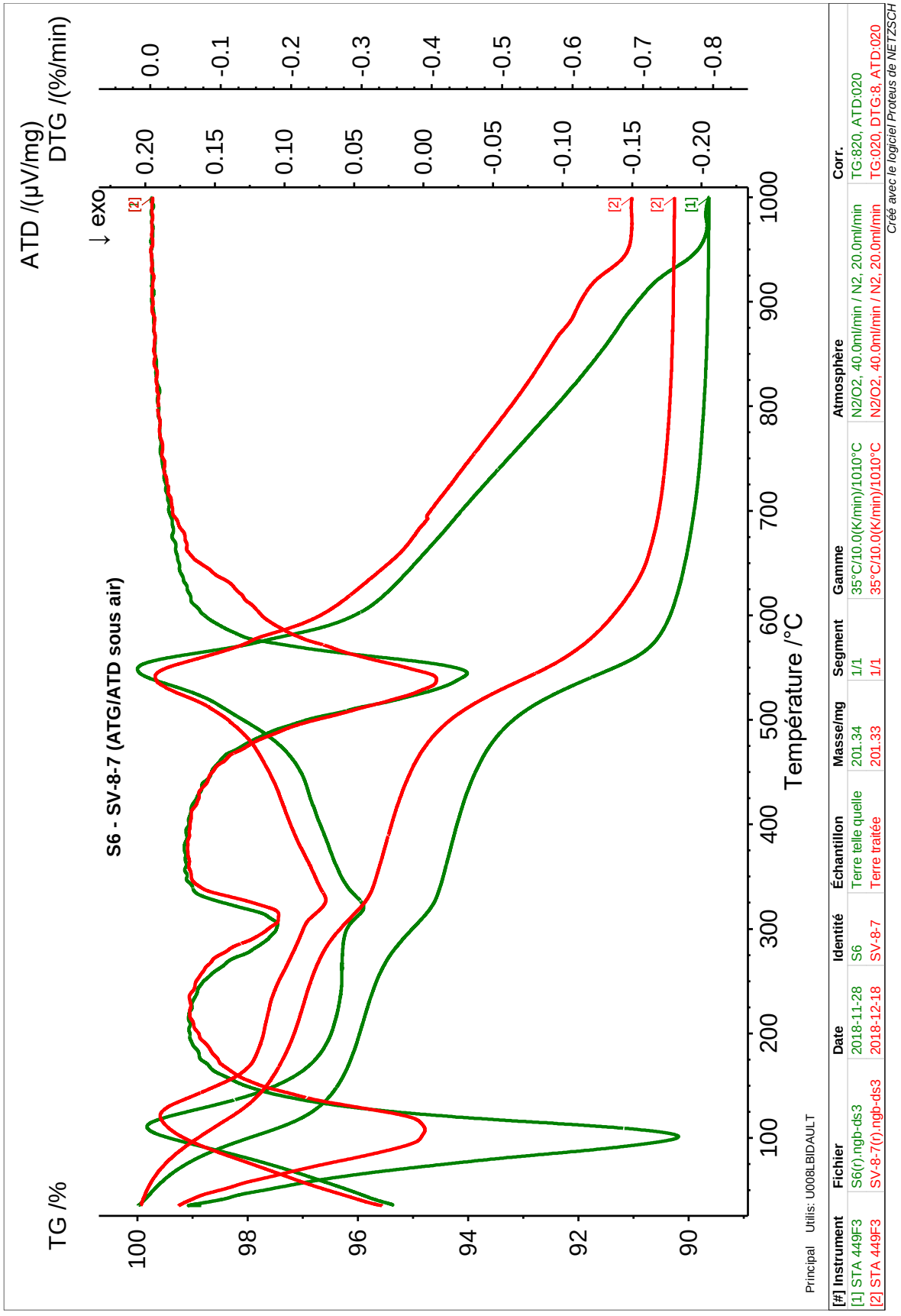
TG /%
ATD /(µV/mg)
DTG /(%/min)
↓ exo
S6 - SV-8-7 (ATG/ATD sous air)
Température /°C
Principal Utilis: U008LBIDAULT
[#] Instrument Fichier Date Identité Échantillon Masse/mg Segment Gamme Atmosphère Corr.
[1] STA 449F3 S6(r).ngb-ds3 2018-11-28 S6 Terre telle quelle 201.34 1/1 35°C/10.0(K/min)/1010°C N2/O2, 40.0ml/min / N2, 20.0ml/min TG:820, ATD:020
[2] STA 449F3 SV-8-7(r).ngb-ds3 2018-12-18 SV-8-7 Terre traitée 201.33 1/1 35°C/10.0(K/min)/1010°C N2/O2, 40.0ml/min / N2, 20.0ml/min TG:020, DTG:8, ATD:020
Créé avec le logiciel Proteus de NETZSCH

SUS vs SM8

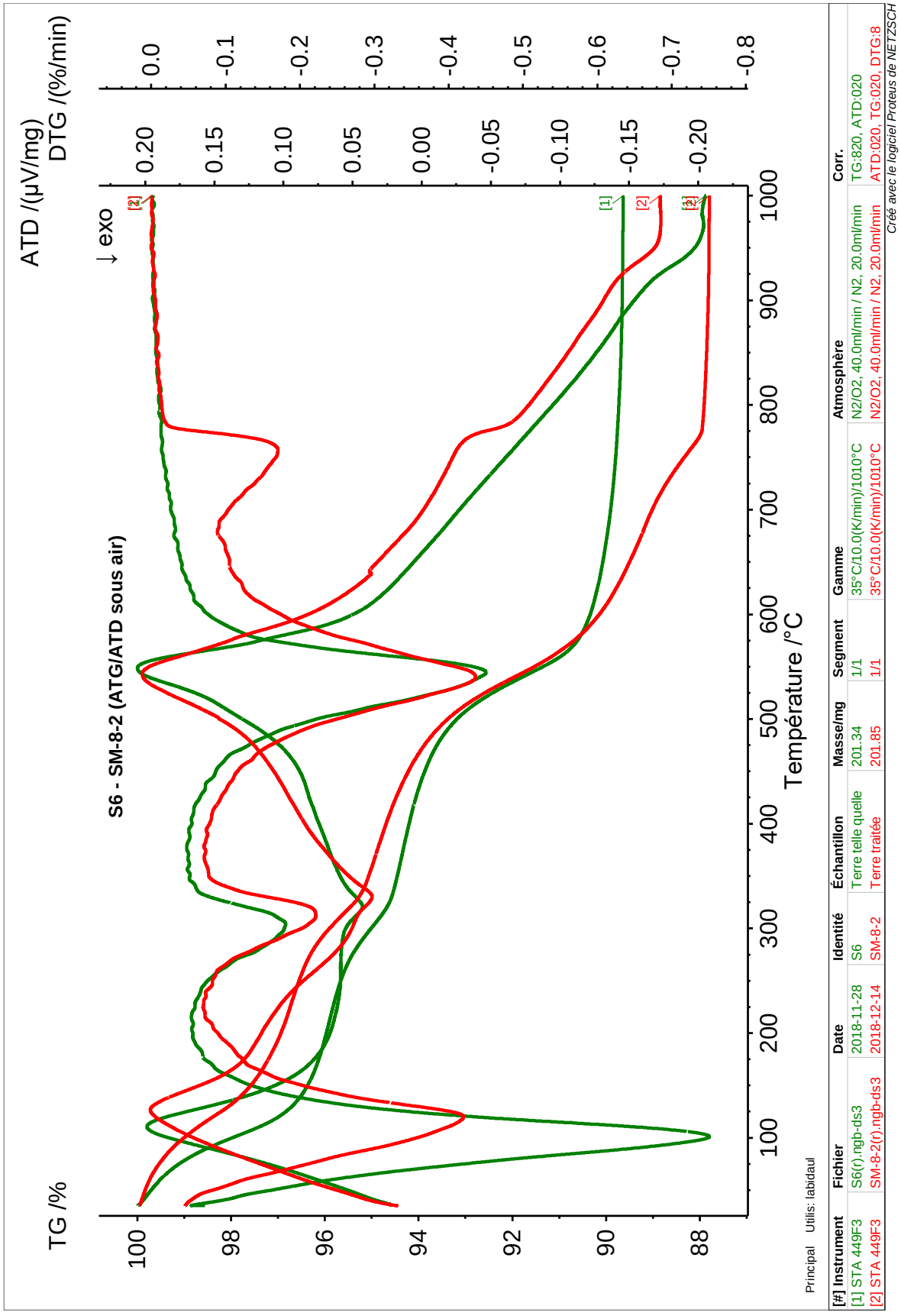
S6 - SM-8-2 (ATG/ATD sous air)
TG /%
ATD /(µV/mg)
DTG /(%/min)
↓ exo
Température /°C
Principal Utilis: labidaul
[#] Instrument Fichier Date Identité Échantillon Masse/mg Segment Gamme Atmosphère Corr.
[1] STA 449F3 S6(r).ngb-ds3 2018-11-28 S6 Terre telle quelle 201.34 1/1 35°C/10.0(K/min)/1010°C N2/O2, 40.0ml/min / N2, 20.0ml/min TG:820, ATD:020
[2] STA 449F3 SM-8-2(r).ngb-ds3 2018-12-14 SM-8-2 Terre traitée 201.85 1/1 35°C/10.0(K/min)/1010°C N2/O2, 40.0ml/min / N2, 20.0ml/min ATD:020, TG:020, DTG:8
Créé avec le logiciel Proteus de NETZSCH

SUS vs SP8

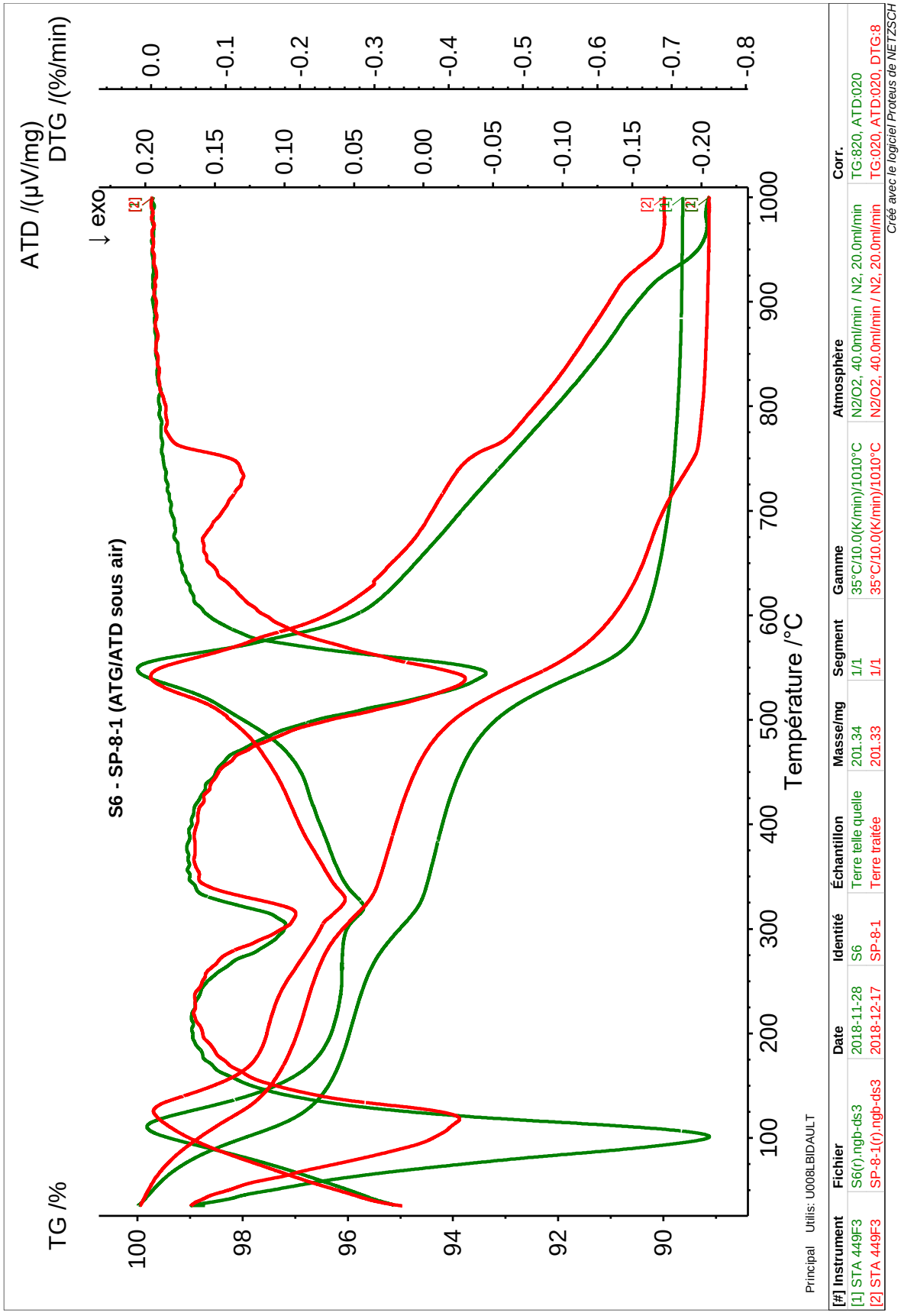

[#]	Instrument	Fichier	Date	Identité	Échantillon	Masse/mg	Segment	Gamme	Atmosphère	Corr.
[1]	STA 449F3	S6(r).ngb-ds3	2018-11-28	S6	Terre telle quelle	201.34	1/1	35°C/10.0(K/min)/1010°C	N2/O2, 40.0ml/min / N2, 20.0ml/min	TG:820, ATD:020
[2]	STA 449F3	SP-8-1(r).ngb-ds3	2018-12-17	SP-8-1	Terre traitée	201.33	1/1	35°C/10.0(K/min)/1010°C	N2/O2, 40.0ml/min / N2, 20.0ml/min	TG:020, ATD:020, DTG:8

Appendix J TGA (curves ENTPE vs curves Calcia)

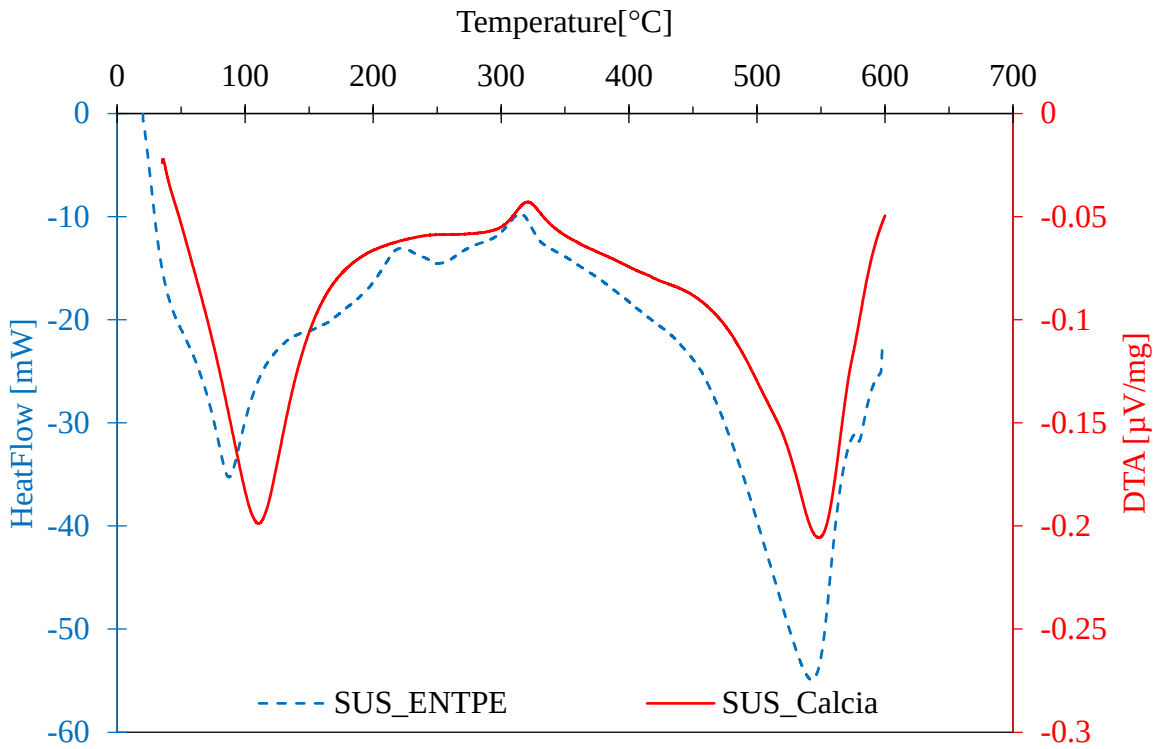

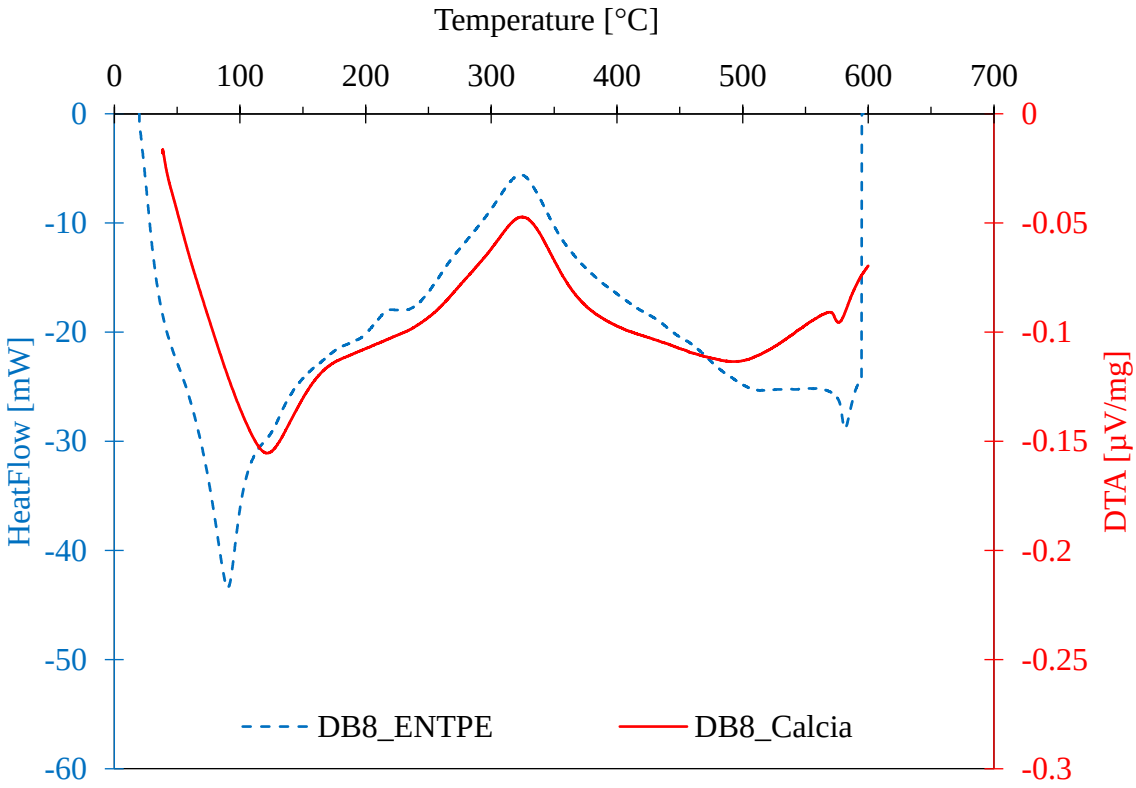

Appendix K TGA peaks of various phases present in concrete

Component	Decomposition temperature [°C]	References
C-S-H	140, peak endothermic	[375]
AFm	200, peak endothermic	[376], [377]
Ettringite	130, peak endothermic	[375], [378]
C_2AH_8	180, peak endothermic	[378]
C_3AH_2	250, peak endothermic	[375]
C_3AH_6	330, peak endothermic	[375]
C_4AH_{12}	270, peak endothermic	[378]
C_2ASH_8	150, peak endothermic	[379]

$Ca(OH)_2$ dehydration temperature [°C]	$CaCO_3$ decarbonation temperature [°C]	References
450 to 600	>600	[380]
600	780	[381]
465	>850	[382]
380 to 600	600 to 750	[383]

References

[1] F. Simon, “Excavated soils: The biggest source of waste you’ve never heard of,” *EURACTIV*, 2021. https://www.euractiv.com/section/circular-economy/news/excavated-soils-the-biggest-source-of-waste-youve-never-heard-of/.

[2] PREDEC, “Plan régional de prévention et de gestion des déchets issus des chantiers du bâtiment et des travaux publics,” 2014.

[3] C. Le Centre D’Etudes des Tunnels and Cerema, “Natural Geological Materials Excavated during Underground Works,” no. May, 2016.

[4] L. Van Eeckhout, “Le Monde: Que faire des 43 millions de tonnes de déblais de terre du Grand Paris ?,” 2016. https://www.lemonde.fr/planete/article/2016/10/21/que-faire-des-43-millions-de-tonnes-de-deblais-de-terre-du-grand-paris_5018057_3244.html.

[5] B. Berge, *The ecology of building materials*, Second edi. Architectural Press, 2009.

[6] H. Houben and H. Guillaud, *Earth Construction: A Comprehensive Guide*. London, England: Intermediate Technology Publications, 1994.

[7] L. Fontaine, R. Ange, P. Doat, H. Houben, H. Van Damme, and R. Piano, *Bâtir en terre: du grain de sable à l’architecture.* Paris, France: Belin : Cité des sciences et de l’industrie, 2009.

[8] F. Champire, “Étude expérimentale du comportement hydro-mécanique de la terre crue compactée pour la construction,” Ecole Nationale des Travaux Publics de l’Etat, 2017.

[9] F. Pacheco-Torgal and S. Jalali, “Earth construction: Lessons from the past for future eco-efficient construction,” *Constr. Build. Mater.*, vol. 29, pp. 512–519, 2012.

[10] L. Keefe, *Earth Building - Methods and materials, repair and conservation*. London: Routledge: Taylor & Francis Group, 2005.

[11] Geological Society, “Earthen Architecture, Engineering Geology Special Publications, v.21,” pp. 387–400, 2006, doi: 10.1144/GSL.ENG.2006.021.01.13.

[12] C. H. Kouakou and J.-C. Morel, “Strength and elasto-plastic properties of non-industrial building materials manufactured with clay as a natural binder,” *Appl. Clay Sci.*, vol. 44, no. 1–2, pp. 27–34, Apr. 2009, doi: 10.1016/j.clay.2008.12.019.

[13] E. Hamard, “Rediscovering of vernacular adaptive construction strategies for sustainable modern building - Application to Cob and Rammed Earth,” ENTPE, 2017.

[14] D. Gandreau and L. Delboy, *sous la direction de Joffroy T., CRAterre-ENSAG, 2010. Patrimoine mondial, Inventaire et situation des biens construits en terre*. Paris, France: UNESCO/CH/CPM, 2010.

[15] B. King, “The renaissance of earthen architecture - a fresh and updated look at clay-based construction,” in *Buildwell Symposium*, 2010, vol. 94903, no. 415, pp. 1–23.

[16] M. K. Dixit, J. L. Fernández-Solís, S. Lavy, and C. H. Culp, “Identification of parameters for embodied energy measurement: A literature review,” *Energy Build.*, vol. 42, no. 8, pp. 1238–1247, 2010, doi: 10.1016/j.enbuild.2010.02.016.

[17] J. C. Morel, A. Mesbah, M. Oggero, and P. Walker, “Building houses with local materials: Means to drastically reduce the environmental impact of construction,” *Build. Environ.*, vol. 36, no. 10, pp. 1119–1126, 2001, doi: 10.1016/S0360-1323(00)00054-8.
[18] D. Allinson and M. Hall, “Humidity buffering using stabilised rammed earth materials,” *Proc. Inst. Civ. Eng. - Constr. Mater.*, vol. 165, no. 6, pp. 335–344, 2012, doi: 10.1680/coma.11.00023.
[19] K. Heathcote, “The thermal performance of earth buildings,” *Inf. la Construcción*, vol. 63, no. 523, pp. 117–126, 2011, doi: 10.3989/ic.10.024.
[20] L. Soudani *et al.*, “Assessment of the validity of some common assumptions in hygrothermal modeling of earth based materials,” *Energy Build.*, vol. 116, pp. 498–511, Mar. 2016, doi: 10.1016/J.ENBUILD.2016.01.025.
[21] F. Pacheco-Torgal and S. Jalali, “Earth construction: Lessons from the past for future eco-efficient construction,” *Constr. Build. Mater.*, vol. 29, pp. 512–519, Apr. 2012, doi: 10.1016/J.CONBUILDMAT.2011.10.054.
[22] L. Zhang, L. Yang, B. P. Jelle, Y. Wang, and A. Gustavsen, “Hygrothermal properties of compressed earthen bricks,” *Constr. Build. Mater.*, vol. 162, no. 2018, pp. 576–583, 2018, doi: 10.1016/j.conbuildmat.2017.11.163.
[23] L. Soudani, A. Fabbri, P. A. Chabriac, J. C. Morel, M. Woloszyn, and A. C. Grillet, “On the relevance of neglecting the mass vapor variation for modelling the hygrothermal behavior of rammed earth,” *Rammed Earth Constr. - Proc. 1st Int. Conf. Rammed Earth Constr. ICREC 2015*, no. April 2016, pp. 151–156, 2015, doi: 10.1201/b18046-31.
[24] E. Quagliarini, A. Stazi, E. Pasqualini, and E. Fratalocchi, “Cob construction in Italy: Some lessons from the past,” *Sustainability*, vol. 2, no. 10, pp. 3291–3308, 2010, doi: 10.3390/su2103291.
[25] M. Hall and D. Allinson, “Assessing the effects of soil grading on the moisture content-dependent thermal conductivity of stabilised rammed earth materials,” *Appl. Therm. Eng.*, vol. 29, no. 4, pp. 740–747, 2009, doi: 10.1016/j.applthermaleng.2008.03.051.
[26] M. Woloszyn, T. Kalamees, M. Olivier Abadie, M. Steeman, and A. Sasic Kalagasidis, “The effect of combining a relative-humidity-sensitive ventilation system with the moisture-buffering capacity of materials on indoor climate and energy efficiency of buildings,” *Build. Environ.*, vol. 44, no. 3, pp. 515–524, Mar. 2009, doi: 10.1016/J.BUILDENV.2008.04.017.
[27] C. Williams, S. Goodhew, R. Griffiths, and L. Watson, “The feasibility of earth block masonry for building sustainable walling in the United Kingdom,” *J. Build. Apprais.*, vol. 6, no. 2, pp. 99–108, 2010, doi: 10.1057/jba.2010.15.
[28] A. M. Forster, G. M. Medero, T. Morton, and J. Buckman, “Traditional cob wall: Response to flooding,” *Struct. Surv.*, vol. 26, no. 4, pp. 302–321, 2008, doi: 10.1108/02630800810906557.
[29] Q. B. Bui, J. C. Morel, S. Hans, and P. Walker, “Effect of moisture content on the mechanical characteristics of rammed earth,” *Constr. Build. Mater.*, vol. 54, no. March, pp. 163–169, 2014, doi: 10.1016/j.conbuildmat.2013.12.067.
[30] P. A. Jaquin, C. E. Augarde, D. Gallipoli, and D. G. Toll, “The strength of unstabilised rammed earth materials,” *Geotechnique*, vol. 59, no. 5, pp. 487–490, 2009, doi: 10.1680/geot.2007.00129.
[31] A. Fabbri and J. C. Morel, “Earthen materials and constructions,” in *Nonconventional and Vernacular Construction Materials*, 2016, pp. 273–299.
[32] P. Gerard, M. Mahdad, A. Robert McCormack, and B. François, “A unified failure criterion for unstabilized rammed earth materials upon varying relative humidity conditions,” *Constr. Build. Mater.*, vol. 95, pp. 437–447, 2015, doi: 10.1016/j.conbuildmat.2015.07.100.

[33] E. E. Alonso, A. Gens, and A. Josa, “A constitutive model for partially saturated soils,” *Geotechnique*, vol. 40, no. 3, pp. 405–430, 1990, doi: 10.1680/geot.1990.40.3.405.
[34] B. T. Lai, H. Wong, A. Fabbri, and D. Branque, “A new constitutive model of unsaturated soils using bounding surface plasticity (BSP) and a non-associative flow rule,” *Innov. Infrastruct. Solut.*, vol. 1, no. 1, pp. 1–8, 2016, doi: 10.1007/s41062-016-0005-z.
[35] THE TRAVEL BLOG, “DJENNE, MALI,” *THE TRAVEL BLOG*, 2015. https://stujarvis.com/2015/10/30/djenne-mali/.
[36] Yemen Art & Architecture, “Examples of Yemen earthen constructions,” 2020. https://www.facebook.com/Yemen.Art.Architecture.
[37] M. JOKAR, “Citadelle de Bam,” *Iran Destination*, 2017. https://fr.irandestination.com/citadelle-de-bam/.
[38] Visit Our China, “Overhanging Great Wall,” 2021. https://www.visitourchina.com/jiayuguan/attraction/overhanging-great-wall.html.
[39] Rilem Association, “Earthen construction techniques,” 2020, [Online]. Available: https://www.linkedin.com/company/rilem-association/.
[40] M. R. Hall, K. B. Najim, and P. Keikhaei Dehdezi, “Soil stabilisation and earth construction: Materials, properties and techniques,” *Mod. Earth Build. Mater. Eng. Constr. Appl.*, pp. 222–255, 2012, doi: 10.1533/9780857096166.2.222.
[41] V. S. Burroughs, “Quantitative criteria for the selection and stabilisation of soils for rammed earth wall construction,” University of New South Wales, Australia, 2001.
[42] P. Faria, V. Silva, C. Pereira, and M. Rocha, “The monitoring of rammed earth experimental walls and characterization of rammed earth samples,” *Rammed Earth Conserv.*, pp. 91–97, 2012.
[43] A. W. Bruno, D. Gallipoli, C. Perlot, and J. Mendes, “Effect of stabilisation on mechanical properties, moisture buffering and water durability of hypercompacted earth,” *Constr. Build. Mater.*, vol. 149, pp. 733–740, 2017.
[44] Y. Millogo, J. E. Aubert, A. D. Séré, A. Fabbri, and J. C. Morel, “Earth blocks stabilized by cow-dung,” *Mater. Struct. Constr.*, vol. 49, no. 11, pp. 4583–4594, 2016, doi: 10.1617/s11527-016-0808-6.
[45] K. Ghavami, R. D. Toledo Filho, and N. P. Barbosa, “Behaviour of composite soil reinforced with natural fibres,” *Cem. Concr. Compos.*, vol. 21, pp. 39–48, 1999.
[46] Y. Millogo, J. E. Aubert, E. Hamard, and J. C. Morel, “Properties of Kenaf fibres from Burkina Faso used as reinforcement of earth blocks,” *Materials (Basel).*, vol. 8, pp. 2332–2345, 2015.
[47] A. Laborel-Préneron, J. E. Aubert, C. Magniont, C. Tribout, and A. Bertron, “Plant aggregates and fibers in earth construction materials: A review,” *Constr. Build. Mater.*, vol. 111, pp. 719–734, 2016.
[48] B. V. Venkatarama Reddy and P. Prasanna Kumar, “Cement stabilised rammed earth. Part B: Compressive strength and stress-strain characteristics,” *Mater. Struct. Constr.*, vol. 44, no. 3, pp. 695–707, 2011, doi: 10.1617/s11527-010-9659-8.
[49] M. Lunt, “Stabilized soil blocks for buildings,” *Overseas Build. Note*, pp. 184:1–15, 1980.
[50] B. V. Venkatarama Reddy and P. Prasanna Kumar, “Cement stabilised rammed earth. Part A: Compaction characteristics and physical properties of compacted cement stabilised soils,” *Mater. Struct. Constr.*, vol. 44, no. 3, pp. 681–693, 2011, doi: 10.1617/s11527-010-9658-9.
[51] K. Heathcote, “Compressive strength of cement stabilized pressed earth blocks,” *Build. Res. Inf.*, vol. 19, no. 2, pp. 101–105, Mar. 1991, doi: 10.1080/09613219108727106.
[52] V. Maniatidis and P. Walker, “A Review of Rammed Earth Construction,” 2003.

[53] V. Rigassi, *Compressed earth blocks: Manual of production*, vol. II. 1995.
[54] P. Walker, R. Keable, J. Martin, and V. Maniatidis, *Rammed earth design and construction guidelines*. BRE Bookshop, Watford, 2005.
[55] M. Hall, "Rammed earth: traditional methods, modern techniques, sustainable future," *Build Eng*, vol. 77, no. 11, pp. 22–14, 2002.
[56] P. L. Verma and S. R. Mehra, "Use of soil–cement in house construction in the Punjab," *Indian Concr. J.*, vol. 24, pp. 91–96, 1950.
[57] D. Easton, "The industrialisation of monolithic earth walling for first world applications," in *5th international conference on building with earth (LEHM 2008)*, 2008, pp. 90–97.
[58] H. Van Damme and H. Houben, "Earth concrete. Stabilization revisited," *Cem. Concr. Res.*, vol. 114, pp. 90–102, 2018, doi: 10.1016/j.cemconres.2017.02.035.
[59] B. V. Venkatarama Reddy and A. Gupta, "Characteristics of soil-cement blocks using highly sandy soils," *Mater. Struct.*, vol. 38, pp. 651–658, 2005, doi: 10.1617/14265.
[60] AENOR, "Compressed earth blocks for walls and partitations. Definitions, specifications and test methods. UNE 41410. Madrid (Spain): Spanish Association for Standardisation and Certification," 2008.
[61] SNZ, *Engineering design of earth buildings. NZS 4297. Wellington: Standards New Zealand*. 1998.
[62] ASTM, *Standard guide for design of earthen wall building systems. Pennsylvania (United States): ASTM International*. 2010.
[63] SLSI, *Specification for compressed stabilized earth blocks. Part 1: Requirements. SLS 1382-1. Sri Lanka: Sri Lanka Standards Institution*. 2009.
[64] G. Middleton, "Bulletin 5. Earth Wall Construction," in *1992 rbSLM, editor. North Ryde (Australia): CSIRO Division of Building, Construction and Engineering*, 1987.
[65] ABNT, *Solo-cimento – determinação da absorção d'água. NBR 13555. Rio de Janeiro (Brasil): Associação Brasileira de Normas Técnicas*. 1996.
[66] ABNT, "Tijolo macico de solo-cemento. Especificacao. NBR 8491. Rio de Janeiro: Associacao brasileira de normas tecnicas," 1986.
[67] BIS, *Specification for soil based blocks used in general building construction. IS 1725 Indian Bureau of Indian Standards*. 1982.
[68] ICONTEC, *Ground blocks cement for walls and divisions. Definitions. Especifications. Test methods. Conditions of delivery*. 2004.
[69] KEBS, *Specifications for stabilized soil blocks. KS02-1070:1993. Nairobi: Kenya Bureau of Standards*. 1999.
[70] B. V. Venkatarama Reddy, *Stabilised soil blocks for structural masonry in earth construction*. Woodhead Publishing Limited, 2012.
[71] G. Minke, "Building with earth, design and technology of a sustainable architecture," *Birkhäuser – Publ. Archit. Basel · Berlin · Bost.*, 2006.
[72] J. Cid-Falceto, F. R. Mazarrón, and I. Cañas, "Assessment of compressed earth blocks made in Spain: International durability tests," *Constr. Build. Mater.*, vol. 37, pp. 738–745, 2012, doi: 10.1016/j.conbuildmat.2012.08.019.
[73] K. Freidin and E. Erell, "Bricks made of coal fly-ash and slag, cured in the open air," *Cem. Concr. Compos.*, vol. 17, no. 4, pp. 289–300, 1995, doi: 10.1016/0958-9465(95)00017-7.
[74] A. Guettala, A. Abibsi, and H. Houari, "Durability study of stabilized earth concrete under both laboratory and climatic conditions exposure," *Constr. Build. Mater.*, vol. 20, no. 3, pp. 119–127, 2006, doi: 10.1016/j.conbuildmat.2005.02.001.
[75] B. V. Venkatarama Reddy and S. Hubli, "Properties of lime stabilised steam-cured blocks for masonry," *Mater. Struct.*, vol. 35, no. 5, pp. 293–300, 2002.

[76] T. Morton, *Earth Masonry: Design and Construction Guidelines*. Berkshire: Construction Research Communications Limited, 2008.
[77] P. J. Walker, "Strength, durability and shrinkage characteristics of cement stabilised soil blocks," *Cem. Concr. Compos.*, vol. 17, no. 4, pp. 301–310, 1995.
[78] B. Venkatarama Reddy and K. S. Jagadish, "Embodied energy of common and alternative building materials and technologies," *Energy Build.*, vol. 35, pp. 129–137, 2003.
[79] B. V. Venkatarama Reddy, "Sustainable materials for low carbon buildings," *Int. J. Low Carbon Technol.*, vol. 4, no. 3, pp. 175–181, 2009.
[80] B. V. Venkatarama Reddy, "The stabilised mud block: a low carbon emission alternative for masonry buildings," in *First International Conference on Building Energy and Environment (C0BEE-2008)*, 2008, pp. 1397–1404.
[81] R. F. Craig, *Soil Mechanics*, Craig, R.F. London, England: E&FN Spon, 1998.
[82] B. M. Das, *Principles of Geotechnical Engineering*, 3rd ed. PWS Publishing Company: PWS Publishing Company, 1994.
[83] A. Casagrande, "Classification and identification of soils," in *American Society of Civil Engineers (ASCE), June 1947*, 1947, pp. 783–810.
[84] Gooding DEM, *Soil testing for soil-cement block preparation*. Development Technology Unit working paper, volume 38, 1993.
[85] EN ISO 17892-4, *Geotechnical investigation and testing - Laboratory testing of soil - Part 4: Determination of particle size distribution*. 2018.
[86] BS 1377-2, *Methods of test for soils for civil engineering purposes - Part 2: Classification tests*. British Standards Institution, 1990.
[87] BNQ 2501-025, *Sols-Analyse granulométrique des sols inorganiques*. Bureau de Normalisation du Québec, 2013.
[88] ASTM C136, *Standard Test Method for Sieve Analysis of Fine and Coarse Aggregates*. ASTM International, 2014.
[89] ASTM D422, *Standard Test Method for Dispersive Characteristics of Clay Soil by Double Hydrometer*. ASTM International, 2011.
[90] EN ISO 14688-1, *Geotechnical investigation and testing - Identification and classification of soil - Part 1: Identification and description*. European Committee for Standardization, 2018.
[91] USDA, *Soil Mechanics Level 1, USDA Textural Soil Classification*. United States Department of Agriculture, 1987.
[92] ASTM D2487, *Standard Practice for Classification of Soils for Engineering Purposes (Unified Soil Classification System)*. ASTM International, 2017.
[93] M. Olivier and A. Mesbah, "Influence of different parametres on the resistance of earth, used as a building material," *Mud Archit.*, no. November, 1987, doi: 10.1111/j.1749-6632.2009.04417.x.
[94] F. J. Pettijohn, *Sedimentary Rocks*. New York, USA: Hopper and Brothers Ltd, 1957.
[95] ILO/UNIDO, *Small-scale Brickmaking*. Geneva, Switzerland: Technology Series, Memorandum No.6. International Labour Organisation, 1984.
[96] R. F. Scot, *Principles of Soil Mechanics*. Addison-Wesley Publishing Inc. London, England, 1963.
[97] B. Vickers, *Laboratory Work in Soil Mechanics*, 2nd ed. London, England: Granada Publishing Ltd, 1983.
[98] B. V. Venkatarama Reddy, L. Richardson, and K. S. Rao, "Optimum Soil Grading for the soil-cement blocks," *J. Mater. Civ. Eng.*, vol. 19, no. 2, pp. 139–148, 2007.
[99] B. V. Venkatarama Reddy and M. S. Latha, "Influence of soil grading on the characteristics of cement stabilised soil compacts," *Mater. Struct.*, vol. 47, pp. 1633–

1645, 2014.
[100] H. B. Nagaraj, A. Rajesh, and M. V. Sravan, “Influence of soil gradation, proportion and combination of admixtures on the properties and durability of CSEBs,” *Constr. Build. Mater.*, vol. 110, pp. 135–144, 2016, doi: 10.1016/j.conbuildmat.2016.02.023.
[101] K. Hyug-Moon, L. Anh Tuan, and N. Ninh Thuy, “Influence of soil grading on properties of compressed cement-soil,” *KSCE J. Civ. Eng.*, vol. 14, pp. 845–853, 2010.
[102] S. R and M. K, *Appropriate building materials: A catalogue of potential solutions*. SKAT Publications, Switzerland, 1981.
[103] EN ISO 17892-12, *Geotechnical investigation and testing - Laboratory testing of soil - Part 12: Determination of Atterberg limits*. European Committee for Standardization, 2018.
[104] ASTM D4318, *Standard Test Methods for Liquid Limit, Plastic Limit, and Plasticity Index of Soils*. ASTM International, 2017.
[105] NF P94-068, *Sols : reconnaissance et essais - Mesure de la capacité d’adsorption de bleu de méthylène d’un sol ou d’un matériau rocheux - Détermination de la valeur de bleu de méthylène d’un sol ou d’un matériau rocheux par l’essai à la tâche*. Association Française de Normalisation, 1998.
[106] NF P11-300, *Classification des matériaux utilisables dans la construction des remblais et des couches de forme d’infrastructures routières*. Association Française de Normalisation, 1992.
[107] D. Lautrin, “Essai au bleu de méthylène-utilisation pratique des paramètres dérivés de l’essai au bleu de méthylène dans les projets de génie civil,” in *Bulletin de liaison des Laboratoires des Ponts et Chaussées*, 1989, p. 160.
[108] A. Chiappone, S. Marello, C. Scavia, and M. Setti, “Clay mineral characterization through the methylene blue test: comparison with other experimental techniques and applications of the method,” *Can. Geotech. J.*, vol. 41, no. 6, 2004.
[109] ASTM D698, *Standard Test Methods for Laboratory Compaction Characteristics of Soil Using Standard Effort (12,400 ft-lbf/ft3 (600 kN-m/m3))*. ASTM International, 2012.
[110] BNQ 2501-250, *Sols-Détermination de la relation teneur en eau-masse volumique-Essai avec energie de compactage normal (600 kNm/m3)*. Bureau de Normalisation du Québec, 2005.
[111] NF P94-093, *Sols : reconnaissance et essais - Détermination des références de compactage d’un matériau - Essai Proctor Normal - Essai Proctor modifié*. Association Française de Normalisation, 2014.
[112] AFNOR, *Compressed earth blocks for walls and partitions: definitions – Specifications – Test methods – Delivery acceptance conditions. XP P13-901*. Saint-Denis La Plaine Cedex: Association française de Normalisation, 2001.
[113] D. P, H. A, H. H, M. S, and V. F, *Construire en Terre*. CRATerre, Paris, 1979.
[114] J. Norton, *Building with Earth: A Handbook*. Great Britain, London: Intermediate Technology Publications Ltd., 1986.
[115] R. J. S. Spence and D. J. Cook, *Building Materials in Developing Countries*. Chichester, England: Wiley, 1983.
[116] P. Donkor and E. Obonyo, “Earthen construction materials: Assessing the feasibility of improving strength and deformability of compressed earth blocks using polypropylene fibers,” *Mater. Des.*, vol. 83, pp. 813–819, 2015, doi: 10.1016/j.matdes.2015.06.017.
[117] A. Laborel-Préneron, J. E. Aubert, C. Magniont, P. Maillard, and C. Poirier, “Effect of plant aggregates on mechanical properties of earth bricks,” *J. Mater. Civ. Eng.*, vol. 29, 2017, doi: 10.1061/(ASCE)MT.1943-5533.0002096.
[118] A. Hakimi, O. Fassi-Fehri, H. Bouabid, S. Charif D’ouazzane, and M. El Kortbi, “Non-

linear behaviour of the compressed earthen block by elasticity-damage coupling," *Mater. Struct.*, vol. 32, pp. 539–545, 1999.
[119] A. Hakimi, N. Yamani, and H. Ouissi, "Results of mechanical strength tests on samples of compressed earth," *Mater. Struct.*, vol. 29, pp. 600–608, 1996.
[120] M. Olivier and A. Mesbah, "Le Matériau Terre: Essai de Compactage Statique Pour La Fabrication de Briques de Terre Compressées," *Bull. des Lab. des Ponts Chaussées*, vol. 146, 1986.
[121] N. M. Code, *New Mexico Earthen Building Materials Code 14.7.4*. Construction Industries Division (CID) of the Regulation and Licensing Department, 2006.
[122] P. Walker and Standards Australia, *HB 195 The Australian Earth Building Handbook*. 2001.
[123] SAZS 724, *Standard Code of Practice for Rammed Earth Structures*. Standards Association of Zimbabwe, 2001.
[124] NZS 4298, *New Zealand Standard - Materials and workmanship for earth buildings*. Standards New Zealand, 1998.
[125] J. Keable, *Rammed earth structure - A code of practice*. London, UK: Intermediate Technology Publications., 1996.
[126] C. Ouellet-Plamondon, N. Soro, and M. J. Nollet, "Characterization, Mix Design, Mechanical Testing of Earth Materials, Stabilized and Unstabilized, for Building Construction," *Poromechanics VI*, 2017, doi: 10.1061/9780784480779.112.
[127] XP P94-047, *Sols : reconnaissance et essais - Détermination de la teneur pondérale en matières organiques d'un matériau - Méthode par calcination*. Association Française de Normalisation, 1998.
[128] XP P94-055, *Sols : reconnaissance et essais - Détermination de la teneur pondérale en matières organiques d'un sol - Méthode chimique*. Association Française de Normalisation, 1993.
[129] BS 1377-3, *Methods of test for soils for civil engineering purposes - Part 3: Chemical and electro-chemical testing*. British Standards Institution, 1990.
[130] BS 1881-124, *Testing concrete. Methods for analysis of hardened concrete*. British Standards Institution, 2015.
[131] EN ISO 10693, *Soil quality - Determination of carbonate content - Volumetric method*. European Committee for Standardization, 1995.
[132] NF P94-048, *Sols : Reconnaissance et essais Détermination de la teneur en carbonate Méthode du calcimètre*. Association Française de Normalisation, 1996.
[133] ASTM D4373, *Standard Test Method for Rapid Determination of Carbonate Content of Soils*. ASTM International, 2014.
[134] EN 15933, *Sludge, treated biowaste and soil; Determination of pH*. Committee for Standardization, 2012.
[135] EN ISO 10390, *Soil quality - Determination of pH*. . European Committee for Standardization, 2020.
[136] ASTM D4972, *Standard Test Method for pH of Soils*. ASTM International, 2001.
[137] NF X31-130, *Qualité des sols - Méthodes chimiques - Détermination de la capacité d'échange cationique (CEC) et des cations extractibles*. Association Française de Normalisation, 1999.
[138] ASTM 7503-18, *Standard Test Method for Measuring the Exchange Complex and Cation Exchange Capacity of Inorganic Fine-Grained Soils*. ASTM International, 2018.
[139] ISO 23470, *Soil quality. Determination of effective cation exchange capacity (CEC) and exchangeable cations using a hexamminecobalt trichloride solution*. International Organization for Standardization, 2018.
[140] ISO 11260, *Qualité du sol - Détermination de la capacité d'échange cationique effective*

et du taux de saturation en bases échangeables à l'aide d'une solution de chlorure de baryum. International Organization for Standardization, 2018.
[141] A. J. Metson, *Methods of chemical analysis for soil survey samples*. New Zealand Soil Bureau Bulletin No. 12., 1956.
[142] P. Walker, R. Keable, J. Martin, and V. Maniatidis, *Rammed earth: Design and construction guidelines*. BRE Bookshop, 2005.
[143] ISO 11265, *Qualité du sol - Détermination de la conductivité électrique spécifique*. International Organization for Standardization, 1994.
[144] ISO 11048, *Qualité du sol - Dosage du sulfate soluble dans l'eau et dans l'acide*. International Organization for Standardization, 1995.
[145] ISO 14256-2, *Qualité du sol - Dosage des nitrates, des nitrites et de l'ammonium dans des sols bruts par extraction avec une solution de chlorure de potassium - Partie 2 : méthode automatisée avec analyse en flux segmenté*. International Organization for Standardization, 2007.
[146] A. Ammari, K. Bouassria, M. Cherraj, H. Bouabid, and S. Charif D'ouazzane, "Combined effect of mineralogy and granular texture on the technico-economic optimum of the adobe and compressed earth blocks," *Case Stud. Constr. Mater.*, pp. 240–248, 2017, doi: 10.1016/j.cscm.2017.08.004.
[147] C. Galán-Marín, C. Rivera-Gómez, and J. Petric, "Clay-based composite stabilized with natural polymer and fibre," *Constr. Build. Mater.*, vol. 24, pp. 1462–1468, 2010, doi: 10.1016/j.conbuildmat.2010.01.008.
[148] H. Houben and H. Guillaud, *Traité de construction en terre*. 2006.
[149] L. Turanli and A. Saritas, "Strengthening the structural behavior of adobe walls through the use of plaster reinforcement mesh," *Constr. Build. Mater.*, vol. 25, pp. 1747–1752, 2011, doi: 10.1016/j.conbuildmat.2010.11.092.
[150] M. Uguryol and F. Kulakoglu, "A preliminary study for the characterization of Kültepe's adobe soils with the purpose of providing data for conservation and archaeology," *J. Cult. Herit.*, vol. 14, pp. 117–124, 2013, doi: 10.1016/j.culher.2012.12.008.
[151] C. A. Dove, F. F. Bradley, and S. V. Patwardhan, "Seaweed biopolymers as additives for unfired clay bricks," *Mater. Struct.*, vol. 49, pp. 4463–4482, 2016, doi: 10.1617/s11527-016-0801-0.
[152] R. Peltier, "La stabilisation des sols," *Rev. Générale des Routes Aérodromes N°304*, pp. 37–60, 1957.
[153] M. Vénuat, *Le traitement des sols à la chaux et au ciment*. 1980.
[154] H. Tremblay, J. Duschene, J. Locat, and S. Leroueil, "Influence of the nature of organic compounds on fine soil stabilization with cement," *Can. Geotech. J.*, vol. 39, pp. 535–546, 2002.
[155] J. Thorez, *Phyllosilicates and Clay Minerals: A Laboratory Hand book for their X-ray Diffraction Examination*, Editions G. 1975.
[156] D. M. Moore and R. C. Reynolds, *X-ray diffraction and the identification and analysis of clay minerals*, Second edi. Oxford University Press, 1997.
[157] K. A. J. Ouedraogo, J. E. Aubert, C. Tribout, and G. Escadeillas, "Is stabilization of earth bricks using low cement or lime contents relevant?," *Constr. Build. Mater.*, vol. 236, p. 117578, 2020, doi: 10.1016/j.conbuildmat.2019.117578.
[158] M. I. Gomes, T. D. Gonçalves, and P. Faria, "Unstabilized rammed earth: Characterization of material collected from old constructions in south portugal and comparison to normative requirements," *Int. J. Archit. Herit.*, vol. 8, no. 2, pp. 185–212, 2014, doi: 10.1080/15583058.2012.683133.
[159] W. A. Deer, R. A. Howie, and J. Zussman, *Rock-Forming Minerals, Sheet Silicates: Clay Minerals*, Second Edi. London: M. J. Wilson. The Geological Society, 2013.

[160] NF EN 197-1 : 2012, *CEMENT - PART 1: COMPOSITION, SPECIFICATIONS AND CONFORMITY CRITERIA FOR COMMON CEMENTS*. 2012.
[161] ASTM C430-17, *Standard Test Method for Fineness of Hydraulic Cement by the 45-μm (No. 325) Sieve*. ASTM International, West Conshohocken, PA, 2017.
[162] ASTM C151 / C151M - 18, *Standard Test Method for Autoclave Expansion of Hydraulic Cement*. ASTM International, West Conshohocken, PA, 2018.
[163] ASTM C266-20, *Standard Test Method for Time of Setting of Hydraulic-Cement Paste by Gillmore Needles*. ASTM International, West Conshohocken, PA, 2020.
[164] ASTM C186-17, *Standard Test Method for Heat of Hydration of Hydraulic Cement (Withdrawn 2019)*. ASTM International, West Conshohocken, PA, 2017.
[165] ASTM C114-18, *Standard Test Methods for Chemical Analysis of Hydraulic Cement*. ASTM International, West Conshohocken, PA, 2018.
[166] E. M. Gartner and J. M. Gaidis, *Hydration mechanisms, I*, J. Skalny. American Ceramic Society, Westerville, OH: Materials Science of Concrete, 1989.
[167] O. G. Ingles and J. B. Metcalf, *Soil stabilization principles and practices*. London, England, 1972.
[168] A. Herzog and J. K. Mitchell, "Reactions Accompanying the Stabilization of Clay with Cement," *Highw. Res. Board Rec.*, vol. 36, pp. 146–171, 1963.
[169] J. R. Harty, "Factors Influencing the Lime Reactivity of Tropically and Subtropically Weathered Soils," University of Illinois, Urbana, Illinois, 1970.
[170] S. of the A. Report, "Lime Stabilization-Reaction, Properties, Design, Construction," *Transp. Res. Board, Washington, D.C.*, 1987.
[171] J. L. Eades and R. E. R.E. Grim, "Reaction of hydrated lime with pure clay minerals in soil stabilization," *Highw. Res. Board Bull.*, vol. 262, pp. 51–63, 1960.
[172] S. Diamond, J. C. White, and W. L. Dolch, "Transformation of Clay Minerals by Calcium Hydroxide Attack : Technical Paper," West Lafayette, Indiana, 1963. [Online]. Available: https://doi.org/10.5703/1288284313640.
[173] P. T. Stocker, "Diffusion and Diffuse Cementation in Lime- and Cement-Stabilized Clayey Soils-Chemical Aspects," *Aust. Road Res.*, vol. 5, no. 9, pp. 6-47., 1975.
[174] S. Diamond and E. B. Kinter, "Absorption of Calcium Hydroxide by Montmorillonite and Kaolinite," *J. Colloid. Interface Sci.*, vol. 22, no. 3, pp. 240–49, 1966.
[175] C. M. Ford, R. K. Moore, and B. F. Hajek, ""Reaction Products of the Lime-Treated Southeastern Soils," *Transp. Res. Rec. Natl. Res. Counc. Washington, D.C*, pp. 38–40, 1982.
[176] W. C. Ormsby and L. H. Bolz, "Microtexture and Composition of Reaction Products in the System Kaolin-Lime-Water," *J. Am. Ceram. Soc.*, vol. 49, no. 7, pp. 364–366, 1966.
[177] B. V. Venkatarama Reddy, M. R. Sudhakar, and M. K. Arun Kumar, "Characteristics of stabilised mud blocks using ash-modified soils," *Indian Concr. J.*, pp. 903–911, 2003.
[178] A. Guettala, A. Abibsi, and H. Houari, "Durability Study of Stabilised Earth Concrete under Both Laboratory and Climatic Conditions Exposure," *Constr. Build. Mater.*, vol. 20, 2006.
[179] J. C. Morrel, A. Pkla, and P. Walker, "Compressive Strength Testing of Compressed Earth Blocks," *Constr. Build. Mater.*, vol. 21, pp. 303 – 309, 2007.
[180] S. Deboucha and R. Hashim, "A Review on Bricks and Stabilised Compressed Earth Blocks," *Sci. Res. Essays*, vol. 6, no. 3, pp. 499 – 506, 2010.
[181] B. V. Venkatarama Reddy and A. Gupta, "Characteristics of soil-cement blocks using highly sandy soils," *Mater. Struct.*, vol. 38, 2005, doi: 10.1007/BF02481596.
[182] N. Al Haffar, A. Fabbri, F. McGregor, and H. Colina, "Cement stabilization effect on mechanical and hygric properties of compacted earth," 2019.
[183] P. Walker, "Specifications for stabilised pressed earth blocks," *Mason. Int.*, vol. 6, no.

1, pp. 1–6, 1996.
[184] J. E. Aubert, A. Fabbri, J. C. Morel, and P. Maillard, “An earth block with a compressive strength higher than 45 MPa!,” *Constr. Build. Mater.*, vol. 47, pp. 366–369, 2013, doi: 10.1016/j.conbuildmat.2013.05.068.
[185] A. Fabbri, J.-C. Morel, and D. Gallipoli, “Assessing the performance of earth building materials: a review of recent developments,” *RILEM Tech. Lett.*, vol. 3, pp. 46–58, 2018, doi: 10.21809/rilemtechlett.2018.71.
[186] J. C. Morel, A. Pkla, and P. Walker, “Compressive strength testing of compressed earth blocks,” *Constr. Build. Mater.*, vol. 21, no. 2, pp. 303–309, 2007, doi: 10.1016/j.conbuildmat.2005.08.021.
[187] J.-C. Morel, A. Pkla, and P. Walker, “Compressive strength testing of compressed earth blocks,” vol. 21, no. 2, pp. 303–309, Feb. 2007, doi: 10.1016/J.CONBUILDMAT.2005.08.021.
[188] F. Champiré, A. Fabbri, J. C. Morel, H. Wong, and F. McGregor, “Impact of relative humidity on the mechanical behavior of compacted earth as a building material,” *Constr. Build. Mater.*, vol. 110, pp. 70–78, 2016, doi: 10.1016/j.conbuildmat.2016.01.027.
[189] A. Koutous and E. Hilali, “Grain shape effects on the mechanical behavior of compacted earth,” *Case Stud. Constr. Mater.*, vol. 11, no. November, p. e00303, 2019, doi: 10.1016/j.cscm.2019.e00303.
[190] French Standard XP P13901, “Blocs de terre comprimée pour murs et cloisons: definitions, specifications, méthodes d’essai et conditions de réception. Association Française de Normalisation (Afnor),” 2001.
[191] M. Olivier, A. Mesbah, Z. El Gharbi, and J. C. Morel, “Mode opératoire pour la réalisation d’essais de résistance sur blocs de terre comprimée,” *Mater. Struct.*, vol. 30, no. 9, pp. 515–517, 1997, doi: 10.1007/BF02486394.
[192] J.-C. Morel and A. Pkla, “A model to measure compressive strength of compressed earth blocks with the ‘ 3 points bending test ,’” *Constr. Build. Mater.*, vol. 16, pp. 303–310, 2002.
[193] M. Mostafa and N. Uddin, “Experimental analysis of Compressed Earth Block (CEB) with banana fibers resisting flexural and compression forces,” *Case Stud. Constr. Mater.*, vol. 5, pp. 53–63, 2016, doi: 10.1016/j.cscm.2016.07.001.
[194] Norma E.080, “Diseño y construcción con tierra reforzada, Ministerio de Vivienda, Construcción y Saneamiento (MVCS), Lima.,” 2017.
[195] ASTM C78/C78M-18, “Standard Test Method for Flexural Strength of Concrete (Using Simple Beam with Third-Point Loading),” ASTM International, West Conshohocken, PA, 2018. doi: 10.1520/C0078.
[196] H. Araki, J. Koseki, and T. Sato, “Tensile strength of compacted rammed earth materials,” *Soils Found.*, vol. 56, no. 2, pp. 189–204, 2016.
[197] T. T. Bui, Q. B. Bui, A. Limam, and S. Maximilien, “Failure of rammed earth walls: From observations to quantifications,” *Constr. Build. Mater.*, vol. 51, pp. 295–302, 2014.
[198] H. Gonçalves *et al.*, “The influence of porogene additives on the properties of mortars used to control the ambient moisture,” *Energy Build.*, vol. 74, pp. 61–68, 2014, doi: 10.1016/j.enbuild.2014.01.016.
[199] A. Arundel, E. Sterling, and J. Biggin, “Indirect health effect of relative humidity in indoor environments,” *Environ. Health Perspect.*, vol. 65, p. 351, 1986.
[200] L. Fang, G. Clausen, and P. O. Fanger, “Impact of temperature and humidity on chemical and sensory emissions from building materials,” *Indoor Air*, vol. 9, pp. 193–201, 1999, doi: 10.1111/j.1600-0668.1999.t01-1-00006.x.
[201] F. Collet, “Caractérisation hydrique et thermiqe de matériaux de génie.,” *Thèse Dr.*

l'université Insa Rennes, 2018.
[202] ISO 12571, *Hygrothermal performance of building materials and products — Determination of hygroscopic sorption properties*. 2013.
[203] G. Minke, *Building with earth: design and technology of a sustainable architecture*. Birkhäuser - Publishers for Architecture, 2012.
[204] F. Champiré, A. Fabbri, J.-C. Morel, H. Wong, and F. McGregor, "Impact of relative humidity on the mechanical behavior of compacted earth as a building material," *Constr. Build. Mater.*, vol. 110, pp. 70–78, 2016, doi: 10.1016/j.conbuildmat.2016.01.027.
[205] A. Fabbri, F. McGregor, I. Costa, and P. Faria, "Effect of temperature on the sorption curves of earthen materials," *Mater. Struct. Constr.*, vol. 50, no. 6, 2017, doi: 10.1617/s11527-017-1122-7.
[206] ISO 12572, *Performance hygrothermique des matériaux et produits pour le bâtiment — Détermination des propriétés de transmission de la vapeur d'eau — Méthode de la coupelle*. 2016.
[207] K. Svennberg, *Moisture buffering in the indoor environment*. Report TVBH-1016 Lund Building Physics LTH, 2006.
[208] H. M. Künzel, *Simultaneous Heat and Moisture Transport in Building Components. One and two dimensional calculation using simple parameters*. IRB Verlag, 1995.
[209] M. Labat, C. Magniont, N. Oudhof, and J. Aubert, "From the experimental characterisation of the hygrothermal properties of straw-cvlay mixtures to the numerical assessment of their bu ering potential.," *Build. Environ.*, vol. 97, pp. 69–81, 2016.
[210] F. Volhard, *Construire en terre allégée,* Actes Sud. 2016.
[211] F. McGregor, A. Fabbri, J. Ferreira, T. Simões, P. Faria, and J. C. Morel, "Impact of the surface film resistance on the hygric properties of clay plasters," *Mater. Struct.*, vol. 50:193, 2017.
[212] D. Allinson and M. R. Hall, "Hygrothermal analysis of a stabilised rammed earth test building in the UK.," *Energy Build.*, vol. 42, pp. 845–852, 2010.
[213] S. Liuzzi, M. R. Hall, P. P. Stefanizzi, and S. P. Casey, "Hygrothermal behaviour and relative humidity buffering of unfired and hydrated lime-stabilised clay composites in a Mediterranean climate," *Build. Environ.*, vol. 61, pp. 82–92, 2013.
[214] P. A. Chabriac, "Mesure du comportement hygrothermique du pisé," ENTPE, 2014.
[215] A. Fabbri, N. Al Haffar, and F. McGregor, "Measurement of the relative air permeability of compacted earth in the hygroscopic regime of saturation," *Comptes Rendus - Mec.*, vol. 347, no. 12, 2019, doi: 10.1016/j.crme.2019.11.017.
[216] H. Cagnon, J. E. Aubert, M. Coutand, and C. Magniont, "Hygrothermal properties of earth bricks," *Energy Build.*, vol. 80, pp. 208–217, 2014.
[217] V. Baroghel-Bouny, M. Thiery, F. Barberon, and G. Villain, "Assessment of transport properties of cementitious materials: a major challenge as regards durability?," *Eur. J. Environ. Civ. Eng.*, vol. 11, no. 6, pp. 671–696., 2007.
[218] I. Gomes, T. D. Gonçalves, and P. Faria, "Hydric Behavior of Earth Materials and the Effects of Their Stabilization with Cement or Lime: Study on Repair Mortars for Historical Rammed Earth Structures," *J. Mater. Civ. Eng.*, vol. 28, no. 7, 2016.
[219] M. Hall and Y. Djerbib, "Moisture ingress in rammed earth: Part 1 - The effect of soil particle-size distribution on the rate of capillary suction," *Constr. Build. Mater.*, vol. 18, no. 4, pp. 269–280, 2004, doi: 10.1016/j.conbuildmat.2003.11.002.
[220] M. Raimondo, M. Dondi, D. Gardini, G. Guarini, and F. Mazzanti, "Predicting the initial rate of water absorption in clay bricks," *Constr. Build. Mater.*, vol. 23, no. 7, pp. 2623–2630, 2009, doi: 10.1016/j.conbuildmat.2009.01.009.
[221] L. C. L. Soudani, "Modelling and experimental validation of the hygrothermal performances of earth as a building material," École Nationale des Travaux Publics de

l'Etat, 2017.
[222] P. J. Walker and Standards Australia, "HB 195: The Australian Earth Building Handbook," 2002.
[223] H. Morris *et al.*, "Engineering design of earth buildings - NZS 4297:1998," *Stand. New Zeal.*, vol. 4297, p. 63, 1998.
[224] J. C. Morel, Q. B. Bui, and E. Hamard, "Weathering and durability of earthen material and structures," in *Modern Earth Buildings: Materials, Engineering, Constructions and Applications*, Woodhead Publishing, 2012, pp. 282–303.
[225] C. T. S. Beckett, P. A. Jaquin, and J. C. Morel, "Weathering the storm: A framework to assess the resistance of earthen structures to water damage," *Constr. Build. Mater.*, vol. 242, no. January, 2020, doi: 10.1016/j.conbuildmat.2020.118098.
[226] F. O. Ogunye and H. Boussabaine, "Diagnosis of assessment methods for weatherability of stabilised compressed soil blocks," *Constr. Build. Mater.*, vol. 16, no. 3, pp. 163–172, 2002, doi: 10.1016/S0950-0618(02)00004-1.
[227] J. Nakamatsu, S. Kim, J. Ayarza, E. Ramírez, M. Elgegren, and R. Aguilar, "Eco-friendly modification of earthen construction with carrageenan: Water durability and mechanical assessment," *Constr. Build. Mater.*, vol. 139, pp. 193–202, 2017, doi: 10.1016/j.conbuildmat.2017.02.062.
[228] R. Aguilar *et al.*, "The potential use of chitosan as a biopolymer additive for enhanced mechanical properties and water resistance of earthen construction," *Constr. Build. Mater.*, vol. 114, pp. 625–637, 2016, doi: 10.1016/j.conbuildmat.2016.03.218.
[229] T. Ashour and W. Wu, "The influence of natural reinforcement fibers on erosion properties of earth plaster materials for straw bale buildings," *J. Build. Apprais.*, vol. 5, no. 4, pp. 329–340, 2010, doi: 10.1057/jba.2010.4.
[230] R. A. Silva, D. V. Oliveira, T. Miranda, N. Cristelo, M. C. Escobar, and E. Soares, "Rammed earth construction with granitic residual soils: The case study of northern Portugal," *Constr. Build. Mater.*, vol. 47, pp. 181–191, 2013, doi: 10.1016/j.conbuildmat.2013.05.047.
[231] A. Seco, P. Urmeneta, E. Prieto, S. Marcelino, B. García, and L. Miqueleiz, "Estimated and real durability of unfired clay bricks: Determining factors and representativeness of the laboratory tests," *Constr. Build. Mater.*, vol. 131, pp. 600–605, 2017, doi: 10.1016/j.conbuildmat.2016.11.107.
[232] DIN 18945:2013-08, "Lehmsteine - Begriffe, Anforderungen, Prüfverfahren," 2013.
[233] H. Schroeder, *Sustainable Building with Earth, Springer*. .
[234] BIS, "IS 3495 Parts 1-4 : Methods of Tests of Burnt Clay building brick," *IS 3495 1992 - Parts 1 to 4 - METHODS TESTS Burn. CLAY Build. BRICKS*, pp. 1–7, 1992.
[235] A. P. da Silva Milani and W. J. Freire, "Physical and mechanical evaluation of bricks of soil-cement-rice husk mixtures," *Rev. Teor. e Prat. na Eng. Civ. 8*, vol. 11, no. 11, pp. 23–30, 2008.
[236] A. P. da Silva Milani and L. C. Labaki, "Physical, Mechanical, and Thermal Performance of Cement-Stabilized Rammed Earth–Rice Husk Ash Walls," *J. Mater. Civ. Eng.*, vol. 24, no. 6, pp. 775–782, 2012.
[237] G. M. Modero, J. H. Kennedy, P. K. Woodward, and M. Banimahd, "Flooding e ect on earth walls," *Sustainability*, vol. 3, no. 1, pp. 1–13, 2010.
[238] XP P13-901, "Blocs de terre comprimée pour murs et cloisons Définitions — Spécifications — Méthodes d'essai — Conditions de réception," 2001.
[239] K. A. Heathcote, "Durability of earth wall buildings," *Constr. Build. Mater.*, vol. 9, no. 3, pp. 185–189, 1995.
[240] R. C. Jaffe, "Understanding Mortar," *J. Mater. Civ. Eng.*, vol. 34, no. 51, pp. 12–19, 2001.

[241] M. Pyle, “Aggregates for mortar,” vol. 1992, 1985.
[242] G. E. Bessey, “Current developments affecting the design and use of mortars for building purposes.,” *J. appl. Chem.*, vol. 16, 1966.
[243] F. Verhelst, E. Kjaer, W. Jaeger, B. Middendorf, K. Van Balen, and P. Walker, “Sustainable Masonry : the Importance of Mortar Quality,” *15th Int. Brick Block Mason. Conf.*, 2012.
[244] L. A. Palmer and D. A. Parsons, “A study of the properties of mortars and bricks and their relation to bond.,” *Bur. Stand. J. Res.*, vol. 12, no. 5, p. 609, 1934.
[245] S. Boynton and A. Gutschick, “Bond of mortar to masonry units.,” *Japanese circulation journal*, vol. 56. p. 748, 1992.
[246] J. C. Thornton, “Relation Between Bond and the Surface Physics of Masonry Units,” *J. Am. Ceram. Soc.*, vol. 36, no. 4, pp. 105–120, 1953, doi: 10.1111/j.1151-2916.1953.tb12847.x.
[247] T. Ritchie and J. Davison, “Factors affecting bond strength and resistance to moisture penetration,” 1963.
[248] L. Miccoli, U. Müller, and P. Fontana, “Mechanical behaviour of earthen materials : A comparison between earth block masonry , rammed earth and cob,” *Constr. Build. Mater.*, vol. 61, pp. 327–339, 2014.
[249] L. A. Palmer and J. V Hall, “Durability and strength of bond between mortar and brick.,” 1931.
[250] B. P. Sinha, “Model Studies Related To Load-Bearing Brickwork,” 1967.
[251] C. Hall and W. Hoff, “Water Transport in Brick, Stone and Concrete,” *Cem. Concr. Res.*, vol. 34, no. 11, p. 2169, 2004.
[252] C. Groot, “Effects of water on mortar-brick bond,” *Heron (Delft)*, vol. 40, no. 1, pp. 57–70, 1995.
[253] C. Groot, “First minutes water transport from mortar to brick,” 1991.
[254] C. Groot and J. Larbi, “Influence of water flow (reversal) on bond strength development in young masonry,” *Heron*, vol. 44, no. 2, pp. 63–78, 1999.
[255] J. P. Forth, J. J. Brooks, and S. H. Tapsir, “The effect of unit water absorption on long-term movements of masonry.,” 2000.
[256] H. Derluyn, H. Janssen, and J. Carmeliet, “Moisture transfer across the interface between brick and mortar joint.,” 2008.
[257] K. Venu Madhava Rao, B. V. Venkatarama Reddy, and K. S. Jagadish, “Flexural bond strength of masonry using various bricks and mortars,” *Mater. Struct.*, vol. 29, pp. 119–124, 1996.
[258] B. V. Venkatarama Reddy and C. Vyas, “Influence of shear bond strength on compressive strength and stress–strain characteristics of masonry,” *Mater. Struct.*, vol. 41, 2008.
[259] P. Walker, “Bond characteristics of earth bocks masonry,” *J. Mater. Civ. Eng.*, pp. 249–256, 1999.
[260] J. S. J. Cheah, P. Walker, A. Heath, and T. K. K. B. Morgan, “Evaluating shear test methods for stabilised rammed earth,” *Proc. Inst. Civ. Eng. - Constr. Mater.*, pp. 325–334., 2012.
[261] P. Fontana, L. Miccoli, and U. Grünberg, “Experimental investigations on the initial shear strength of masonry with earth mortars,” *Int. J. Mason. Res. Innov.*, vol. 3, no. 1, pp. 34–49, 2018, doi: 10.1504/IJMRI.2018.089051.
[262] L. Miccoli, D. V. Oliveira, R. A. Silva, U. Müller, and L. Schueremans, “Static behaviour of rammed earth : experimental testing and finite element modelling,” *Mater. Struct.*, pp. 3443–3456, 2015.
[263] R. Silva, D. Olliveira, L. Schueremans, T. Miranda, and J. Machado, “Shear behaviour

of rammed earth walls repaired by means of grouting," in *9th International Masonry Conference*, 2014, pp. 1–12.
[264] A. Corbin and C. Augarde, "Investigation into the shear behaviour of rammed earth using shear box tests," in *First International Conference On Bio-based Building Materials*, 2015, pp. 93–98.
[265] R. El-Nabouch, Q. -B. Bui, O. Plé, and P. Perrotin, "Characterizing the shear parameters of rammed earth material by using a full-scale direct share box," *Constr. Build. Mater.*, vol. 171, pp. 414–420, 2018.
[266] L. Xu, K. K. Wong, A. Fabbri, F. Champiré, and D. Branque, "Loading-unloading shear behavior of rammed earth upon varying clay content and relative humidity conditions," *Soils Found.*, 2018.
[267] J. A. Thamboo and M. Dhanasekar, "Characterisation of flexural bond strength in thin bed," 2012.
[268] N. Walliman, B. Baiche, and R. Ogden, "Thin-joint glued brickwork : Building in the British context," vol. 22, pp. 1081–1092, 2008.
[269] G. Van Zijl, "Modeling Masonry Shear-Compression : Role of Dilatancy Highlighted Modeling Masonry Shear-Compression : Role of Dilatancy Highlighted," 2004.
[270] A. Gabor, E. Ferrier, E. Jacquelin, and P. Hamelin, "Analysis and modelling of the in-plane shear behaviour of hollow brick masonry panels," vol. 20, pp. 308–321, 2006.
[271] R. Shaan, "Etude du comportement mecanique de la maconnerie en briques," 1987.
[272] H. K. Hilsdorf, "Investigation into the failure mechanism of brick masonry loaded in axial compression," pp. 34–41, 1991.
[273] A. Page, "The biaxial compressive strength of brick masonry of brick masonry," 1981.
[274] M. Dhanasekar, "The failure of brick masonry under biaxial stresses.," 1985.
[275] A. N. Narayanaswamy, "Mechanical Testing Procedure for Local Building Materials : Rammed Earth and Laterite Building Stones," École Nationale des Travaux Publics de l'Etat, 2016.
[276] L. XU, "Mechanical behaviour of compacted earth with respect to relative humidity and clay content : experimental study and constitutive modelling," École Nationale des Travaux Publics de l'Etat, 2018.
[277] AFNOR, "Compressed Earth Blocks for walls and partitions : definitions - specifications - test methods - delivery acceptance conditions," 2001.
[278] V. Maniatidis and P. Walker, "A review of rammed earth construction," *Dev. rammed earth UK Hous.*, no. May, p. 109, 2003, [Online]. Available: http://staff.bath.ac.uk/abspw/rammedearth/review.pdf.
[279] A. P'KLA, "Caractérisation en compression simple des blocs de terre comprimée (BTC) : application aux maçonneries 'BTC-mortier de terre,'" ENTPE, 2002.
[280] M. A. Rahman, "Effects of Cement-Rice Husk Ash Mixtures On Geotechnical Properties of Lateritic Soils," *Soils Found.*, 1987.
[281] M. Olivier, M. Ali, and A. Mesbah, "Influence du malaxage et du type de presses sur la fabrication des briques de terre compressée," no. June 2016, 1989.
[282] M. Olivier, "Optimisation de la Fabrication de Briques de Terre Crue pour la Construction," no. June, 1985.
[283] S. Maini, "Production and Use of Compressed Earth Stabilised Earth Block," vol. 91, no. 0, 2010.
[284] B. V. Venkatarama Reddy and M. S. Latha, "Influence of soil grading on the characteristics of cement stabilised soil compacts," *Mater. Struct. Constr.*, vol. 47, no. 10, pp. 1633–1645, 2014, doi: 10.1617/s11527-013-0142-1.
[285] B. V. Venkatarama Reddy and A. Gupta, "Influence of sand grading on the characteristics of mortars and soil-cement block masonry," *Constr. Build. Mater.*, vol.

22, no. 8, pp. 1614–1623, 2008, doi: 10.1016/j.conbuildmat.2007.06.014.
[286] K. S. Venkatarama Reddy, B. V.; Richardson Lal; Nanjunda Rao, "Optimum soil grading for the soil-cement blocks," *Mater. Civ. Eng.*, pp. 139–148, 2007, doi: https://doi.org/10.1061/(ASCE)0899-1561(2007)19:2(139).
[287] M. Ben Mansour, E. Ogam, A. Jelidi, A. S. Cherif, and S. Ben Jabrallah, "Influence of compaction pressure on the mechanical and acoustic properties of compacted earth blocks: An inverse multi-parameter acoustic problem," *Appl. Acoust.*, vol. 125, pp. 128–135, 2017, doi: 10.1016/j.apacoust.2017.04.017.
[288] J. R. González-López, C. A. Juárez-Alvarado, B. Ayub-Francis, and J. M. Mendoza-Rangel, "Compaction effect on the compressive strength and durability of stabilized earth blocks," *Constr. Build. Mater.*, vol. 163, pp. 179–188, 2018, doi: 10.1016/j.conbuildmat.2017.12.074.
[289] K. Scrivener, A. Ouzia, P. Juilland, and A. Kunhi Mohamed, "Advances in understanding cement hydration mechanisms," *Cem. Concr. Res.*, vol. 124, no. August, p. 105823, 2019, doi: 10.1016/j.cemconres.2019.105823.
[290] C. F. Dunant, J. Granja, A. Muller, M. Azenha, and K. L. Scrivener, "Microstructural simulation and measurement of elastic modulus evolution of hydrating cement pastes," *Cem. Concr. Res.*, vol. 130, no. February, p. 106007, 2020, doi: 10.1016/j.cemconres.2020.106007.
[291] F. J. Ulm and O. Coussy, "Modeling of thermochemomechanical couplings of concrete at early ages," *J. Eng. Mech.*, vol. 121, no. 7, pp. 785–794, 1995, doi: 10.1061/(ASCE)0733-9399(1995)121:7(785).
[292] F. Lea and P. Hewlett, *Lea's Chemistry of Cement and Concrete*. Arnold, 1998.
[293] H. Taylor, *Cement Chemistry*, Second edi. 1997.
[294] W. Ma, D. Sample, R. Martin, and P. Brown, "Calorimetric Study of Cement Blends Containing Fly Ash, Silica Fume, and Slag at Elevated Temperatures," *Cem. Concr. Aggregates*, vol. 16, no. 2, pp. 93–99, 1994.
[295] J. Brooks and A. Al-Kaisi, "Early strength development of Portland and slag cement concretes cured at elevated temperatures," *Materials (Basel).*, vol. 87, pp. 503–507, 1990.
[296] F. Sajedi and H. A. Razak, "Effects of curing regimes and cement fineness on the compressive strength of ordinary Portland cement mortars," *Constr. Build. Mater.*, vol. 25, no. 4, pp. 2036–2045, 2011, doi: 10.1016/j.conbuildmat.2010.11.043.
[297] K. P. Teixeira, I. P. Rocha, L. D. S. Carneiro, J. Flores, E. A. Dauer, and A. Ghahremaninezhad, "The effect of curing temperature on the properties of cement pastes modified with TiO2 nanoparticles," *Materials (Basel).*, vol. 9, no. 11, pp. 1–15, 2016, doi: 10.3390/ma9110952.
[298] J. Tinnea and J. F. Young, "Influence of Citric Acid on Reactions in the System 3CaO·Al 2 O 3 - CaSO 4 ·2H 2 O-CaO-H 2 O," *J. Am. Ceram. Soc.*, vol. 60, pp. 9–10, 1977.
[299] P. J. Walker, "Strength, durability and shrinkage characteristics of cement stabilised soil blocks," *Cem. Concr. Compos.*, vol. 17, no. 4, pp. 301–310, Jan. 1995, doi: 10.1016/0958-9465(95)00019-9.
[300] K. A. Heathcote, "Durability of earthwall buildings," *Constr. Build. Mater.*, vol. 9, no. 3, pp. 185–189, 1995, doi: 10.1016/0950-0618(95)00035-E.
[301] J. Rouquerol, F. Rouquerol, P. Llewellyn, G. Maurin, and K. Sing, *Adsorption by Powders and Porous Solids: Principles, Methodology and Applications*, 2nd Editio. Academic Press, 2013.
[302] I. Langmuir, "The adsorption of gases on plane surfaces of glass, mica and platinium," *J. Am. Chem. Soc.*, 1918.
[303] J. Carmeliet, M. H. D. De Wit, and H. Janssen, "Hysteresis and moisture buffering of

wood," *Symp. Build. Phys. Nord. Ctries.*, no. 3, pp. 55–62, 2005.
[304] A. Patera, H. Derluyn, D. Derome, and J. Carmeliet, "Influence of sorption hysteresis on moisture transport in wood," *Wood Sci. Technol.*, vol. 50, no. 2, pp. 259–283, 2016, doi: 10.1007/s00226-015-0786-9.
[305] J. A. Palyvos, "A survey of wind convection coefficient correlations for building envelope energy systems' modeling," *Appl. Therm. Eng.*, vol. 28, no. 8–9, pp. 801–808, 2008, doi: 10.1016/j.applthermaleng.2007.12.005.
[306] D. Lelievre, T. Colinart, and P. Glouannec, "Hygrothermal behavior of bio-based building materials including hysteresis effects: Experimental and numerical analyses," *Energy Build.*, vol. 84, pp. 617–627, 2014, doi: 10.1016/j.enbuild.2014.09.013.
[307] H. Derluyn, D. Derome, J. Carmeliet, E. Stora, and R. Barbarulo, "Hysteretic moisture behavior of concrete: Modeling and analysis," *Cem. Concr. Res.*, vol. 42, no. 10, pp. 1379–1388, 2012, doi: 10.1016/j.cemconres.2012.06.010.
[308] P.-A. Chabriac, "Mesure du comportement hygrothermique du pisé.," ENTPE, Université de Lyon, France, 2014.
[309] F. McGregor, A. Heath, A. Shea, and M. Lawrence, "The moisture buffering capacity of unfired clay masonry," *Build. Environ.*, vol. 82, pp. 599–607, 2014, doi: 10.1016/j.buildenv.2014.09.027.
[310] ISO 12572:2001, "Hygrothermal performance of building materials and products — Determination of water vapour transmission properties," *Therm. Insul. Build.*, 2001.
[311] F. McGregor, A. Heath, E. Fodde, and A. Shea, "Conditions affecting the moisture buffering measurement performed on compressed earth blocks," *Build. Environ.*, vol. 75, pp. 11–18, 2014, doi: 10.1016/j.buildenv.2014.01.009.
[312] K. Svennberg, "Moisture Buffering in the Indoor Environment," Byggnadsfysik LTH, Lunds Tekniska Högskola, 2006.
[313] J. Mitchell, D. Hooper, and R. Campanella, "Permeability of compacted clay," *J. Soil Mech. Found. ASCE*, pp. 41–65.
[314] S. Tsivilis *et al.*, "The effect of clinker and limestone quality on the gas permeability, water absorption and pore structure of limestone cement concrete," *Cem. Concr. Compos.*, vol. 21, no. 2, pp. 139–146, 1999, doi: 10.1016/S0958-9465(98)00037-7.
[315] P. Walker, R. Keable, J. Martin, and V. Maniatidis, *Rammed Earth : Design and Construction Guidelines*. BRE Bookshop, 2005.
[316] K. A. Heathcote, "An investigation into the erodibility of earth wall units," University of Sydney, 2002.
[317] J. L. Briaud, *Geotechnical Engineering: Unsaturated and Saturated Soils*. John Wiley&Sons, 2013.
[318] J. P. Magnan, "Description, identification et classification des sols," *Tech. l'Ingénieur*, 1997.
[319] M. Földvári, *Handbook of thermogravimetric system of minerals and its use in geological practice*, vol. 213. Hungary, 2011.
[320] K. L. Scrivener, P. Juilland, and P. J. M. Monteiro, "Advances in understanding hydration of Portland cement," *Cem. Concr. Res.*, vol. 78, pp. 38–56, 2015, doi: 10.1016/j.cemconres.2015.05.025.
[321] J. W. Bullard *et al.*, "Mechanisms of cement hydration," *Cem. Concr. Res.*, vol. 41, no. 12, pp. 1208–1223, 2011, doi: 10.1016/j.cemconres.2010.09.011.
[322] Y. Sun, K. Q. Wang, and H. S. Lee, "Prediction of compressive strength development for blended cement mortar considering fly ash fineness and replacement ratio," *Constr. Build. Mater.*, vol. 271, p. 121532, 2021, doi: 10.1016/j.conbuildmat.2020.121532.
[323] E. M. Golafshani and A. Behnood, "Automatic regression methods for formulation of elastic modulus of recycled aggregate concrete," *Appl. Soft Comput. J.*, vol. 64, pp. 377–

400, 2018, doi: 10.1016/j.asoc.2017.12.030.
[324] E. M. Golafshani and A. Ashour, “Prediction of self-compacting concrete elastic modulus using two symbolic regression techniques,” *Autom. Constr.*, vol. 64, pp. 7–19, 2016, doi: 10.1016/j.autcon.2015.12.026.
[325] S. M. Mousavi, P. Aminian, A. H. Gandomi, A. H. Alavi, and H. Bolandi, “A new predictive model for compressive strength of HPC using gene expression programming,” *Adv. Eng. Softw.*, vol. 45, no. 1, pp. 105–114, 2012, doi: 10.1016/j.advengsoft.2011.09.014.
[326] K. M. Alexander, “The relationship between strength and the composition and fineness of cement,” *Cem. Concr. Res.*, vol. 2, no. 6, pp. 663–680, 1972, doi: 10.1016/0008-8846(72)90004-X.
[327] S. Tsivilis and G. Parissakis, “A Mathematical model for the prediction of cement strength.” 1995.
[328] K. Omine, H. Ochiai, and N. Yoshida, “Estimation of In-Situ Strength of Cement-Treated Soils Based on a Two-Phase Mixture Model,” *Soils Found.*, vol. 38, no. 4, pp. 17–29, 1998.
[329] N. C. Consoli, R. A. Q. Samaniego, S. F. V. Marques, G. I. Venson, E. Pasche, and L. E. G. Velasquez, “Single model establishing strength of dispersive clay treated with distinct binders,” *Can. Geotech. J.*, vol. 53, no. 12, pp. 2072–2079, 2016.
[330] G. A. Lorenzo and D. T. Bergado, “Fundamental Parameters of Cement-Admixed Clay—New Approach,” *J. Geotech. Geoenvironmental Eng.*, vol. 130, no. 10, pp. 1042–1050, 2004.
[331] J. K. Mitchell, T. S. Veng, and C. L. Monishith, “Behavior of stabilized soils under repeated loading, Performance evaluation of cementstabilized soil layers and its relationship to pavement design,” California University, Berkeley, California, 1974.
[332] S. C. Chian, S. T. Nguyen, and K. K. Phoon, “Extended strength development model of cement-treated clay,” *J. Geotech. Geoenvironmental Eng.*, vol. 142, no. 2, 2016.
[333] S. Horpibulsuk, N. Miura, and T. . S. Nagaraj, “Assessment of strength development in cement-admixed high water content clays with Abrams’ law as a basis,” *Geotechnique*, vol. 53, no. 4, pp. 439–444, 2003.
[334] T. A. Pham, J. Koseki, and D. Dias, “Optimum material ratio for improving the performance of cement-mixed soils,” *Transp. Geotech.*, vol. 28, no. March, p. 100544, 2021, doi: 10.1016/j.trgeo.2021.100544.
[335] ASTM, “ASTM D559-96. Standard test methods for wetting and drying compacted soil-cement mixtures.,” 1996.
[336] BIS, “IS 1725: Stabilized Soil Blocks Used in General Building Construction - Specifications,” 2013.
[337] W. H. Wischmeïer and D. D. Smith, *Predicting rainfall erosion losses - a guide to conservation planning*. Science and Education Administration, United States Department of Agriculture, 1958.
[338] S. M. Brooks and T. Spencer, “Vegetation modification of rainfall characteristics: implication for rainfall erosivity following logging in Sabah, Malaysia.,” *J. Trop. For. Sci.*, vol. 7, no. 3, pp. 435–446, 1995.
[339] A. Moussouni, L. Mouzai, and M. Bouhadef, “The effects of rain and overland flow powers on agricultural soil erodibility,” *Waset*, vol. 76, pp. 439–442, 2013.
[340] R. P. C. Morgan, *Soil Erosion and Conservation*, 2nd ed. Addison Wesley Longman, England, 1995.
[341] C. Quansah, “The effect of soil type, rain intensity and their interactions on splash detachment and transport,” *J. Soil Sci.*, vol. 32, pp. 215– 224, 1981.
[342] J. Poesen, “An improved splash transport model,” *Zeitschrift fur Geomorphol.*, vol. 29,

no. 2, pp. 193–211, 1985.
[343] C. J. Rosewell, “Rainfall kinetic energy in eastern Australia,” *J. Clim. Appl. Meteorol.*, vol. 25, pp. 695 – 1701, 1986.
[344] R. P. C. Morgan *et al.*, *The European Soil Erosion Model (EUROSEM): Documentation and User Guide*. Silsoe, Bedford: Silsoe College, Cranfield University, 1998.
[345] W. H. Wischmeier and D. D. Smith, *Predicting rainfall erosion losses*. USDA Agricultural Research Service Hand-book, 1978.
[346] M. R. Hall, “Assessing the environmental performance of stabilised rammed earth walls using a climatic simulation chamber,” *Build. Environ.*, vol. 42, no. 1, pp. 139–145, 2007.
[347] P. Gerard, M. Mahdad, and B. McCormack, A. R. Francois, “A uni ed failure criterion for unstabilized rammed earth materials upon varying relative humidity conditions,” *Constr. Build. Mater.*, vol. 95, pp. 437–447, 2015.
[348] P. A. Jaquin, C. E. Augarde, D. Gallipoli, and D. G. Toll, “The strength of unstabilised rammed earth materials,” *Géotechnique*, vol. 59, no. 5, pp. 487–490, 2009.
[349] C. T. S. Beckett, C. E. Augarde, D. Easton, and T. Easton, “Strength characterisation of soil-based construction materials,” *Geotechnique*, vol. 68, no. 5, pp. 400–409, 2018, doi: 10.1680/jgeot.16.P.288.
[350] A. G. Killip and D. W. Cheetham, “The prevention of rain penetration through external walls and joints by means of pressure equalization,” *Build. Environ.*, vol. 19, no. 81–91, 1984.
[351] F. J. Heymann, “Erosion by liquids,” *Mach. Des.*, pp. 118–124, 1970.
[352] F. J. Heymann, “A survey of clues to the relationship between erosion rate and impact parameters,” in *Second Meersburg conference on rain erosion and allied phenomena*, 1967, pp. 683–760.
[353] F. J. Heymann, “On the time dependence of the rate of erosion due to impingement or cavitation,” *Eros. by Cavitation or Impingement, ASTM STP 408, Philadelphia*, pp. 70–110, 1967, doi: 10.1520/STP46046S.
[354] F. P. Bowden and J. H. Brunton, “The deformation of solids by liquid impact at supersonic speeds,” *Proc. R. Soc. London, Ser. A (Mathematical Phys. Sci.*, vol. 263, pp. 433–450, 1961.
[355] C. T. S. Beckett, P. A. Jaquin, and J. C. Morel, “Weathering the storm: A framework to assess the resistance of earthen structures to water damage,” *Constr. Build. Mater.*, vol. 242, p. 118098, 2020, doi: 10.1016/j.conbuildmat.2020.118098.
[356] BS EN 12504-4, *Testing concrete. Determination of ultrasonic pulse velocity*. 2004.
[357] J. H. Bungey, *The use of ultrasonics for NDT of concrete*. Brit J NDT, 1984.
[358] S. Dimter, T. Rukavina, and I. Barišić, “Application of the ultrasonic method in evaluation of properties of stabilized mixes,” *Balt. J. Road Bridg. Eng.*, vol. 6, no. 3, pp. 177–184, 2011, doi: 10.3846/bjrbe.2011.23.
[359] D. G. Aggelis, E. Leonidou, and T. E. Matikas, “Subsurface crack determination by one-sided ultrasonic measurements,” *Cem. Concr. Compos.*, vol. 34, no. 2, pp. 140–146, 2012, doi: 10.1016/j.cemconcomp.2011.09.017.
[360] J. Zhu, S. H. Kee, D. Han, and Y. Te Tsai, “Effects of air voids on ultrasonic wave propagation in early age cement pastes,” *Cem. Concr. Res.*, vol. 41, no. 8, pp. 872–881, 2011, doi: 10.1016/j.cemconres.2011.04.005.
[361] I. Barišić, S. Dimter, and T. Rukavina, “Characterization of cement stabilized pavement layers with ultrasound testing,” *Teh. Vjesn.*, vol. 23, no. 2, pp. 447–453, 2016, doi: 10.17559/TV-20140916142451.
[362] M. Hamidian, M. Shariati, M. M. K. Arabnejad, and H. Sinaei, “Assessment of high strength and light weight aggregate concrete properties using ultrasonic pulse velocity technique,” *Int. J. Phys. Sci.*, vol. 6, no. 22, pp. 5261–5266, 2011, doi:

10.5897/IJPS11.1081.
[363] I. Facaoaru, “Non-Destructive Testing of Concrete in Romania,” in *Symposium on NDT of Concrete and Timber*, 1970, pp. 39–49.
[364] D. Breysse, “Nondestructive evaluation of concrete strength: An historical review and a new perspective by combining NDT methods,” *Constr. Build. Mater.*, vol. 33, pp. 139–163, 2012, doi: 10.1016/j.conbuildmat.2011.12.103.
[365] M. Duriez, F. Vieux-Champagne, R. Trad, P. Maillard, and J. E. Aubert, “A methodology for the mix design of earth bedding mortar,” *Mater. Struct. Constr.*, vol. 53, no. 1, 2020, doi: 10.1617/s11527-020-1443-9.
[366] B. V. Venkatarama Reddy, V. Nikhil, and M. Nikhilash, “Moisture Transport in Cement Stabilised Soil Brick-Mortar Interface and Implications on Masonry Bond Strength,” in *Earthen Dwellings and Structures - Current Status in their Adoption*, 2019.
[367] EN 1052-3, “Methods of test for mortar for masonry – Part 11: Determination of flexural and compressive strength of hardened mortar (includes Amendment A1:2006),” 2007.
[368] N. E. 1015-18, “Méthodes d’essai des mortiers pour maconnerie Partie 18 : détermination du coefficient d’absorption d’eau par cappillarité du mortier durci,” 2003.
[369] C. Egenti, J. M. Khatib, and E. Negim, “Performance of Compressed Earth Brick in Comparison With the Prevailing Sand-Cement Wall Construction in Nigeria.,” *Int. J. Eng. Res. Rev.*, vol. 3, no. 4, pp. 37–41, 2015.
[370] A. J. Fopossi, R. N. Mutuku, and F. Ngapgue, “Effects of stabilizers on water absorption of compressed earth blocks made from Mangu soil.,” *Int. J. Eng. Sci. Emerg. Technol.*, vol. 7, no. 1, pp. 490–495, 2014.
[371] D. C. Hughes and N. L. Crossley, “Pore structure characterization of GGBS/OPC Grouts using solvent techniques,” *Cem. Concr. Res.*, vol. 24, no. 7, pp. 1255–1266, 1994.
[372] L. J. Parrott, “Thermogravimetric and sorption studies of methanol exchange in an alite paste,” *Cem. Concr. Res.*, vol. 13, pp. 18–22, 1983.
[373] L. J. Parrott, “An examination of two methods for studying diffusion kinetics in hydrated cements,” *Mater. Struct.*, vol. 17, pp. 131–137, 1981.
[374] R. F. Feldman, “Diffusion measurements in cement paste by water replacement using propan-2-ol,” *Cem. Concr. Res.*, vol. 17, pp. 602–612, 1987.
[375] E. H. Schwiete and U. Ludwig, “Crystal structure and properties of cement hydration products (hydrated calcium aluminates and ferrites,” in *5th Int. Symposium on the Chemistry of Cement*, 1968, pp. 36–37.
[376] F. Massazza and U. Costa, “Effect of superplasticizers on the C3A hydration,” in *7th International Congress on the Chemistry of Cement*, 1980, pp. 529–534.
[377] S. Monosi, G. Morinoci, M. Pauri, and M. Collepardi, “Effect of retarding admixtures on the Portland cement hydration,” in *8th International Congress on the Chemistry of Cement*, 1986, pp. 130–141.
[378] R. Sersale, V. Sabatelli, and G. L. Valenti, “Influence of some retarders on the hydration, at early ages, of tricalcium aluminate,” 1980.
[379] G. Cassagnabère, F. Escadeillas and M. Mouret, “Study of the reactivity of cement/metakaolin binders at early age for specific use in steam cured precast concrete,” *Constr. Build. Mater.*, vol. 23, no. 2, pp. 775–784, 2009.
[380] A. Bajza and I. Rousekova, “Effect of heat treatment conditions on the pore structure of cement mortars,” *Cem. Concr. Res.*, vol. 13, no. 5, pp. 747–750, 1983.
[381] C. J. Fordham and I. . Smalley, “A simple thermogravimetric study of hydrated cement,” *Cem. Concr. Res.*, vol. 15, no. 1, pp. 141–144, 1985.
[382] A. Xu, “Structure of hardened cement-fly ash systems and their related properties,” Chalmers University of Technology,Göteborg (Sweden), 1992.
[383] E. A. Helsing Atlassi, “Quantitative thermogravimetric study on the non evaporable

water in mature silica fume concrete," Chalmers University of Technology, Göteborg (Sweden), 1993.
[384] V. Maniatidis and P. Walker, "A Review of Rammed Earth Construction," 2003.
[385] D. Ciancio and C. Beckett, "Rammed earth: An overview of a sustainable construction material," 2013.
[386] M. C. Jiménez Delgado and I. C. Guerrero, "The selection of soils for unstabilised earth building: A normative review," *Constr. Build. Mater.*, vol. 21, no. 2, pp. 237–251, 2007, doi: 10.1016/j.conbuildmat.2005.08.006.